NASA Contractor Report 4049

Space Shuttle Flying Qualities and Criteria Assessment

T. T. Myers, D. E. Johnston,
and D. T. McRuer

Systems Technology, Inc.
Hawthorne, California

Prepared for
Ames Research Center
Dryden Flight Research Facility
under Contract NAS2-11900

National Aeronautics
and Space Administration

**Scientific and Technical
Information Branch**

1987

TABLE OF CONTENTS

LIST OF FIGURES

LIST OF FIGURES (Continued)

LIST OF FIGURES (Continued)

LIST OF FIGURES (Continued)

LIST OF FIGURES (Continued)

LIST OF FIGURES (Concluded)

LIST OF TABLES

NOMENCLATURE

a, b, c	Constant coefficients of quadratic equations
AR	Aspect ratio
c or $\overline{c}$	Reference chord length
c.g.	Center of gravity
C_D	Drag coefficient; $\frac{2D}{\rho U^2 S}$
C_{D_o}	Zero lift drag coefficient
C_L	Lift coefficient; $\frac{2L}{\rho U^2 S}$
C_{L_o}	Lift coefficient, $\alpha = \delta_e = 0$
C_{L_α}	$\frac{\partial C_L}{\partial \alpha}$
C_{L_δ}	$\frac{\partial C_L}{\partial \delta}$
C_M	Pitching moment coefficient; $\frac{2M}{\rho U^2 Sc}$
C_{M_u}	$\frac{U}{2}\frac{\partial C_M}{\partial U}$
C_{M_α}	$\frac{\partial C_M}{\partial \alpha}$
$C_{M_{\dot{\alpha}}}$	$\frac{\partial C_M}{\partial(\dot{\alpha}c/2U)}$
C_{M_q}	$\frac{\partial C_M}{\partial(qc/2U)}$
C_{M_δ}	$\frac{\partial C_M}{\partial \delta}$
C_N or CN	Normal force coefficient

dB	Decibel
D	Aerodynamic drag
F	Force
g	Acceleration due to gravity (32.2 ft/sec^2)
G_f	Forward loop transfer function
G_i	Command path filter transfer function
h	Path deviation; altitude
H	Altitude AGL
H_f	Flare initiation altitude
H_o	Altitude at start of shallow glide
I_y, I_x	Moment of inertia in pitch and roll, respectively
k, K	Gain, particularized by subscript
$K_{\dot{V}}$	Average acceleration parameter, see Fig. 32
L	Aerodynamic lift; aircraft length
ℓ_x	Distance along aircraft axis from c.g., positive forward
m	Aircraft mass
ms	Millisecond
M	Aerodynamic pitching moment; Mach number
M_q	(Single degree-of-freedom) pitch damping; pitching acceleration per unit pitching velocity; $M_q = \frac{\rho S U c^2}{4 I_y} C_{M_q}$
M_u	Pitching acceleration per unit forward velocity; $M_u = \frac{\rho S U c}{I_y} (C_M + C_{M_u})$

M_w, (M_α) — Weathercock stability; pitching acceleration per unit vertical velocity (angle-of-attack);

$$M_\alpha = U_o M_w \quad ; \quad M_w = \frac{\rho S U c}{2 I_y} C_{M_\alpha}$$

$M_{\dot{\alpha}}$ — Pitching acceleration per unit angle-of-attack rate

$$M_{\dot{\alpha}} = \frac{\rho S U c^2}{4 I_y} C_{M_{\dot{\alpha}}}$$

M_δ — Pitching acceleration per unit control surface deflection

$$M_\delta = \frac{\rho S U^2 c}{2 I_y} C_{M_\delta}$$

n — Load factor

n_z — Load factor in z direction

$N^h_{\delta_e}$ — Altitude-to-elevator numerator

$N^\theta_{\delta_e}$ — Pitch attitude-to-elevator numerator

psf — Pounds per square inch

q — Pitching velocity (perturbation)

$\bar{q}$ — Dynamic pressure

R, R_T — Turn radius

s — Laplace Operator

S — Reference planform area

t — Time measure

T — Time constant; sampling period

T_f — Flare time constant

T_{h_1}, T_{h_2}, T_{h_3} — Time constants, altitude numerator

T_q — Lead time constant in augmentation system

T_r	Rise time
T_{SP_1}, T_{SP_2}	Time constants, real short period roots
T_{θ_1}, T_{θ_2}	Time constants, pitch attitude numerator
U_o	Speed in reference condition
V	Speed
$\overline{V}$	Velocity vector
V_s	Stall speed
w	Vertical velocity
W	Gross weight; aircraft weight
X	Flight path displacement along runway line
X_{ICR}	Location of ICR along aircraft X axis, positive forward of c.g.
X_w, X_α	Forward acceleration per unit vertical velocity

$$X_\alpha = U_o X_w \quad ; \quad X_w = \frac{\rho SU}{2m} (C_L - C_{D_\alpha})$$

Y	Flight path displacement perpendicular to runway line
Z_u	Vertical acceleration per unit forward velocity

$$Z_u = \frac{\rho SU}{m} (-C_L - C_{L_u})$$

Z_w, $(Z\alpha)$	Heave damping; vertical acceleration per unit vertical velocity (angle-of-attack);

$$Z_\alpha = U_o Z_w \quad ; \quad Z_w = \frac{\rho SU}{2m} (-C_{L_\alpha} - C_D)$$

Z_δ	Vertical acceleration per unit control surface deflection

$$Z_\delta = \frac{\rho SU^2}{2m} (-C_{L_\delta})$$

α	Angle-of-attack
γ	Flight path angle
δ	Generic control (elevator, manipulator, etc.) deflection, particularized by subscript
Δ	Difference increment; denominator of airframe transfer function
ζ	Damping ratio, particularized by subscript
θ	Pitch attitude (perturbation)
$\dot{\theta}$	Pitch attitude rate
π	3.1416
ρ	Atmospheric density
$\rho^2(\omega)$	Correlation coherence function between input and output spectra
σ	Real component of complex variable, s
τ	Time delay
Φ, ϕ	Bank angle
ϕ_{ii}	Spectral or cross spectral density distributions; particularized by subscripts
ϕ_M	Phase margin
ω	Imaginary component of complex variable, s
ω_{c_a}	Crossover frequency of amplitude ratio asymptote
ω_n	Natural frequency
ω_u	Instability frequency ($\phi_M = 0$)

MATH SYMBOLS

$\measuredangle$	phase angle
$\propto$	proportional to
$>$	greater than
d( ) or ($\cdot$)	first derivative of ( )
∂( )	partial derivative of ( )
f( )	function of ( )
($\cdot\cdot$)	second derivative of ( )
( )$'$	closed-loop value of ( )

SUBSCRIPTS

a	actuator
B	FCS bending filter; below runway level
BW	bandwidth
c	command or crossover
d	delay
e	elevator
f	flare
F	FCS smoothing filter
FB	feedback
h	altitude
max	maximum
min	minimum
n or n'	aircraft-FCS closed-loop effective vehicle damped natural frequency
o	initial or trim state; initiation of shallow glide
p	pilot or phugoid
q, Q	pitch rate
SB	speed brake
SF	FCS equalization shaping filter
SP	short period
SS	steady-state
TD	touchdown
X,Y,Z	aircraft axis system; forces along aircraft axis
ε	error
θ	pitch attitude

ACRONYMS AND ABBREVIATIONS

ACAH	Attitude command, attitude hold
ACIP	Aerodynamic Coefficient Identification Package
AGL	Above ground level
ALT	Approach and Landing Test
AR	Aspect ratio
ARC	Ames Research Center
BFCS	Backup flight control system
CAP	Control anticipation parameter
CHPR	Cooper Harper Pilot Rating (also HQR, PR)
CONV	Conventional
CSS	Control stick steering
DFRF	Dryden Flight Research Facility
DOF	Degrees-of-Freedom
ELBFK	FCS filter, see Fig. 9
ELERROR	FCS filter, see Fig. 9
ELVCMD	FCS filter, see Fig. 9
FCS	Flight control system
FFT	Fast Fourier Transform
FREDA	Frequency Domain Analysis Digital Program (STI proprietary)
GDQ	FCS gain, see Fig. 9
GPC	General purpose computer
GS	Glide slope
HAC	Heading alignment cylinder
HOS	Higher order system

HQR	Handling quality rating (also CHPR, PR)
HUD	Head-up display
ICR	Instantaneous center of rotation for elevator inputs
KEAS	Knots equivalent airspeed
LAHOS	Landing and Approach Higher Order System
LOES	Lower order equivalent system
MMLE	Modified maximum likelihood estimator
NLR	National Aerospace Laboratory (the Netherlands)
OEX	Shuttle Orbiter experiments program
OFQ	Shuttle Orbiter flying qualities and flight control design experiment
OFT	Orbiter Flight Test
OGS	Outer glide slope
PAPI	Precision approach path indicator
PIO	Pilot induced oscillation
PR	Pilot rating (also CHPR, HQR)
RCAH	Rate command, attitude hold
RHC	Rotational hand controller
RSS	Relaxed static stability
SAA	Superaugmented aircraft
S.M.	Static margin
STI	Systems Technology, Inc.
STS	Space Transportation System
TAEM	Terminal area energy management
TAGR	Total available gain range, see Eq. 18
TIFS	Total Inflight Simulator

SECTION I

INTRODUCTION

This report is a summary of work accomplished under a series of study tasks (Refs. 1-4) for the Flying Qualities and Flight Control Systems Design Criteria Experiment (OFQ) of the Shuttle Orbiter Experiments Program (OEX). The major tasks have involved review of applicability of existing flying quality and flight control system specification and criteria for the Shuttle; identification of potentially crucial flying quality deficiencies; dynamic modeling of the Shuttle Orbiter pilot/vehicle system in the terminal flight phases; devising a non-intrusive experimental program for extraction and identification of vehicle dynamics, pilot control strategy, and approach and landing performance metrics; and preparation of an OEX approach to produce a data archive and optimize use of the data to develop flying qualities criteria for future space Shuttle craft in general.

The detailed accomplishments of the various task segments have been documented in Refs. 1-4. But due to some of the dead ends and twists and turns of this study and other related research, it is somewhat difficult to follow a given topic through the four documents. Thus, this report and a companion document (Ref. 5) provide a (hopefully) more comprehensible summary of key results from the program. This report concentrates on analytic modeling of the Orbiter unconventional closed-loop dynamics in landing, modeling pilot control strategies, verification of vehicle dynamics and pilot control strategy from flight data, review of various existent or proposed aircraft flying quality parameters and criteria in comparison with the unique dynamic characteristics, and control aspects of the Shuttle in landing; and finally a summary of conclusions and recommendations for developing flying quality criteria and design guides for future Shuttle craft. The Ref. 5 companion document presents the proposed organization and means of implementing a flying quality data archive, and a system for experimenter access to and analysis of archival data.

At the outset of this flying quality and flight control system criteria assessment, which was initiated prior to the first Orbiter entry and landing, a number of potential problem areas were identified. These were based to some extent on uncertainties in vehicle aerodynamics, the recognized unusual vehicle dynamic and control properties as compared to conventional aircraft, the anticipated high pilot workload in achieving an acceptable solution to the manual terminal control problem in landing a large glider on a runway, allowance for possible failures in the vehicle electronic/hydraulic control system, etc. These and other uncertainties and potential problem areas were examined and prioritized in Ref. 1. A number of these were subsequently eliminated from further consideration after a few highly successful landings. Some have not yet had the opportunity to be exposed (e.g., possible control surface rate limiting due to APU failure, and subsequent reduced hydraulic power supply). Others involving longitudinal attitude and path control in the final approach and landing flare have been reinforced by the first few flights and are the main focus of this report.

In Section II the Shuttle landing task and vehicle dynamics are developed. Kinematics of the steep glide, preflare, shallow glide, and final flare are described along with ground and cockpit aids to manual path control. The Shuttle Orbiter longitudinal dynamics and flight control system characteristics are developed to demonstrate the unusual or non-conventional attitude and path response nature of this superaugmented vehicle. Finally, the effective pitch dynamics of the Orbiter in the landing phase are identified from flight data, and are shown to be essentially as predicted by quasi-linearized analytic models.

Section III is devoted to prediction and verification of the manual control loop structure, and the influence of different flare strategies in landing. Flight traces are examined for six landings and, with the aid of altitude vs. sink rate phase plane (hodograph) analysis, pilot adopted control strategies and techniques are identified. Final flare strategies are found to run the gamut from highly skilled, precisely timed, single control pulse, precognitive (almost open-loop) step attitude change to an almost continuous input exponential flare via tight

pitch attitude control proportional to altitude decay. The latter closely approximates an ideal exponential flare in which sink rate is inversely proportional to altitude. Despite the differing strategies and control techniques, values for key flight path and touchdown parameters extracted from the flight data indicate the pilot's concern for touchdown sink rate and velocity as opposed to runway position.

A review of flying quality criteria relevant to pitch attitude and flight path control is presented in Section IV. It is shown that aircraft responses and criteria derived from conventional fighter aircraft are not generally applicable to large superaugmented aircraft such as the Shuttle. More appropriate pitch rate response and time delay criteria are suggested. Problems with pitch rate command/attitude hold (RCAH) control in the landing flare as opposed to attitude command/attitude hold (ACAH) are addressed, and the preference for the latter noted. Possible influence of the pilot's control manipulator configuration on the preference for ACAH over RCAH is also explored along with some preliminary design guide considerations for Shuttle-like wrist action manipulators.

Recommendations for future Shuttle craft flying qualities criteria and/or further experimentation are summarized in Section V.

SECTION II

SHUTTLE LANDING TASK AND VEHICLE DYNAMICS

In Section II the Shuttle landing task and vehicle dynamics are developed. Kinematics of the steep glide, preflare, shallow glide, and final flare are described along with ground and cockpit aids to manual path control. The Shuttle Orbiter longitudinal dynamics and flight control system characteristics are developed to demonstrate the unusual or non-conventional attitude and path response nature of this superaugmented vehicle. Finally, the effective pitch dynamics of the Orbiter in the landing phase are identified from flight data, and are shown to be essentially as predicted by quasi-linearized analytic models.

A. LANDING TASK AND LANDING AIDS

1. Shuttle Return from Orbit

As in almost all aspects of its design, the space shuttle has been a pioneering vehicle in the discipline of flight control. As the first vehicle to return from orbit and operate and land as an aircraft, the shuttle provided its flight control designers with a formidable challenge. The complexity of the problem derived basically from the wide range of flight conditions, altitude, Mach number, and dynamic pressures in the entry. These requirements have resulted in a sophisticated digital flight control system, which employs both reaction jets and aerodynamic surfaces. Further, both automatic guidance and human pilots are essential elements in the system.

Guidance and control in the return from orbit involves three phases which are reflected in the basic mode selection logic of the flight control system (FCS). These are: entry, terminal area energy management (TAEM), and the approach and landing phase. Because the shuttle is a glider, energy management is a dominant concern in all three phases. The basic guidance activity in the entry phase involves modulation of a series of S-turns to keep the shuttle's total energy within the allowed

"window." The TAEM phase begins at about 80,000 ft and the major maneuver here is the Heading Alignment Cylinder (HAC) turn. The two HACs are imaginary cylinders (see Fig. 1) tangent to a vertical plane through the runway centerline. The shuttle may enter a HAC from any direction and then fly around its surface until the runway heading is reached. At this point the approach and landing phase begins. Thus, the major guidance activity in the TAEM is adjustment of the HAC diameter to put the shuttle within the correct energy window at the start of the approach and landing phase.

There have been challenging FCS design problems over the entire return from orbit (Ref. 6). Interestingly though, like many aircraft before, the primary flying qualities concerns have been in the landing phase; primarily in the final flare in the last few feet before touchdown. To paraphrase an astronaut/pilot: the importance of flying qualities in the shuttle is inversely proportional to altitude. These

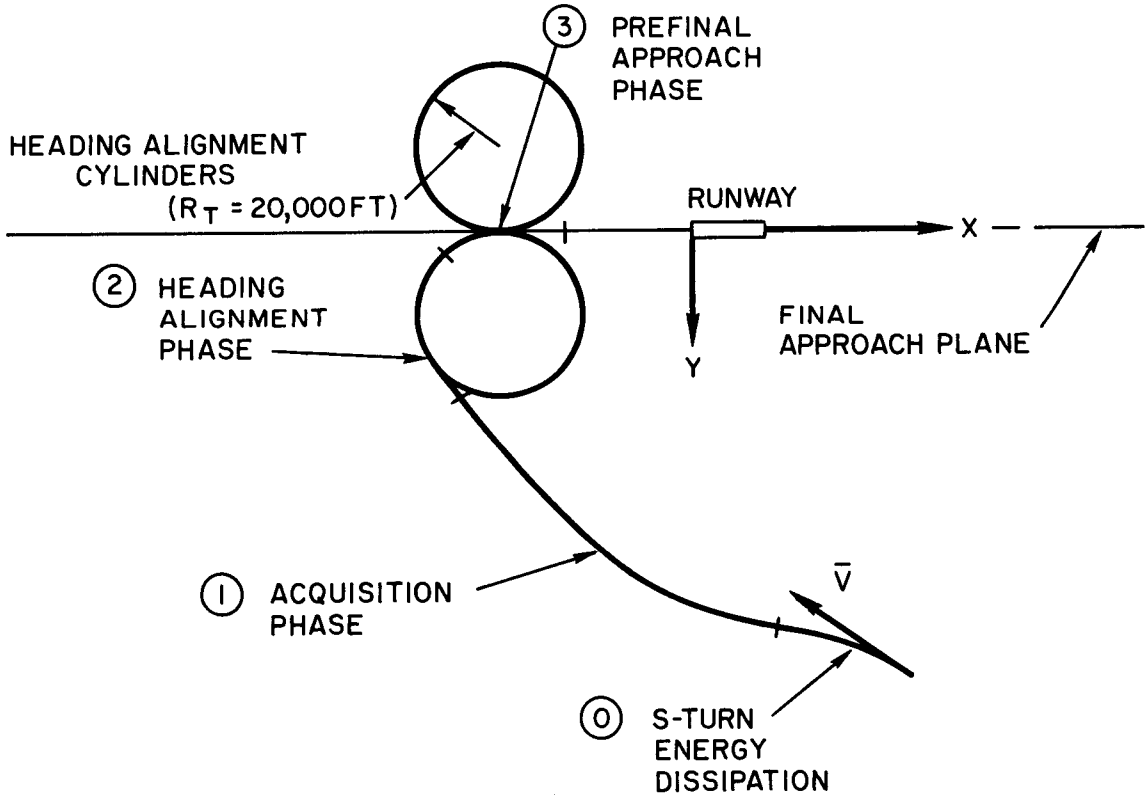

Figure 1. TAEM Guidance Phases

concerns existed before the first Orbiter Flight Test (OFT) flight, particularly after the PIO incident which occurred in the fifth Approach and Landing Test (ALT) flight (Ref. 7). Despite these concerns and a general recognition that the shuttle has unconventional handling qualities, the shuttle has now made a large number of successful manual landings. Furthermore, autoland flight testing, which was to have been a major activity from OFT flight STS-3 on, has now been long postponed while confidence in manual landings has grown.

Because of the particular importance of the landing for shuttle flight control system design and flying qualities, and the implications for other advanced "superaugmented" aircraft, this report will focus on the landing phase. Since the approach and landing is fundamentally a longitudinal maneuver and because of important unconventional aspects of the shuttle longitudinal dynamics and pitch control system, this report will further concentrate on longitudinal dynamics and control.

The basic technique for landing the shuttle as a glider was evolved over many years of experimentation with lifting body research aircraft. The maneuver basically consists of a steep "outer" glide followed by a pull-up to a shallow inner glide slope.

2. The Landing Task

Figure 2a shows a nominal trajectory for the Orbiter approach and landing. This reference trajectory is based on considerations of basic flight mechanics (Ref. 2) and autoland system design data (Ref. 8). While actual trajectories will vary of course depending on pilot technique, disturbances, etc., Fig. 2 will serve as a reference for developments to follow.

The approach and landing phase begins with capture of the steep glide slope shortly after leveling the wings following the HAC turn -- nominally at 15,000 ft altitude and approximately 40,000 ft from the runway threshold. The primary purpose of the steep glide slope is to set up and stabilize the vehicle on a constant equivalent airspeed (i.e., constant dynamic pressure). The steep flight path angle is

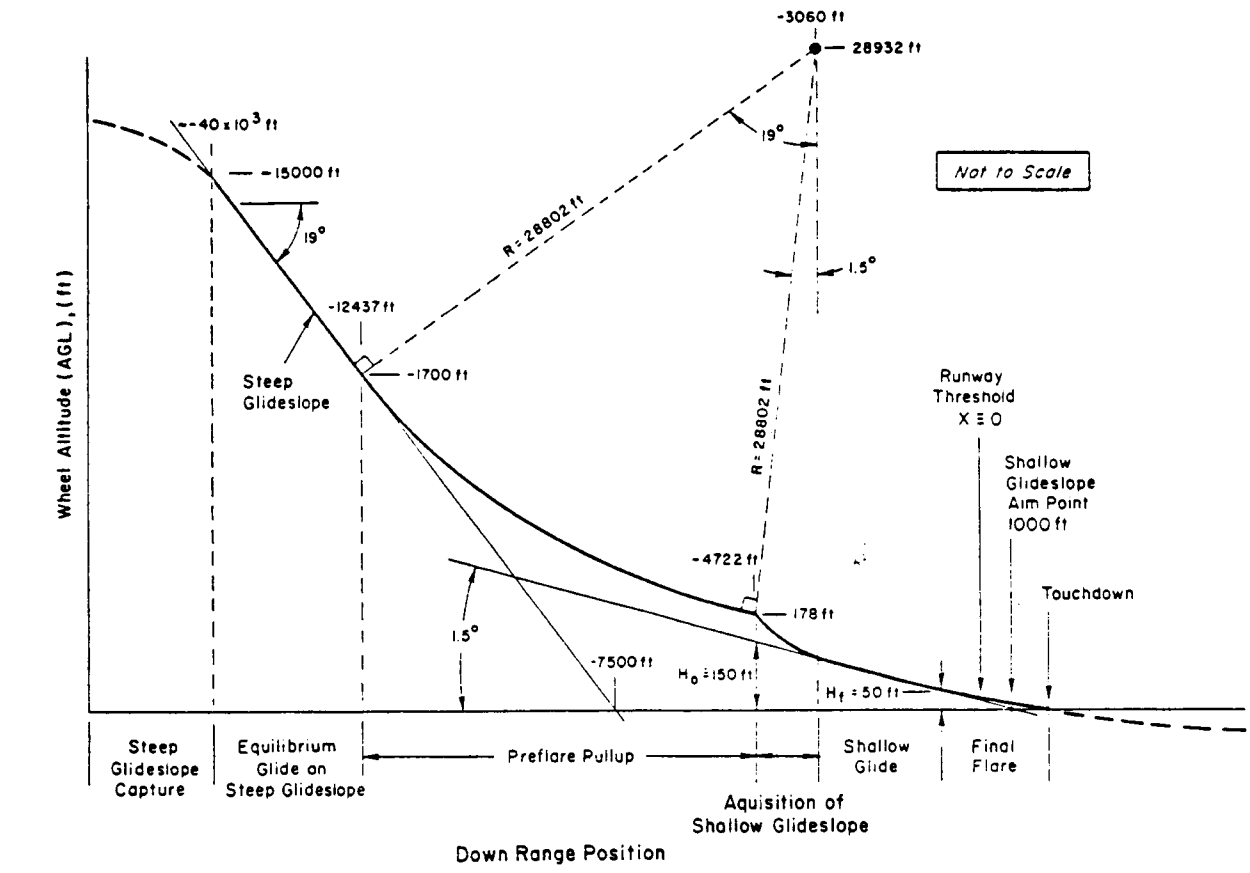

a) Trajectory

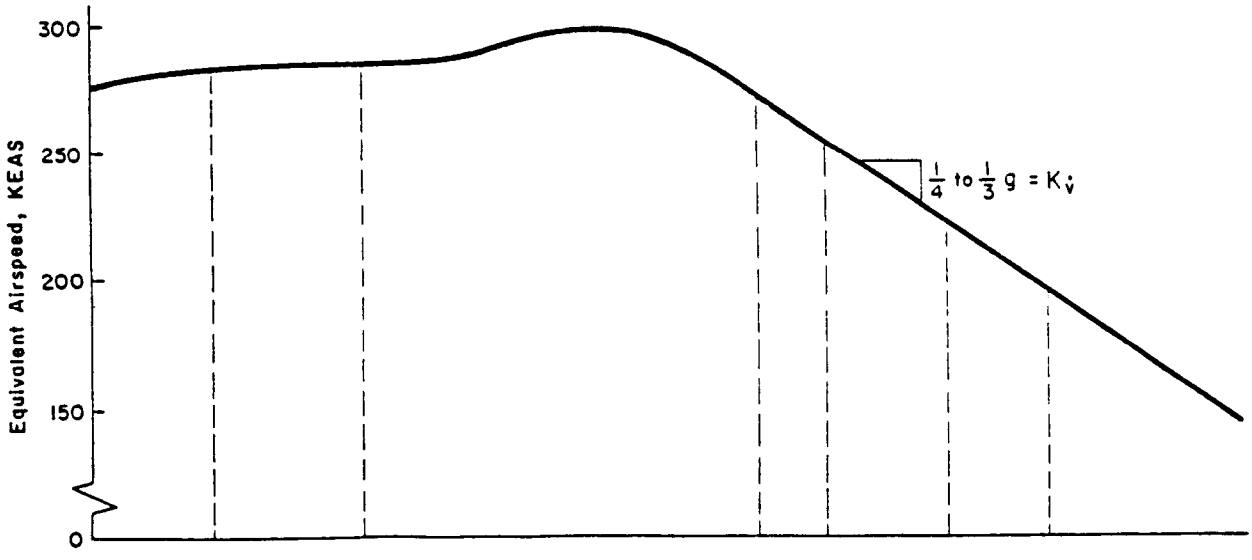

b) Equivalent Airspeed Variation

Figure 2. Nominal Trajectory and Airspeed Variation for Shuttle Approach and Landing

selected such that the gravity component balances the drag. Precise control of airspeed is then achieved through modulation of the speed brakes. Figure 2b shows the nominal airspeed variation. While the equivalent airspeed remains essentially constant during the equilibrium glide, true airspeed decreases due to variation of atmospheric density with altitude (Ref. 2). Thus, adjustment of the airspeed on the outer glide slope with modulation of the speed brakes is the final major energy management operation before touchdown. At the end of the steep glide, the speed brakes are fixed and no further active energy management is performed.

At an altitude of approximately 1700 ft, a preflare pull-up maneuver is initiated which "circularizes" the trajectory. The pull-up is terminated when the flight path angle matches that for the shallow glide slope -- nominally -1.5 deg. Speed change during the preflare pull-up is very slow until the flight path angle departs significantly from the equilibrium value, therefore, the pull-up may be considered a constant speed maneuver to a first approximation.

3. Shallow Glide and Final Flare

In principal, the preflare pull-up is followed by the $\gamma = -1.5$ deg shallow glide on the inner glide slope down to a final flare for touchdown. As noted previously, this final phase has been the focus of the greatest controversy concerning shuttle longitudinal FCS design, flying qualities, and design criteria. Further (as will be discussed in Section III) there has been considerable variation in pilot technique for this maneuver. However, some important points can be noted here about the flight mechanics of this maneuver, which will serve as a departure point for examination of manual control in Section III.

Beginning with the lift and drag equations

$$mV\dot{\gamma} = -mg\cos\gamma + L \tag{1a}$$

$$m\dot{V} = -mg\sin\gamma - D \tag{1b}$$

and the simple aerodynamic model of Fig. 3 and noting that γ is a small angle during the shallow glide, the approximate rate of change of speed is

$$\dot{V} = -g\gamma - \bar{q}SC_D/m \tag{2}$$

While the details of elevon deflection and normal acceleration will vary depending on pilot technique, the increments in lift and drag due to elevon will be negligible and the pilot will use only small changes in normal acceleration to accomplish the final flare. That is

$$mV\dot{\gamma} \ll L \text{ or } mg\cos\gamma \tag{3}$$

Thus

$$\begin{aligned} \dot{V} &\doteq -\gamma_o g - g\frac{C_D}{C_L} \\ &= a + bV^2 + cV^{-2} \end{aligned} \tag{4}$$

where the (constant) coefficients are

$$a = -\gamma_o g$$

$$b = -\frac{gC_{D_o}\rho}{2W/S} \qquad \text{(parasite drag)}$$

$$c = \frac{-2gC_{D_L}W/S}{\rho} \qquad \text{(induced drag)}$$

Equation 4 may be examined from Fig. 4 which indicates that the dominant (C_D/C_L) term is roughly constant over the shallow glide. Thus, regardless of pilot technique, the shuttle will decelerate at a roughly constant 1/3 to 1/4 of a "g" as indicated in Fig. 2b.

Strictly speaking, this implies that the shuttle dynamics are time varying in the shallow glide. However, the variation on pitch and path

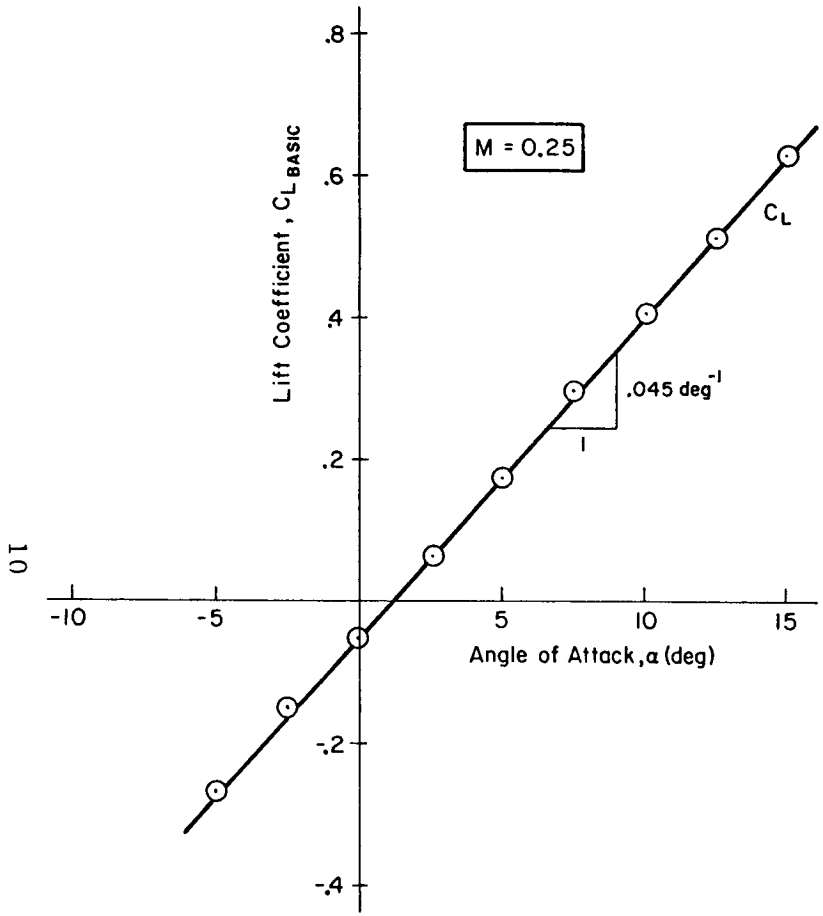

a) Low Speed C_L vs. α, $\delta_e = 0$

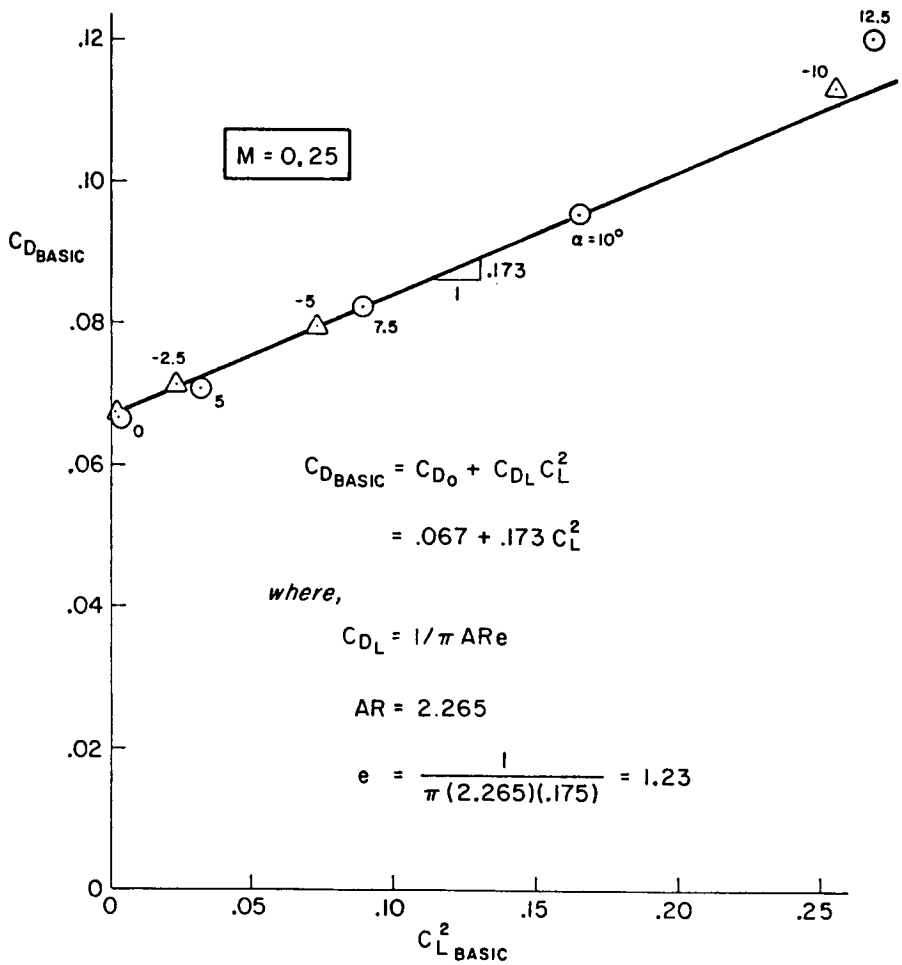

b) Extraction of Drag Polar Constrants, $\delta_{SB} = 0$, Gear Up

Figure 3. Shuttle Lift and Drag Characteristics in Approach and Landing

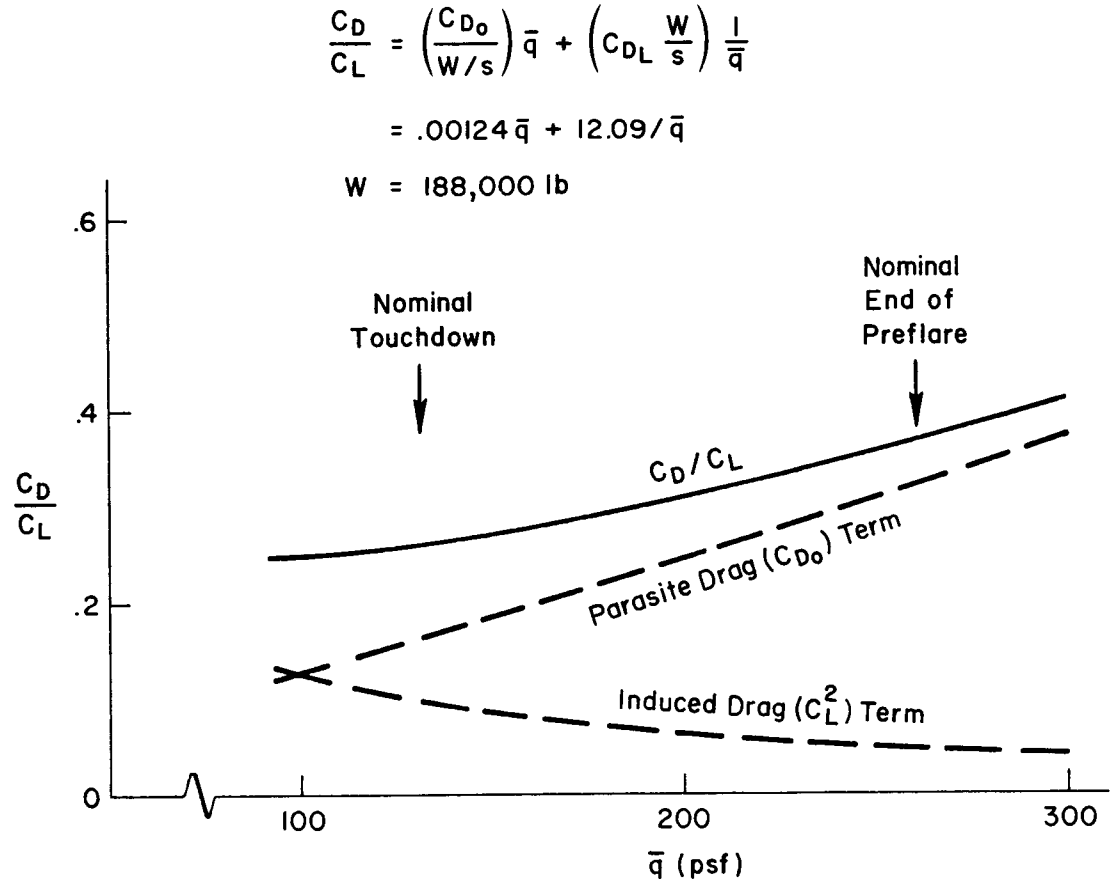

Figure 4. Typical Relative Contribution of Parasite and Induced Drag to Deceleration

response poles and zeros are small and, as will be discussed in Section II-B, the scheduling of the pitch rate to elevon feedback gain is such as to cancel the effect at least in the dominant mode. Thus, the primary effect on pilot technique of the shuttle being a decelerating glider (rather than a conventional transport aircraft) is that the pilot has a finite time window in which he must touchdown to avoid exceeding maximum or minimum touchdown speed limits. An analysis of the effects of this constraint on shuttle pilot's landing strategy is presented in Appendix A of Ref. 4. Operational experience with the shuttle implies that while this constraint exists for the shuttle in distinction with conventional aircraft, it is not "tight" enough to have caused problems to date.

4. Ground Aids for Flight Path Control

Ground aids for manual control of approach and landing have been steadily improved as the program progressed (Ref. 9). For the first few flights the principal ground aids consisted of steep and shallow glide aim markers on the lakebed at Edwards Air Force Base. Two aim markers were provided for the steep glide, one at 7500 ft before the runway threshold for nominal energy approaches and one at 6500 ft in case the shuttle should be at a low energy level. The shallow glide slope aim point is 1000 ft beyond the runway threshold.

An additional ground aid for the later portion of the preflare pull-up and shallow glide was then added (Fig. 5). This consisted of a cluster of very high intensity white lights mounted on a pole on the left side of the runway near the runway threshold and a row of similar red lights, also on the left side but perpendicular to the runway at the shallow glide aim point. The height of the pole was selected so that a 1.5 deg glide slope is defined when the white light is superimposed on the red row of lights. This is called the ball-bar aid and is similar in function to the fresnel lens optical landing aid employed on aircraft carriers.

With this ball-bar system, if the white ball appears to be below the red bar, the vehicle is high or on a steeper glide. If the ball is above the bar the vehicle is below the desired 1.5 deg glide slope. Thus, this system provides a reference to guide the pilot to the correct termination of the preflare maneuver and to maintain the proper shallow glide in manually controlled flight. It also provides a means of monitoring guidance and control performance for fully automatic landings.

Yet another ground based optical aid for the steep glide slope was added following Mission 5. This consists of red and white high intensity lights located at the steep glide aim point. These are aimed upward at differing angles such that specific glide slopes are defined by the number of red and white lights visible. This is called the Precision Approach Path Indicator (PAPI) and is represented in Fig. 6. The aircraft is on the correct 19 deg steep glide path when the crew can see two white and two red lights.

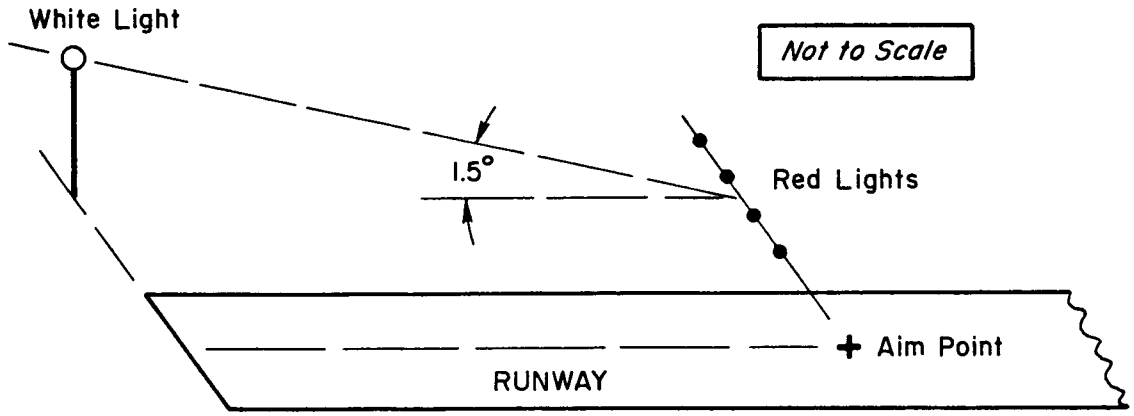

Figure 5. Ball-Bar Shallow Glide Slope Flight Path Aid

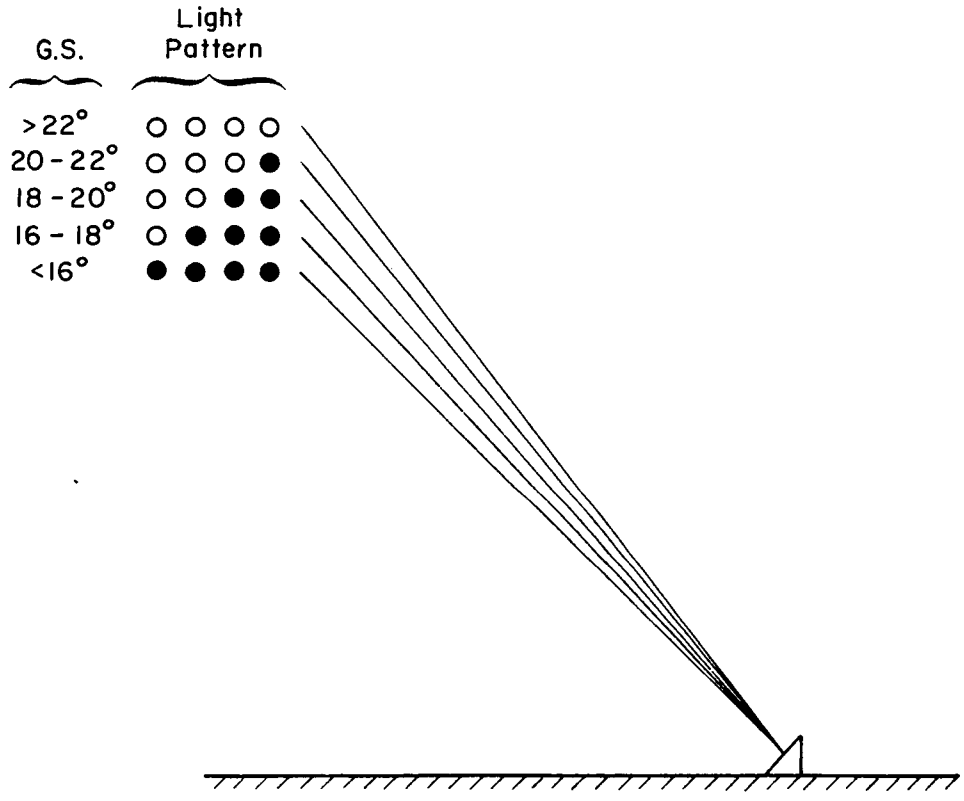

Figure 6. Steep Glide Precision Approach Path Indicator (PAPI) Ground Aid

5. Cockpit Display Aids

The primary change in the Orbiter vehicle occurred for STS-6 and -7 in which the "flight test" vehicle Columbia was replaced by the "operational" vehicle Challenger. Although there were no significant flight control system changes affecting the final approach and landing, the Challenger did introduce the head-up display (HUD).

For the first five landings the principal onboard longitudinal path and energy references were head down instruments: a flight path flight director and airspeed and altimeter indicators for the steep glide (energy management setup) phase; a pitch rate indicator and g-meter for preflare; and airspeed and altitude indicators for shallow glide and final flare. These were supported at all times by pitch attitude display for inner loop control and out the window ground aim point references for path guidance.

One of the original intended uses of the HUD was an adjunct to the autoland system. The HUD was to provide an initial check on guidance system accuracy at this terminal phase, to inform the crew when the approach path variables were within tolerances for engagement of the autoland, and then to help monitor performance of the autoland through approach and landing to flare (Ref. 10). The HUD (Fig. 7a) provided a computer generated runway symbol which initially informs the crew that the guidance computer speed, distance, etc. are good via the runway symbol being superimposed over the actual runway. A runway extended centerline with an outer glide slope (OGS) aim point was also presented. Other information displayed included: velocity vector, flight path angle reference, altitude, airspeed, speedbrake command and actual position, and the pitch and roll ladder.

It appears this was the basic HUD for STS-6 and -7. However, this configuration provided so much information that "declutter" provisions were included for STS-8 and future flights (Ref. 9) to allow elimination of undesired or unnecessary data and symbology clutter as various phases of approach and landing are completed.

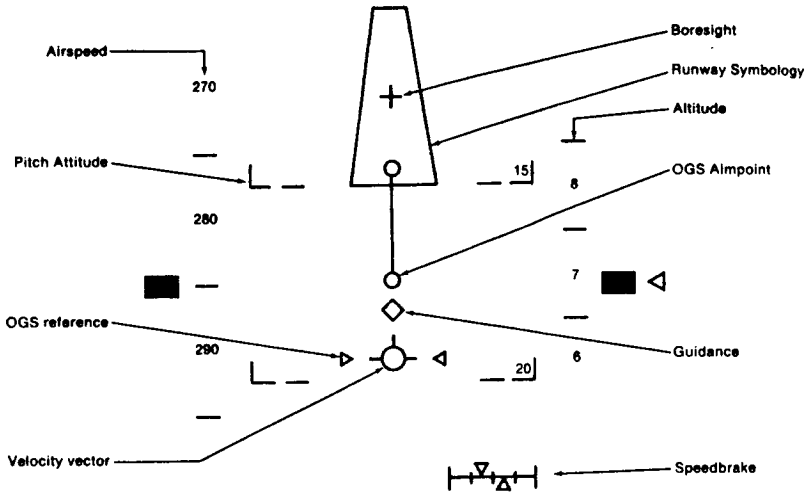

a) No Declutter

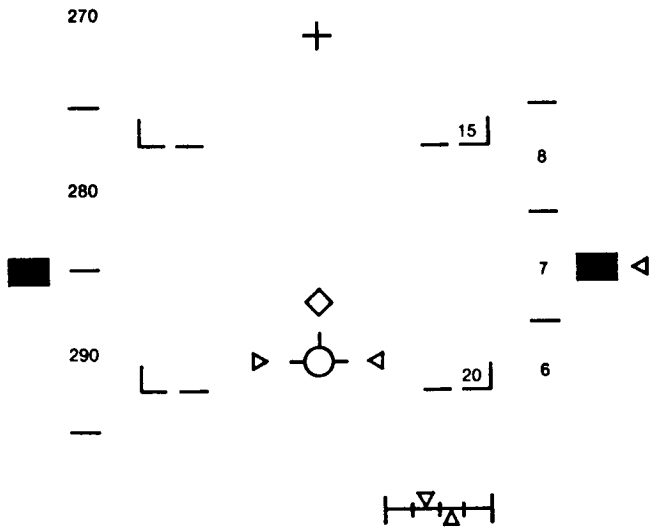

b) First Declutter

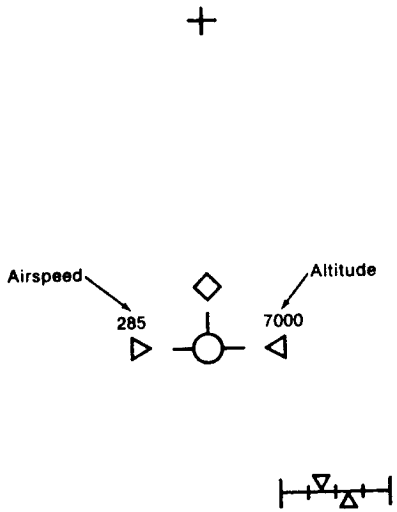

c) Second Declutter

Figure 7. HUD Approach and Landing Symbology (from Ref. 9)

Per Ref. 9, the symbology configuration of Fig. 7a would now be selected upon exiting the HAC for getting set up on the steep glide (OGS) path. Figure 7a depicts the vehicle approaching the OGS. When actually on the OGS aimpoint, the velocity vector symbol and PAPI light (out the window) would be superimposed and bracketed by the glide slope reference markers. The first declutter would then be selected to remove the runway symbology. This reduces the display to that of Fig. 7b.

Just before preflare (1850 ft altitude) a second set of path reference markers come into play and move up from the bottom of the display. When these reach the OGS reference it signals the start of preflare. One set of path markers then continues to move up while the second set disappears (Ref. 10). This signifies the proper altitude and airspeed to initiate transition. The pilot then flies the velocity vector symbol to the path reference markers as they continue to move up the display. Preflare ends when the markers stop moving. The velocity vector should then be directed at the close end of the runway or between the close end and the shallow glide aim point. At this juncture the shallow glide ground aid should also signify a 1.5 deg glide slope. The pilot should then accomplish a second declutter (Fig. 7c) and keep the velocity vector symbol and ground glide slope reference steady until reaching the desired flare altitude.

As a result of these various ground and onboard landing aids being operational with successive flights, the control strategies (path control loop structure, gains, etc.), and hence workload for preflare and shallow glide would be expected to vary somewhat from flight-to-flight. This will be quite apparent in the later detailed analysis of the STS-2 through -7 landings. It might also be expected that path and landing performance should come closer to ideal or target values and become more uniform with each flight. Only the final flare has remained essentially the same unaided task for all landings. [An exception is HUD direct display of altitude and airspeed information on STS-6 and -7 in place of verbal callouts on previous flights.]

B. SHUTTLE LONGITUDINAL DYNAMICS AND FLIGHT CONTROL SYSTEM CHARACTERISTICS

1. FCS Pitch Channel

Perhaps the most important aerodynamic consideration for longitudinal flight control in landing is the relaxed static stability condition. Figure 8 shows a representative (flexible) longitudinal stability plot with the relevant C_L and δ_e ranges indicated for the landing. It may be seen that flexibility effects are negligible and that the static margin is:

$$\frac{dC_M}{dC_L} \doteq 3.7\%\bar{c} \text{ unstable}$$

The maneuver margin is:

$$\frac{dC_M}{dC_L} - \frac{\rho S\bar{c}}{4m} C_{M_q} \doteq 0.9\%\bar{c} \text{ unstable}$$

The primary effect of relaxed static stability is the degeneration of the normally complex short period mode into two real roots. When the static margin becomes unstable, one of the real roots $(1/T_{sp_2})$ becomes divergent (3 DOF model, Ref. 11). This may be seen in a typical quasi-steady shuttle approach condition (h = 2420 ft, U_o = 190 KEAS, $\bar{q}$ = 122 psf). The airframe-alone three degrees-of-freedom pitch transfer function is (Ref. 12):

$$\frac{q}{\delta_e}(s) = \frac{A_\theta s(1/T_{\theta_1})(1/T_{\theta_2})}{(1/T_{sp_1})(1/T_{sp_2})[\zeta_p, \omega_p]} \qquad (5)^*$$

$$= \frac{-0.92(0)(0.036)(0.54)}{(0.85)(-0.17)[0.42,\ 0.016]} \frac{\text{deg/sec}}{\text{deg}}$$

*Transfer function notation: $(a) \equiv (s + a)$; $[\zeta,\omega] \equiv [s^2 + 2\zeta\omega s + \omega^2]$. A_θ, etc. are high frequency gains.

MACH NO.	DEL BF	DEL SB	XCG (IN)	ZCG (IN)	QBAR1-PSF	QBAR2-PSF
0.400	-11.700	25.000	1098.630	375.000	0.0	300.000

QBAR1 = SOLID QBAR2 = DASH

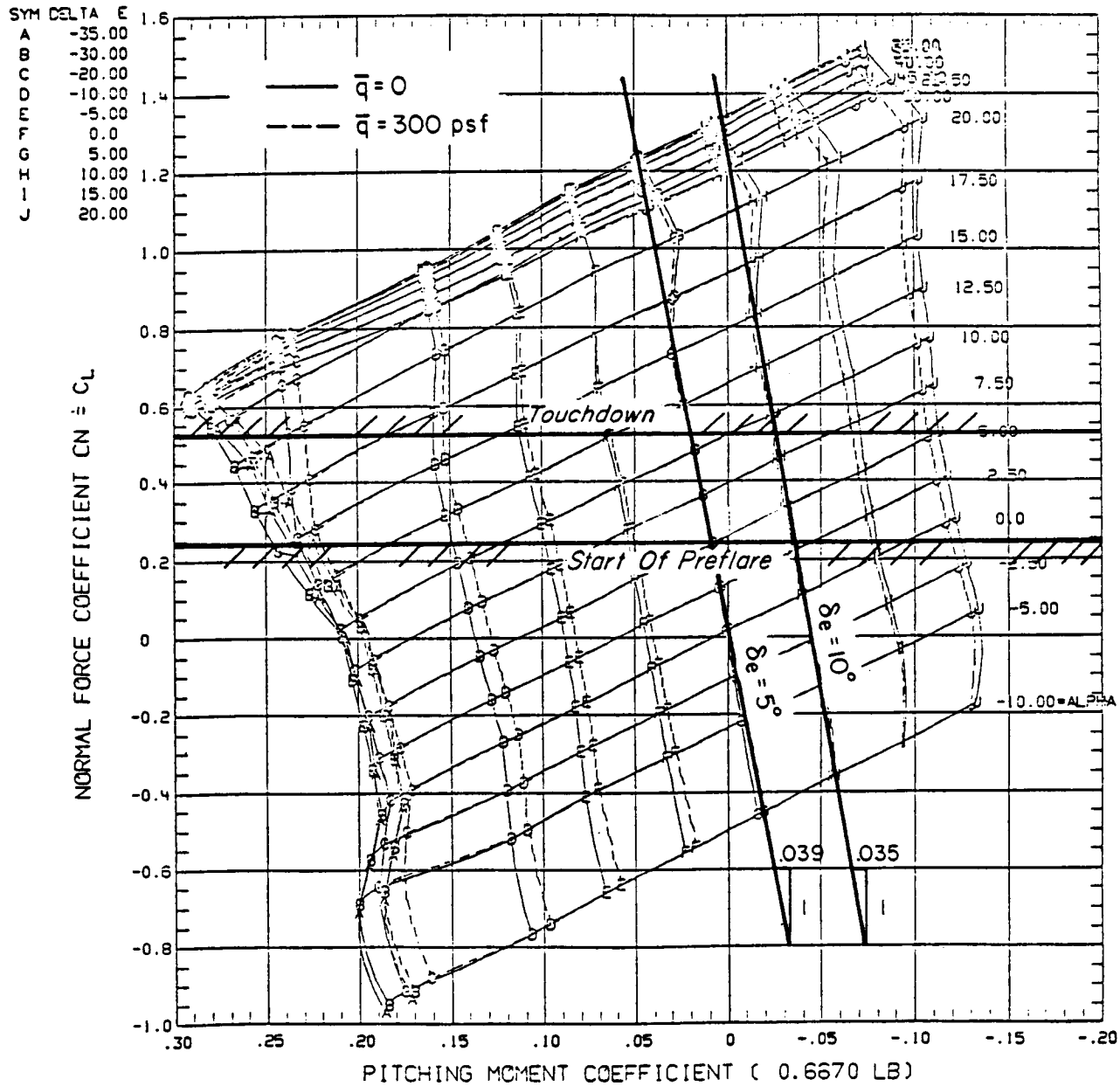

Figure 8. Shuttle Airframe Longitudinal Stability, Flexible-Approach and Landing

A basic function of the shuttle FCS is stabilization of the divergent, real short-period root $(1/T_{sp_2} = -0.17)$. This is accomplished through the FCS pitch channel shown in simplified linearized form in Fig. 9 for the Orbiter Flight Test (OFT) vehicle. Several of the gains and filter time constants are scheduled, but are shown for the flight condition corresponding to Eq. 5. Stabilization of the aircraft requires forward loop integration (to cancel the free s in Eq. 5). In the shuttle, this is provided by the $\delta_e \rightarrow \delta_c$ inner loop through the first-order "ELFBK" filter. With the inner loop closed:

$$\frac{\delta_e}{\delta_{cc}} \doteq \left(\frac{s + \omega_e}{s}\right) G_f(s) \tag{6}$$

where ω_e is fixed at 1.5 rad/sec below Mach 3, and the (inner) forward loop transfer function, G_f, is composed of the high frequency bending and smoothing filters, actuator, and computational delay terms:

$$\begin{aligned} G_f(s) &= \frac{0.373[0.02;\ 32.75]}{[0.4;\ 20.7]} \times \frac{36.0^2}{[0.7;\ 36.0]} \times \frac{20}{(20)} \times e^{-0.0455s} \\ &\doteq e^{-(0.0388 + 0.0397 + 0.05 + 0.0455)s} \\ &\doteq e^{-0.174s} \qquad \text{for } |s| \ll 20 \text{ rad/sec} \end{aligned} \tag{7}$$

Feeding back pitch rate in the outer loop through this effective proportional/integral equalization provides an effective q, $\int q \rightarrow \delta_e$ system. The outer loop closure system survey in Fig. 10 reveals that the gain $K_q = 1.425$ deg/deg/sec, is sufficient to drive the short-period roots into the attitude zeros $(1/T_{\theta_1})(1/T_{\theta_2})$ as shown by root loci 1 and 3. Closed-loop roots are shown by the symbol ■. The augmented phugoid, $[\zeta_p', \omega_p']$, then becomes the dominant closed-loop mode. A literal approximate expression for the closed-loop q/q_c transfer function may be

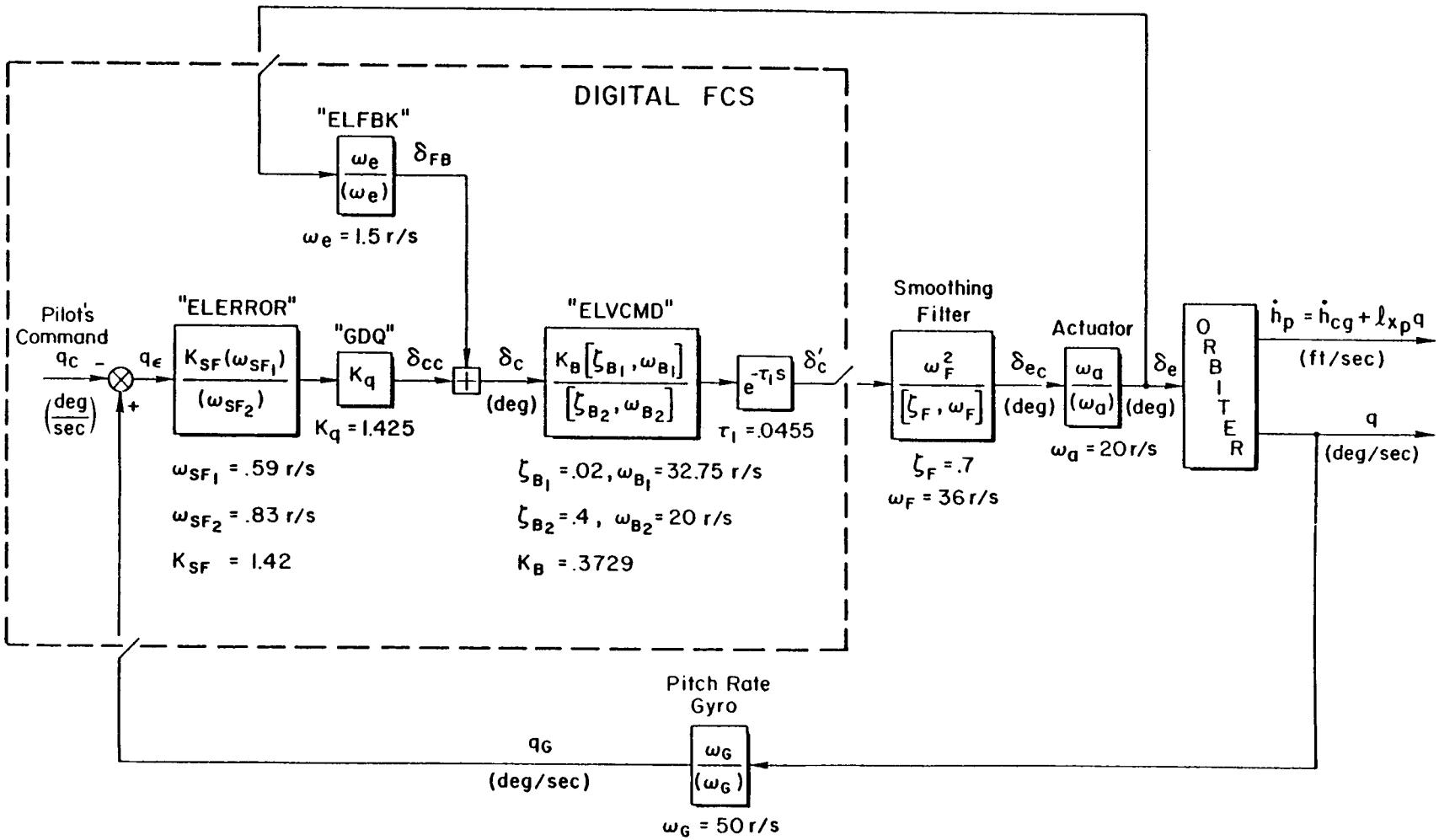

Figure 9. Linearized OFT Shuttle Pitch Channel Landing Approach
Condition: h = 2420 ft, V = 190 kt EAS, $\bar{q}$ = 122 psf

ORIGINAL PAGE IS
OF POOR QUALITY

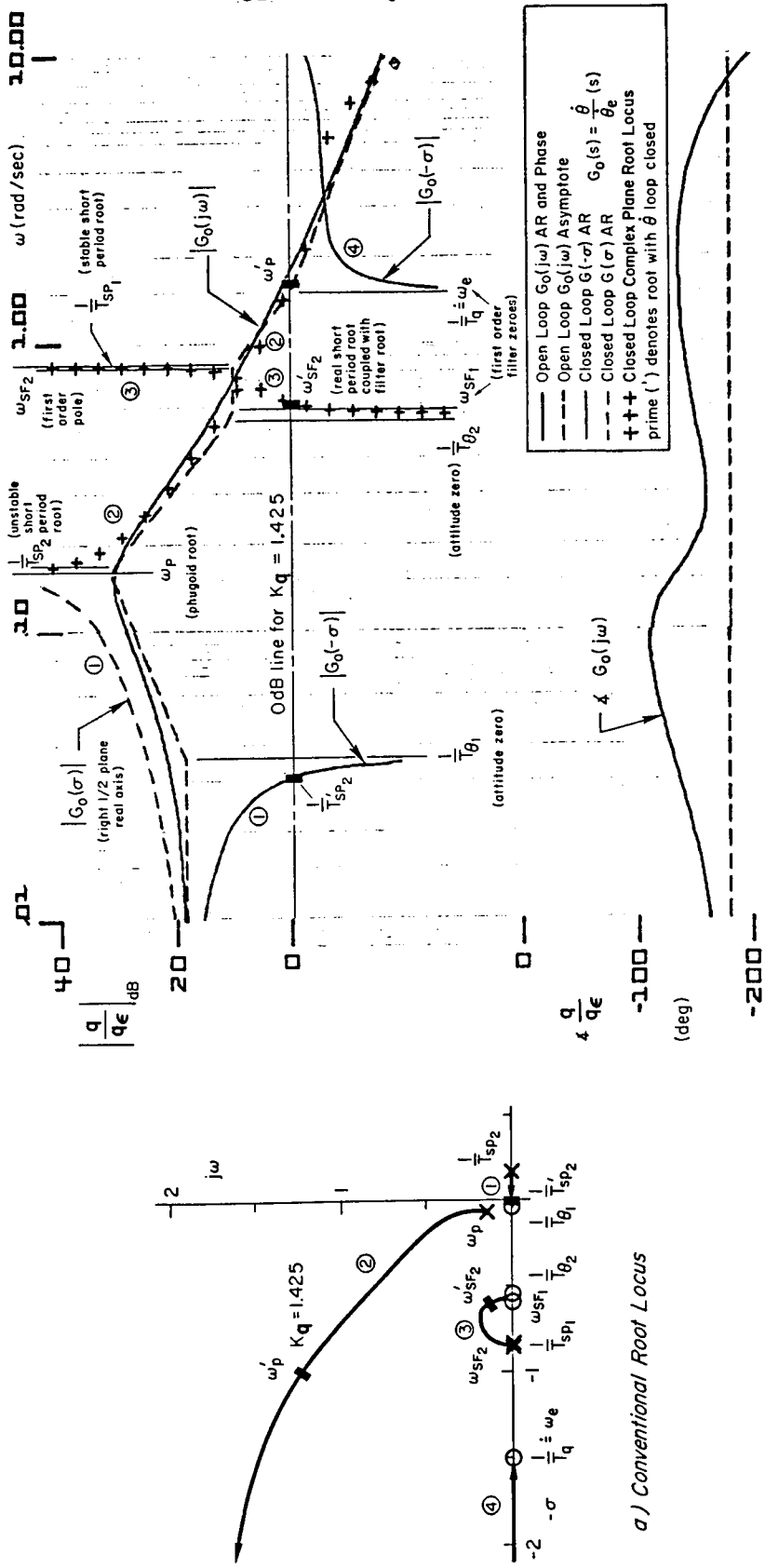

a) Conventional Root Locus

b) jω Bode and Bode Root Locus

Figure 10. System Survey of Outer Pitch Rate Loop Closure

derived from Bode asymptote approximation in the crossover region (Ref. 1) as

$$\frac{q}{q_c} \doteq \frac{K_1(1/T_q)e^{-\tau s}}{[\zeta_p', \omega_p']} \tag{8a}$$

$$= \frac{-M_{\delta_e} K_q (\omega_e) e^{-\tau s}}{\left[(1/2)\sqrt{-M_{\delta_e} K_q/\omega_e}, \sqrt{-M_{\delta_e} K_q \omega_e}\right]} \tag{8b}$$

$$= \frac{1.31(1.5)e^{-0.174s}}{[0.468, 1.40]} \tag{8c}$$

where

$$M_{\delta_e} = \rho U_0^2 S c C_{m_{\delta_e}} / 2Iy$$

2. Superaugmentation

The foregoing is a prototypical example of a "superaugmented" longitudinal flight control system. The literal approximations of Eq. 8 are made primarily for insight into the dominant parameters and effects, and have been generalized as part of a detailed examination of superaugmentation design issues in Refs. 11, 13. Some of these issues will be briefly reviewed here as they relate specifically to the shuttle, and as a starting point for discussion of manual control in landing (Section III), and FCS design criteria (Section IV).

"Superaugmented" aircraft are an important subclass of actively controlled highly-augmented aircraft. In Refs. 11 and 13, the term superaugmented is applied to aircraft which:

- are statically unstable without augmentation,
- have a degree of pitch attitude stability with respect to inertial space (as opposed to weathercock stability) which is provided by the flight control system, and

> have command response characteristics which are largely independent of the basic airframe aerodynamic stability derivatives except for pitch control effectiveness.

In this usage an unstable aircraft stabilized with a high gain $\alpha \rightarrow \delta_e$ feedback would be considered "conventional" and <u>not</u> be termed superaugmented. Superaugmented FCS designs are defined by the feedback loops which establish the dominant poles. However, for a given feedback loop structure the response to command can vary widely depending on the characteristics of any command path filter, G_i in Fig. 11.

To a much greater extent than in past aircraft designs, the basic issues of FCS stability, robustness, dominant modes, and disturbance rejection for superaugmented aircraft can be separated from the flying qualities issues associated with response to command. The first group of issues is associated with the closure of the pitch rate (or alternative) loop and is essentially set by defining just 2 parameters -- the crossover frequency and T_q. Once the basic pitch loop bandwidth is set, the command response/flying qualities issues become largely a matter of determining the appropriate command path filter characteristics, G_i (at least for single longitudinal control point aircraft). However, there are issues for superaugmented aircraft design which are intimately connected to both basic stability and response to command. The primary examples are nonlinear effects, in particular control surface rate and position limiting.

Thus in the following, consideration of the dominant mode and stability will be distinguished from response to command. This is done because even though the shuttle has the simplest possible effective command path transfer function, $G_i \triangleq$ constant (neglecting the effect of the PIO filter, Ref. 7), more complex G_i's are relevant to current research in superaugmentation and possible design criteria for future shuttle craft.

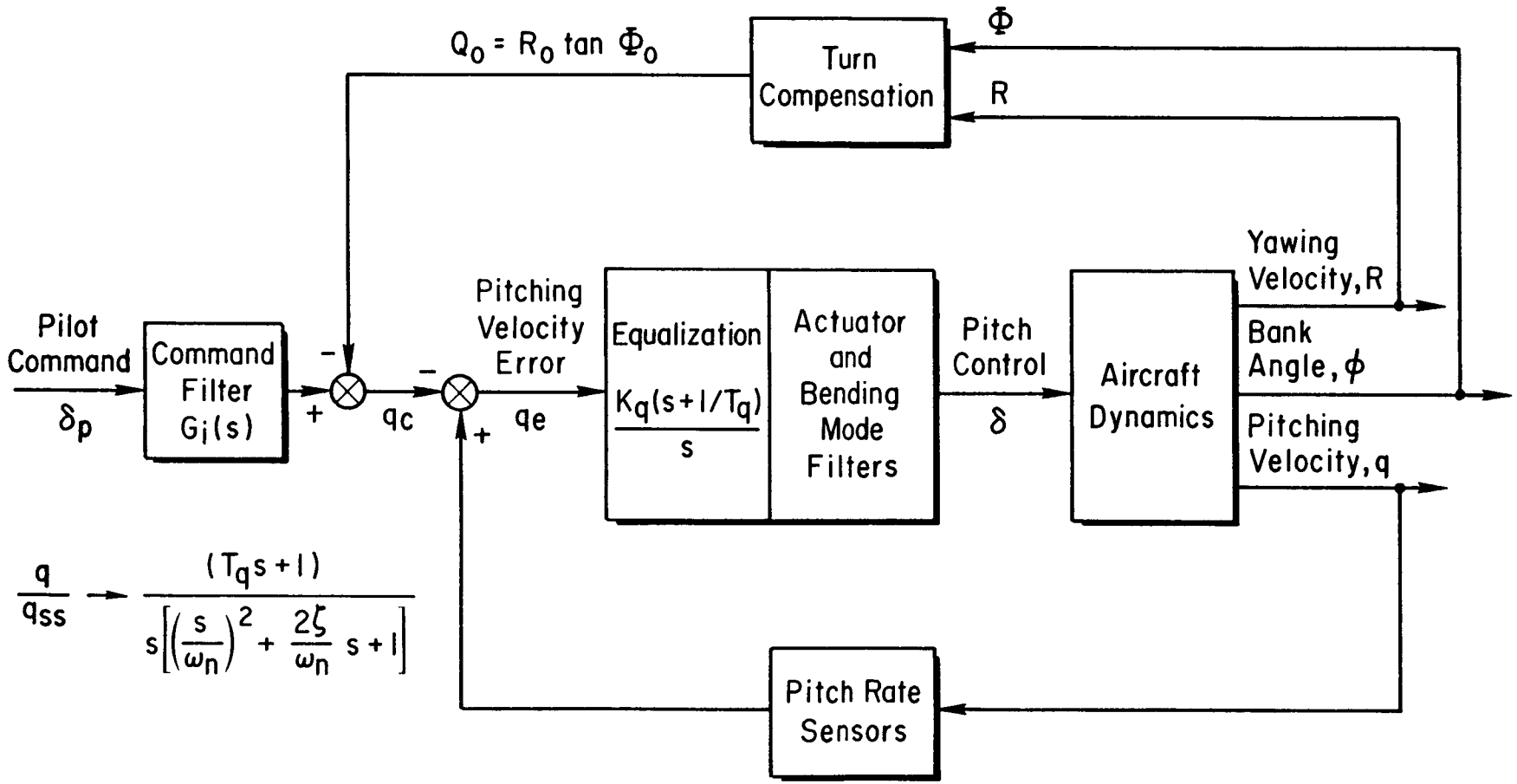

Figure 11. Typical Pitch Control System for Superaugmented Aircraft

3. Closure of the Pitch Rate Loop

There are a variety of specific FCS feedback architectures which could be used in a superaugmented design. Some of these are reviewed in Ref. 11. For the shuttle and many other modern aircraft, an equalized $q \rightarrow \delta_e$ loop based on use of rate gyros has great appeal. This comes from considerations such as simplification of redundancy management, freedom from measurement noise in aerodynamic sensors, etc. (see Ref. 11). Once a $q \rightarrow \delta_e$ structure is selected, equalization requirements may be established. To stabilize the unstable $1/T_{sp_2}$ root, forward loop integration is required as noted previously to cancel the free s in the pitch numerator. This is equivalent to stabilizing the vehicle by creating an artificial "pitching moment due to pitch attitude" stability derivative.

When the forward loop integrator is inserted, the open-loop q/q_ε transfer function is

$$\frac{q}{q_\varepsilon} \doteq \frac{K}{s^2}$$

at frequencies above the upper range of the aircraft rigid body dynamics ($1/T_{sp_1}$ in Fig. 10). If a lead $(s + 1/T_q)$ is introduced to complete the equalization indicated in Fig. 11, then a region of "K/s" (high frequency asymptote in Fig. 10) is created in which the pitch loop can be readily closed.

In this superaugmented approach, system design is basically a selection of two parameters -- the $1/T_q$ lead (ω_e in the "ELFBK" filter in Fig. 9), and the crossover frequency ω_c (equivalently the loop gain -- "GDQ" in Fig. 9). The basic shuttle design philosophy was to set $1/T_q$ well above the aircraft dynamics $(1/T_{sp_1})$ and set the (asymptotic) crossover frequency (ω_{c_a}) at or above $1/T_q$ in the K/s region (see Fig. 10). (Other recent designs, e.g., the X-29 have placed $1/T_q$ differently.) As noted previously, the real "short period" poles are thus driven into the attitude zeros, and the dominant (pitch) mode is defined in the crossover region as summarized in Fig. 12. This shows that the

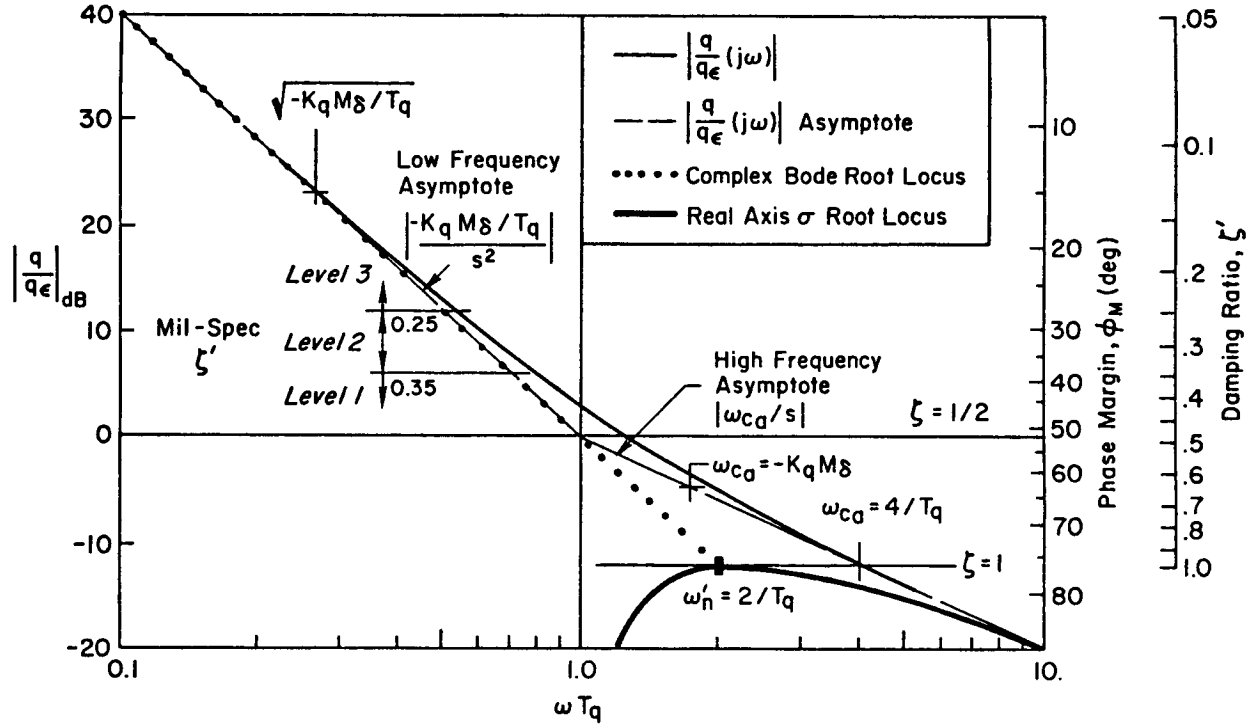

$$\bullet \quad \left.\frac{q}{q_\epsilon}\right|_{\substack{\text{open}\\\text{loop}}} \doteq \frac{-K_q M_\delta (s + 1/T_q)}{s^2}$$

$$\bullet \quad \left.\frac{q}{q_c}\right|_{\substack{\text{closed}\\\text{loop}}} \doteq \frac{(T_q s + 1)}{\left[\left(\frac{s}{\omega_n'}\right)^2 + \frac{2\zeta'}{\omega_n'} s + 1\right]}$$

$$\bullet \quad \zeta' \doteq \frac{1}{2}\sqrt{-K_q M_\delta T_q} = \frac{1}{2}\sqrt{\omega_{ca} T_q}$$

$$\omega_n'^2 \doteq -K_q M_\delta / T_q = \omega_{ca} / T_q$$

Figure 12. Superaugmented Dominant Pitch Mode Approximation

closed-loop characteristics [ζ' and ω_n'] are functions of only T_q, and the asymptotic crossover frequency, $\omega_{c_a} = -K_q M_\delta$. Thus, the only aerodynamic stability derivative of first-order importance in the attitude dynamics is the elevon effectiveness in pitch, M_δ. M_δ in turn determines the level of the high frequency asymptote in the crossover region, and since M_δ is a function of dynamic pressure, the asymptote will "sink" as the shuttle decelerates. From preflare through touchdown, this variation is typically about

$$\left|\frac{290 \text{ psf}}{135 \text{ psf}}\right|_{dB} = 6.6 \text{ dB}$$

Thus the shuttle GDQ gain scheduling must account for this to set the crossover frequency as desired.

The asymptotic crossover frequency is:

$$\omega_{c_a} \doteq -M_\delta K_q = \left(\frac{ScC_{M_{\delta_e}}}{I_y}\right) \bar{q} K_q \tag{9}$$

for the shuttle situation in which $\omega_{c_a} > 1/T_q$. The basic scheduling (GDQ_COMP) is shown in the block diagram of Fig. 13 and indicates that

$$K_q \propto \frac{f(M)}{\sqrt{q}} \tag{10}$$

It should be noted that none of the relevant nondimensional aerodynamic coefficients are functions of Mach number in this region, thus the rationale for the Mach number schedule is of interest. At these low altitudes (below 2000 ft AGL) where density and acoustic velocity are roughly constant, the Mach number schedule effectively provides an additional dynamic pressure schedule. When approximate calculations of this effect are made, the resulting crossover frequency schedule is

$$\omega_{c_a} \doteq 0.177(\sqrt{\bar{q}} - 0.026 \bar{q}) \text{ rad/sec} \tag{11}$$

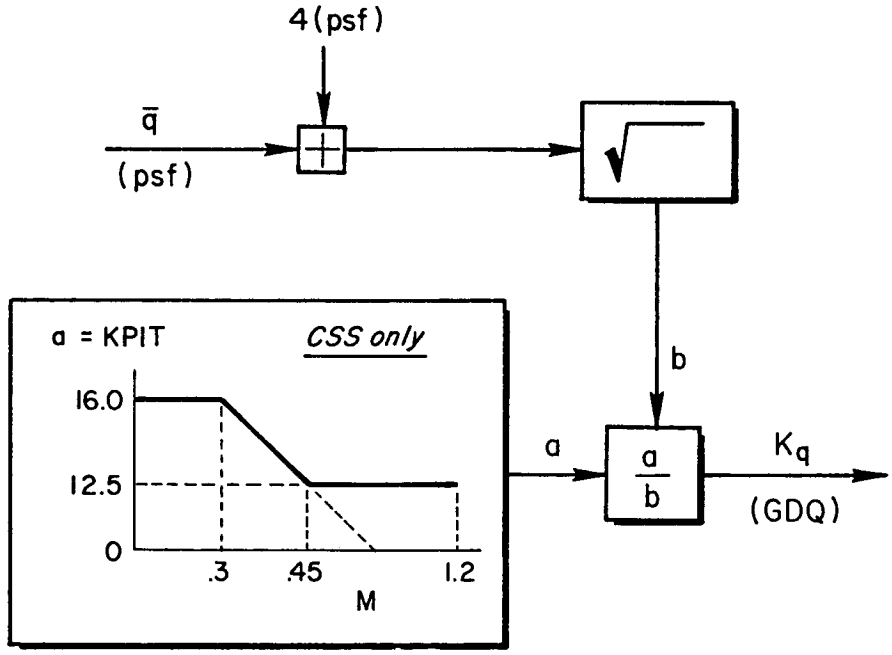

Figure 13. Schedule for Pitch Rate Loop Gain, K_q (GDQ_COMP)

Figure 14 shows this ω_{c_a} variation from the start of preflare through touchdown compared to a fixed crossover schedule (i.e., $K_q \propto \bar{q}^{-1}$) and a crossover frequency schedule proportional to the square root of $\bar{q}$ (no Mach schedule). In the flights of the Approach and Landing Test (ALT) vehicle, K_q was scheduled inversely proportional to dynamic pressure (Ref. 14); thus giving an effectively constant crossover frequency. This has been modified to the present OFT schedule primarily because of problems with elevon saturation at low speeds when using the original schedule.

As noted previously, $1/T_q = \omega_e$ is fixed at 1.5 rad/sec below Mach 3. Thus, Fig. 14 shows that the basic strategy of setting the crossover in the K/s region (i.e., $\omega_{c_a} > 1/T_q$) is essentially achieved through the approach and landing. The fact that $\omega_{c_a} \doteq 1/T_q$ for landing implies (from the Fig. 12 literal approximation) a dominant pitch mode damping ratio of

$$\zeta' = 0.5$$

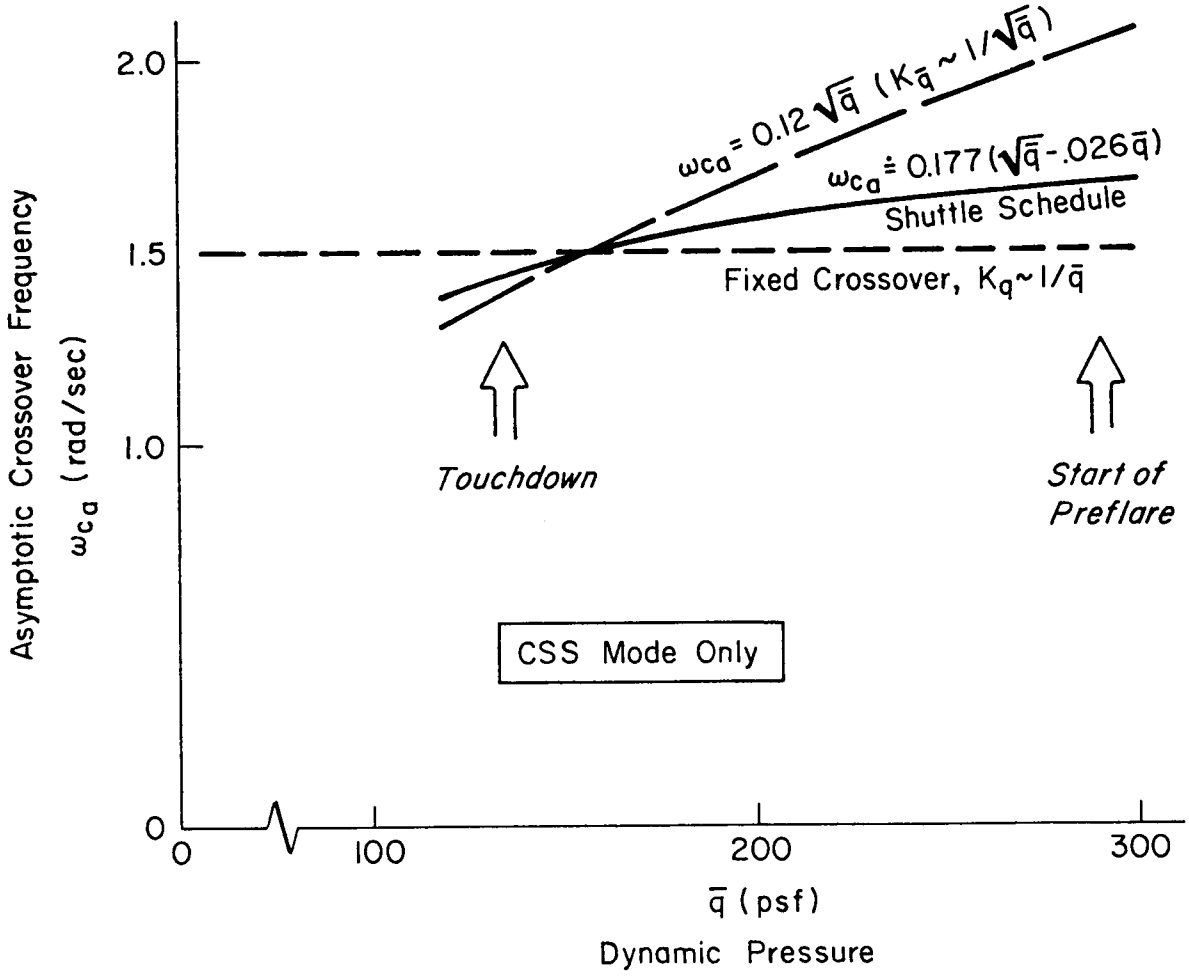

Figure 14. Effective Pitch Gain Scheduling of Shuttle

Complete calculations indicate a somewhat higher value ($\zeta' > 0.6$) for the shuttle. This can be traced to extra phase lead in the crossover region from the "ELERROR" filter (Fig. 9).

4. Compensation for Stability and Robustness

In the previous section the design strategy for the shuttle pitch loop was analyzed in some detail. Next we will generalize this to consider what can be recommended for future shuttlecraft. The aircraft considered here are superaugmented shuttlecraft or transatmospheric or atmospheric transport aircraft (essentially MIL-F-8785C Class II or III). It is assumed that these aircraft are only moderately unstable,

however, use of canard surfaces could lead to relatively large unstable static margins. For this aircraft type it is assumed that there is a pitch control surface but not necessarily direct lift capability. It is further assumed that the aircraft are powered or, if gliders, have some capability for modulating drag but that thrust vectoring for maneuvering is not used.

a. Crossover Frequency

The crossover frequency is the first consideration in setting the pitch loop compensation parameters. This is set primarily to position the pitch mode root to achieve adequate loop bandwidth. For the aircraft of interest, minimum bandwidths around 2 rad/sec should be adequate (the shuttle bandwidth in landing is about 1.5 rad/sec) for terminal area operations. A primary concern is maintaining pitch bandwidth well above the flare inverse time constant -- an issue that will be discussed in detail in the following section. Higher crossovers could be considered (and would be generally necessary for fighter and other high maneuverability aircraft) but may not be worth the additional cost of potential actuator and structural mode complications for transports and shuttlecraft.

b. Selection of T_q

Once the crossover frequency is selected, the major consideration is selection of T_q. Several consideration are involved.

The first consideration is the position (i.e., frequency) of the desired crossover region with respect to the upper end of the bare aircraft rigid body dynamics region. The later is generally defined by the $1/T_{sp_1}$ -- the stable real "short period" root. This root can be estimated as the larger of

$$\frac{1}{T_{sp_1}} \doteq \begin{array}{l} -(Z_w + M_q) = \rho SU\left(\frac{1}{2m}C_{L_\alpha} + \frac{C^2}{4I_x}C_{M_q}\right) \quad \text{or} \\ \sqrt{M_\alpha} = \sqrt{\rho\frac{SU^2c}{2I_y}C_{M_\alpha}} \end{array} \qquad (12)$$

Both of these factors are proportional to speed and on this basis we could expect variations in the subsonic range (from M=1 to typical touchdown speeds) on the order of a factor of four. However, air density and compressibility effects also influence $1/T_{sp_1}$ with generally opposing effects. Density should be the dominant effect (especially when quasi-static aeroelastic effects are accounted for). This should be more true for shuttlecraft descending from high altitudes (such that the density ratio increases by an order magnitude in the subsonic phase) than for conventional atmospheric transports. Thus, we can expect the upper frequency range of the aircraft rigid body dynamics to vary (for a given configuration) not much more than an octave in terminal area operations.

In the critical landing phase the shuttle $1/T_{sp_1}$ decreases over the range

$$0.73 < 1/T_{sp_1} < 1.03 \text{ rad/sec}$$

Assuming landings are made at

$$V = 1.4\, V_S = 1.4 \sqrt{\frac{2(W/S)}{\rho C_{L_{max}}}}$$

Equation 12 can be reformulated as

$$\frac{1}{T_{sp_1}} \doteq \begin{cases} -(Z_w + M_q) = 1.4g\sqrt{\dfrac{\rho}{2(W/S)C_{L_{max}}}}\left(C_{L_\alpha} + \dfrac{1}{2}\left(\dfrac{c}{k}\right)^2 C_{M_q}\right) \\ \sqrt{M_\alpha} = 1.4\sqrt{\dfrac{gC_{L_\alpha}(S.M.)c}{k^2 C_{L_{max}}}} \end{cases} \tag{13}$$

The primary configuration factors for landing can be seen from Eq. 13. Wing aspect ratio is a dominant factor through its effect on lift curve slope. However, shuttlecraft as a class can be expected to have considerably lower aspect ratios than conventional atmospheric transports and consequently lower $1/T_{sp_1}$ values. This may be offset somewhat by lower shuttlecraft $C_{L_{max}}$ values associated with simpler

landing flap systems. Transport aircraft or shuttlecraft of fairly conventional configurations (i.e., aft tails or tailless) can be expected to have only moderately unstable static or maneuver margins and thus wing loading becomes a factor but airplane size is otherwise a second-order influence.

From the above considerations it appears that the shuttle is reasonably representative of shuttlecraft to come and we can expect the crossover frequency to be somewhat above the upper end of the vehicle dynamics region. In this case, as for the shuttle, $1/T_q$ should be below the crossover to assure crossover in a region of K/s. See Fig. 10.

Positioning $1/T_q$ slightly below the crossover will establish a damping ratio somewhat above 0.5. Reducing $1/T_q$ will increase the damping ratio. As long as $1/T_q$ is above $1/T_{sp_1}$, as it is with the shuttle, then the dominant pitch mode will be second-order. Otherwise the root locus topology will transition so that the dominant pitch mode is first-order. Maintaining $1/T_q$ above $1/T_{sp_1}$ is not an absolute requirement but rather a strategy that leads to effective dynamics comparable (in some respects) to conventional short period dynamics. This seems to be a reasonable strategy for the transports and shuttlecraft but may not be the best for advanced fighters and other highly maneuverable aircraft.

c. Effective Time Delay and Phase Margin

To this point it has not been necessary to explicitly consider the effects of high frequency elements in the loop. However, to address stability margins and robustness these elements must be accounted for. In the crossover region, the dominant effect can generally be treated as a lumped, effective time delay. For the present generation of superaugmented aircraft the primary contributors to this effective time delay are structural mode filters, actuators, and throughput delay in digital FCS computers. For the shuttle, bending and smoothing filters contributed just under half of the total estimated delay of 170 ms (see Eq. 7).

Time delay influences the phase margin in the crossover region. With T_q positioned as proposed above, the phase margin is given approximately by (Ref. 11)

$$\phi_M \doteq \tan^{-1}(T_q\omega) - \tau\omega \tag{14}$$

Thus the effect of the time delay is to create a high frequency phase 180 deg crossover at

$$\omega_{u_2} \doteq \frac{\pi}{2\tau} - \frac{2}{\pi}\frac{1}{T_q} \tag{15}$$

At lower frequencies there may be another 180 deg phase crossover terminating a conditional instability region (Ref. 11). This does not quite occur in the shuttle (largely due to the ELERROR filter, Fig. 9), instead there is a relative phase minimum between the phugoid and the degenerate short period modes (Fig. 10). Between the two 180 deg crossovers (or between the minimum phase dip and the high frequency 180 deg crossover) there will be a relative maximum in phase at

$$\omega\Big|_{\phi_{M_{max}}} = (\tau T_q)^{-1/2} \tag{16}$$

with corresponding phase margin

$$\phi_{M_{max}} \doteq \frac{\pi}{2} - 2\sqrt{\tau/T_q} \tag{17}$$

Thus, if it is desired to maximize phase margin in the desired gain crossover region, say 2 rad/sec, then $1/T_q$ should be

$$\frac{1}{T_q} = 4\tau = 0.68 \text{ rad/sec for } \tau = 0.17 \text{ ms}$$

and the maximum phase margin would be

$$\phi_{M_{max}} = 51^0$$

However, this generally would put $1/T_q < 1/T_{sp_1}$ and result in the dominant pitch mode being first-order. A compromise is therefore called for. Phase margin above 30 deg should be obtainable with $1/T_q$ placed as suggested in the previous subsection. Additional margins can be obtained via lead-lag equalization near the crossover region, such as the ELERROR filter in the shuttle.

d. Total Effective Gain Range

The high frequency phase margin sets an upper bound on crossover frequency/loop gain. For superaugmented aircraft there are lower bounds on gain as well. One may be created by the lower frequency conditional stability region noted above (and detailed in Ref. 11). A more definite lower bound is provided by the requirement to drive the unstable $1/T_{sp_2}$ root into the left half plane. It is shown in Ref. 11 that this requires the 0 dB line (which determines the crossover frequency) to be below the low frequency Bode asymptote of q/q_e (Fig. 15). The difference between the maximum and minimum allowable gain is the Total Available Gain Range (TAGR). As developed in Ref. 11, the TAGR is a basic measure of the robustness of the basic feedback loop and TAGR should exceed a minimum level for good design. One important indication TAGR can provide is sensitivity to control power limitations.

As derived in Ref. 11 (for the basic superaugmented compensation)

$$TAGR = \frac{\frac{1}{T_q}\left(\frac{\pi}{2\tau} - \frac{2}{\pi T_q}\right)}{M_\alpha\left(T_{\theta_1} T_{\theta_2} \omega_p^2\right)} \tag{18}$$

The numerator expression in Eq. 18 is defined entirely by FCS parameters and will generally be positive for realistic values of T_q and τ. The denominator is determined entirely by the airframe characteristics and will generally be positive for statically unstable aircraft. As

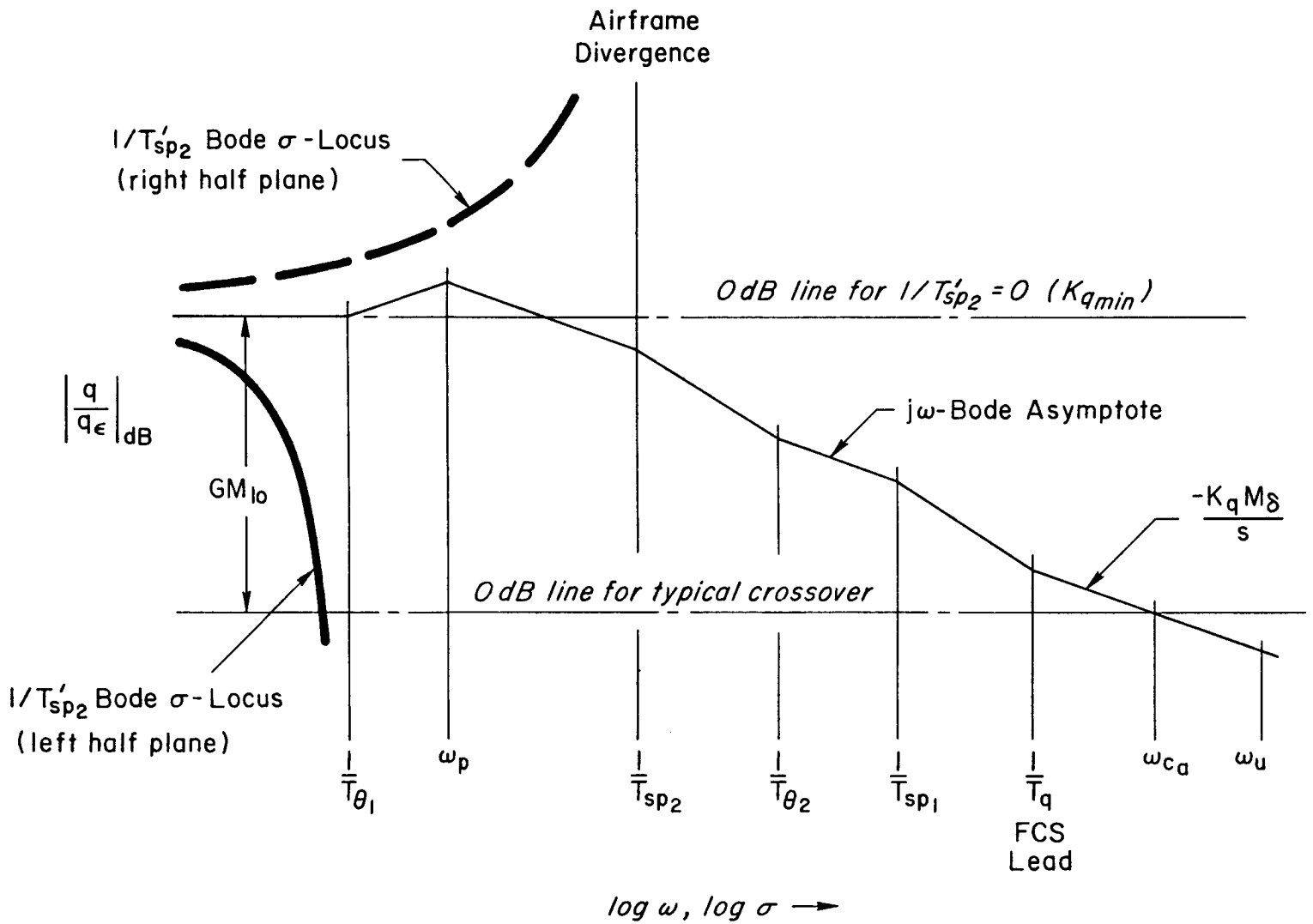

Figure 15. Partial Bode Sketch Showing $K_{q_{min}}$ Set by Requirement for Stabilization of the Divergent Real Pole, $1/T_{sp_2}$

discussed in Ref. 11 the denominator factor can become large, having the undesirable effect of reducing TAGR, if the airplane is operating on or near the "backside" of the power required curve.

From Eq. 18 it can be seen tht the primary parameter the designer has for adjusting TAGR is the compensation lead parameter T_q. The sensitivity of TAGR to the breakpoint $1/T_q$ is given by

$$\frac{\partial(\text{TAGR})}{\partial(1/T_q)} = \frac{\left[\frac{\pi}{2\tau} - \frac{4}{\pi}\left(\frac{1}{T_q}\right)\right]}{M_\alpha\left(T_{\theta_1} T_{\theta_2} \omega_p^2\right)} \tag{19}$$

Both terms in the numerator are positive and, for realistic values of τ and $1/T_q$ the first term will be much larger than the second. Thus the sensitivity derivative

$$\partial(\text{TAGR})/\partial(1/T_q)$$

will generally be positive. This implies that TAGR can generally be increased by moving the $1/T_q$ breakpoint to higher frequencies.

5. Responses to Command Inputs

The closed-loop pitch attitude response to pitch rate command for the shuttle has the form

$$\frac{\theta}{q_c} = \frac{1}{s}\frac{q}{q_c} \doteq \frac{K_q M_\delta \left(1/T_{\theta_1}\right)\left(1/T_{\theta_2}\right)\left(1/T_q\right) e^{-\tau s}}{s\left(1/T'_{sp_1}\right)\left(1/T'_{sp_2}\right)\left[\zeta', \omega'_n\right]} \tag{20}$$

As noted previously, the short period roots are driven into the attitude zeros such that

$$\frac{\theta}{q_c} \doteq \frac{K_q M_\delta \left(1/T_q\right) e^{-\tau s}}{s\left[\zeta', \omega'_n\right]} \tag{21}$$

Since the command filter for the shuttle is effectively a pure gain, Eq. 21 is a good approximation of the pitch attitude response to the pilot's rotational hand controller (RHC). However, it should be noted that the response to command for a superaugmented aircraft can be significantly modified by shaping the command filter, G_i. This will be considered further in Section IV in connection with recent research activity, but here we will consider only the shuttle ($G_i \doteq$ constant) design.

It is useful to compare the above shuttle pitch rate response to the 3 DOF response of a conventional aircraft

$$\frac{\theta}{\delta_e} = \frac{M_\delta \left(1/T_{\theta_1}\right) \left(1/T_{\theta_2}\right) e^{-\tau_c s}}{\left[\zeta_p,\ \omega_p\right] \left[\zeta_{sp},\ \omega_{sp}\right]} \tag{22}$$

and its "short period" approximation (Ref. 12).

$$\frac{\theta}{\delta_e} \doteq \frac{M_\delta \left(1/T_{\theta_2}\right) e^{-\tau_c s}}{s\left[\zeta_{sp},\ \omega_{sp}\right]} \tag{23}$$

A comparison of the key pitch attitude response parameters for Eqs. 21 and 23 is accomplished in Fig. 16 and Table 1. Figure 16a is idealized with no control system or other lags between the pilot step function input and the control response. Figure 16b includes such delays and approximates their net effect as a delay time τ. For the conventional airplane at the left in Table 1, the attitude lead and short-period undamped natural frequency, and hence the rise time in Fig. 16a, depend primarily on aircraft configuration characteristics and the way the aircraft is balanced. The damping ratio also is predominantly a function of configuration, although a pitch damper can provide a good deal of design latitude.

For the shuttle as noted before, there is a relative lack of sensitivity to aircraft configuration characteristics and a dominance of the controller properties as they affect the closed-loop aircraft/augmenter

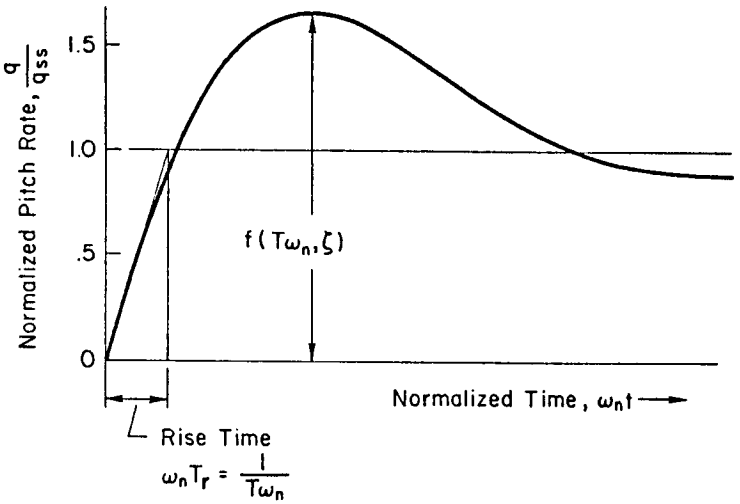

General Form:

$$\frac{q}{q_{ss}} = \frac{(Ts+1)}{s\left[\left(\frac{s}{\omega_n}\right)^2 + \frac{2\zeta_n}{\omega_n}s+1\right]}$$

a) Idealized Dynamics for the Shuttle or for Short-Period Attitude Dynamics for a Conventional Aircraft With Large Static Stability

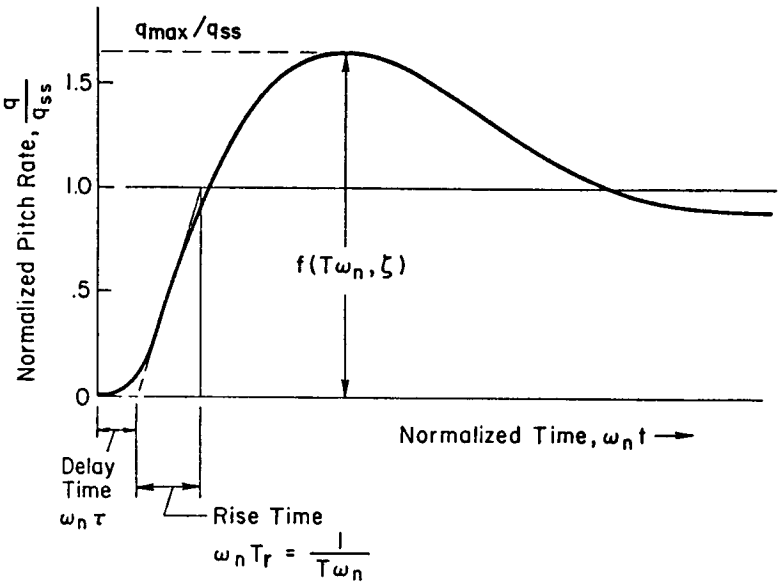

General Form:

$$\frac{q}{q_{ss}} = \frac{(Ts+1)e^{\tau s}}{s\left[\left(\frac{s}{\omega_n}\right)^2 + \frac{2\zeta}{\omega_n}s+1\right]}$$

b) Attitude Dynamics With Effective Time Delay

Figure 16. General Pitch Rate Response to Step Pilot Input

TABLE 1. COMPARISON OF PITCH ATTITUDE RESPONSE GOVERNING PARAMETERS FOR CONVENTIONAL AIRCRAFT AND THE SHUTTLE

DYNAMIC PROPERTY	CONVENTIONAL		SHUTTLE	
	PARAMETERS	PRIMARY DESIGN FACTORS	PARAMETERS	PRIMARY DESIGN FACTORS
Lead Time Constant T	$\frac{1}{T_{\theta 2}} \doteq -Z_w + \frac{Z_\delta}{M_\delta} M_w$	Set Predominantly by Airframe: C_{L_α}; wing	T_q	Governed predominantly by closed-loop control system Stability, Response, and Margins **Control System Parameters** T_q - Lead time constant K_q - Gain **Airframe Parameter** M_δ - Surface effectiveness (C_{m_δ})
Undamped Natural Frequency ω_n	$\omega_{sp}^2 = Z_w M_q - M_\alpha$	Maneuver Margin; $C_{M_{CL}}$; Tail	$\omega_n^2 = \frac{\omega_{ca}}{T_q}$ $= \frac{K_q}{T_q}[M_\delta]$	
Normalized Rise Time $\omega_n T_r$	$\frac{1}{T_{\theta 2}\omega_{sp}}$		$\frac{1}{T_q\omega_n} = \frac{1}{\sqrt{T_q\omega_{ca}}}$ $T_r = \frac{1}{\omega_{ca}}$	
Damping Ratio ζ	$(\zeta\omega)_{sp} = -(Z_w + M_q + M_{\dot{\alpha}})$	C_{L_α}; Wing C_{m_q}; Tail Pitch Damper	$\zeta = \frac{\sqrt{T_q\omega_{ca}}}{2}$ $= \frac{1}{2}\sqrt{K_q T_q [M_\delta]}$	
Delay Time τ_d		Actuator and Manual Control lags		Actuator lag + Stick filters + Bending Mode filters + Computational delays

system. As can be seen from Table 1, the factors underlying the dynamics of the shuttle are the closed-loop crossover frequency (of the asymptote), ω_{c_a}, and the controller lead, T_q. The crossover frequency is of overwhelming importance because it defines:

- The total system gain comprising both controller (K_q) and aircraft control effectiveness (M_δ) parameters.
- The system bandwidth which indicates the frequency range of good command following and disturbance suppression.
- The rapidity of system response, i.e., rise time $T_r = 1/\omega_{c_a}$.
- The system damping ratio in that ω_{c_a} is a key factor (together with the controller lead time constant, T_q) in setting the damping ratio, ζ.

The first three properties of the crossover frequency listed above are qualitatively applicable to all feedback control systems which have a low-pass closed-loop character. (Low pass here means that at frequencies up to the bandwidth, the output follows the input quite well; whereas, at higher frequencies the output will drop off in amplitude relative to the input -- thus the low frequencies are "passed" through the system while frequencies higher than the bandwidth are attenuated or "not passed.") The fourth property is a special one for "superaugmented" systems which share the specific characteristics of the shuttle. It is one reflection of the idealized superaugmented situation wherein only two parameters, the attitude lead (T_q) and crossover frequency (ω_{c_a}), define <u>all</u> the system input/output characteristics except the overall response scaling between output and input.

A final manifestation of the two parameter character of the idealized shuttle is the maximum pitch rate overshoot vs. $1/T_q\omega_n$ shown in Fig. 17. It may be seen that a distinguishing feature of the shuttle q_c step response is a relatively low pitch rate overshoot (i.e., low q_{max}/q_c). In fact an approximate upper overshoot limit on shuttle type designs is (Ref. 11)

$$\frac{q_{max}}{q_c} < \left.\frac{q_{max}}{q_c}\right|_{\omega_{c_a} = 1/T_q} = 1 + e^{-2\pi/3\sqrt{3}} \doteq 1.30 \qquad (24)$$

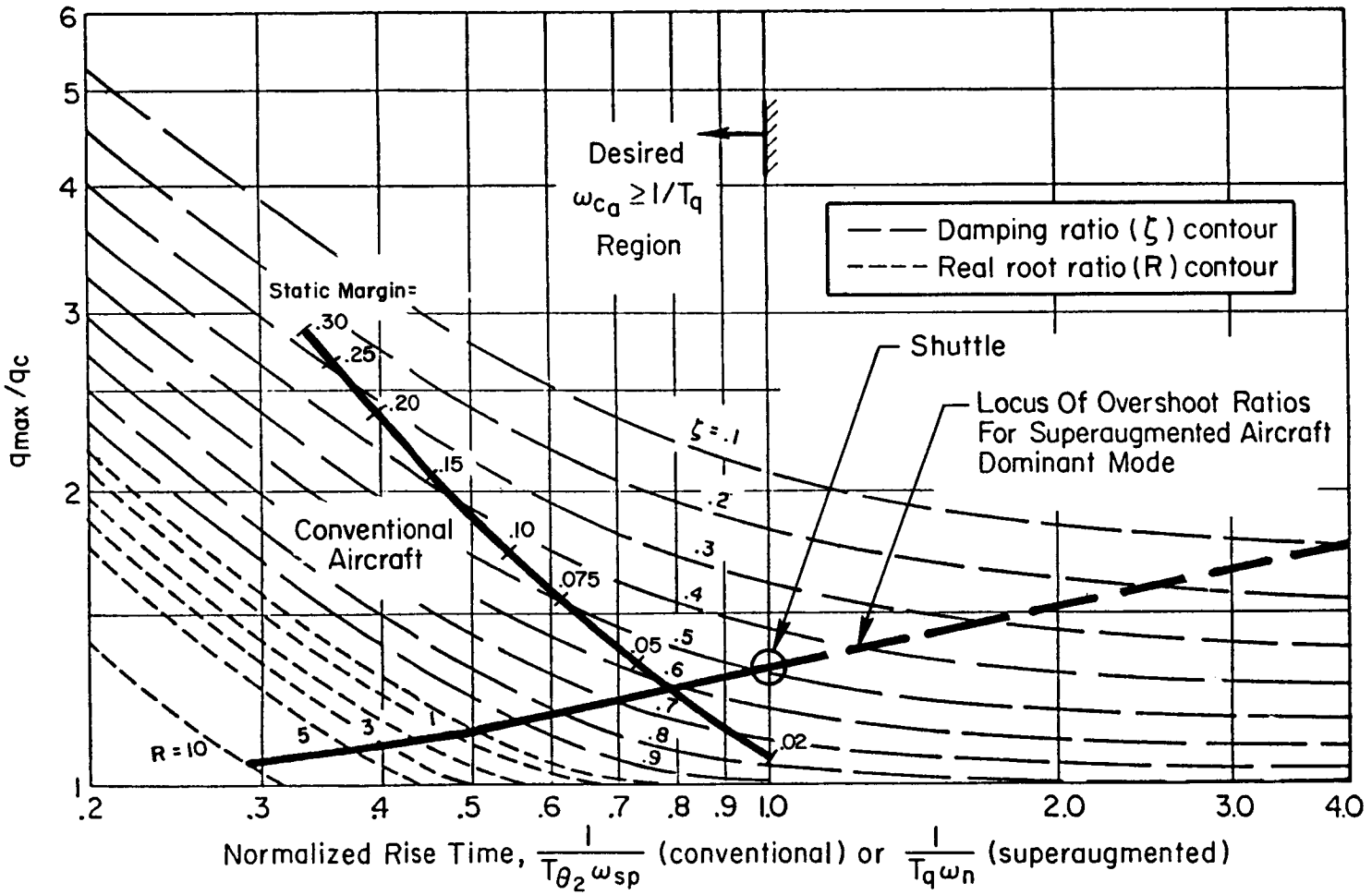

Figure 17. Maximum Pitch Rate Overshoot Variation for Shuttle-like and Conventional Aircraft

which corresponds to $\omega_{c_a} = 1/T_q$. Furthermore, if one desires to decrease the normalized rise time by increasing loop gain and hence ω_{c_a} at fixed $1/T_q$, the overshoot decreases. At $\omega_{c_a} > 2/T_q$, the closed-loop pitch response becomes overdamped.

It is instructive to compare the pitch overshoot variation with static margin of conventional aircraft in Fig. 17 with the law of overshoot for the shuttle. As noted in Table 1, for the conventional case the usual variable is the way the aircraft is balanced, i.e., the static margin (while T_{θ_2} is fixed and based on wing design). Increased static margin has a concomitant increase in the undamped natural frequency and decrease in the normalized rise time. This aspect is similar to that for ω_n and normalized rise time, $1/T_q\omega_n$, for the shuttle. On the other hand, the damping ratio of the short period decreases and the overshoot increases for the conventional aircraft while the opposite trend is present for the superaugmented airplane.

A major distinction can also be made between the shuttle and conventional aircraft with reference to the aerodynamic characteristics which underlie their responses. For the conventional aircraft the stability derivatives Z_w, M_q, and M_α together with their variations with flight condition are major governing parameters in the short period. When the complete three degrees-of-freedom airplane characteristics are also taken into account, several more derivatives become important (e.g., Z_u, M_u, X_w, etc.). On the other hand to the extent that the shuttle augmentation system can be made to approach the superaugmented characteristics, the aerodynamic parameters of importance reduce to the surface effectiveness, M_δ. Potential variations in other derivatives must, of course, be assessed in the design process to assure that no possible variation could upset this applecart, but in actual system operation the primary sensitivity and variations of interest are those of M_δ. In some ways this sparsity of airplane characteristic dependence for aircraft which approach the superaugmented state offers a major advantage when one is faced with identifying the effective airframe from flight data or in validating simulations. This will be demonstrated later.

Finally, the ultimate comparison of the shuttle and conventional vehicles is connected with the closed-loop precision path control dynamic responses. A block diagram that indicates the pilot's activities in precision path control is shown in Fig. 18. On the right the augmented aircraft has path deviation and pitch attitude as the output variables stemming from aircraft dynamics, which are forced by external atmospheric disturbances and the pilot control output, δ. The augmented aircraft itself is a closed-loop system comprising the airplane and augmentation system. Thus the sensors, computation, and actuation elements involved in the feedback control augmentation system as well as the aircraft are encompassed by the "Augmented Aircraft Pitch Dynamics" block in Fig. 18. (An underlying assumption in this diagram is that other aircraft control effectors such as speed brake or body flap are not being continuously modulated by pilot control action; trim management using these aircraft effectors, however, is not excluded.)

Even though trimmed precisely, the augmented aircraft will not by itself maintain exactly the prescribed path and attitude in the presence of disturbances. Consequently, the pilot must exert control not only to establish the desired path, but also to correct any deviations from the desired attitude and path. This is accomplished by the pilot acting as a closed-loop controller, which means simply that the pilot's control output is dependent on (i.e., a function of) path deviation and attitude. Thus, a component of the pilot's control output is correlated with an attitude error, and another component is correlated with the difference between the desired and actual path. This relationship is depicted in the Fig. 18 block diagram as a "series" pilot closure, i.e., the pilot's action on path deviation acts in series with and provides an internal "attitude command" for the pilot's action on attitude error.

Figure 19 shows a simplified comparison of conventional and heavily augmented (shuttle) dynamic response to the pilot's controller input. For the conventional aircraft, the pitch numerator and path denominator contain dynamic elements characterized by $1/T_{\theta_2}$ which thus cancel. The path deviation is then the integral of pitch attitude. For the shuttle however, $1/T_{\theta_2}$ is approximately one-third $1/T_q$, these dynamic parameters

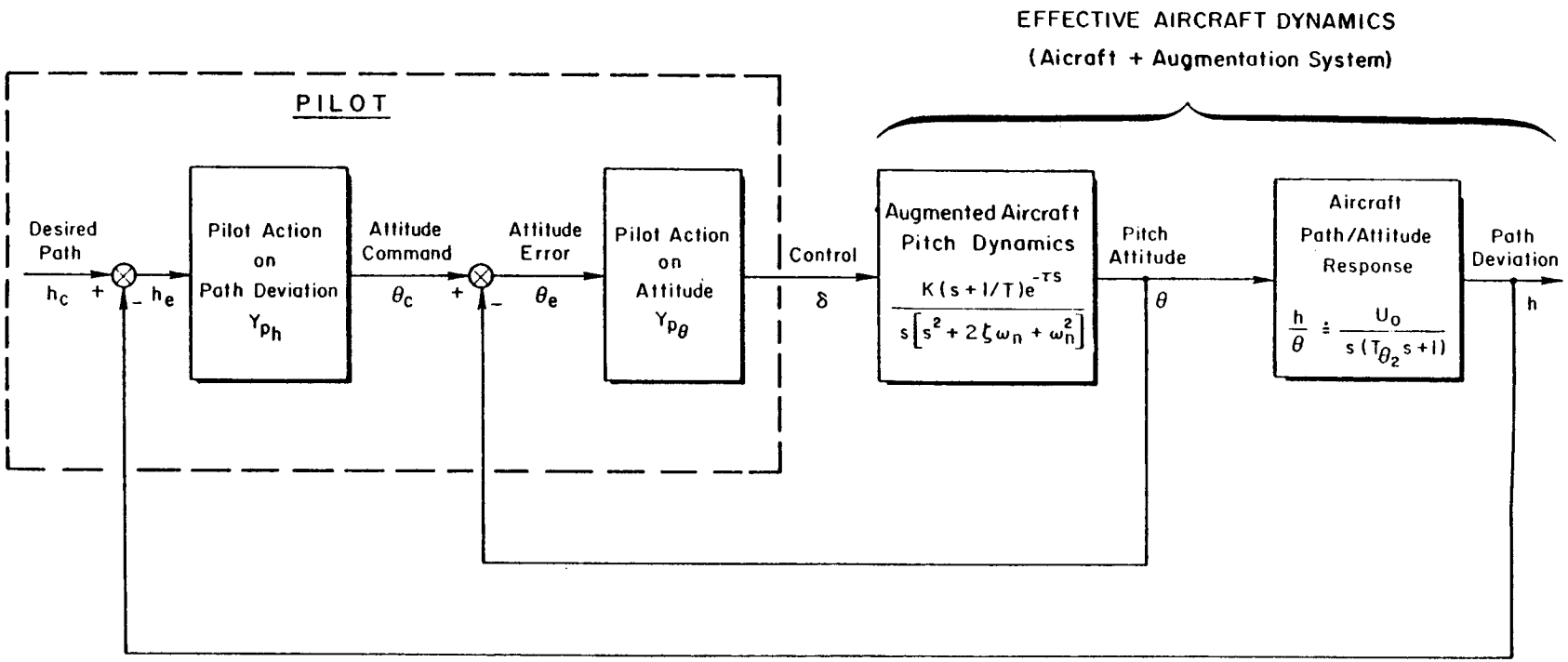

Figure 18. Closed-Loop Precision Path Control with Attitude Control Inner Loop

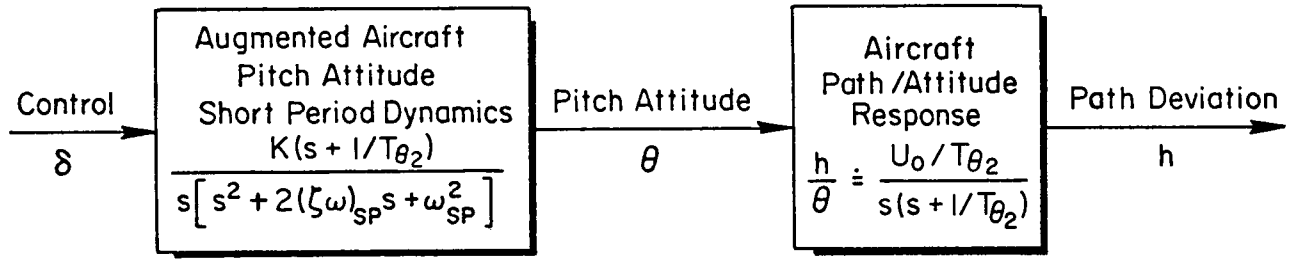

a) Conventional Aircraft

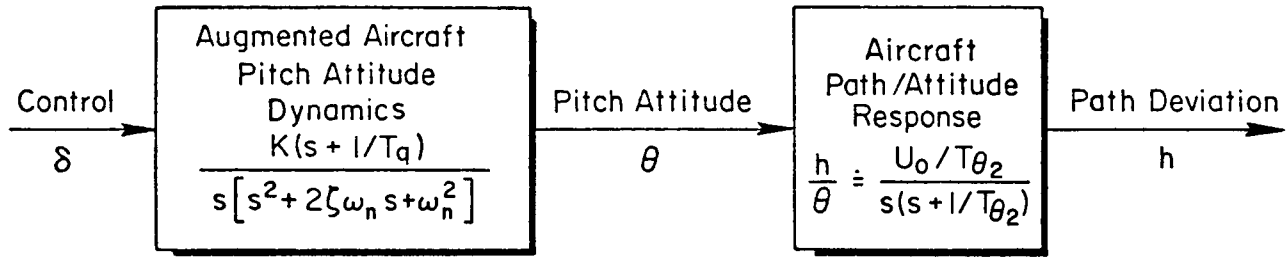

b) Shuttle-Like Aircraft

Figure 19. Effective Aircraft Dynamics (Aircraft + Augmentation System) for Conventional and Shuttle-like Aircraft

do not cancel, and the path response lags pitch attitude change by this additional time constant, T_{θ_2}. This also applies to other shuttle responses. For example, Table 2 and Fig. 20 present a hypothetical conventional aircraft compared to a shuttle-like (G_i = constant) superaugmented aircraft. For this comparison the superaugmented dominant pitch mode frequency ω_n' is selected to match the conventional short period frequency ω_{sp} and the two aircraft are assumed to have the same "stick force per g." (ω_n' has been made a little higher than the shuttle value to clarify the distinctions with the conventional aircraft.) In Fig. 20 only the Bode asymptotes are shown to emphasize the important poles and zeros.

The effect on pitch attitude response of the shuttle attitude lead being about three times higher than the conventional $1/T_{\theta_2}$ value can be seen in the θ/δ_p Bode asymptotes. The superaugmented form is more "K/s-like" out to the second-order mode and the response to pilot input is essentially invariant.

The conventional aircraft on the other hand exhibits an increased response in the frequency range above $1/T_{\theta_2}$ but may also exhibit considerable pitch "droop" or "drop back" at low frequencies. The latter is due to T_{θ_1} and the phugoid (ω_p).

The result is that insofar as pitch response is concerned, the shuttle responds as a rate command/attitude hold vehicle while the conventional aircraft responds essentially as an attitude command/attitude hold vehicle.

Examination of Table 2 and Fig. 20 also shows distinctions between the superaugmented (shuttle) and conventional command respond in angle-of-attack, flight path angle, and speed response. All of these differences can be traced to differences in the system poles. For the superaugmented aircraft, the second-order pole at ω_n is not a true "short period" in that it is essentially a pure attitude mode; whereas the conventional airplane short period is a coupled heave-pitch mode. The presence of an essentially pure attitude mode for a superaugmented aircraft such as the shuttle is a consequence of the near neutral or somewhat

TABLE 2. SUMMARY OF CONVENTIONAL AND SUPERAUGMENTED RESPONSE TO PILOT INPUTS

	CONVENTIONAL		SUPERAUGMENTED $G_i \triangleq$ constant (Approximate Form)	
$\frac{\theta}{\delta_p}$	$\frac{A_\theta(1/T_{\theta_1})(1/T_{\theta_2})}{[\zeta_p, \omega_p][\zeta_{sp}, \omega_{sp}]}$	$\frac{A_\theta(0.05)(0.40)}{[0.116, 0.174][0.402, 2.50]}$	$\frac{k(1/T_q)}{(0)[\zeta', \omega_n']}$	$\frac{k(2.0)}{(0)[0.75, 2.5]}$
$\frac{\alpha}{\delta_p}$	$\frac{A_\alpha[\zeta_\alpha, \omega_\alpha]}{[\zeta_p, \omega_p][\zeta_{sp}, \omega_{sp}]}$	$\frac{A_\alpha[0.137, 0.183]}{[0.116, 0.174][0.402, 2.50]}$	$\frac{k(1/T_q)}{(0)[\zeta', \omega_n']} \cdot \frac{[\zeta_\alpha, \omega_\alpha]}{(1/T_{\theta_1})(1/T_{\theta_2})}$	$\frac{k(2.0)[0.137, 0.183]}{(0)[0.75, 2.5](0.05)(0.40)}$
$\frac{\gamma}{\delta_p}$	$\frac{A_\gamma(1/T_{h_1})}{[\zeta_p, \omega_p][\zeta_{sp}, \omega_{sp}]}$	$\frac{A_\gamma - 0.0337}{[0.116, 0.174][0.402, 2.50]}$	$\frac{k(1/T_q)}{(0)[\zeta', \omega_n']} \cdot \frac{(1/T_{h_1})}{(1/T_{\theta_1})(1/T_{\theta_2})}$	$\frac{k(2.0)(-0.0337)}{(0)[0.75, 2.5](0.05)(0.40)}$
$\frac{u}{\delta_p}$	$\frac{A_u(1/T_{u_1})}{[\zeta_p, \omega_p][\zeta_{sp}, \omega_{sp}]}$	$\frac{A_u(0.40)}{[0.116, 0.174][0.402, 2.50]}$	$\frac{k(1/T_q)}{(0)[\zeta', \omega_n']} \cdot \frac{(1/T_{u_1})}{(1/T_{\theta_1})(1/T_{\theta_2})}$	$\frac{k(2.0)(0.40)}{(0)[0.75, 2.5)(0.05)(0.40)}$

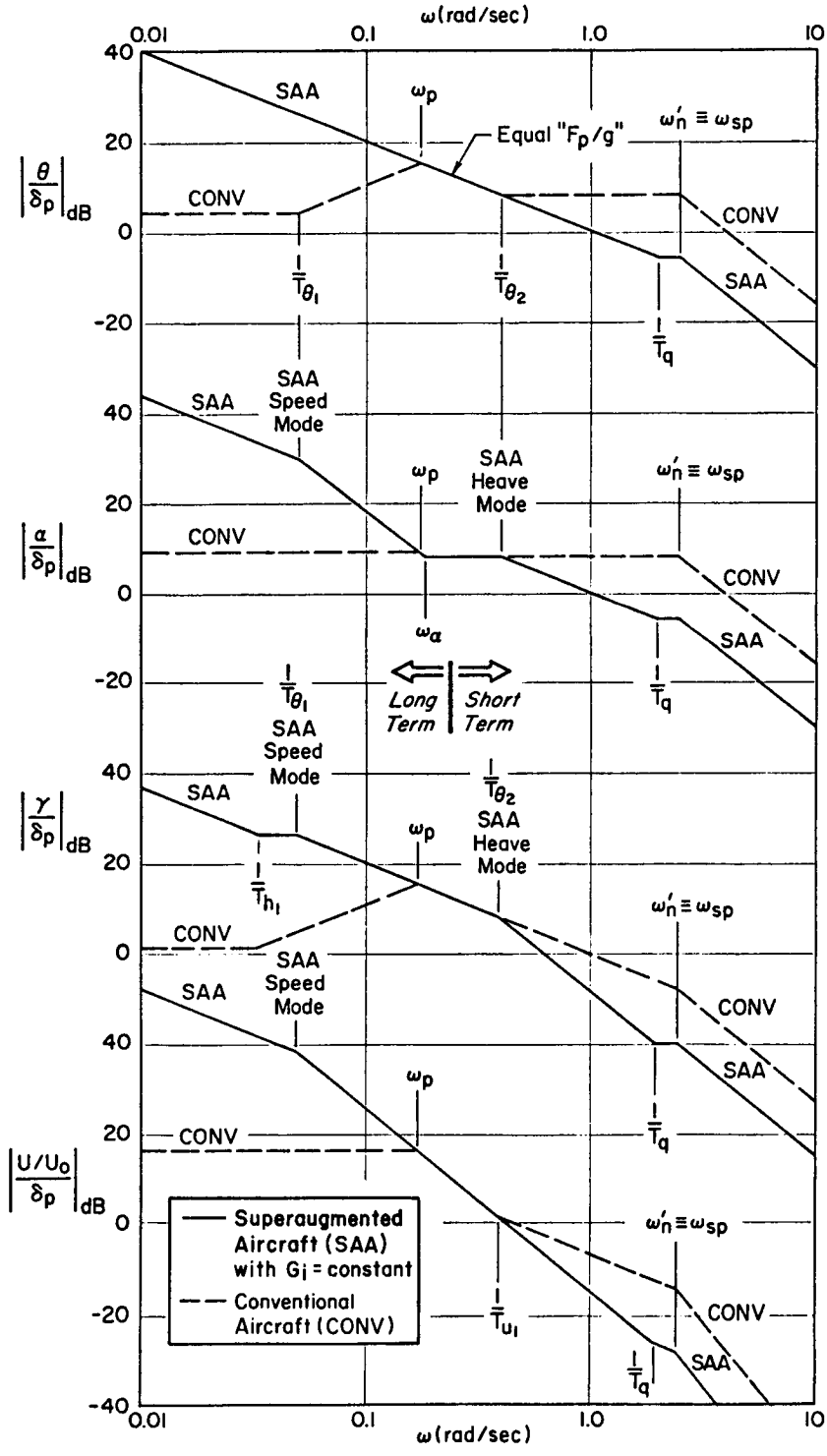

Figure 20. Asymptotic Comparison of Conventional and Superaugmented (G_i = Constant) Response to Pilot's Controller

unstable static margin, which implies that the "heave-into-pitch" coupling derivative M_w is small, combined with the fact that the superaugmentation system is based on an effective pitch attitude to elevator feedback. The superaugmented aircraft is also distinct from the conventional aircraft in that is does not have a phugoid. Rather the two remaining poles are driven close to the attitude zeros $1/T_{\theta_1}$ and $1/T_{\theta_2}$ to create real "speed" and "heave" modes, respectively (see Fig. 10). These two modes are comparable to those of a neutrally stable (i.e., zero static margin) conventional aircraft, although the well damped second-order attitude mode of the superaugmented aircraft is not characteristic of a neutral airframe (see Ref. 11).

Several of the differences seen in Fig. 20 deserve special note in light of manual control issues to be addressed in Section IV. In the region of the short period responses, all shuttle motion quantities lag those of the conventional counterpart by virtue of the separation between $1/T_{\theta_2}$ and $1/T_q$ as noted previously. The result is that a "G_i = constant" superaugmented aircraft like the shuttle will have a reduction in α/δ_p bandwidth associated with achieving a wider K/s range in the attitude response. In the time domain this means that the shuttle will have a longer (slower) path response rise time for a step RHC command. Also, in the frequency band between $1/T_{\theta_2}$ and $1/T_q$ the path and speed response is "K/s^2-like" and would be expected to elicit pulse-like control activity if the pilot were to attempt direct control of these motion responses within this frequency band.

In the low frequency region, i.e., below the conventional phugoid, differences between the two types of vehicles are related primarily to an additional integration present in each of the shuttle responses. This derives from the shuttle's overpowering pitch attitude stability and indicates that the shuttle has no path, speed, or angle-of-attack "stability," or more correctly, zero "stick force/speed gradient," etc.

It should be noted that the above distinctions are <u>not</u> necessary characteristics of superaugmented aircraft, only of shuttle-like designs with $G_i \doteq$ constant. By suitably shaping G_i, the path response to pilot command can be changed at will, even to approximate the conventional

response. However, for a single control point (e.g., elevator) aircraft the attitude and path responses cannot be adjusted independently. For instance if the path response is made more "conventional" by shaping G_i, the attitude response will become more conventional as well. Thus, the FCS designer must consider the tradeoffs carefully to seek an adequate compromise.

There is a possible way out of this tradeoff. If a second independent control point (e.g., a canard) is available, then the attitude and path responses can in theory be tailored independently. However, creating a successful FCS design will require, as a minimum, a good understanding of task specific manual control requirements and appropriate design requirements -- topics to be discussed in Section IV and Section V.

6. Command Response at the Pilot's Location

There is yet another unusual characteristic of the shuttle path (altitude, normal acceleration, etc.) response which is related to the vehicle elevon design and mass distribution. This is <u>not</u> a superaugmentation issue and will not in general be an issue for other advanced aircraft. It arises from the fact that the instantaneous center-of-rotation (ICR) for elevon inputs is relatively far forward for the shuttle. Thus, while the shuttle cockpit is located conventionally, the pilot position with respect to the ICR is unusual. The pilot is about 10 ft behind the ICR. Figure 21 compares the shuttle pilot position with several other aircraft. Only for the HLIO -- a lifting body precursor of the shuttle -- is the pilot also behind the ICR.

The ICR is the point at which the normal acceleration due to $Z_{\delta_e}\delta_e$ is just canceled by the pitching component $X_{ICR}M_{\delta_e}\delta_e$ so that

$$X_{ICR} = \frac{Z_{\delta_e}}{M_{\delta_e}} = \frac{k_y^2}{\ell_{\delta_e}} \text{ (ft, positive forward from c.g.)} \qquad (25)$$

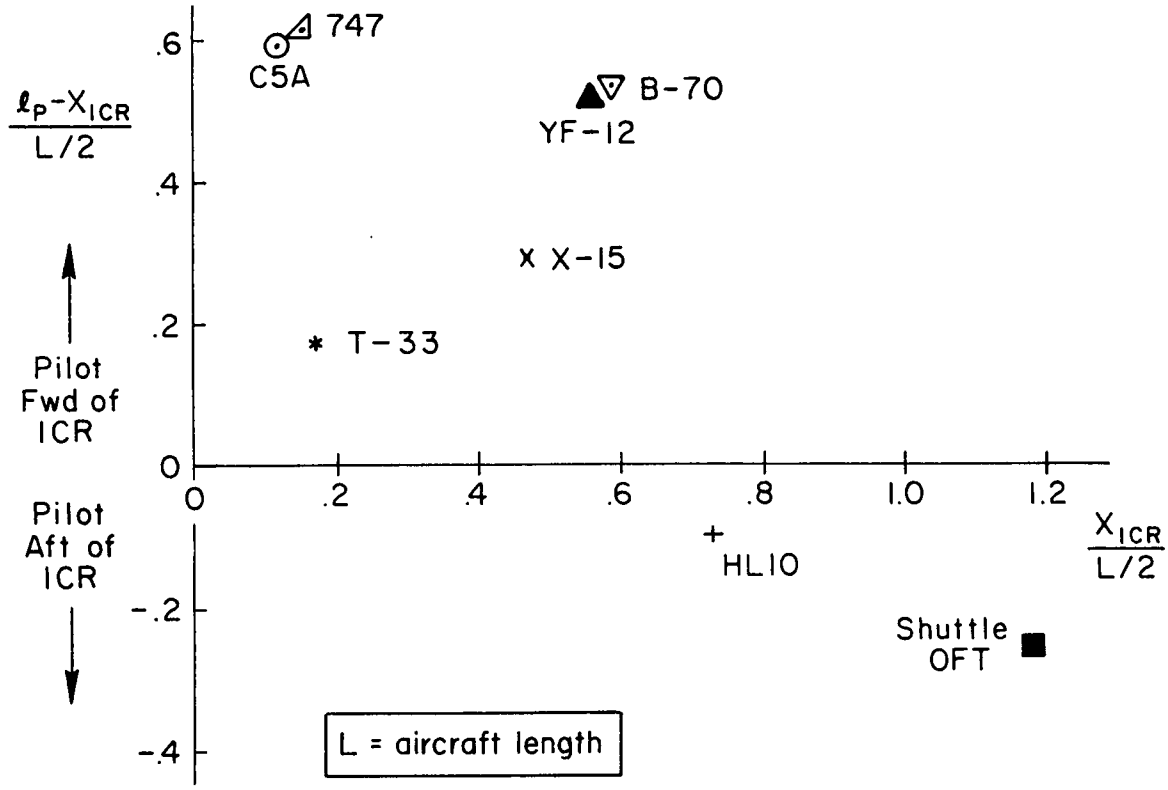

Figure 21. Comparison of Pilot Location with Respect to the Instantaneous Center of Rotation for Eight Aircraft

The extreme forward position of the shuttle's ICR is attributable to the large radius of gyration from the engines mounted behind a (nearly) empty payload bay combined with short effective tail length for the elevons. The segregation of aircraft along the ordinate in Fig. 21, which separates transport/bomber types from smaller "fighter" types stems largely from the pilot being located relatively further forward geometrically in large aircraft.

The interest in pilot location stems from the influence on effective path dynamics, which the pilot must control in landing. The general form of the 3 DOF path-to-elevator numerator for any aircraft (including the shuttle) is a third-order consisting of one low frequency zero, which is almost independent of location relative to the ICR, and two high frequency zeros, which vary widely with location (Refs. 1, 15). In Fig. 20, the two high frequency zeros were neglected since they have no

bearing on the superaugmentation issue per se. It is shown in Ref. 1 that in the conventional situation where the pilot is ahead of the ICR, the high frequency zeros will generally form a lightly damped complex pair in the left half s plane. For the shuttle, these two zeros are real and one is a non-minimum phase zero in the right hand plane. A physical view of this situation is provided in Fig. 22. It may be seen that immediately after a step elevator input for a pull-up, a pilot at A (the conventional location) will immediately rise, i.e., he will lead the c.g. motion. A pilot at B (the shuttle location) will "go down before he goes up" as does the c.g. (and also the main landing gear, the altitude of which is of primary concern for landing). This pilot perceives an initial response reversal or an effective time delay in the path response.

C. IDENTIFICATION OF ORBITER EFFECTIVE PITCH DYNAMICS FROM FLIGHT DATA

1. STS-4 Flight Data

Because of the dominant effect of the FCS on the Orbiter's pitch response, identification of airframe characteristics alone is not adequate to characterize the effective vehicle as seen by the pilot. In Ref. 3 the effective vehicle pitch rate response to rotational hand controller (RHC) inputs in landing was extracted from flight data for one flight -- STS-4. This was accomplished by application of a fast Fourier transform spectral analysis technique implemented in a STI Frequency Domain Analysis (FREDA) digital program. The spectral identification of the q/δ_{RHC} describing function requires δ_{RHC} and q time histories (Fig. 23) for the approach and landing. The FREDA program obtains the spectral density distributions $\phi_{\delta\delta}$ and ϕ_{qq}, and cross spectral $\phi_{q\delta}$ by direct Fourier transform of the time series using the Wiener-Khinchin relationship (Ref. 16). The q/δ_{RHC} describing function is then given by

$$\frac{q}{\delta_{RHC}}(j\omega) = \frac{\phi_{q\delta}(j\omega)}{\phi_{\delta\delta}(j\omega)} \tag{26}$$

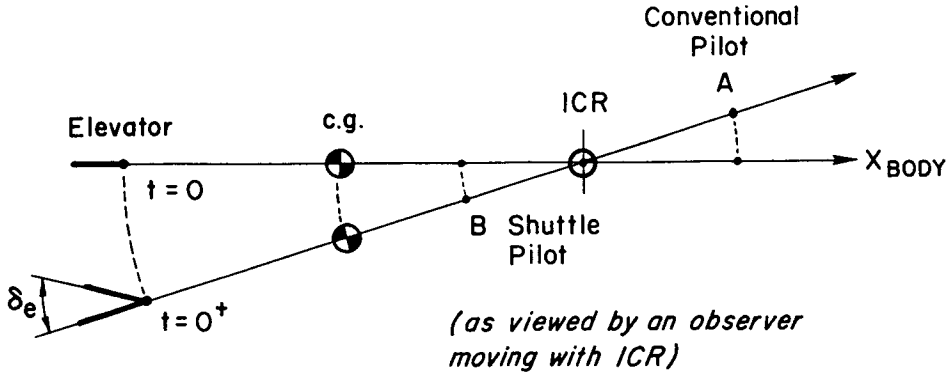

Figure 22. Illustration of Initial Motion Following a Step (Trailing Edge Up) Elevator Input at 2 Pilot Positions

The FREDA program produces discrete magnitude and phase angle pairs for q/δ_{RHC}, $\phi_{\delta\delta}$, and ϕ_{qq}. A coherence function

$$\rho^2(\omega) = \frac{|\phi_{q\delta}(j\omega)|^2}{\phi_{qq}(\omega)\ \phi_{\delta\delta}(\omega)} \tag{27}$$

is also computed and gives a measure of the degree to which the output is linearly correlated with the input. A ρ^2 of zero implies no correlation and a ρ^2 of 1 indicates perfect correlation between output and input. For vehicle dynamic identification, ρ^2 values between 0.8 and 0.9 are generally indicative of meaningful identification.

Implicit in the use of the spectral procedure is the assumption that the describing function will be time invariant. Because of the properties of superaugmentation, this will be true to a first approximation for q/δ_{RHC} in the region of interest given the fixed value of T_q, and the small variation of the dominant closed-loop mode during approach and landing. This situation would not occur for a conventional airframe transfer function such as q/δ_e, and special accommodation would be required. There are in addition system nonlinearities which could, in principal, compromise the use of FREDA; in particular the PIOs filter and the stick shaping. During the STS-4 landing the PIOs filter was active only when the commander executed the preflare termination. To examine possible PIOs effects, FREDA runs were made over the entire

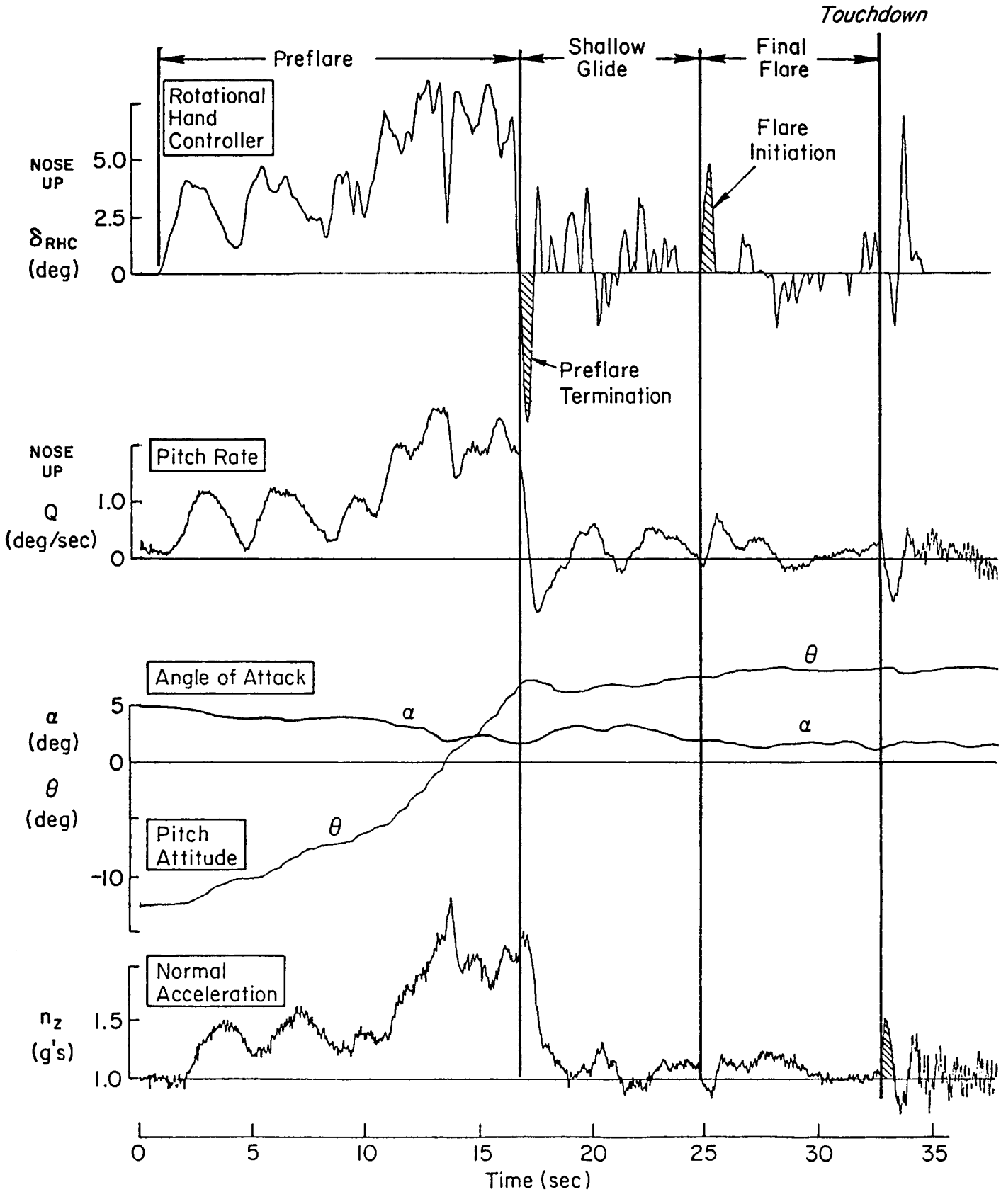

Figure 23. Attitude Control Time Histories STS-4

period from the start of preflare to touchdown, and for subsegments excluding the PIOs activity. The above considerations of time varying system parameters and occasional nonlinear events (e.g., PIOs activity) imply a desire for a short identification run length T_{RUN}. On the other hand, maximizing run length is desirable to obtain good low frequency data since the theoretical lower bound on the frequency response ω_{min} is

$$\omega_{min} = 2\pi/T_{RUN} \tag{28}$$

The FREDA output plots for maximum feasible run length (start of preflare to touchdown, T_{RUN} = 30 sec, ω_{min} = 0.2 rad/sec) are shown in Fig. 24. The coherence ρ^2 values are above 0.8 out to approximately 10 rad/sec. Above this frequency the coherence decreases, and thus 10 rad/sec is taken as limit of validity for the frequency response (the describing function plot symbols are changed when ρ^2 drops below 0.8).

Figure 25 presents the corresponding FREDA output for the shallow glide and final flare starting just after the PIOs activity, and terminating just before touchdown. The results are quite consistent with the Fig. 24 data, except for the reduction in low frequency data due to the shorter run length (T_{RUN} = 12.0 sec). These results are valuable because they imply usable results may be obtained for T_{RUN} on the order of a flight segment length, and they confirm the approximate time invariance of q/δ_{RHC}.

The FREDA program defines the q/δ_{RHC} describing function as a set of discrete magnitude and phase angle points. Definition of the specific parameter values in the superaugmented response form (i.e., the poles and zeros) requires "fitting" this form to the FREDA output. This was done (Ref. 3) with the STI Multi-Frequency Parameter Identification program (MFP), which provides a weighted least squares fit to the specified response form.

The fitting operation was performed both with the lead $1/T_q$ fixed at the shuttle FCS value ($1/T_q$ = 1.5 rad/sec), and also with the $1/T_q$ free.

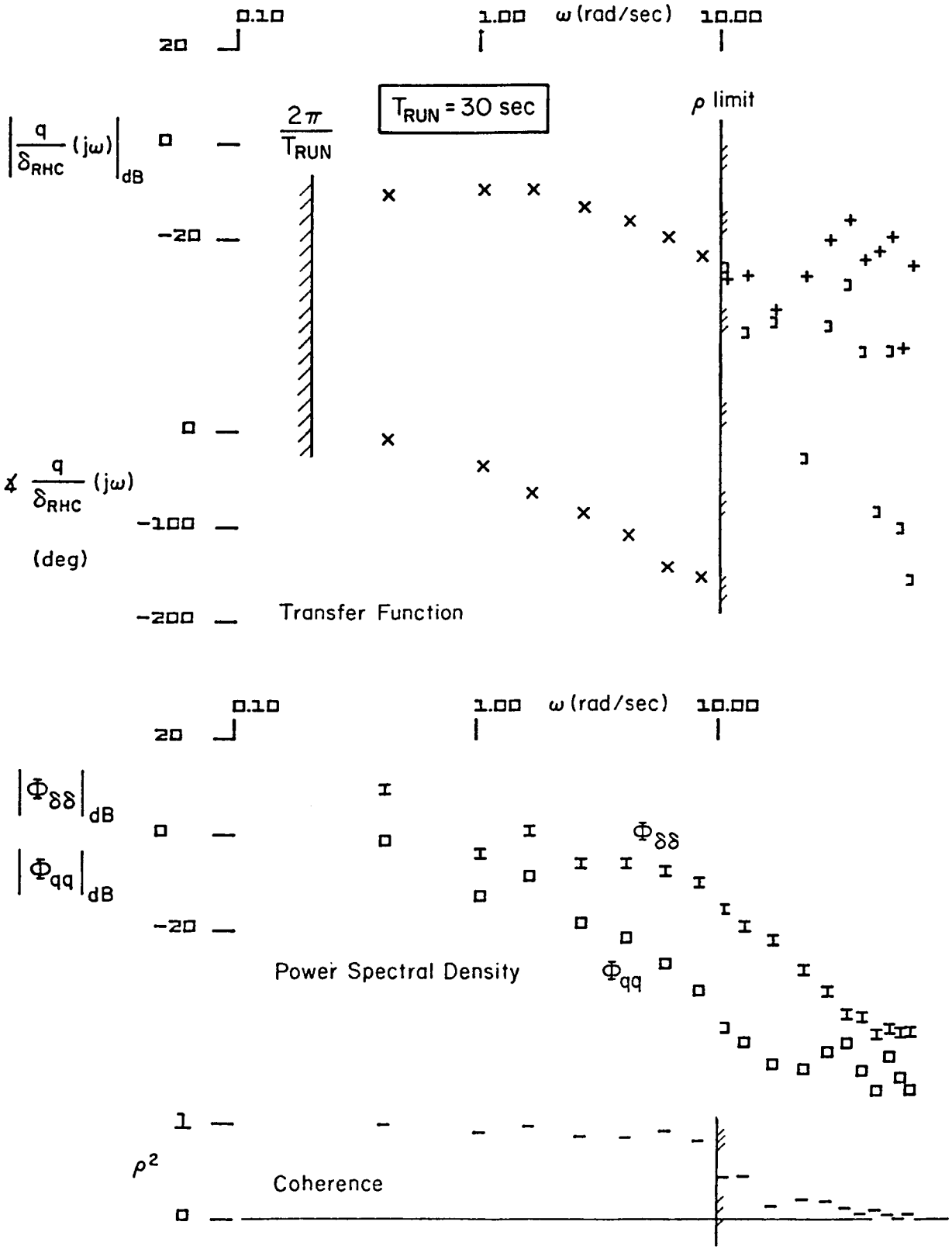

Figure 24. FREDA Output for q/δ_{RHC}, STS-4 Preflare Through Touchdown

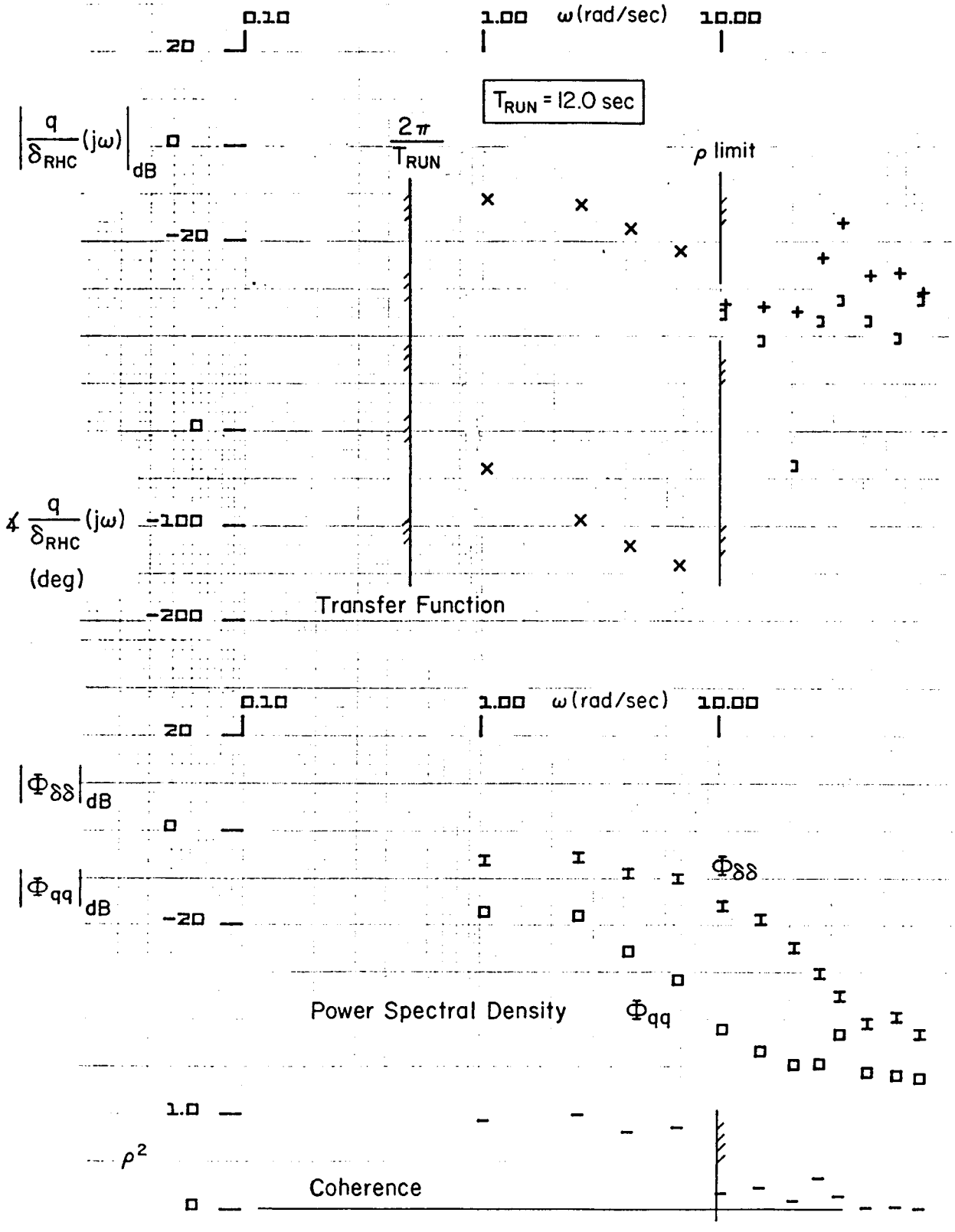

Figure 25. FREDA Output for q/δ_{RHC}, STS-4 Shallow Glide and Final Flare

The two results are shown in Fig. 26a. It may be seen that the two cases are very similar, and that both provide a very satisfactory fit. A time domain comparison (Fig. 26b) leads to a similar conclusion.

Table 3 shows a comparison between the analytic low order equivalent system (LOES) (Eq. 21) model parameters, and values extracted from the STS-4 flight data (both for fixed and free numerator time constant). The first line compares steady state gain values, and shows the largest difference of any of the comparisons. The extracted values are approximately 80 percent higher than the estimated values. While this difference has not been totally resolved, it appears to be due to the recorded δ_{RHC} signal being obtained from the Backup Flight Control System (BFCS), which does not contain all of the forward loop elements of the primary control system used to compute the gain in Eq. 21. Additionally, the precise point at which the signal is picked off was not tracked down.

The fixed value of flight derived numerator inverse time constant exactly matches the analytic model by definition. The extracted value with $1/T_{q_{free}}$ is somewhat lower at 1.03. However, it is still well above the range of values for $1/T_{\theta_2}$ in the identification region (0.44 to 0.64 rad/sec). The values of the damping ratio obtained from flight are approximately 50 percent higher than the prediction. It is presently felt that the primary cause of the higher in-flight damping ratio, and perhaps also the lower in-flight value of $1/T_q$, is the "ELERROR" filter (see Fig. 9) which has been ignored in the simplified model (Eq. 21). To a first approximation, the ELERROR filter increases the open-loop phase margin in the crossover region, which would correspond to the effect of a low value of $1/T_q$ and to a higher closed-loop damping ratio.

The flight extracted values of natural frequency are slightly higher for the fixed T_q case and slightly lower for the free T_q case with respect to the theoretical value of 1.5 rad/sec. Finally, the flight extracted values of time delay are actually somewhat lower than obtained by adding the low frequency phase lag approximates of the forward loop elements (Eq. 7).

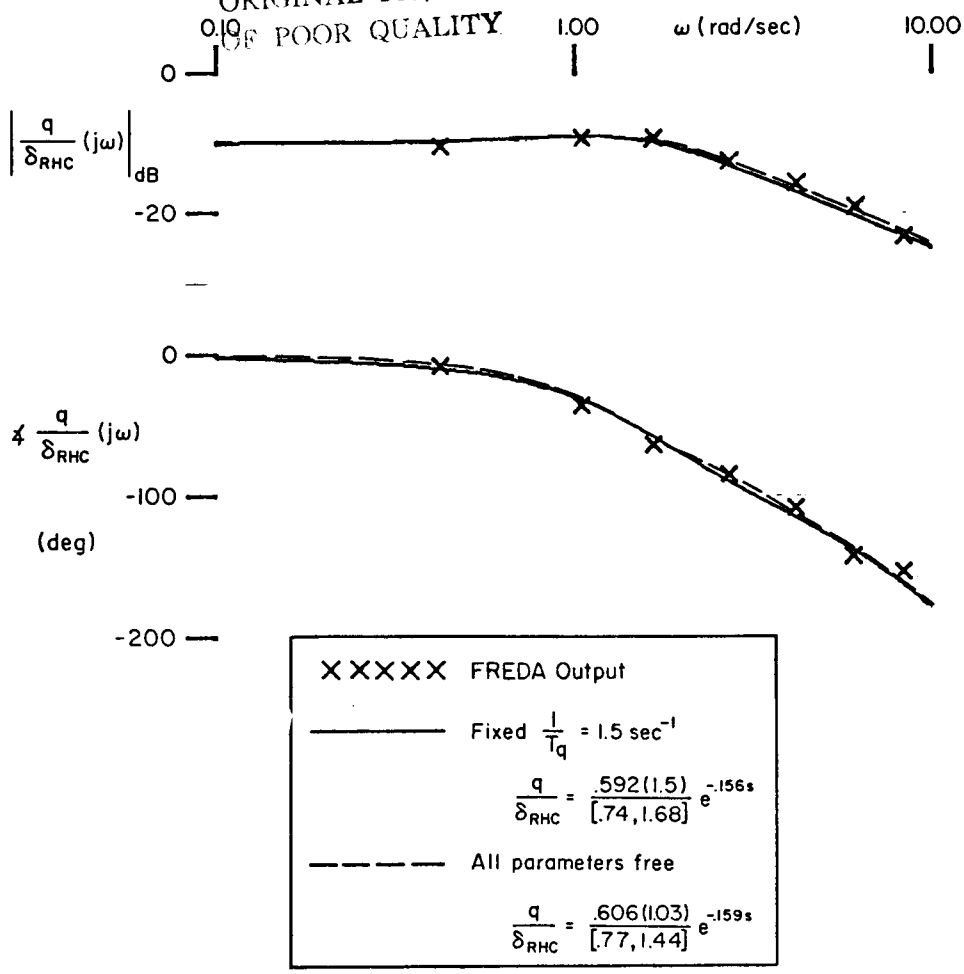

a) Frequency Response Of Fitted Superaugmentation Forms Compared To FREDA Output

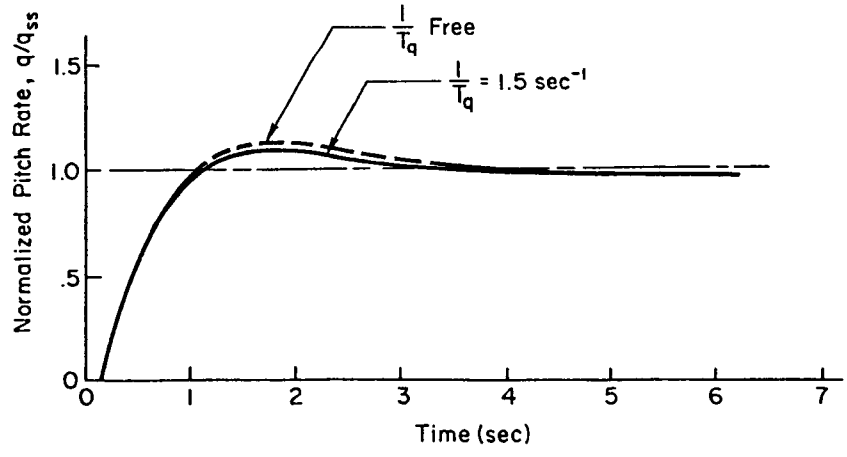

b) Normalized Pitch Rate Response To A δ_{RHC} Step

Figure 26. Comparison of Flight-Derived Effective q/δ_{RHC} with $1/T_q$ Fixed and Free

TABLE 3. COMPARISON OF PARAMETER EXTRACTED FROM STS-4 FLIGHT DATA WITH THE SUPERAUGMENTATION MODEL

PARAMETER	SUPERAUGMENTED MODEL (Eq. 21)	EXTRACTED FROM STS-4 FLIGHT	
		$1/T_q$ = 1.5 r/s	$1/T_q$ free
$q/\delta_{RHC}(0)$ (rad/rad/sec)	0.17	0.31	0.30
$1/T_q$ (rad/sec)	1.5	1.5	1.03
ζ	0.5	0.74	0.77
ω_n (rad/sec)	1.5	1.68	1.44
τ (sec)	0.174	0.156	0.159

From the standpoint of flight validation of the superaugmentation model, probably the most important issue is whether the attitude zero is really closer to $1/T_q$ than to $1/T_{\theta_2}$. This issue may be addressed by considering an alternative fit to the FREDA data with the attitude zero constrained to $1/T_{\theta_2} \doteq 0.50$ rad/sec. Figure 27 shows such a comparison in terms of asymptote fits for the transfer function parameter values of Fig. 26, and for a $1/T_{\theta_2}$ fit with ω_n = 1.5 rad/sec. For this alternative fit there is a significant region of +20 dB/decade slope which is inconsistent with the low frequency FREDA points. In this connection it should be noted that these FREDA points are averages of three "raw" FFT points, and are reliable within the context of this comparison. No adjustments of ω_n would provide a satisfactory fit using the $1/T_{\theta_2}$ value.

2. STS-5 and -7 Flight Data

As additional flight data became available, the FREDA program was again applied to determine the repeatability of the results. The describing function summaries comparable to Fig. 24 are shown for STS-5 and -7 in Figs. 28 and 29, respectively (from Ref. 4). The discrete

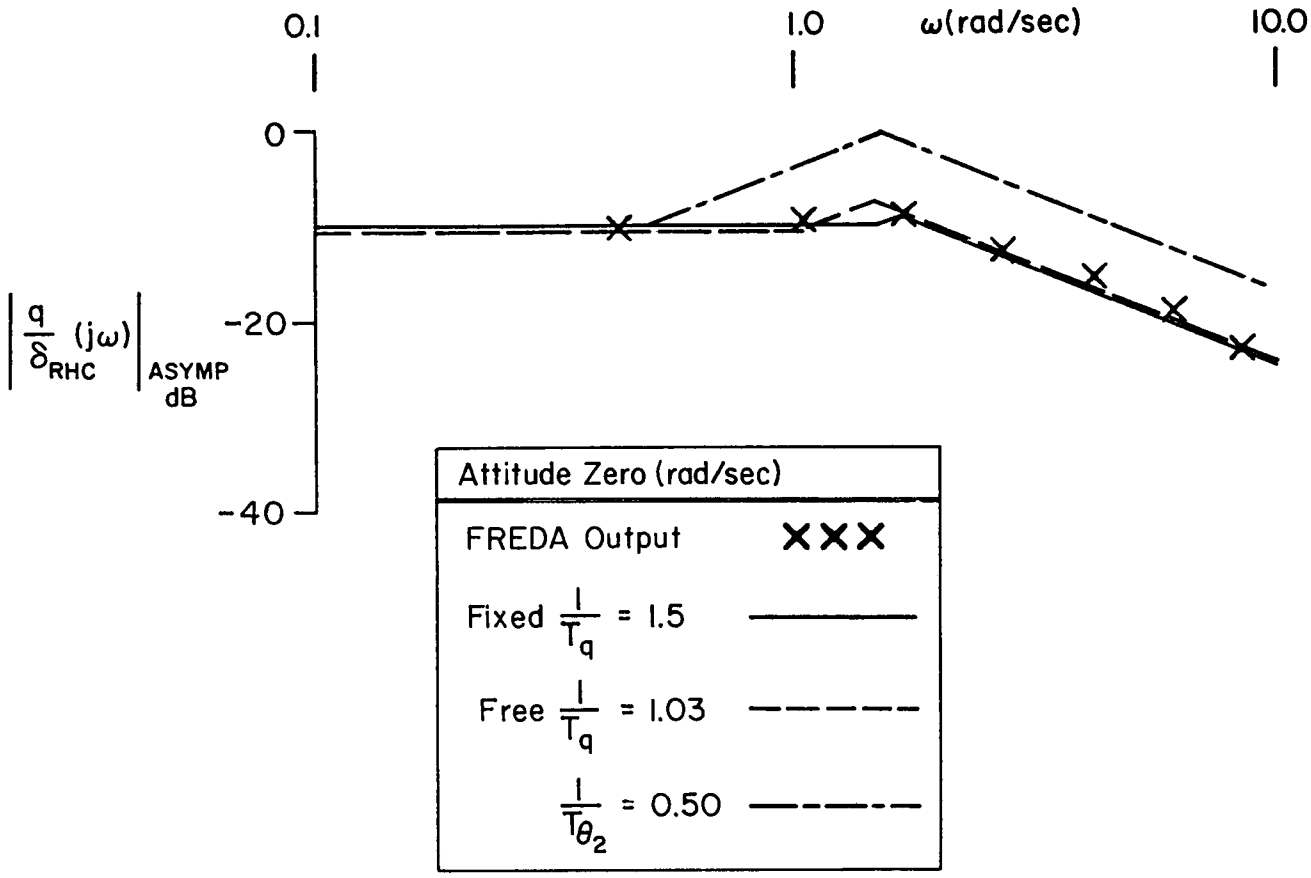

Figure 27. Asymptotic Comparison of $|q/\delta_{RHC}|$ with Three Different Numerator Constraints

frequency response data is superimposed for the three flights in Fig. 30, which also contains the superaugmented model form based on the fixed $1/T_q$, STS-4 data fit. Only those points with a correlation coefficient (ρ) greater than 0.8 are shown. Figure 30 shows that with respect to the major issues in the superaugmentation response, i.e., the effective attitude lead and time delay, there is no indication of a significantly different interpretation than that the effective attitude lead is dominated by the FCS parameter $1/T_q$.

The slight difference in the flight data amplitude at the 1 rad/sec frequency point for STS-7 (Challenger) vs. STS-4 and -5 (Columbia) may reflect a small decrease in $1/T_q$ due to FCS gain changes. The very close agreement of the data from the three flights does increases confidence in the technique and results obtained.

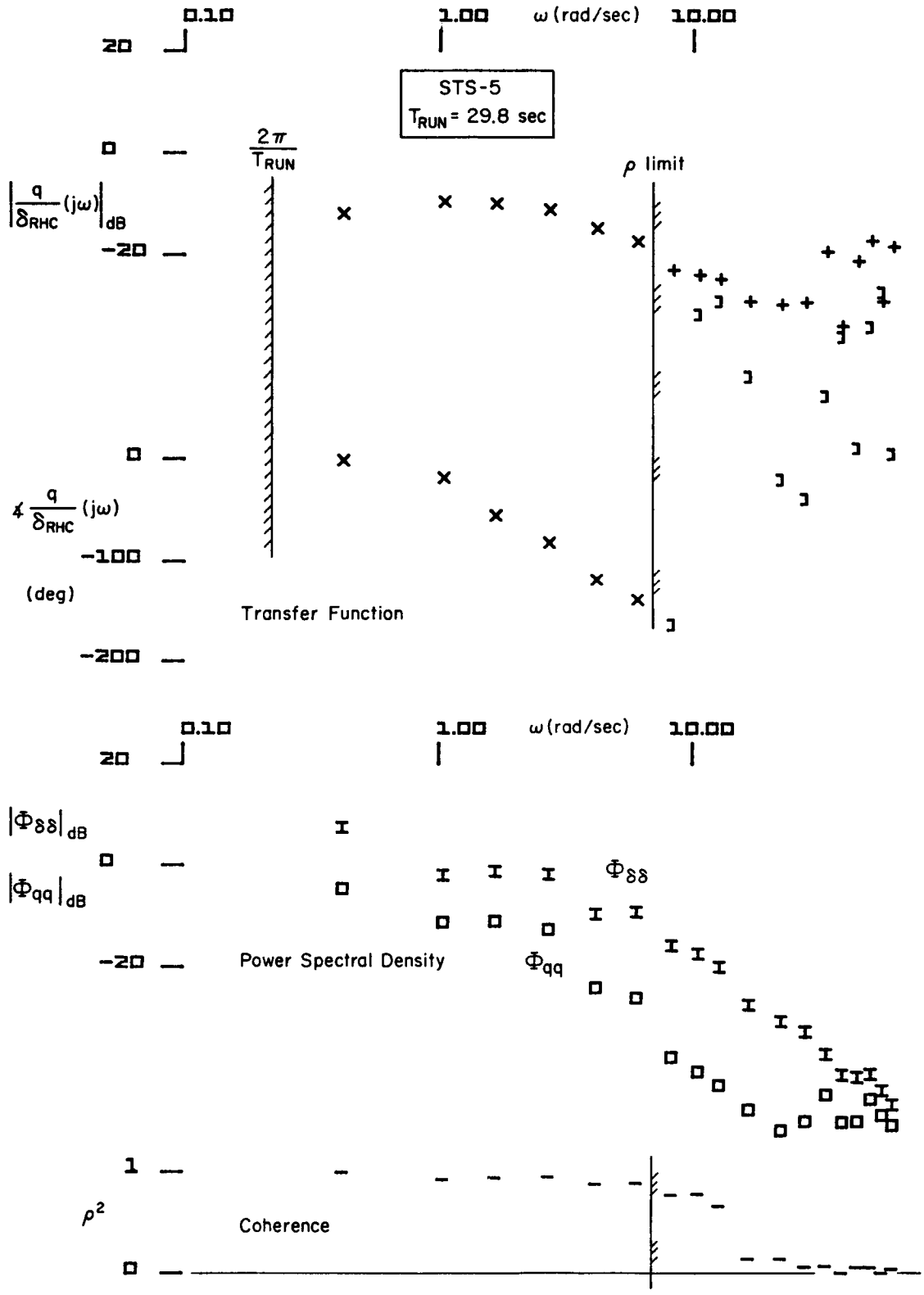

Figure 28. FREDA Output for q/δ_{RHC}, STS-5 Preflare Through Touchdown

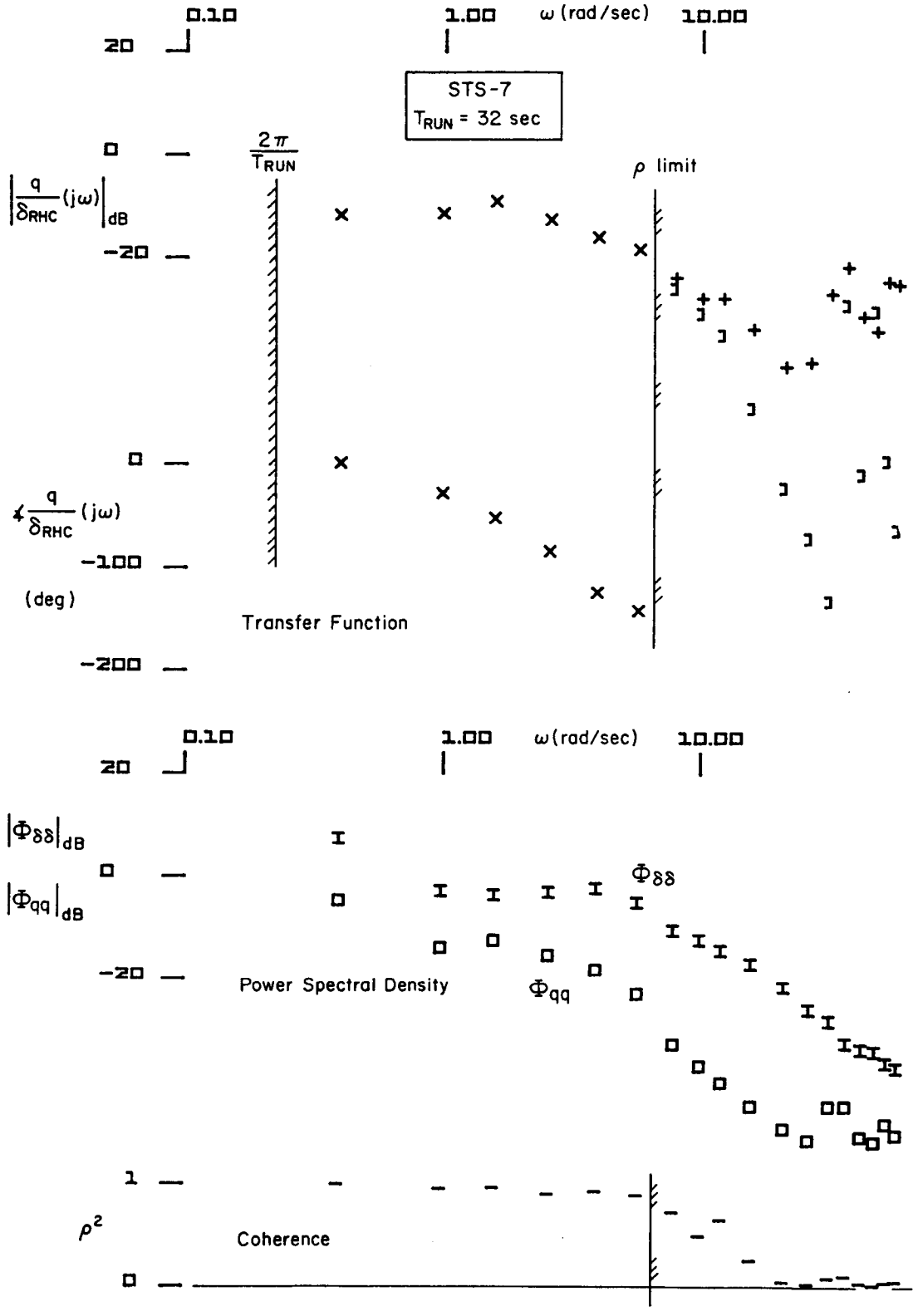

Figure 29. FREDA Output for q/δ_{RHC}, STS-7 Preflare Through Touchdown

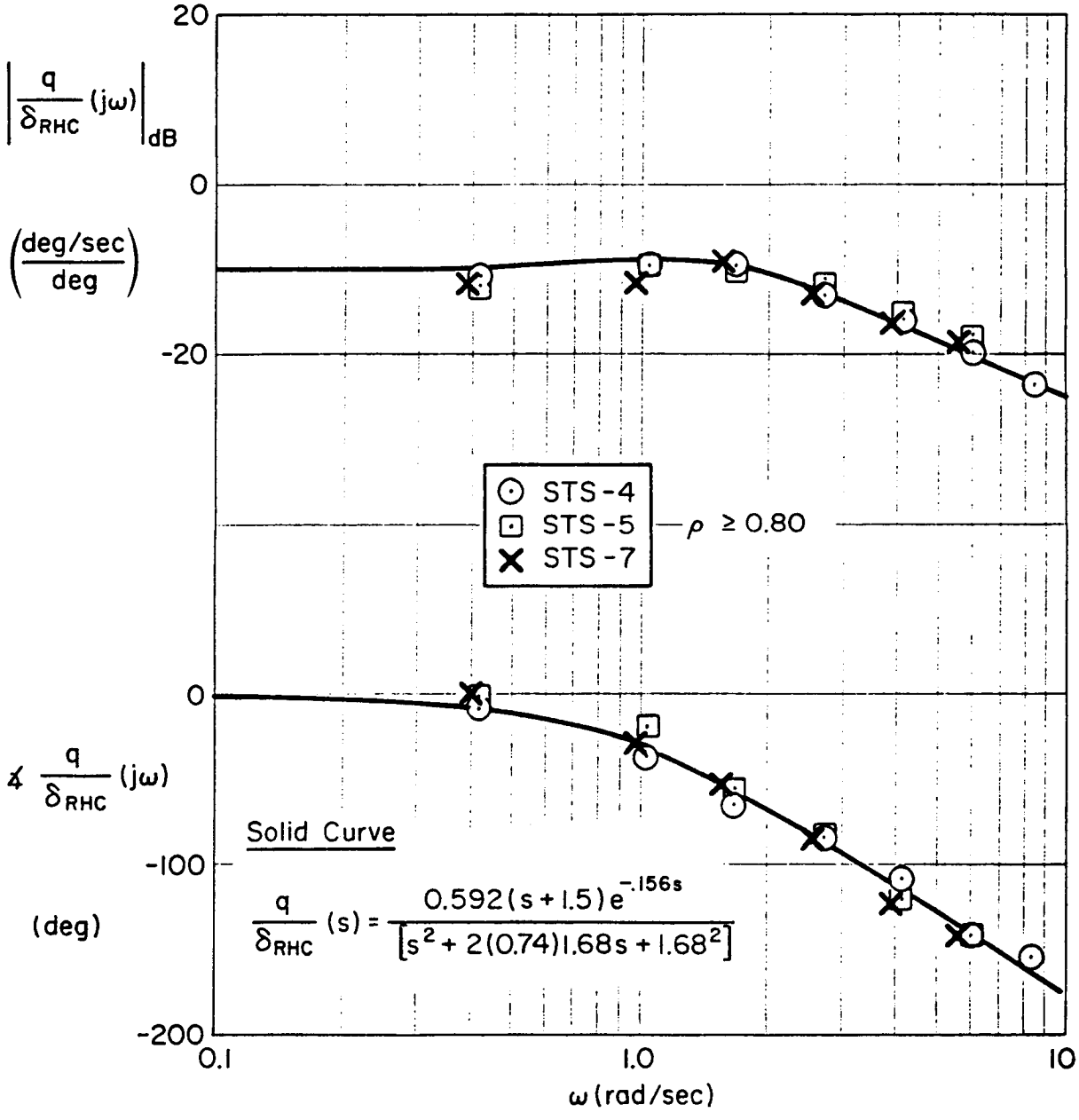

Figure 30. Comparison Between Theoretical Superaugmentation Model and Flight Data

SECTION III

SHUTTLE MANUAL CONTROL IN LANDING

Section III is devoted to prediction and verification of the manual control loop structure, and the influence of different flare strategies in landing. Flight traces are examined for six landings and, with the aid of altitude vs. sink rate phase plane (hodograph) analysis, pilot adopted control strategies and techniques are identified. Final flare strategies are found to run the gamut from highly skilled, precisely timed, single control pulse, precognitive (almost open-loop) step attitude change to an almost continuous input exponential flare via tight pitch attitude control proportional to altitude decay. The latter closely approximates an ideal exponential flare in which sink rate is inversely proportional to altitude. Despite the differing strategies and control techniques, values for key flight path and touchdown parameters extracted from the flight data indicate the pilots concern for touchdown sink rate and velocity as opposed to runway position.

A. PILOT STRATEGY IN LANDING

1. Strategy and Manual Control

In this section we will examine OFT flight data from the perspective of manual control theory focused on the landing task. The goal of this section is to develop insights and understanding of the shuttle landing task and the impact of the FCS design.

The landing task has always been critical in flight control design, but experience with the shuttle and other advanced aircraft with unconventional FCS characteristics (i.e., superaugmentation) has focused on landing as a task of primary concern. This understanding will provide the basis for consideration of advanced FCS design criteria in the next section.

We focus first on simplified flight mechanics involved in approach and flare path control, i.e., the guidance aspects of approach, flare,

and touchdown. Next we look at the influence of various flare techniques, or strategies, on a hodograph of altitude vs. sink rate. This sets the stage for a similar analysis of actual flight data from STS-2 through -7 to identify the multiloop structure and flare strategy employed by the pilot in each landing.

One of the difficulties of the Orbiter vehicle flying qualities experiment (OFQ) program is that the "experimenter" has no control over the test vehicle configuration or the operational and environmental conditions surrounding the experiment. The shuttle system (vehicle, ground aids, operational constraints, etc.) was in a state of evolution during the first dozen OFT flights. Furthermore, most landings have been a first for each commander and crew, and atmospheric conditions may have played a significant role in several of the landings. However, analysis of the OFQ flight data has been performed with an eclectic approach, and augmented with data from some specific simulations.

A number of local approximations and limiting cases in an overall pilot-vehicle model will be used to examine specific aspects of the task. This approach will be used to decompose the complex problem into comprehensible elements. In general, this examination will procede from an "outer loop" (guidance/flight mechanics) focus down through to "inner" higher frequency attitude and manipulator considerations (treated in the next section). The emphasis here is on developing theoretical connections between the requirements of the task and the implied requirements for flying qualities and flight control system design. Making an analytical connection from task requirements to the flying qualities/flight control system requirements rests on quantitative definition of three elements.

- Vehicle: the aircraft can generally be quantified in precise detail. This is certainly true in the case of the shuttle and, in addition, valuable simplifications are available from its superaugmentation model which has been defined theoretically and confirmed from flight data analysis (Section II).

- Task: in principal the task can be defined in terms of inequality constraints on specific system variables. For the shuttle landing task, the most basic requirements will include constraints on touchdown sink rate, speed, and distance. Realistic definition of the constraints is essential for strategy analysis, but is complicated by the fact that pilots apply weightings to physical constraints that are difficult to determine.

- Pilot: the pilot is the most difficult element to define, and the particular difficulties of the OFQ situation have led to an eclectic combination of pilot identification methods. For our purposes here the identification process begins by distinguishing between the pilot's guidance strategy to accomplish the task, and his control activity by which he attempts to implement his strategy.

Here the term "pilot strategy" is applied to the pilot's guidance activities, and the term "pilot behavior" will refer to flight control activity performed to implement the strategy.

- Pilot strategy (guidance activity): generally refers to the pilot's plan for achieving an acceptable trajectory and energy management to meet performance constraints for the task. This is largely a precognitive plan developed from the pilot's experience and simulator training. Feedback structures associated with this activity are generally related to discrete switching from one task phase to the next. The parameters associated with strategy are usually set in these discrete switching steps. Understanding the strategy involves separating what the pilot was attempting to do from the details of what actually happened in a particular flight. A search for landing strategy can be made in the long wavelength shape of the H, $\dot{H}$ phase plane trajectory (hodograph) which we expect to be roughly constant for a well trained pilot over an ensemble of flights.

- Pilot behavior (flight control activity): generally refers to the pilot's closed-loop control activity in response to internal commands derived from his strategy. The details of the behavior seen in response time histories and in the short wavelength activity in the hodographs, will vary

greatly from flight-to-flight; although the spectral content of this activity can be expected to be roughly constant for a well trained pilot. However, the pilot's control activity will tend to interfere with identification of strategy from the hodographs.

The performance constraints which shape the pilots strategy are set by operational and aircraft factors which are independent of the FCS design and flight control factors. Performance constraints arise from factors such as runway length, structural load limits, maximum tire speeds, etc., and can be expressed as inequality constraints on several variables. In general, there will be an upper bound on touchdown distance, X_{TD}, and upper and lower bounds on touchdown sink rate, $\dot{H}_{TD}$. For a decelerating glider like the shuttle, there are also direct constraints on touchdown velocity, V_{TD}. Defining the constraints for analysis is complicated by the fact that pilots apply their own "fuzzy" weightings and subjective adjustments.

In addition to the performance constraints, there are also constraints imposed by the FCS; in particular, control surface rate and deflection limits. A flexible (or at least transparent) control system design will be such that the pilot can select almost any strategy which is feasible with respect to the performance constraints without exceeding FCS limits. Control surface effectiveness, FCS transport lags, and the aircraft dynamic response to the pilot's controllers generally impose limits on the pilot which affect his strategy and influence the manner in which he uses the aircraft control system to implement his strategy. For the shuttle, elevon surface rate limits are critical for the landing task and have lead to the introduction of the PIOS filter (Ref. 7).

Understanding the pilot's strategy and the constraints which influence it is important because this provides the link between task requirements and the pilot's opinion of the aircraft's flying qualities. Strategy must be understood in order to develop commands to inner loop flight control elements in pilot-vehicle models. Pilot's evolve their strategies from experience and training activity with new aircraft and

tasks. For the shuttle, pilot's develop their strategies in simulator (ground based and in-flight) training before ever landing the real vehicle.

Any manual landing will involve a mix of open-loop programmed inputs and closure of feedback loops. A simplified (ideal attitude dynamics) conceptual pilot model for landing is shown in Fig. 31. Experience and training allows the pilot to develop an altitude program (desired trajectory) which is to be executed in an actual landing. The pilot compares his H program to the perceived altitude to form an outer feedback loop.

According to the Successive Organization of Perception theory (Ref. 17), the pilot will develop precognitive control input programs (a θ program as shown in Fig. 31, and ultimately a manipulator (δ_p) program at a more detailed level) as his experience with the task and aircraft increase. If the pilot's H and θ_c programs are consistent, and his perception of H is perfect, H_e will be zero and the landing will be truly open-loop. In actuality some feedback error will occur, i.e., while the pilot may claim to perform an "open-loop" landing, his performance (not to mention his confidence) would probably be degraded if he was "blind folded" in the flare. A more detailed pilot model might also include distinct $\dot{H}$, θ, and δ_p feedbacks, and corresponding precognitive programs for these variables.

In the OFQ work, altitude-sink rate hodographs (H, $\dot{H}$ phase plane trajectories) have been used as a primary means of identifying pilot strategy and technique. In the following, connections are made between task constraints, elementary strategies, and the resulting hodograph forms. To establish limiting cases this is done first with ideal (instantaneous) sink rate response and then with more realistic aircraft path-to-attitude dynamics under the assumption of ideal attitude response. These ideal cases are then used to provide a context for assessing the actual shuttle landing hodographs.

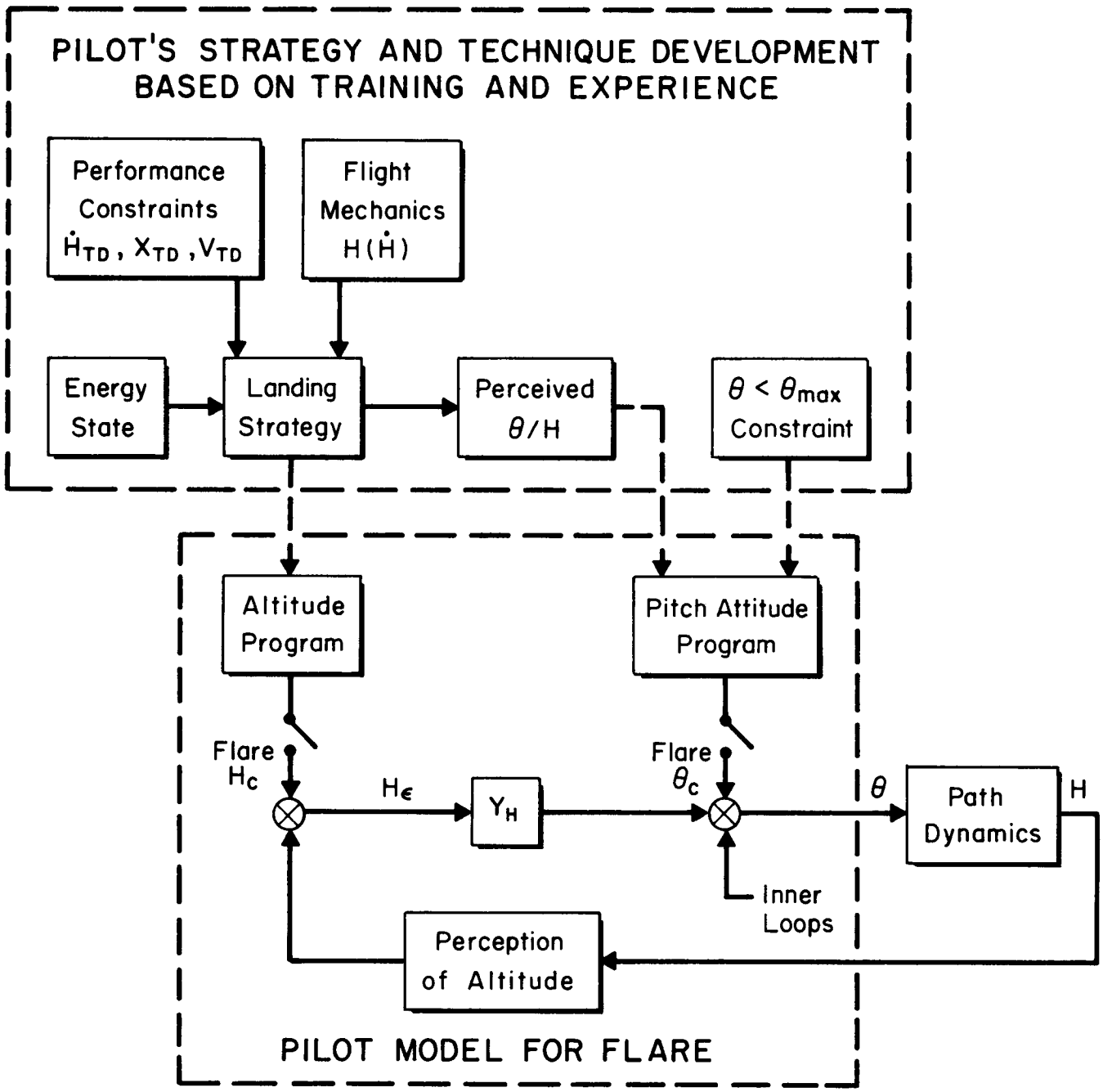

Figure 31. Conceptual Pilot Model for Landing

2. Shallow Glide and Flare Strategy

The shallow glide reduces the decelerating shuttle's sink rate to the order of 10 fps -- about the limit for the main gear at touchdown. The final flare is used to reduce touchdown sink rate to a nominal level of about 1 fps. However, the pilot's strategy for glide and flare must satisfy touchdown speed and distance constraints as well.

To examine the strategy issues, we start with a shallow glide and flare model which begins with the flight mechanics of Section II-A and add some assumptions about the pilot's strategy. The shuttle is assumed to decelerate at a constant rate and the shallow glide is a constant flight path angle from H_o to H_f (see Fig. 32). A final hypothesis is that flare is executed by scheduling sink rate proportional to altitude

$$\dot{H} \doteq -\frac{1}{T_f}(H + H_B) \tag{29}$$

This latter assumption creates an exponentional flare asymptotic to a level H_B below the runway. The model (Refs. 2 and 8) is summarized in Fig. 32. It is implicit in this model that the pilot controls sink rate directly. That is, the attitude and sink rate response to command bandwidths are considered "infinite" -- i.e., well above the inverse flare time constant, $1/T_f$. Thus we are not concerned here with the pilot's attitude control technique or whether this is open or closed-loop. In fact the scheduling of sink rate with altitude could also be either open-loop (precognitive), closed-loop, or a mix of both. What is of interest is what task factors influence development of the strategy rather than details of its execution.

The strategy model goes beyond the relationships of Fig. 32 in the way that the different variables are classified. Here the altitude and velocity at the end of preflare (H_o and V_o) are considered to be given initial conditions (observed values for the STS-2 through -7 analysis). However, these variables are to some extent under the control of the crew through execution of the preflare, and in an extended model they would become strategy variables. The touchdown sink rate ($-\dot{H}_{TD}$), the

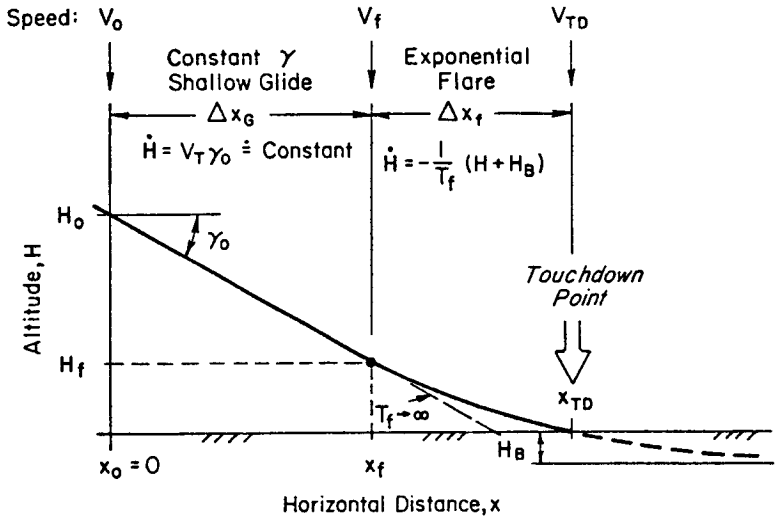

Speed at flare initiation

$$V_f = [2K_v^{\bullet}(H_o - H_f)/\gamma_o + V_o^2]^{1/2}$$

where: $K_v^{\bullet}$ = average $(-dv/dt)$

Depth of flare asymptote

$$H_B = -T_f V_f \gamma_o - H_f$$

Touchdown time measured from flare initiation

$$t'_{TD} = -T_f \ln\left(H_B/(H_f + H_B)\right)$$

Touchdown speed

$$V_{TD} = V_f - K_v^{\bullet} t'_{TD}$$

Touchdown sink rate

$$\dot{H}_{TD} = \gamma_o V_f + H_f/T_f$$

Distance traveled in glide

$$X_g = (H_o - H_f)/\tan \gamma_o$$

Distance traveled in flare

$$X_f = V_f t'_{TD} - \frac{K_v^{\bullet}}{2} t'^2_{TD}$$

Glide and flare distance

$$X_t = X_g + X_f$$

Figure 32. Summary of Glide and Flare Landing Model

touchdown speed (V_{TD}), and the distance traveled in the shallow glide and flare (X_T), are "constrained variables" which for various reasons must meet the Table 4 performance constraints. (Actually, the constraints of Table 4 are somewhat simplistic and will be reexamined later in light of flight results.) Finally, there are three "strategy variables" that the pilot has at his disposal to accomplish the task: the shallow glide slope angle (γ_o) the flare height (H_f), and the flare time constant (T_f).

Given the above definitions, the landing strategy is idealized as the sequential decision making process in which the pilot first selects a shallow glide slope, then a flare height, and finally a flare time constant. However, the selection of the three strategy variables for a shuttle landing is certainly a long process which evolves over the crew's simulator and STA training, and culminates in the actual landing. The selection of shallow glide slope is now predetermined to the nominal value (-1.5 deg) set up by landing aids. However, at least in the early flights examined here, minimal aids were available, glide slope was probably adjusted by the pilot, and it is treated conceptually as a strategy variable in the model at this stage.

The glide and flare model summarized above has intentionally been maintained as simple as possible, and involves only about a half dozen parameters. The computational problems associated with the model are not particularly difficult; however, even with such a simple model, interpretation of the implications and consideration of it's validity is complex. The difficulty in interpretation stems in part from the inequality constraints (Table 4) which must be examined in multi-dimensional parameter spaces (here three dimensions: γ_o, H_f, and T_f).

To simplify this problem somewhat, we initially consider sensitivity to two strategy variables γ_o and T_f with the third, H_f, fixed. This may be seen in Fig. 33 (from Ref. 3) which is based on applying initial conditions derived from the STS-4 landing and the constraints of Table 4 to

TABLE 4. CONSTRAINTS ON TOUCHDOWN PARAMETERS

Design sink rate at TD: -1.5 fps $> \dot{H}_{TD} > -2.5$ fps
Maximum sink rate at TD: $\dot{H}_{TD} = -9$ fps
Maximum sink rate at TD, crosswind: $\dot{H}_{TD} = -6$ fps
Nominal V_{TD} = 195 kts (329 fps)
Maximum V_{TD} = 225 kts (380 fps)
Minimum $V_{TD} \equiv 0.9$ nominal V_{TD} (296 fps)

the model of Fig. 32. Examination of these curves leads to the following indications for strategy development.

- For γ_o near nominal, the pilot has very little margin on T_f below the nominal $T_f \doteq 2$ sec to avoid $\dot{H}_{TD} > 0$ (ballooning). However, there is considerably more margin for larger T_f with respect to the main gear $\dot{H}_{TD}$ limit.

- For a given value of T_f, shallow γ_o leads to ballooning ($\dot{H}_{TD} > 0$). This is consistent with STS-3 crew comments that low flat approaches in the STA are prone to ballooning.

- For γ_o values near nominal, the pilot's T_f margin is reduced greatly in crosswinds due to the reduction in the crosswind $\dot{H}_{TD}$ limit.

- If the pilot executes a slow flare, i.e., $T_f >$ 10 sec, the importance and roles of γ_o and T_f are reversed. T_f no longer makes significant difference, and touchdown speed and sink rate are essentially determined by γ_o. In this situation T_f adjustments cannot make up for an improper γ_o decision made earlier unless the pilot employs a "fast T_f," precise flare strategy.

- Control of touchdown speed is essentially a matter of how soon the vehicle touches down. Since it is decelerating, touching down quickly implies high touchdown speed and vice versa.

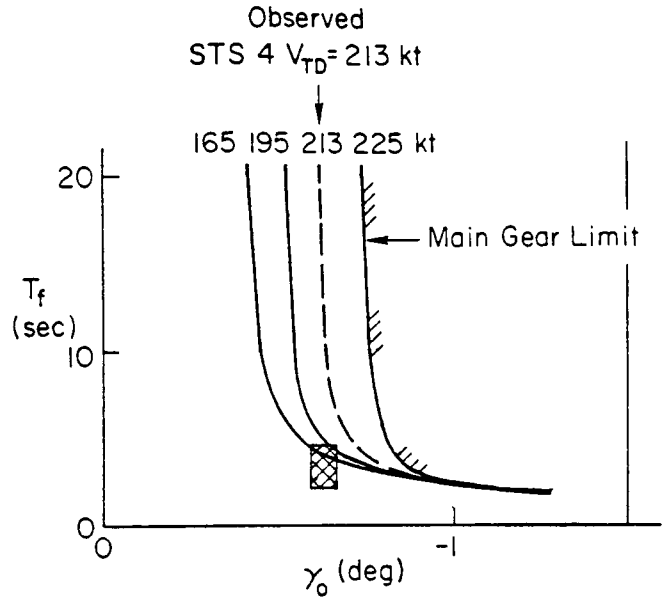

b) Touchdown Speed

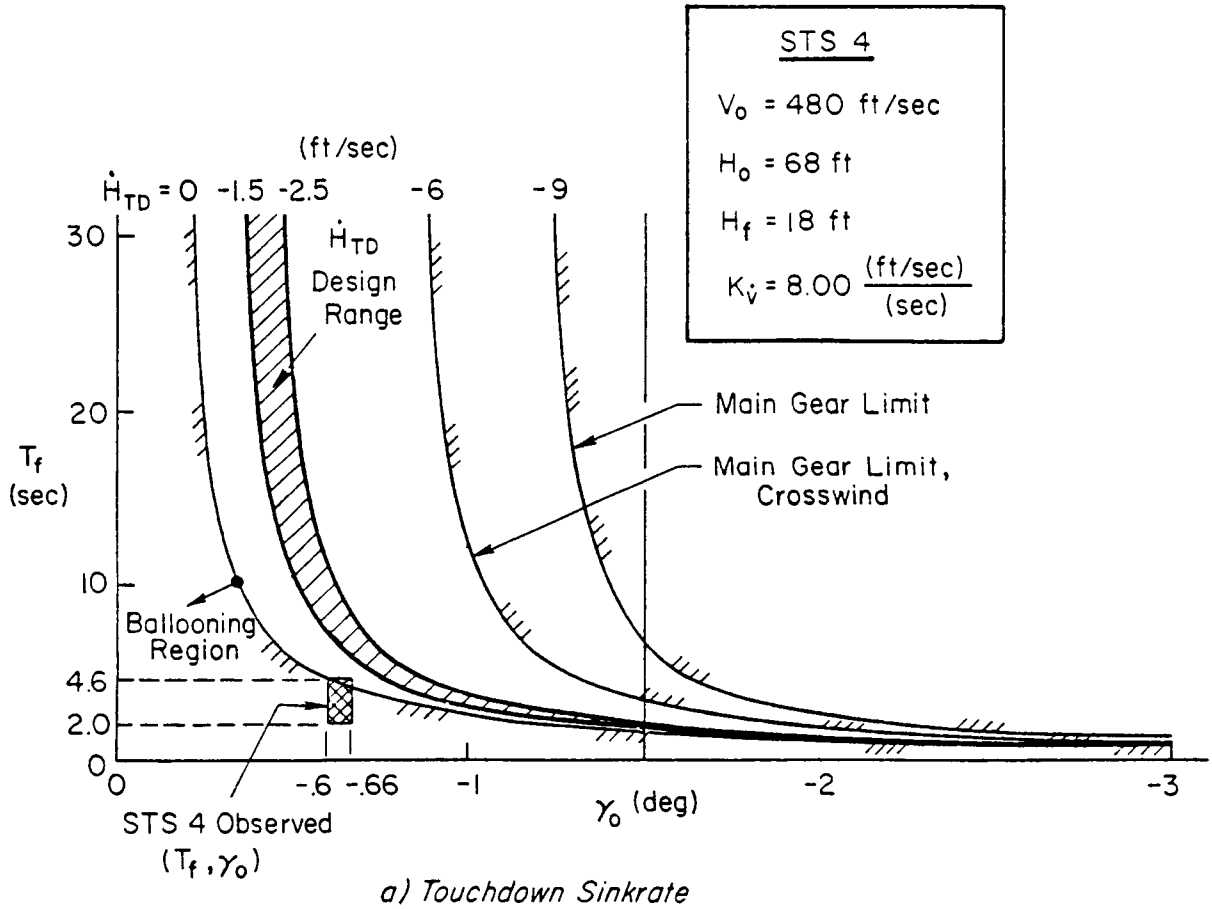

a) Touchdown Sinkrate

Figure 33. Variations of Touchdown Parameters in the Pilot's T_f-γ_o Control Plane (Based on Experimental Flare Model and Initial Conditions from STS-4)

3. Flare Strategies

To this point we have considered a two parameter (γ_o, T_f) strategy. In the early landings before shallow glide landing aids (ball-bar indicator, HUD) were available, γ_o varied significantly from the nominal value and the pilot's adjustment of γ_o was probably a significant part of his strategy. We shall see that in later flights (after STS-5), there is an indication that the aids available were employed to come close to the nominal value, γ_o = -1.5 deg. Thus in the next analyses we will consider γ_o fixed at the nominal value. This will allow considering flare strategies other than the $\dot{H} \sim H$ exponential flare. While the exponential flare is a good working hypothesis, there are other possibilities which need to be considered in the detailed examination of the flight hodographs to follow. We consider these possibilities next; first retaining the assumption of direct sink rate control by the pilot, then relaxing this by considering realistic path-to-attitude response with direct pilot control of attitude.

The trajectory of an idealized flared landing is shown in Fig. 34. The aircraft is assumed on the nominal glide slope ($\gamma = \gamma_o$) until the flare altitude H_f is reached, where a positive perturbation (h) in altitude is initiated to arrest the sink rate. The flare extends touchdown to a point X_{TD} beyond the glide slope intercept (X=0). Note that the origin is now at the glide slope intercept which is fixed in the runway; whereas, the flare initiation point (X_f) will vary with pilot strategy.

a. Flare with Idealized Sink Rate Control

Continuing from the previous case, we pretend the pilot can instantaneously change incremental sink rate $\dot{h}$. The problem will be further simplified by assuming constant total speed V_o and no wind. The total sink rate $\dot{H}$ is then

$$\dot{H} = \gamma_o V_o + \dot{h} \tag{30}$$

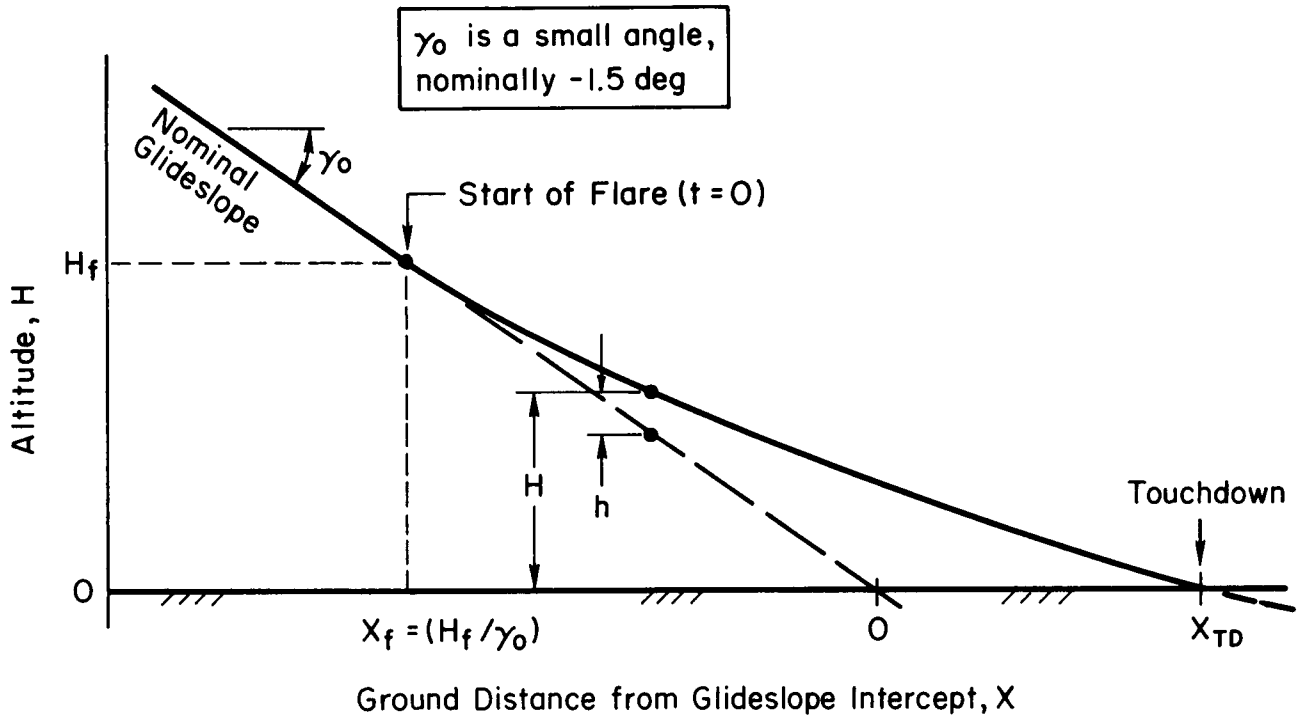

Figure 34. Flared Landing Trajectory

and the total altitude H during the flare (see Fig. 35) is

$$H(t) = \gamma_o V_o t + \int_o^t \dot{h}(t)dt + H_f \qquad (31)$$

where time t is measured from the start of flare. Distance from the glide slope intercept is

$$X \doteq V_o t + H_f/\gamma_o$$

Note that $t > 0$ when $X=0$.

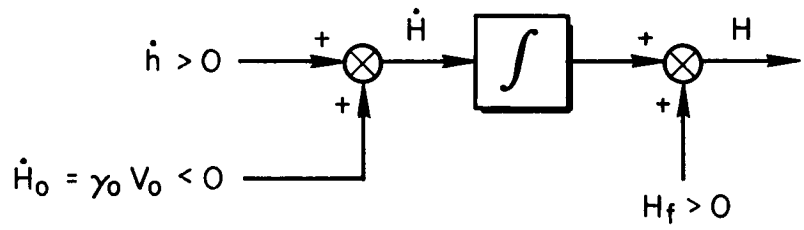

Figure 35. Ideal (Infinite Bandwidth) Aircraft Model

1) Step $\dot{H}$ Strategy

Figure 36 shows the characteristics of a "two slope" flare resulting from a perturbation sink rate ($\dot{h}$) step. The step characteristic is reflected in the H, $\dot{H}$ hodograph. The total sink rate and altitude are

$$\dot{H} = \gamma_o V_o + \dot{h} \tag{32}$$

$$H(t) = (\gamma_o V_o + \dot{h})t + H_f \tag{33}$$

The time (measured from flare initiation) for touchdown, t_{TD}, is found by setting H(t)=0 to be:

$$\begin{aligned} t_{TD} &= -H_f/(\gamma_o V_o + \dot{h}) \\ &= -H_f/\dot{H}_{TD} \end{aligned} \tag{34}$$

The touchdown distance from the glide slope intercept is

$$X_{TD} = -H_f V_o/\dot{H}_{TD} + H_f/\gamma_o \tag{35}$$

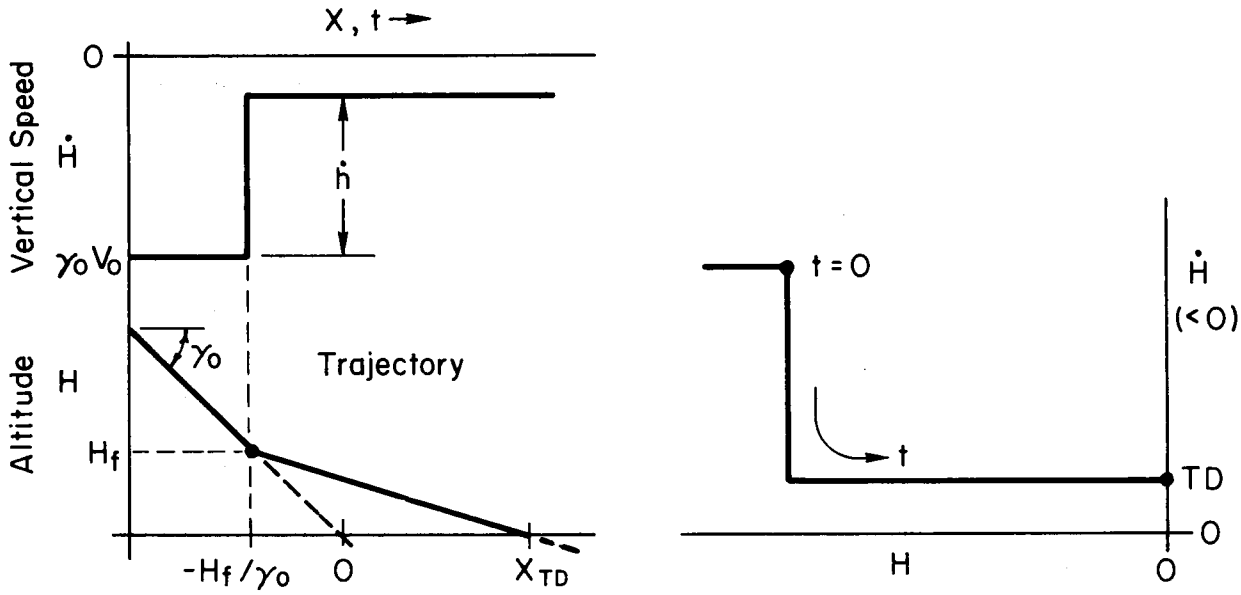

a) Vertical Speed and Altitude as a Function of Ground Distance

b) Altitude-Sink Rate Hodograph

Figure 36. The "Step $\dot{H}$" Landing Strategy for an Ideal Aircraft

This relation is plotted in Fig. 37 in the X_{TD}, $\dot{H}_{TD}$ "constrained variable plane" for various flare heights, and can be used to examine the impact of constraints. Consider the hypothetical constraints shown in

$$0 < X_{TD} < 4000 \text{ ft} \tag{36a}$$

$$-1.5 > \dot{H}_{TD} > -2.5 \text{ fps} \tag{36b}$$

Fig. 37. It may be seen that these impose an upper limit on the pilot's choice of flare height (just over 40 ft). All curves eminate from $\dot{H}_{TD} = \gamma_o V_o$ (the value for no flare), and are asymptotic to $\dot{H}_{TD} = 0$ (corresponding to zero slope for the second leg of the flare). It should be noted that Fig. 37 implies that any $\dot{H}_{TD} > 0$ constraint can be met even as $H_f \to 0$. This is a consequence of the assumed capability for instantaneous γ change, and will not be true when real airplane lags are added.

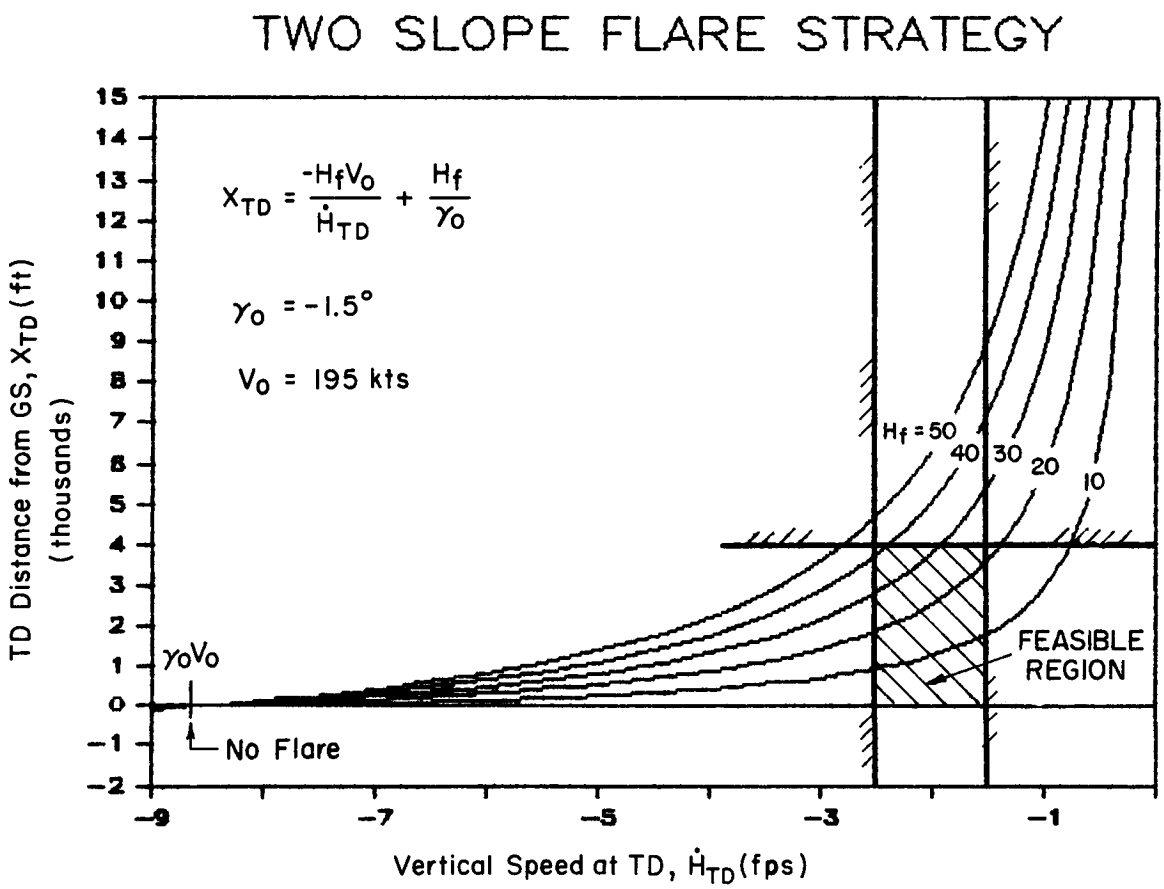

Figure 37. Application of Landing Constraints in the Constrained Variable Plane, "Step $\dot{H}$" Strategy

2) Ramp $\dot{H}$ Strategy

Figure 38 shows an ideal ramp decay of sink rate, which produces a parabolic trajectory and hodograph since

$$\dot{H}(t) = \gamma_o V_o + \ddot{h}t \tag{37}$$

where $\ddot{h}$ is a constant given by $(\dot{H}_{TD} - \gamma_o V_o)/t_{TD}$ and

$$H(t) = \ddot{h}\frac{t^2}{2} + \gamma_o V_o t + H_f \tag{38}$$

C-2

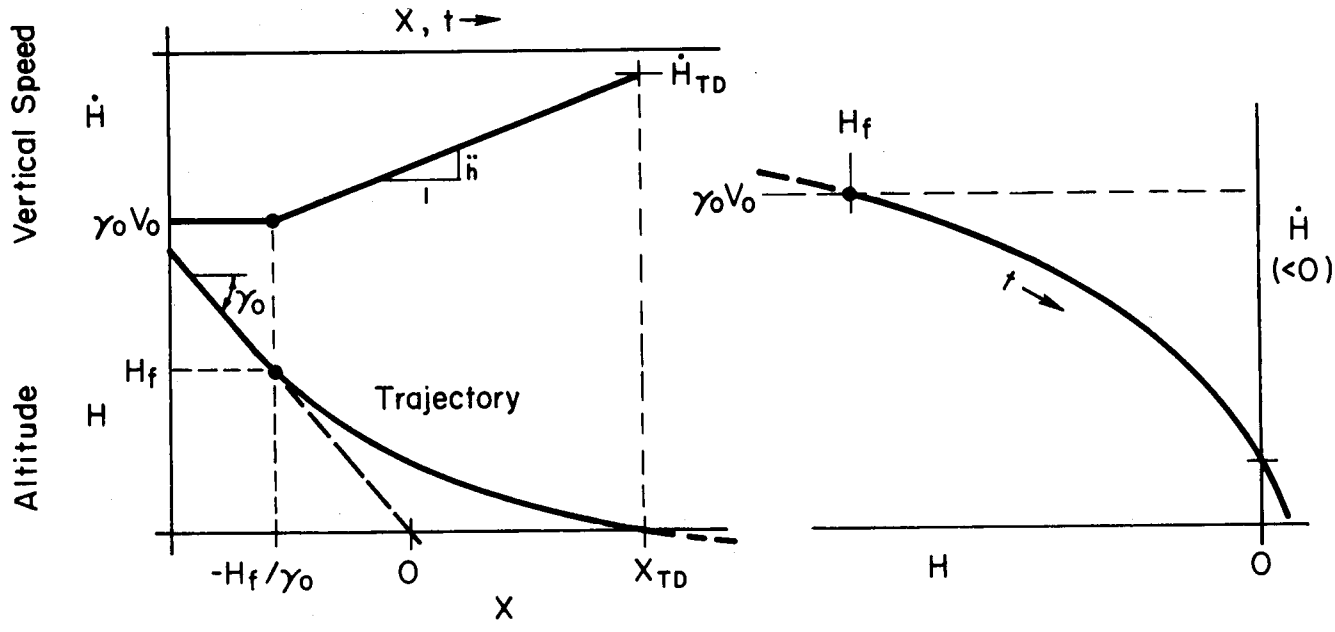

a) Vertical Speed and Altitude as a Function of Ground Distance

b) Altitude - Sink Rate Hodograph

Figure 38. The "Ramp $\dot{H}$" Landing Strategy for an Ideal Aircraft

Figure 39 shows the relation between the constrained variables corresponding to Fig. 37 computed from

$$X_{TD} = \frac{-H_f V_o}{(\dot{H}_{TD} + \gamma_o V_o)/2} + \frac{H_f}{\gamma_o} \qquad (39)$$

This relation is the same as Eq. 35, except that $\dot{H}_{TD}$ is scaled with the "no flare" point fixed; thus, the curves of Figs. 37 and 39 have the same shape except for the scaling of the abscissa. The constraints are much easier to meet in the ramp $\dot{H}$ case, since for a given H_f, the higher initial sink rate reduces time to touchdown, and thus reduces X_{TD}. With a ramp $\dot{H}$, there is also less sensitivity to H_f strategy decisions. However, with a ramp $\dot{H}$, an H_f error which makes the actual H_f lower than nominal will increase the touchdown sink rate (see Fig. 38) -- this would not occur with the step $\dot{H}$ strategy.

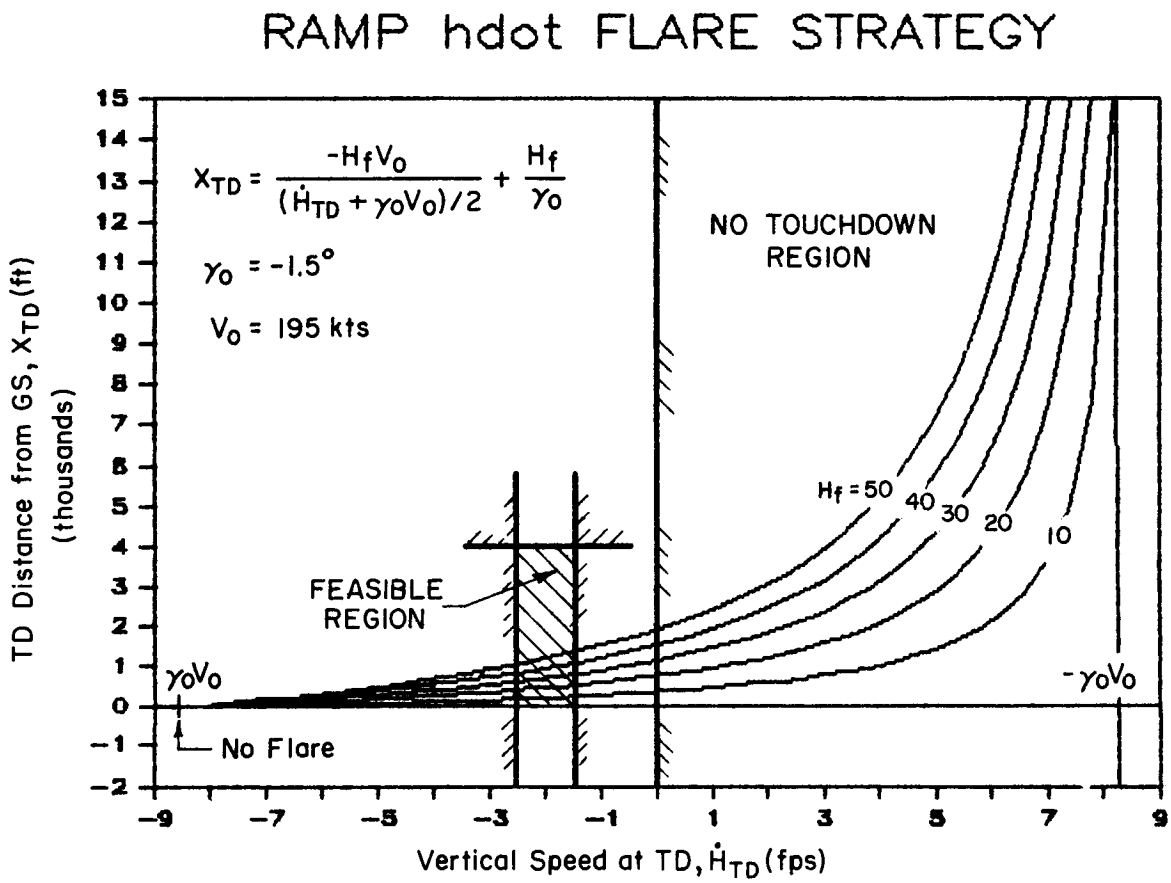

Figure 39. Application of Landing Constraints in the Constrained Variable Plane, "Ramp $\dot{H}$" Strategy

3) Exponential Flare

To combine the best features of both strategies, i.e., low X_{TD} with ramp $\dot{H}$, and low $\dot{H}_{TD}$ sensitivity to H_f errors with the step $\dot{H}$ strategy, an $\dot{H} \sim H$ schedule as sketched in Fig. 40 might be used. The exponential flare considered previously (Figs. 32, 33) is a good candidate in part because it can be approximated with a simple closed-loop control law.

In comparison to the Fig. 33 situation, we now consider the effect of flare time constant T_f as the strategy variable with γ_o and H_f fixed. That is, in the hypothesized multi-stage decision process we consider the final strategy decision as selection of T_f.

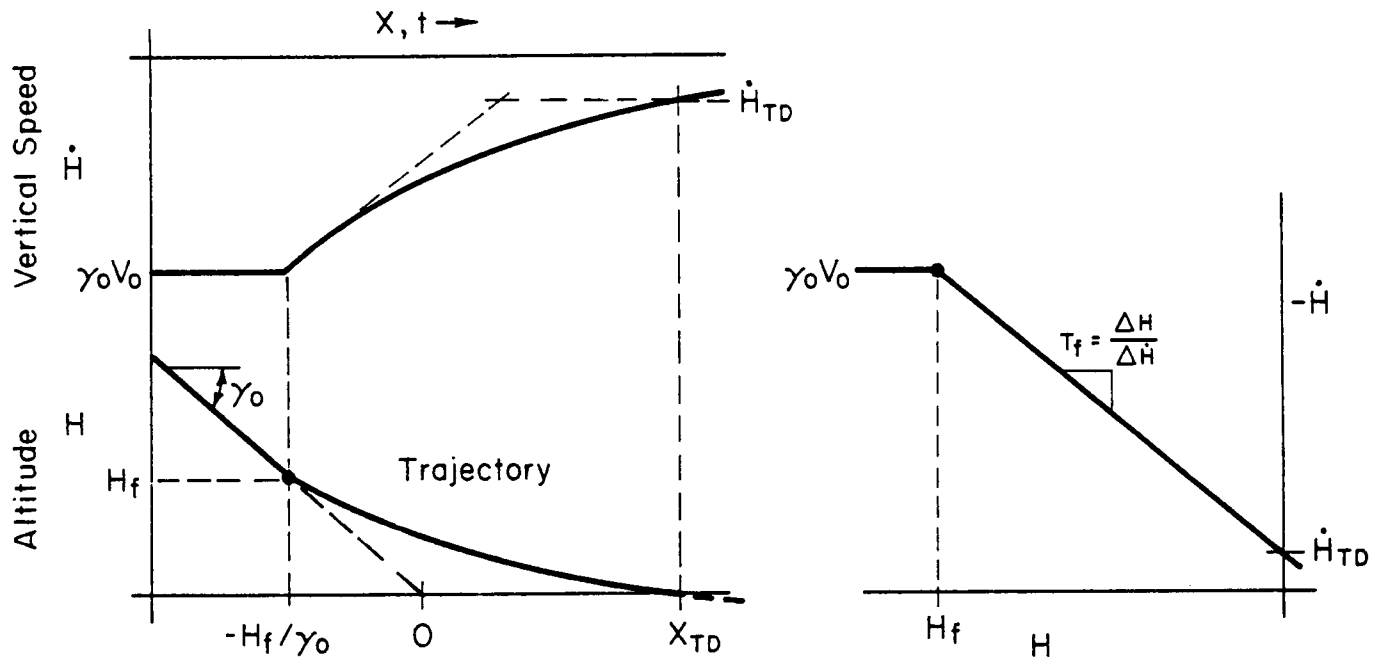

a) Vertical Speed and Altitude as a Function of Ground Distance

b) Altitude-Sink Rate Hodograph

Figure 40. The Exponential Flare Landing for an Ideal Aircraft

The effect of the flare time constant may be examined from the curves of Fig. 41 computed for the nominal conditions indicated in the figure. If the flare is very slow (very large T_f), there is essentially no flare, and the trajectory is an extension of the glide. Thus, the minimum flare distance is

$$(X_F)_{min} \doteq -H_f/\gamma_o \qquad \text{as } T_f \to \infty \tag{40}$$

As T_f is reduced for a faster flare, the trajectory approaches a level parallel to H_B feet below the runway. When T_f is reduced to H_B

$$T_f^* = -H_f/V_f\gamma_o \tag{41}$$

goes to zero, and the runway is approached asymptotically ($X_f \to \infty$). For still lower T_f values, the runway is never reached and a "ballooning"

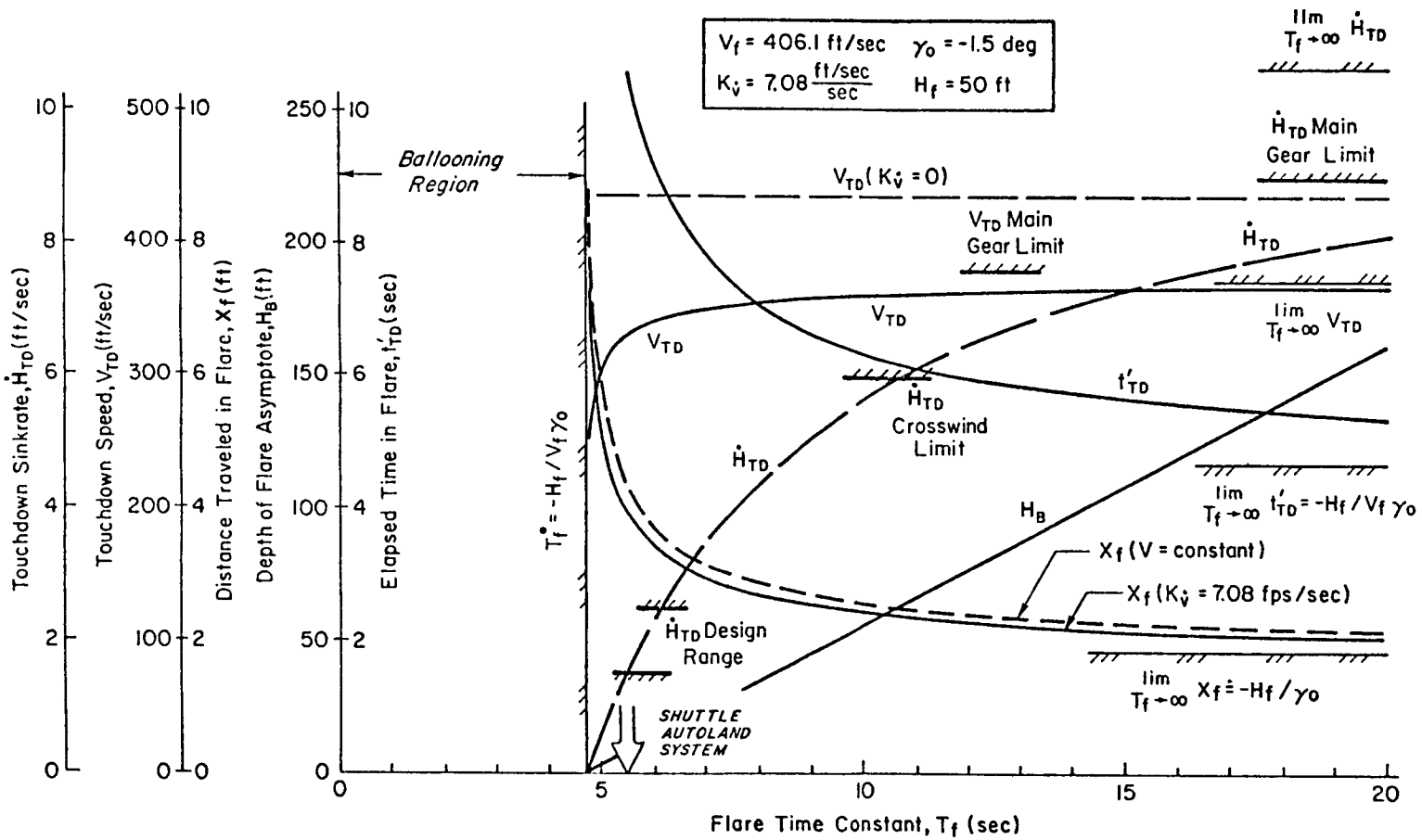

Figure 41. Effect of Flare Time Constant on Touchdown

situation results. Thus for low values of T_f a lower H_f must be selected as implied from Fig. 37. Touchdown speed remains fairly constant until $T_f \doteq T_f^*$, at which point the increasing flare time causes considerable speed bleed off. Touchdown sink rate is strongly affected by the trajectory slope, and thus decreases steadily as $T_f \to T_f^*$.

b. Flare With Idealized Pitch Control

The effects of realistic path-to-attitude aircraft dynamics can now be included as shown in Fig. 42, where θ is the perturbation attitude change from the (stability axis) reference attitude $\theta_o = \gamma_o$. We pretend at this point that the pilot can change θ instantaneously (i.e., the aircraft attitude dynamics have very high bandwidth).

1) Step θ Strategy

The closest the pilot can now come to a step $\dot{H}$ flare is a step θ. Figure 43 shows the step θ trajectory and hodograph for $T_{\theta_2} = 2$ (roughly the shuttle landing value). The two second path-to-attitude lag has reduced the touchdown distance (compared to the ideal $\dot{H}$ step) by 3300 ft because of the lag in the $\dot{H}$ reduction.

Figure 44 shows the effect of H_f variation with a 1.26° step θ. H_f can be reduced to about 20 ft without a significant increase in touchdown sink rate. The hodographs become essentially straight lines with slope $\Delta H/\Delta\dot{H} \doteq T_{\theta_2}$ with low H_f, but the $\dot{H}_{TD}$ becomes unacceptable for $H_f <$ 20 ft.

2) Ramp θ Strategy

The ideal ramp $\dot{H}$ strategy can be approached with a ramp θ input as shown in Fig. 45. For $H_f = 40$, the ramp θ strategy reduces X_{TD} by over 3500 ft compared to a θ step with comparable $\dot{H}_{TD}$. The hodograph shows a concave down parabolic shape similar to the ideal $\dot{H}$ ramp characteristic in Fig. 38.

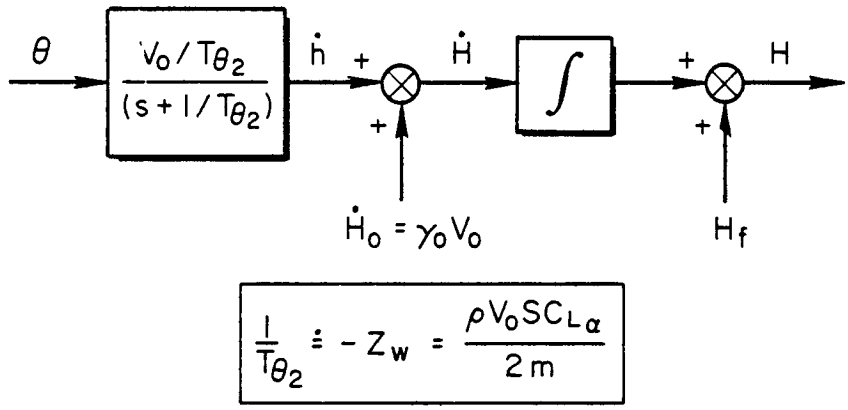

Figure 42. Aircraft Model with Ideal (Infinite Bandwidth) Pitch Attitude Dynamics

B. REVIEW OF LANDING DATA

With the foregoing considerations of pilot strategy hypotheses, we can now turn to examination of actual shuttle landing data.

1. Landing Conditions/Situations

A summary of factors related to the STS-2* through -7 landings, extracted from Refs. 18 through 29, are presented in Table 5. This indicates that there were a minimum of external or head-up landing aids for the first few landings. Also the assistance of the third crew member to reduce cockpit workload was not available until STS-5 and subsequent flights. The commander of STS-4 actually commented that he had difficulty judging preflare, and worked hard during the landing. With the additional aids starting at STS-5, one might expect that the pilot workload to be lower with perhaps improved touchdown performance.

The first four flights were considered test flights, and there was interest in validating performance of the automatic guidance and path

*An in-flight data recorder malfunction resulted in the loss of essential data from STS-1 and thus this first flight is not included in our analysis.

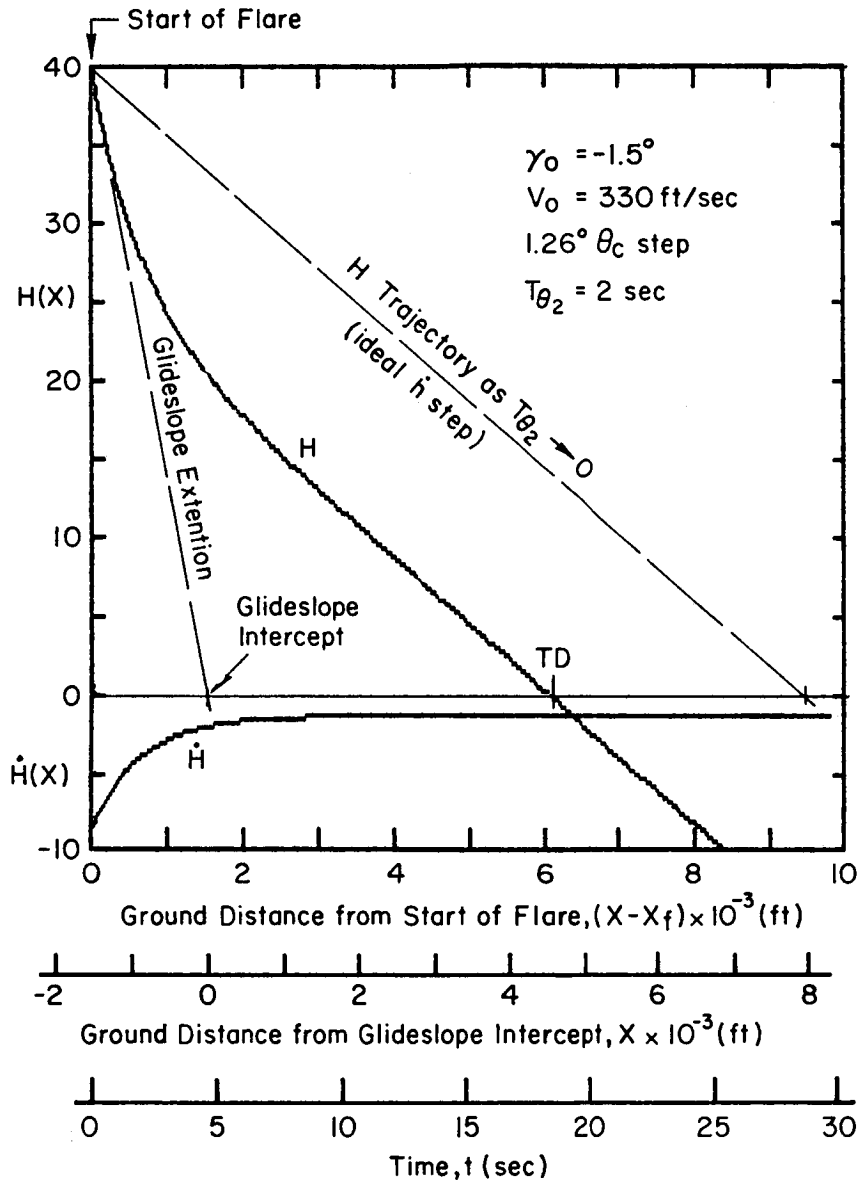

a) Vertical Speed and Altitude as a Function of Ground Distance and Time

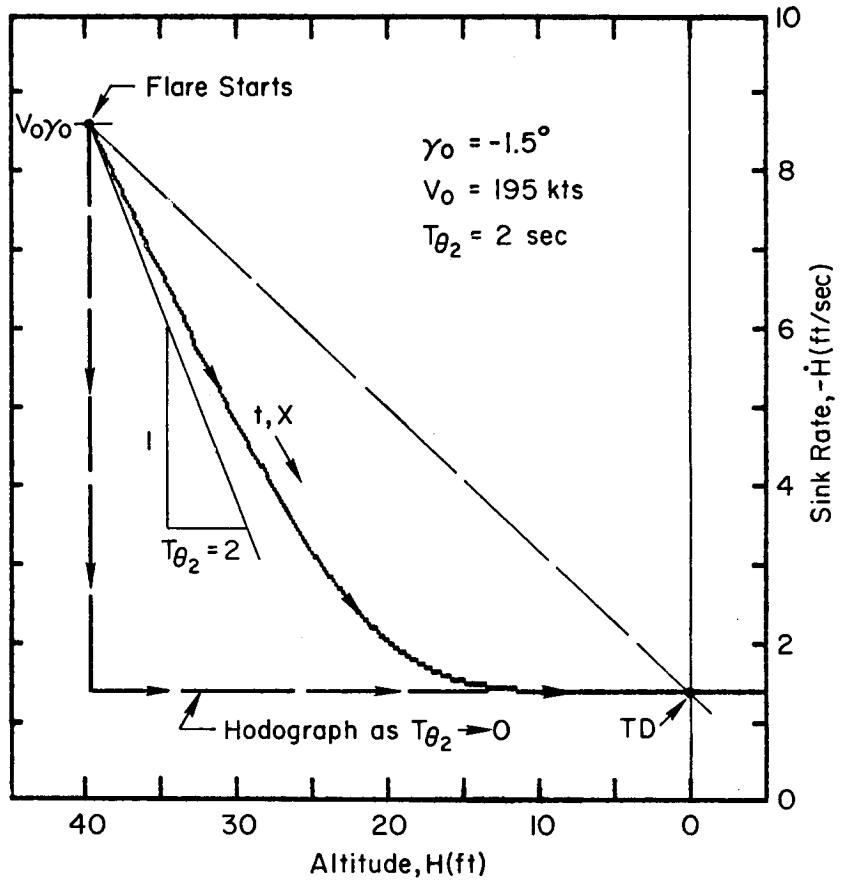

b) Altitude - Sink Rate Hodograph

Figure 43. The "Step θ" Strategy for an Aircraft with Ideal Pitch Response

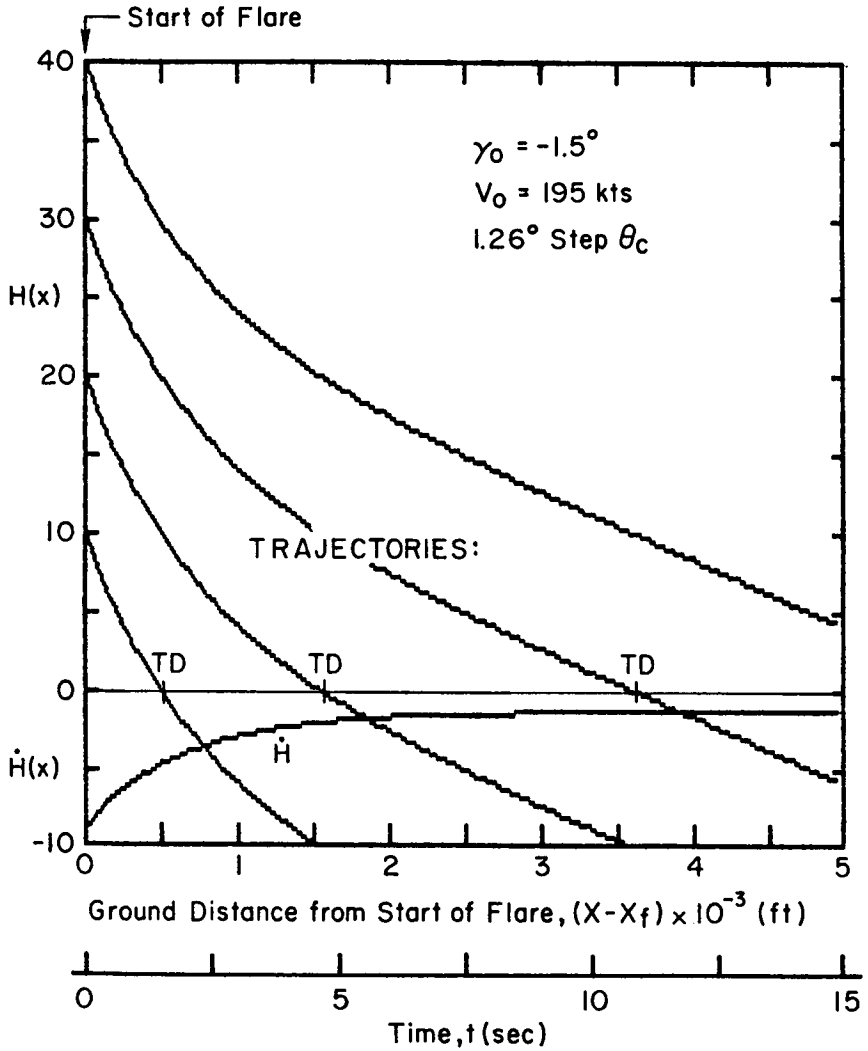

a) Vertical Speed and Altitude as a Function of Ground Distance and Time

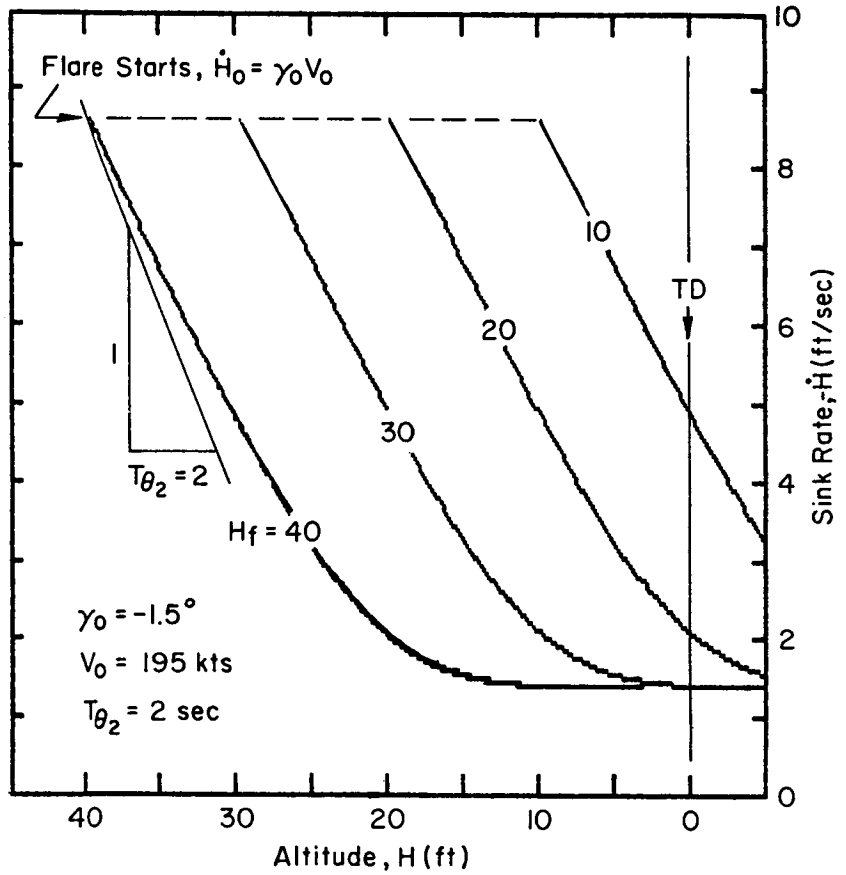

b) Altitude - Sink Rate Hodograph

Figure 44. The Effect of Flare Height Variation with the "Step θ" Strategy

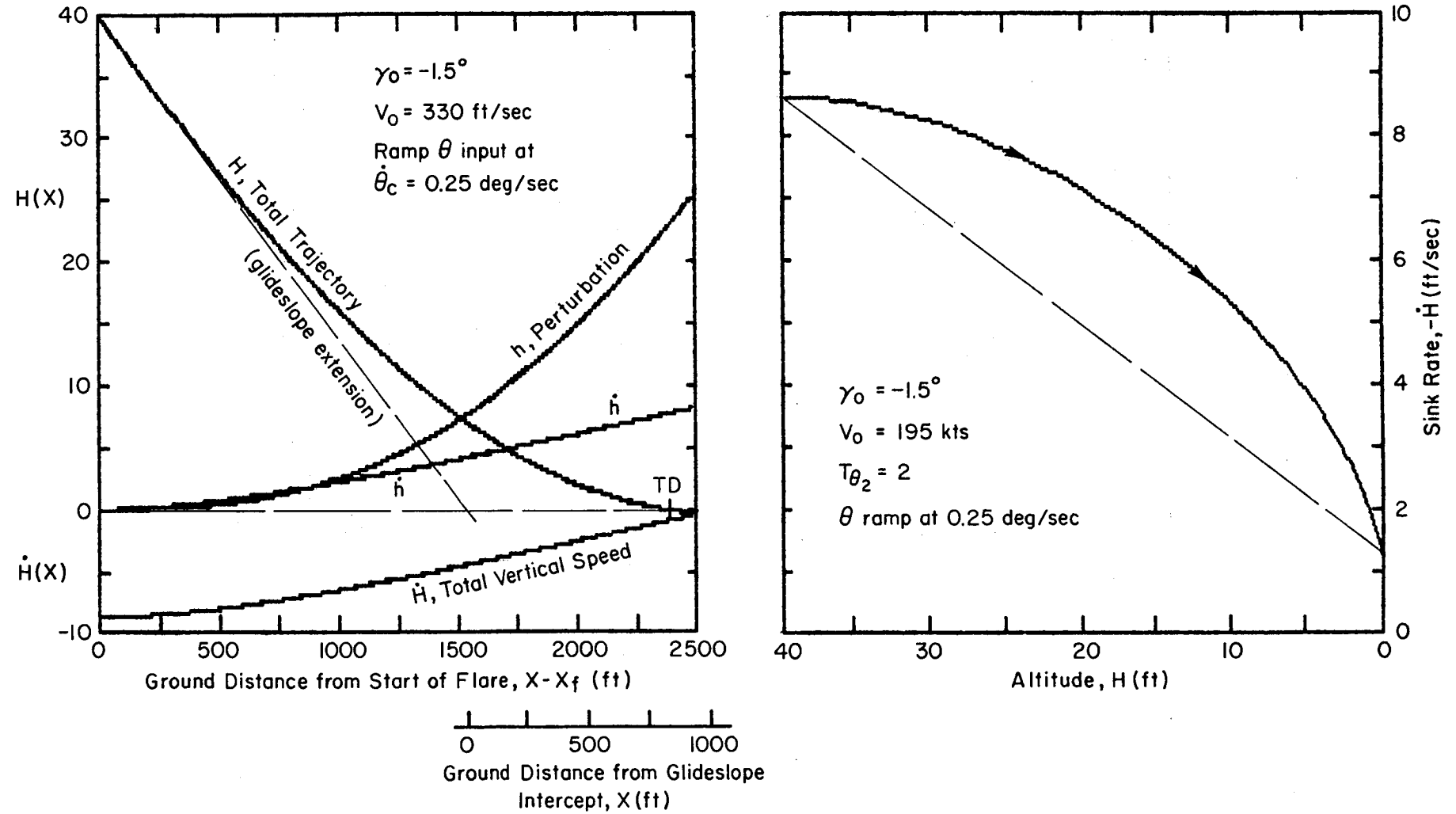

a) Vertical Speed and Altitude as a Function of Ground Distance

b) Altitude Sink Rate Hodograph

Figure 45. The "Ramp θ" Strategy for an Aircraft with Ideal Pitch Response

TABLE 5. ORBITER APPROACH AND LANDING CONDITION SUMMARY

FLIGHT	STS-2	STS-3	STS-4	STS-5	STS-6	STS-7
AIDS						
PAPI LIGHTS	NO	NO	NO	YES	YES	YES
BALL-BAR	NO	NO	NO	YES	YES	YES
HUD	NO	NO	NO	NO	YES	YES
3rd CREWMAN	NO	NO	NO	YES	YES	YES
MANUAL						
TAKEOVER ALT.	2000'	120'	2500'	HAC	HAC	HAC
PREFLARE	1750'	AUTO	?	1750'	?	1750'
TOUCHDOWN						
SURFACE	LAKEBED	SAND STRIP	RUNWAY	RUNWAY	RUNWAY	LAKEBED
DISTANCE	SHORT	SHORT	SHORT	SHORT	SHORT	ON
SPEED	SLOW	FAST	FAST	FAST	FAST	FAST
ENVIRONMENT						
VISIBILITY	CLEAR	BLOWING SAND	CLEAR	CLOUDS ~19K'	CLEAR	CLEAR
WIND	HIGH HEADWIND	HIGH	HIGH	CALM	GUSTY 22 KT HEADWIND	10 KT HEADWIND

control modes leading eventually to a fully automatic landing. Therefore, manual takeover was initiated at different points in the steep glide or preflare on STS-2, -3, and -4. It became apparent on STS-3 that the time required for the pilot to adapt to his closed-loop control task was significant, and that early manual takeover was advisable to provide time for the pilot to obtain a feel for the Orbiter response characteristics and settle into the control task. For the next four flights the crew not only took over manual control for the heading alignment circle (HAC) phase, but retained manual control through to touchdown.

The touchdown surface is of interest in that the lakebed offers a much longer and less constrained landing and rollout target than does the concrete runway. Therefore, touchdown performance is more important for runway landings. This leads to tighter closed-loop control (as demonstrated by the PIO which occurred with the ALT-5 landing) and the need for more precise setup through each of the approach segments leading up to the final flare. Most touchdowns have occurred short of the landing aim point. On STS-2 this might be attributed in part to a low energy state brought about by high winds, an untimely sweep of the speed brake, and re-engagement of the automatic approach/landing system at termination of the HAC. As a result, the crew had to fly a maximum L/D attitude to get to the lakebed. This touchdown was slow and only some 900 ft beyond the runway threshold. The other short touchdowns all occurred at higher than nominal speeds. Pilot comments tend to indicate problems in judging touchdown or in "holding off" touchdown to bleed off airspeed because of being located slightly behind the center of rotation for pitch attitude changes while the main gear is far aft. The pilots not only have problems in judging pitch attitude, but also in judging the sinking of the main gear due to small attitude adjustments to "hold off" the sink rate at the cockpit.

Finally, environmental conditions may have contributed to touchdown problems encountered on STS-3 in that the pilot's visibility and depth perception may have been adversely affected by blowing sand. Gusty winds and a large increasing wind shear from 2500 ft to the ground were

encountered by STS-6. Also for this flight the outer aim point marker was underwater, and the crew was advised to use the inner marker. The crew was then confused as to whether the HUD was aligned to the outer or inner glide slope. This may have increased the workload somewhat.

The foregoing factors should be kept in mind when interpreting the time traces for each landing as presented and discussed in following sections of this report.

2. Extraction of Control Strategies

To briefly review the landing task, the preflare, shallow approach, and flare nominally are individual segments which may involve different control loop structures. The preflare is a constant pitch rate maneuver and vehicle pitch rate, or its equivalent is displayed to the pilot (either head down or up). The superaugmented vehicle dynamics response is that of pitch rate command/attitude hold (RCAH). Pilot actuation of the rotational hand controller (RHC) directly commands vehicle pitch rate. During this flight segment one would expect the time traces to show relatively constant RHC deflection, pitch rate, and normal acceleration.

For the shallow glide portion, the control task is more complicated in that pitch control becomes an inner loop to sink rate or flight path control. The approximate short-term (quasi-steady speed) path to attitude transfer function is

$$\frac{\dot{h}}{\theta} = \frac{sN_{\delta}^{h}}{N_{\delta}^{\theta}} \doteq \frac{U_o}{(T_{\theta_2} s + 1)} \tag{42}$$

where the Orbiter path lag, T_{θ_2} is about 2.0 sec.

The shallow glide and final flare control strategy may be identified from the altitude/sink rate phase plane (hodograph) shown hypothetically in Fig. 46. If the shallow glide region has constant flight path angle γ_o, the phase plane trajectory will be a straight sloping line. If the sink rate is constant, the glide trajectory will be horizontal. In the

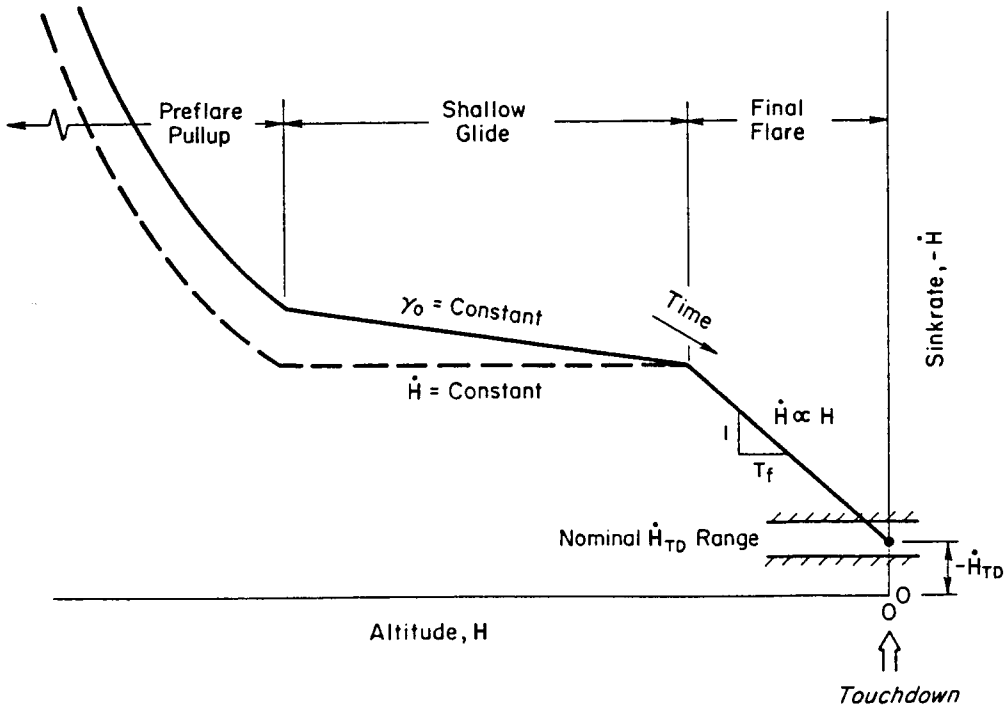

Figure 46. Idealized Altitude/Sink Rate Phase Plane Trajectory for the Shallow Glide and Flare Assuming an Exponential Flare

final flare region, if sink rate is scheduled proportional to altitude (an exponential flare), the phase plane is a straight line with slope $-1/T_f$. The slope reflects the relative weighting given to arresting sink rate as altitude decreases and therefore can vary significantly. If any other relationship is employed, the flare phase plane will be curved as noted in the previous subsection.

Perhaps the easiest strategy for the final flare is to change pitch attitude in a stepwise manner, and let sink rate decay with the open-loop 2 sec (T_{θ_2}) time constant noted above. If sink rate should be controlled in a closed-loop manner as a function of altitude, flare response time constants greater than T_{θ_2} could result. Detection of either of these two path control strategies should be evident from the pilot's RHC inputs. They are also indicated by the flare time constant obtained from the hodograph, i.e., $T_f \doteq T_{\theta_2}$ and little or no RHC activity in the final seconds of the flare indicates precognitive control of sink rate; whereas a $T_f \neq T_{\theta_2}$ implies closed-loop piloted control of

sink rate. Interpretation of the hodographs will be considered further in the following subsection.

a. Time History and Hodograph Views

Time traces and altitude/sink rate hodographs for the STS-2 through -7 landings are presented in Figs. 47 through 57. The RHC, pitch rate, and normal acceleration time traces are from the MMLE database (see Ref. 4). Altitude and vertical speed are from the cinetheodolite database (Ref. 4). The figures which contain only H, $\dot{H}$, and hodograph plots are expanded scale data which covers only the final 10 to 15 sec of the landing. This generally includes the portion of flight which would encompass the end of preflare, shallow glide, and final flare, if such segments are identifiable. It should be noted in the hodographs that the altitude reference point (Orbiter nose) is set to zero ground level at the touchdown point (to remove the 20 to 30 ft nose altitude biases seen in the altitude time histories).

Termination of each path segment and start of the next is generally signalled in the time traces by a larger than usual RHC pulse, which is then followed by a somewhat changed control technique. An excellent example is Fig. 50 in which the discrete pilot inputs that terminate the preflare and initiate the final flare appear quite distinct on the RHC trace. Gaining confidence that these spikes do represent such precognitive pilot activity requires examining the resulting responses in aircraft attitude and normal acceleration, and finally relating these events to "corners" of the hodograph. This process must account at least approximately for the associated vehicle response lags among the state variables. By accepting a certain amount of subjectivity and judgment, shallow glide and final flare initiation points can be defined on the RHC trace for each flight (except STS-2 where recorded data dropout again was encountered). But tracing these discrete events through the attitude and path responses to the hodograph is complicated since "precognitive" pilot inputs are generally more complex than a series of simple impulses. Thus, the effective lag between an identified RHC "event" and the resulting response in the hodograph varies somewhat.

After some iteration the shallow glide and final flare initiation response points have been defined as ⓪ and ⓕ respectively on the hodographs. There is an inevitable subjectivity and uncertainty in the extracted parameters which might ultimately be improved by the use of more sophisticated identification algorithms and computational procedures; however, such steps were felt to be inappropriate at this stage of analysis. Thus, the approach here has been to make a simple best estimate of the basic model parameters, and then examine the implications for the six flights examined. The most fundamental test of the validity of the parameter extraction process is whether or not gross inconsistencies and obvious impossibilities are implied downstream in the analysis.

In all flights an attempt is made to identify each sequential segment; although in some instances the short time span between ⓪ and ⓕ make it unlikely that the segments are indeed separable, rather than one continuous flare to touchdown.

The flights will be analyzed individually in the following:

STS-2 -- The onboard data recording system suffered data dropout during most of the time segments of interest (Fig. 47a). However, the relatively smooth responses of the pitch rate and normal acceleration traces are indications the initial preflare was accomplished on autoland. Reversion to manual occurred at about 12 sec on the trace time scale. The flight segments are identified on the basis of the Fig. 47b $\dot{H}$ time trace in which the sudden oscillation is interpreted as an attempt to terminate the preflare and initiate shallow glide. However, the short time span of this transient certainly leaves it open to question as to whether this was the start of final flare. If one assumes the final flare was initiated at f , the average slope for the hodograph between that point and touchdown produces a flare time constant of 2 sec, which is the same as the T_{θ_2} path time constant. Prior to this final flare the hodograph is essentially a straight line which indicates one long exponent preflare with a time constant T_f = 2.84 sec. The generally concave downward trajectory following the point identified as (o) could also reflect a final ramp θ strategy (as in Fig. 45) and the

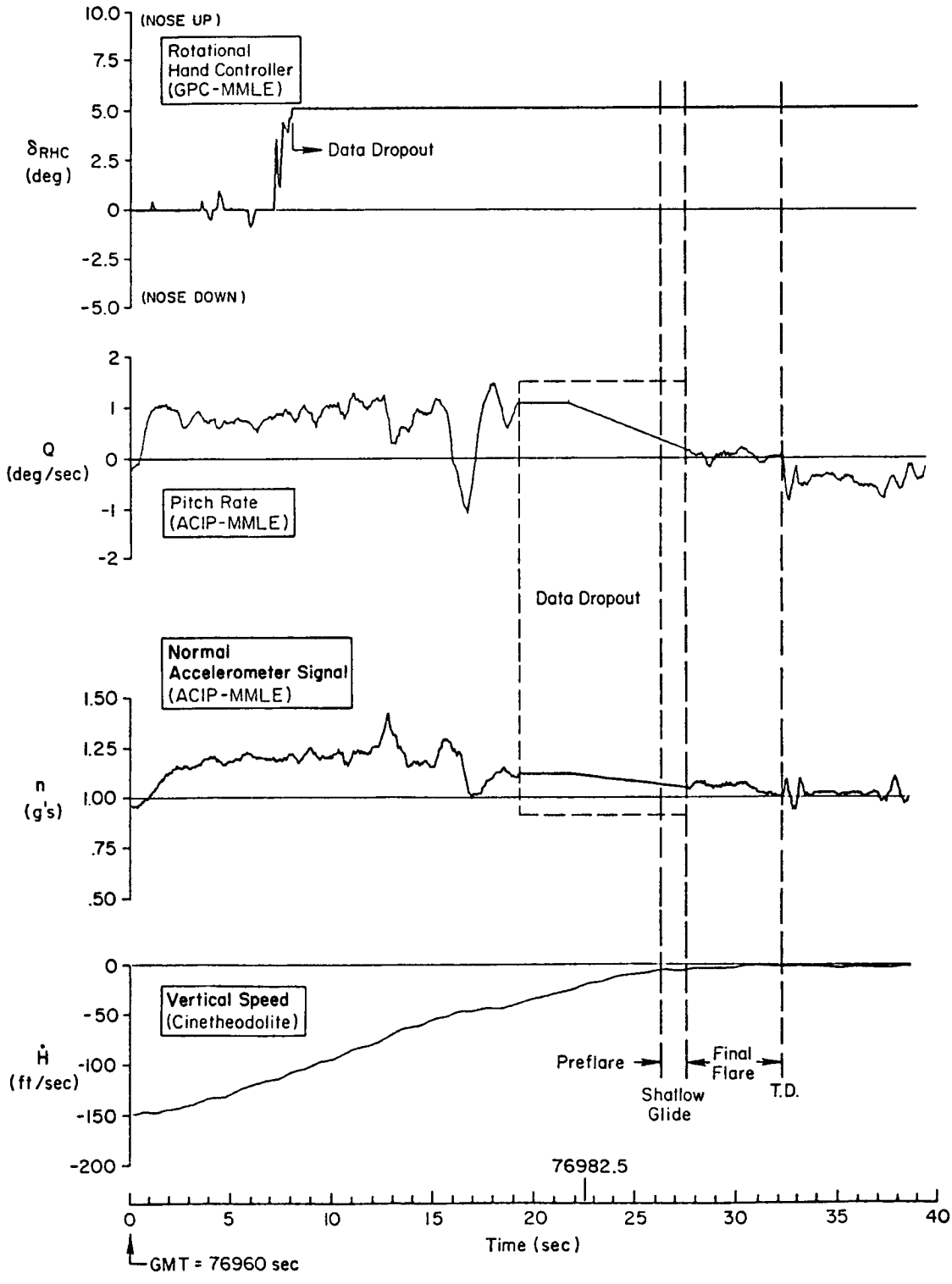

Figure 47a. STS-2 Preflare Through Touchdown Time Traces

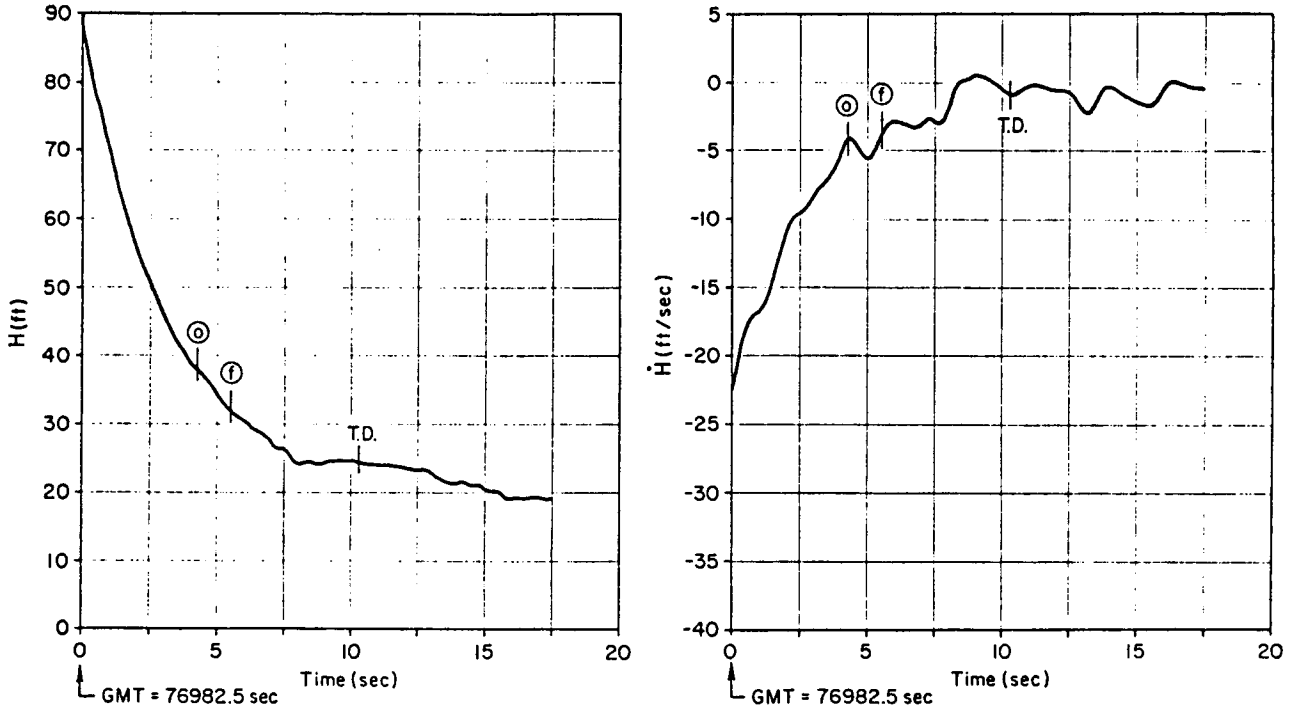

a) Altitude Time History

b) Vertical Speed Time History

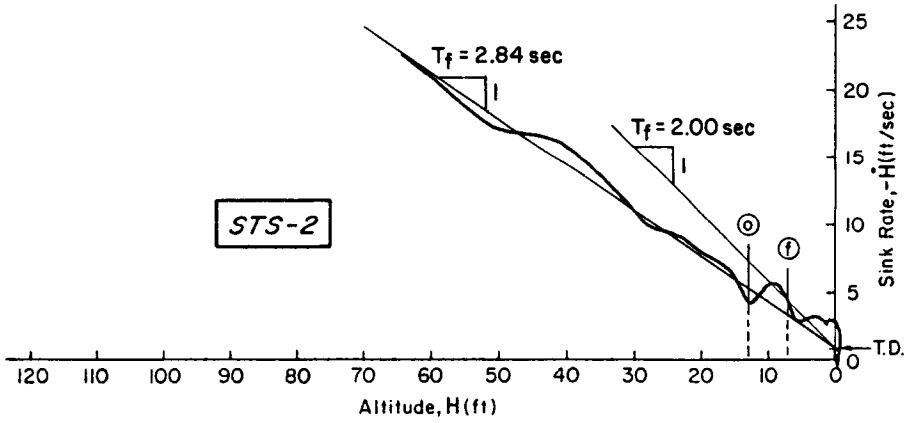

Figure 47b. STS-2 Preflare Through Touchdown Hodograph

THIS PAGE INTENTIONALLY LEFT BLANK

roughly 3.5 rad/sec oscillations at 5 sec before touchdown, a slight PIO due to tightening of attitude control as the vehicle approached touchdown.

STS-3 -- The first 20 sec of the Fig. 48 time traces again reflect autoland operation since δ_{RHC} is zero. At 20 sec the commander took over manual control, and made several large nose-down (and up) inputs prior to touchdown at about 30 sec. The initial input appears to be to stop the preflare, increase sink rate, and avoid ballooning. This is followed by a large pilot induced oscillation to touchdown. Two aspects of the RHC inputs are of particular interest. First, there is an absence of the pulse and wait type control, which one would expect with rate command/attitude hold type inner loop control where path control is well in hand. Second, the large one and one-half cycle divergent input oscillation may indicate the pilot was concentrating on gaining direct control over altitude or sink rate, and may have dropped the inner attitude closure.

The H, $\dot{H}$, and hodograph traces of Fig. 49 also reflect the rather unstable nature of the STS-3 landing. The hodograph seems to indicate an attempt to establish a shallow glide at the rather high sink rate of 15 ft/sec. This was followed by the 4 to 4.5 rad/sec oscillation between 6 and 8 sec on the $\dot{H}$ time history. This frequency is too high to be a path mode response, and indeed is not apparent in the normal acceleration (n) trace of Fig. 48. Therefore the oscillation preceding point ⓕ on the $\dot{H}$ trace and hodograph may be some anomaly of the cine measurement of nose movement. The large amplitude oscillation from point ⓕ to touchdown (last 2.5 or 3 sec) is visible in the $\dot{H}$ and n traces, and apparently was an attempt to arrest the high sink rate. Note that within this time frame the vehicle could have touched down at a sink rate anywhere from 0 to -7.5 ft/sec. The flare time constant averaged about 2 sec while arresting the sink rate from -15 ft/sec to the -2.5 ft/sec at touchdown.

It appears from the hodograph that there was sufficient time following manual takeover to establish a shallow glide at a sink rate of about -10 ft/sec, and then a smooth flare to touchdown. However, it is also

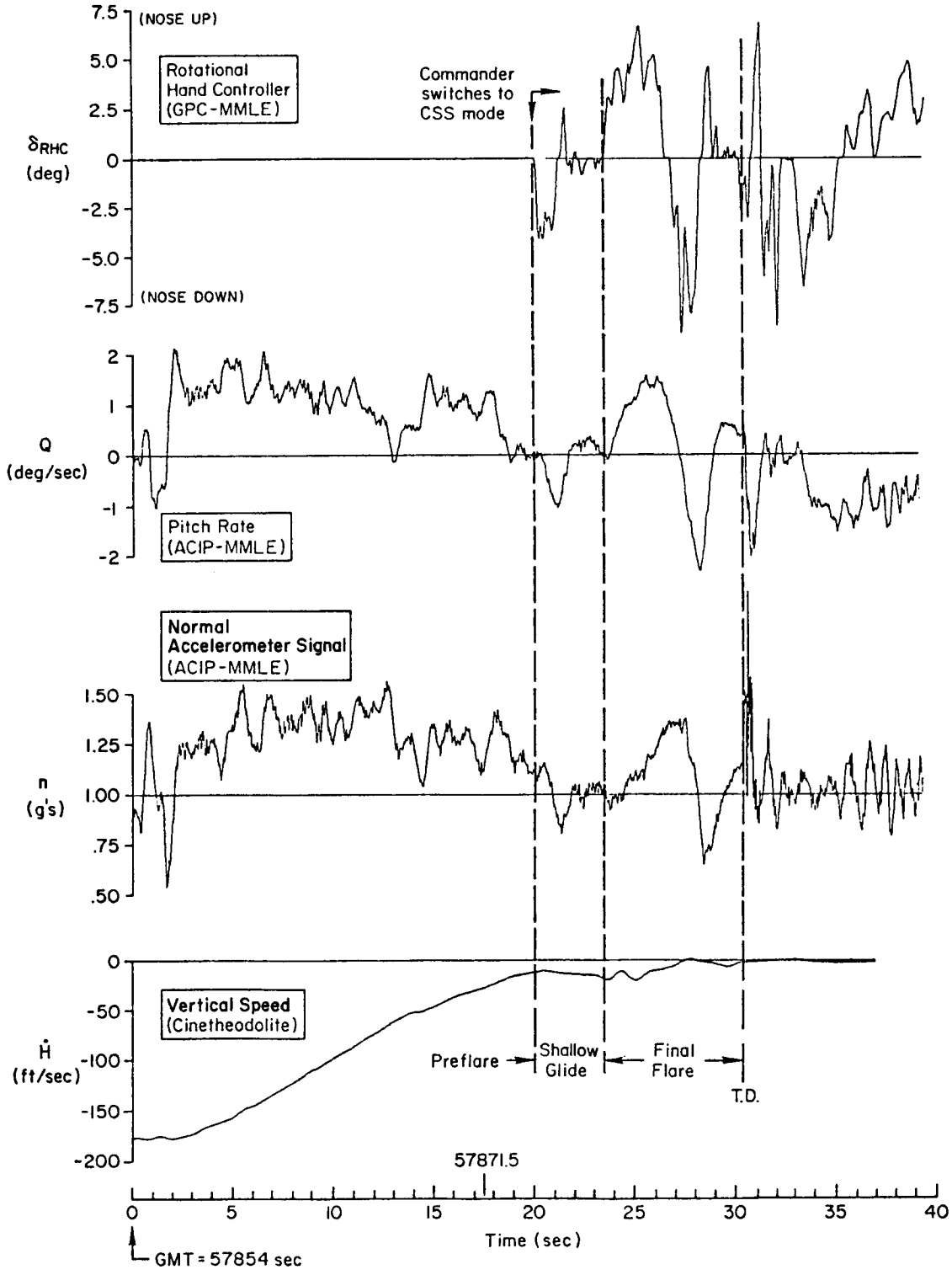

Figure 48. STS-3 Preflare Through Touchdown Time Traces

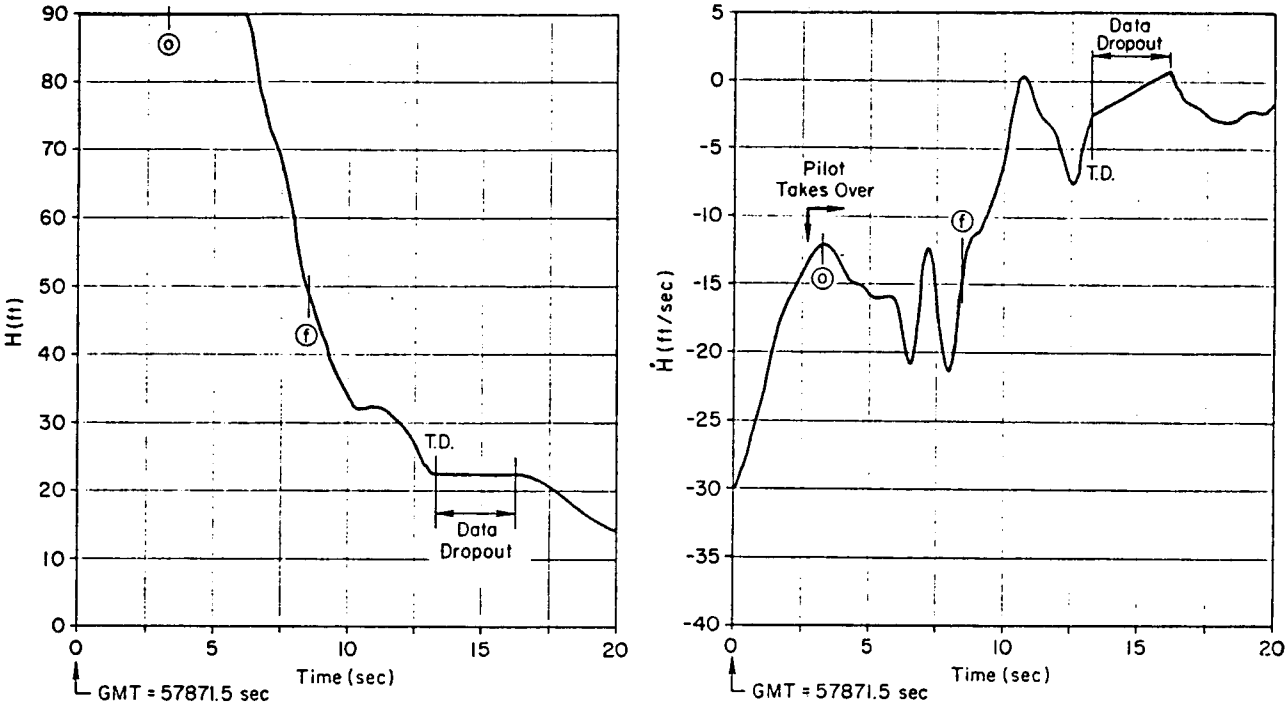

a) Altitude Time History

b) Vertical Speed Time History

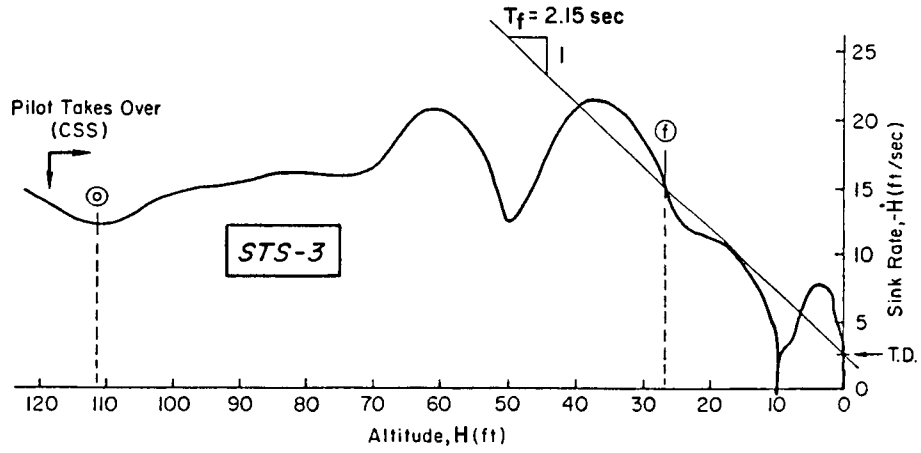

Figure 49. STS-3 Preflare Through Touchdown Hodograph

THIS PAGE INTENTIONALLY LEFT BLANK

apparent that the pilot RHC inputs were overly large, perhaps because he had not established a "feel" for the aircraft response, and the situation rapidly deteriorated following the initial large nose-down input. This has implications for the safety of any last second manual takeover from an autoland system failure, and for much earlier takeover on other flights in order for the pilot to adapt to the landing control task.

STS-4 -- This was the first runway landing at Edwards, and was accomplished with only the external aim point aids. The time traces of Fig. 50 reflect the early manual takeover for STS-4 in which the pilot performed the preflare, shallow glide, and final flare. The traces show that the preflare was accomplished in a two step sequence with the initial pitch rate averaging about 0.7 deg/sec, and then increasing to about 2 deg/sec. This is consistent with the pilot's comments that he had trouble judging the preflare, that he started preflare, but it felt "hard" so he relaxed and then did another preflare when he had better "visual." The RHC trace for the shallow glide slope segment shows a transition from essentially continuous rate command type control to a rapid pulsing type control. This is followed by two nose-up pulses to initiate final flare, and several small nose-down corrective pulses. It should be noted that this is one of the rare landings where pilot commentary regarding the landing and flare technique (or strategy) is available. In Ref. 23 the commander commented that he relied upon altitude calls by the pilot during flare. He then estimated sink rate based upon the altitude and cadence of the calls and adjusted pitch attitude accordingly. This clearly reflects an outer loop sink rate "error" command to an inner attitude loop control.

The traces and hodograph of Fig. 51 show the late part of the preflare, a definite shallow glide with a sink rate of about -5 ft/sec, and a final flare with time constant of about 1.26 sec. This T_f value and the pilot's RHC activity again indicate closed-loop control of sink rate throughout the flare.

STS-5 -- This flight also landed on the runway at Edwards, and was the first to have the ball-bar shallow glide aid. The traces of Fig. 52

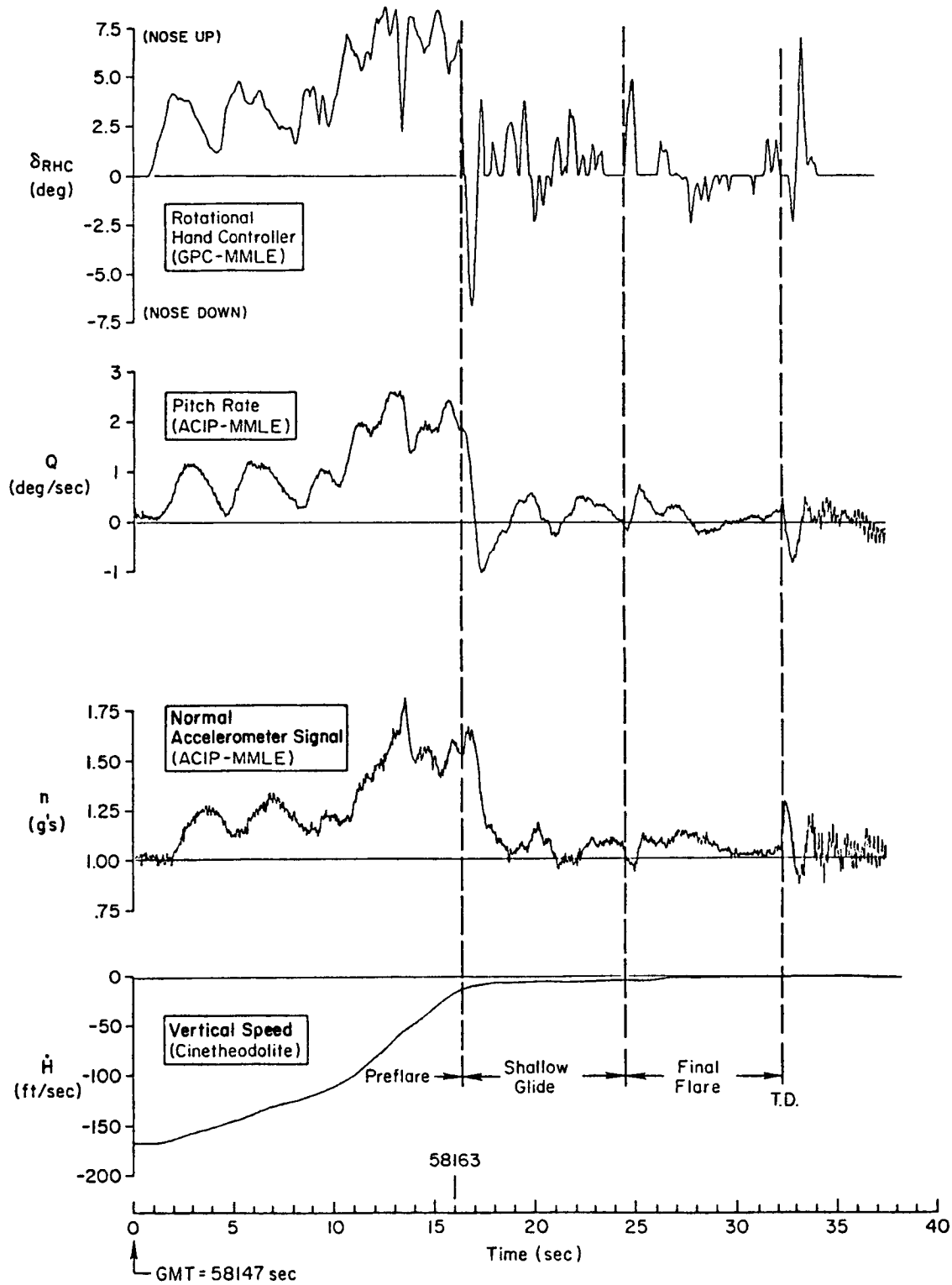

Figure 50. STS-4 Preflare Through Touchdown Time Traces

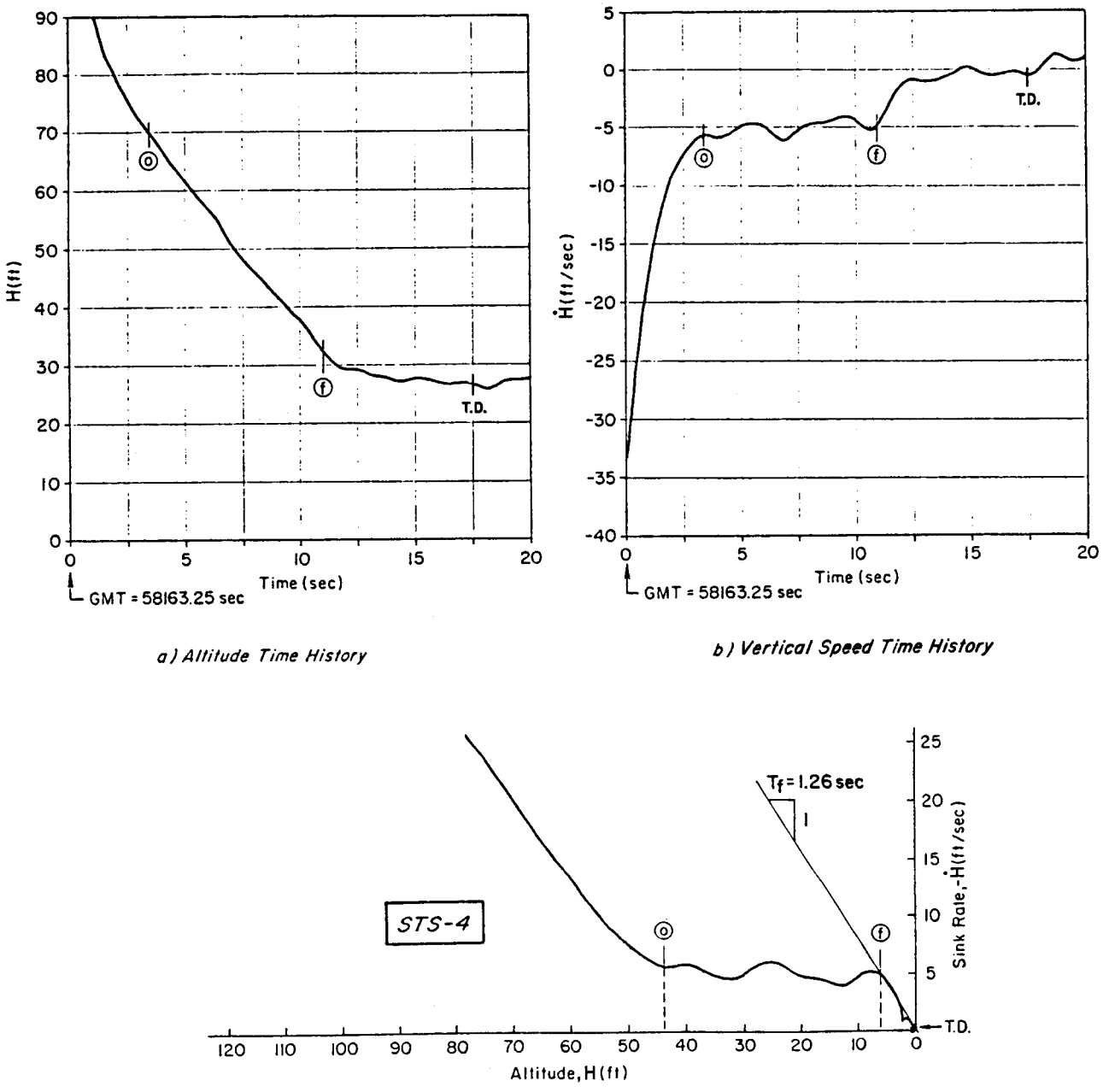

Figure 51. STS-4 Preflare Through Touchdown Hodograph

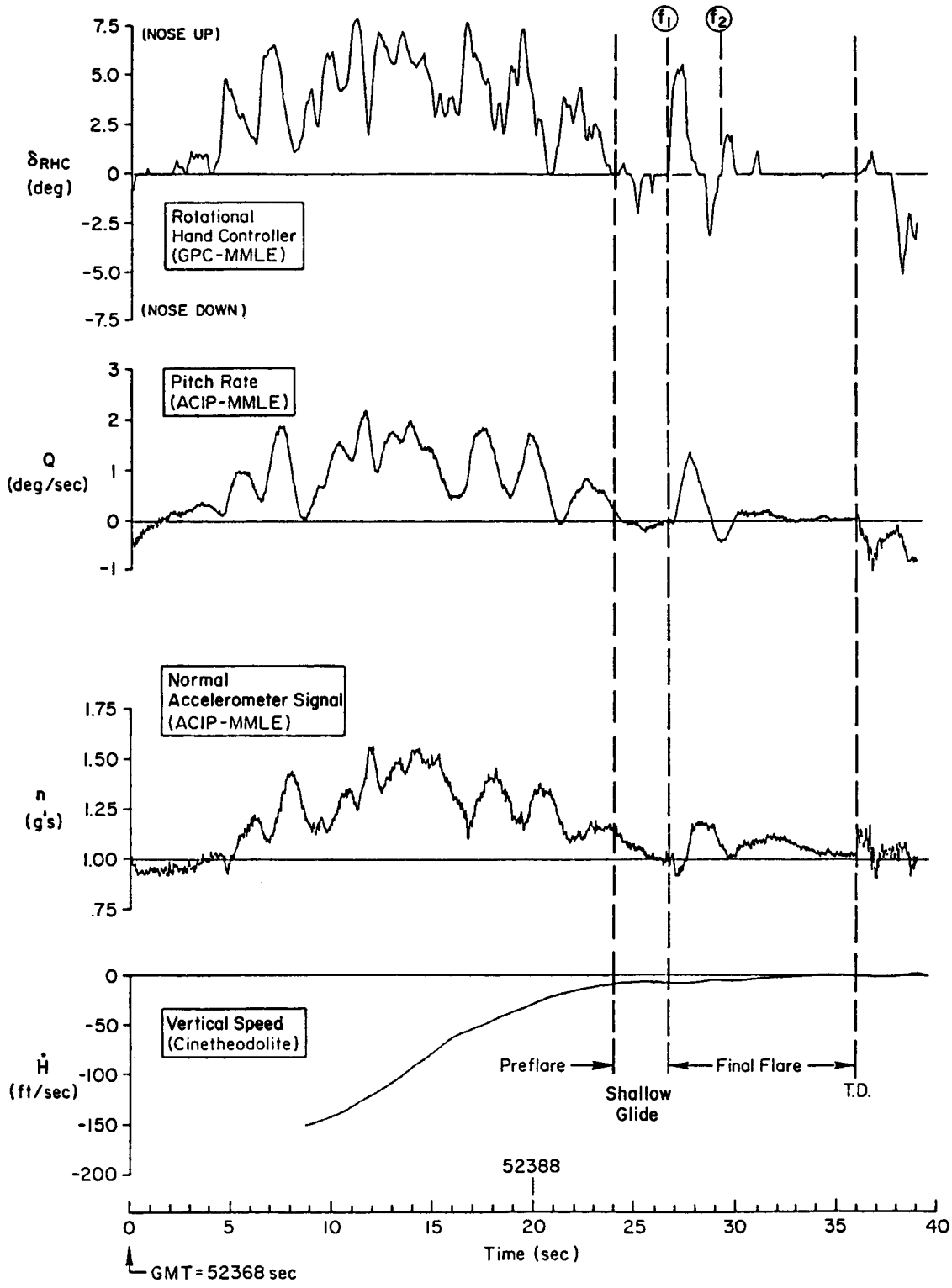

Figure 52. STS-5 Preflare Through Touchdown Time Traces

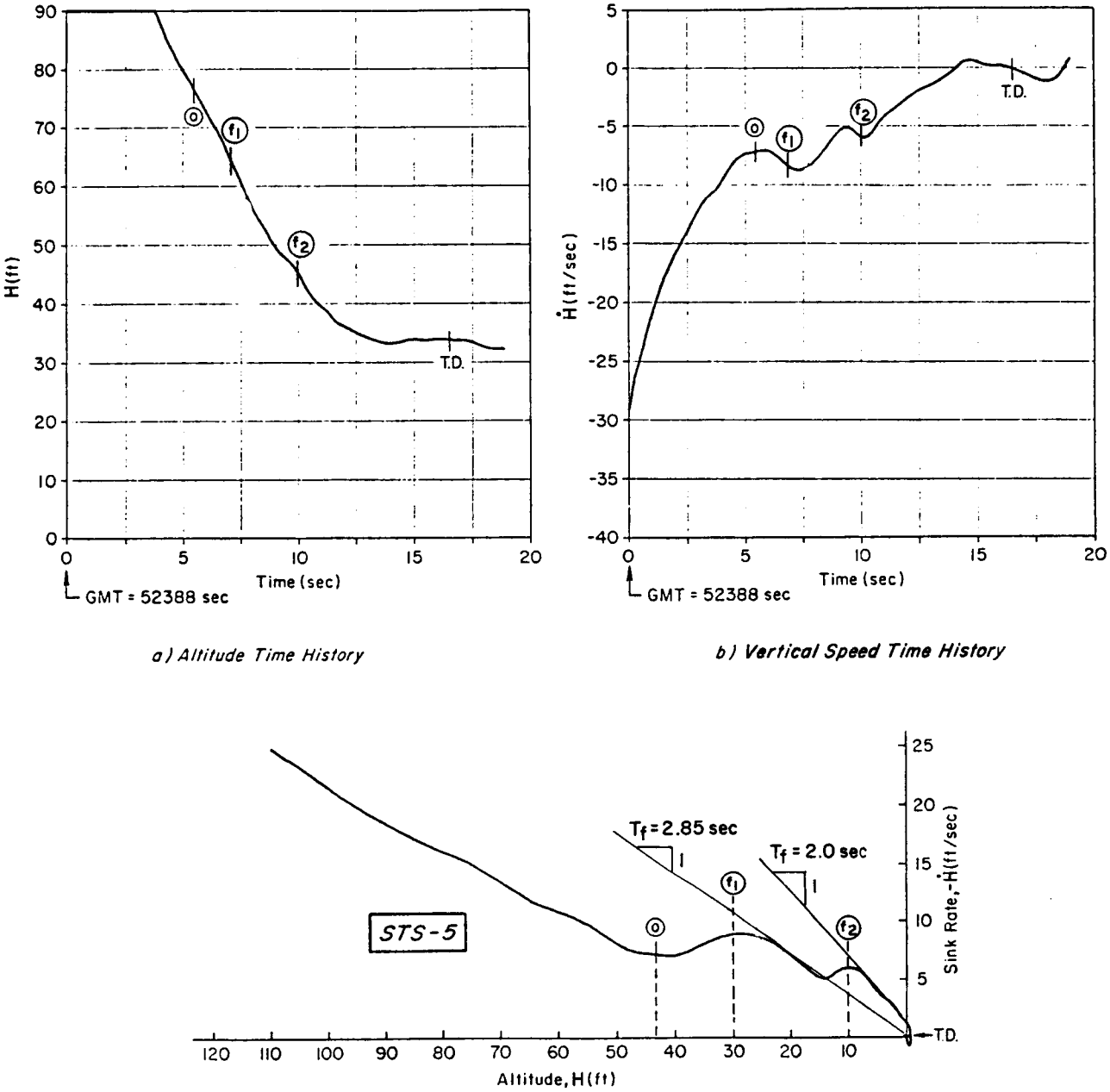

a) Altitude Time History

b) Vertical Speed Time History

Figure 53. STS-5 Preflare Through Touchdown Hodograph

THIS PAGE INTENTIONALLY LEFT BLANK

cover preflare, shallow glide, and final flare. It is somewhat difficult to detect where preflare ends and shallow glide begins on these traces. This would tend to indicate the pilot was following the ball-bar aid since its purpose is to guide a smooth transition from steep to shallow glide slope. The pilot also commented that he had no problem judging preflare. However, it is interesting to note the neutrally damped oscillation which developed in pitch rate during the later portion of preflare. This indicates a very tight pitch loop closure.

By the time the shallow glide slope was reached, the pilot had adopted the pulse control technique. The transition to final flare was accomplished by a series of up-down-up pulses after which the vehicle was allowed to settle to touchdown in the attitude hold mode during the final 5 sec of the landing. This final flare appears to have been initiated by the large δ_{RHC} pulse at (f$_1$) and the following inputs were probably vernier adjustments to achieve the desired increment in pitch attitude. Thus, the landing was nearly a precognitive step attitude change. The flare time constant (Fig. 53) starts out to be approximately 2.85 sec but the later nose-up input at (f$_2$) results in a second identifiable path time constant of T_f = 2 sec = T_{θ_2}.

STS-6 -- This flight landed on the runway at Edwards with the aid of the PAPI lights, ball-bar system, and HUD. It is relatively easy to identify preflare, shallow glide, and final flare in the time traces of Fig. 54. Again a neutrally damped pitch oscillation developed near the end of preflare. There is a distinct transition to pulse type control for the shallow glide slope and landing. There is essentially no RHC activity for the last 5 sec prior to touchdown.

The time histories and hodograph of Fig. 55 also show very decisive segments for this landing. The shallow glide is held quite precisely at -10 ft/sec until final flare, which is initiated at a nose altitude of about 50 ft. The final flare is almost an ideal exponential with a time constant of 2.42 sec.

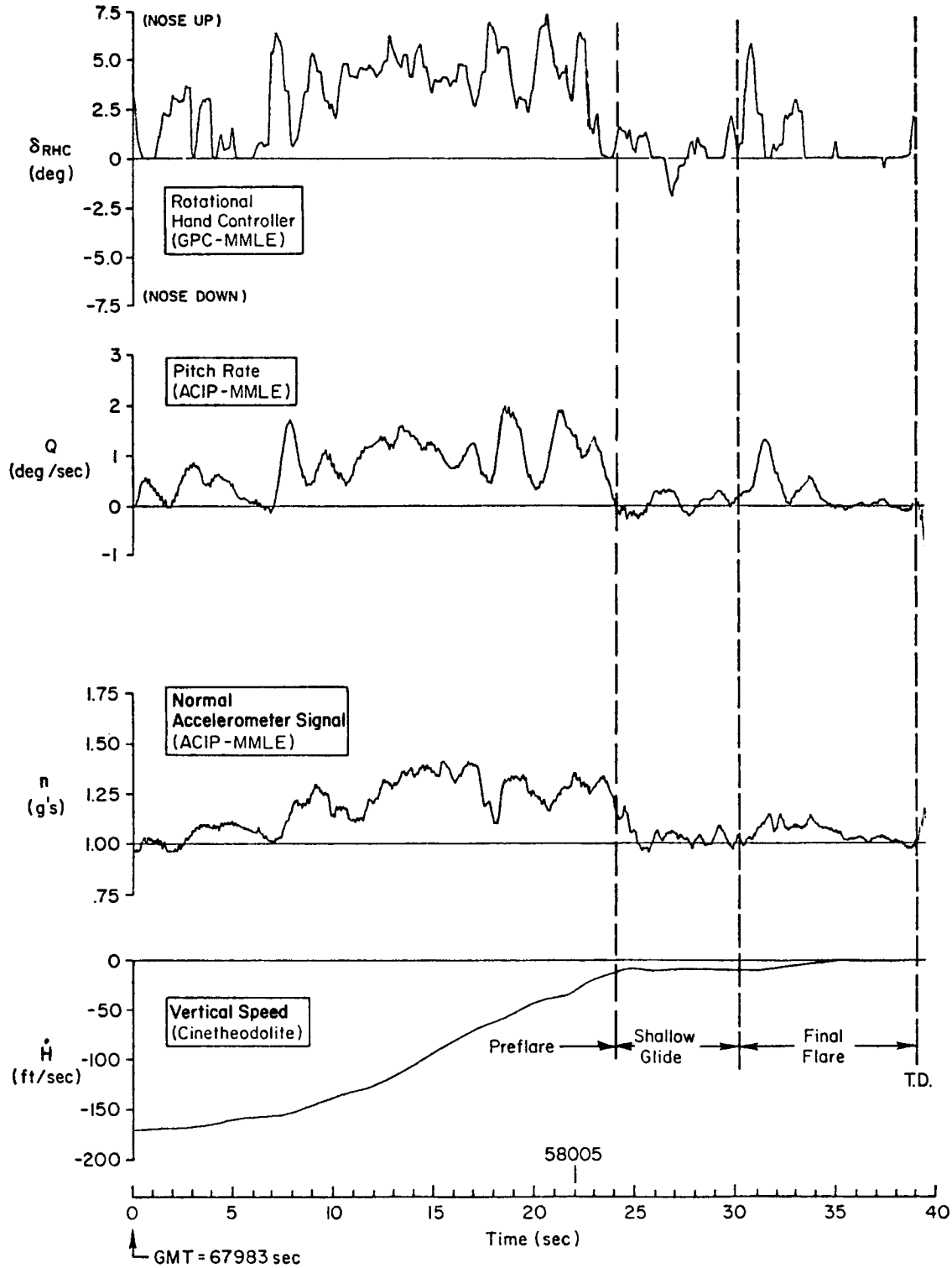

Figure 54. STS-6 Preflare Through Touchdown Time Traces

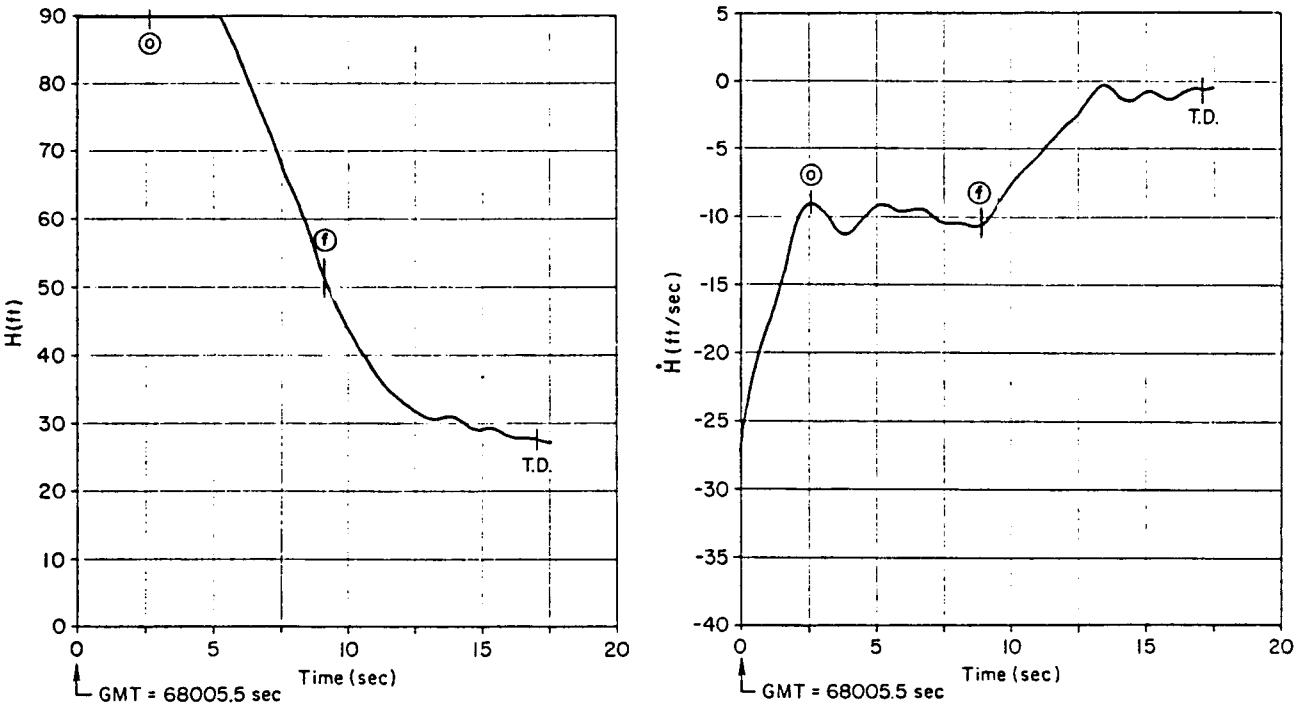

a) Altitude Time History

b) Vertical Speed Time History

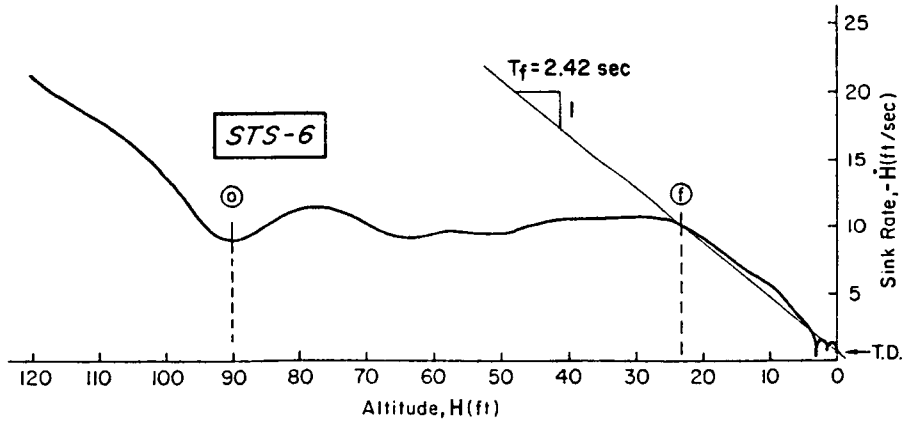

Figure 55. STS-6 Preflare Through Touchdown Hodograph

THIS PAGE INTENTIONALLY LEFT BLANK

Based on the minimum RHC activity in Fig. 54 and the smooth transitions and segments of Fig. 55, it appears that the ground based landing aids and HUD have reduced the control workload significantly.

STS-7 -- This flight was diverted at virtually the last minute from landing at Kennedy to the lakebed at Edwards. The PAPI and ball-bar ground aids were available, and it was the second landing with the HUD. The time traces of Fig. 56 show a gradual change in RHC activity from continuous rate command to a 3 cycle PIO (at about 4.2 rad/sec) and finally the distinctly pulsive type control. Thus, there is little to distinguish separate path segments. The time histories and hodograph of Fig. 57 provide additional clues to indicate a possible transition between ⓪ and ⓕ from the preflare to an apparent final flare. There is a large nose-up pulse which produce a hesitation at a sink rate of about -12 ft/sec and suggests start of shallow glide, but this is followed immediately by a flare with a time constant of 4.6 sec. Since this landing is on the lakebed where there is little concern for touchdown point and landing roll, it appears the pilot was concentrating on achieving a specific touchdown sink rate (and possibly speed). The lightly damped path oscillation at about 2.3 rad/sec (also discernable in the pitch rate of Fig. 56) and the rapid RHC pulsing suggests a rather tightly closed sink rate loop which results in an almost neutrally stable path mode. This terminal RHC activity and the $T_f \doteq 4.6$ sec flare time constant make it very clear that the pilot was able to maintain sink rate proportional to altitude and was in closed-loop control throughout the flare. Interestingly, the neutrally damped closed-loop attitude and path modes demonstrated here are very close to those predicted in the analysis of Ref. 12.

Figure 58 is a composite of the STS-2 through -7 hodographs, which provides yet another perspective among the landings. There is considerable similarity in the two lakebed landings (STS-2 and -7) in that neither has a discernable shallow glide phase, but rather one almost continuous flare. It is likely the control strategy and loop structure were the same in both. The three runway landings (STS-4, -5, and -6) are similar in that each has a fairly distinct shallow glide at a sink

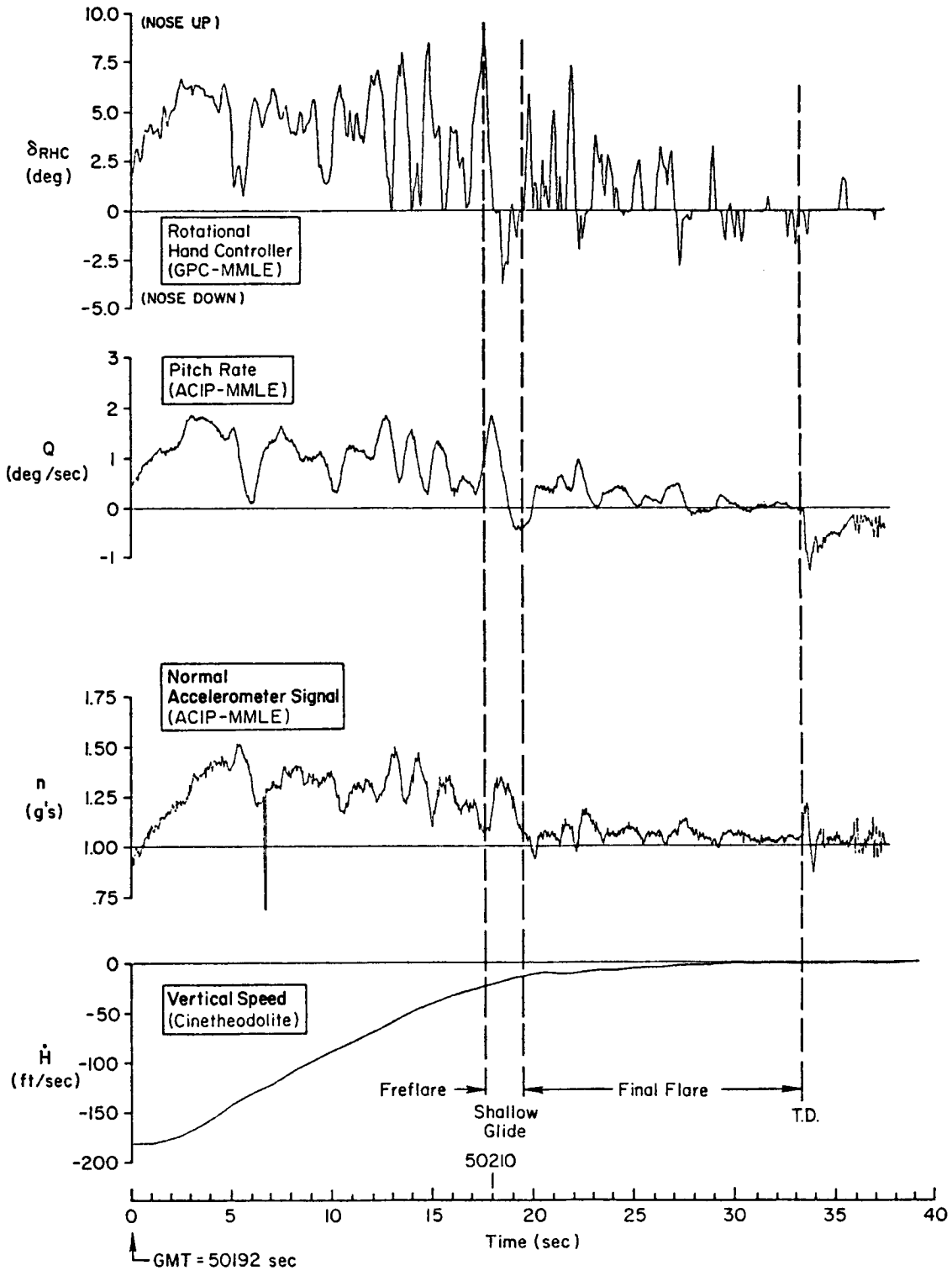

Figure 56. STS-7 Preflare Through Touchdown Time Traces

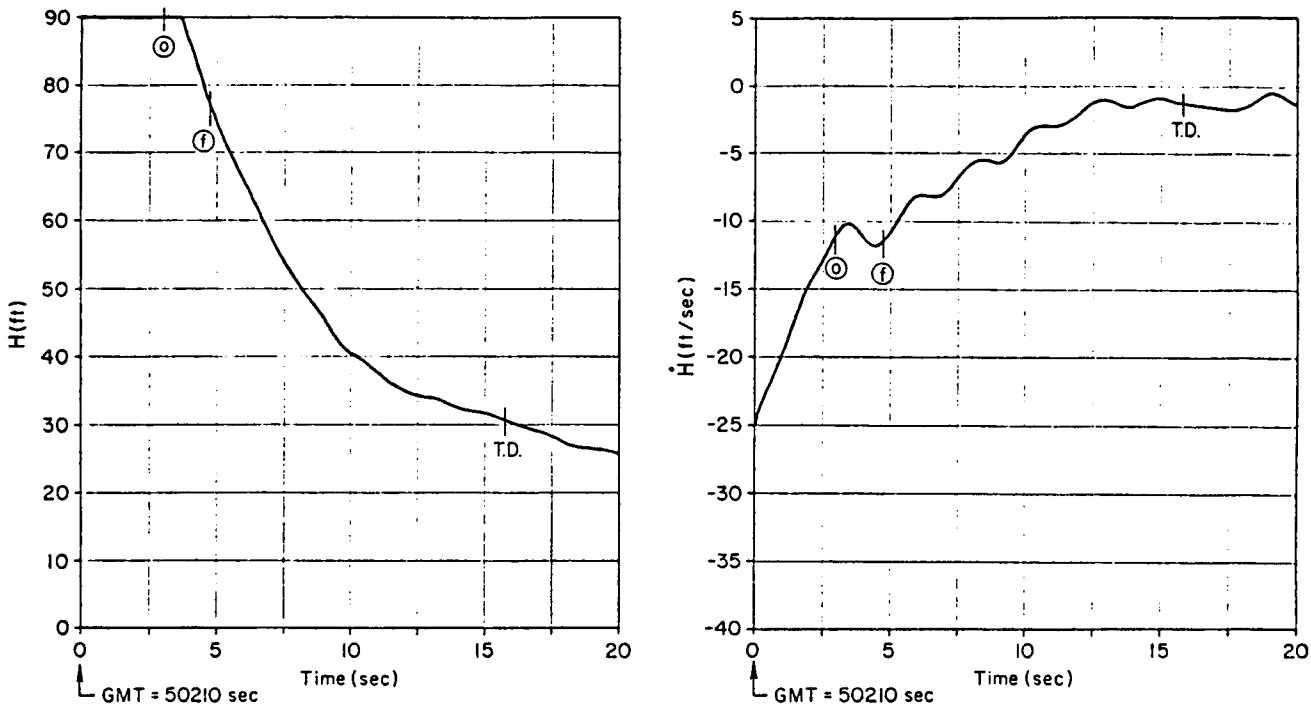

a) Altitude Time History

b) Vertical Speed Time History

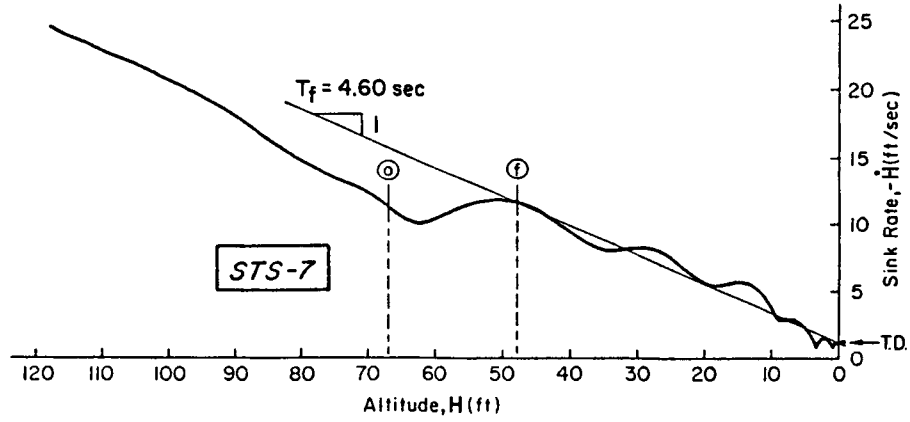

Figure 57. STS-7 Preflare Through Touchdown Hodograph

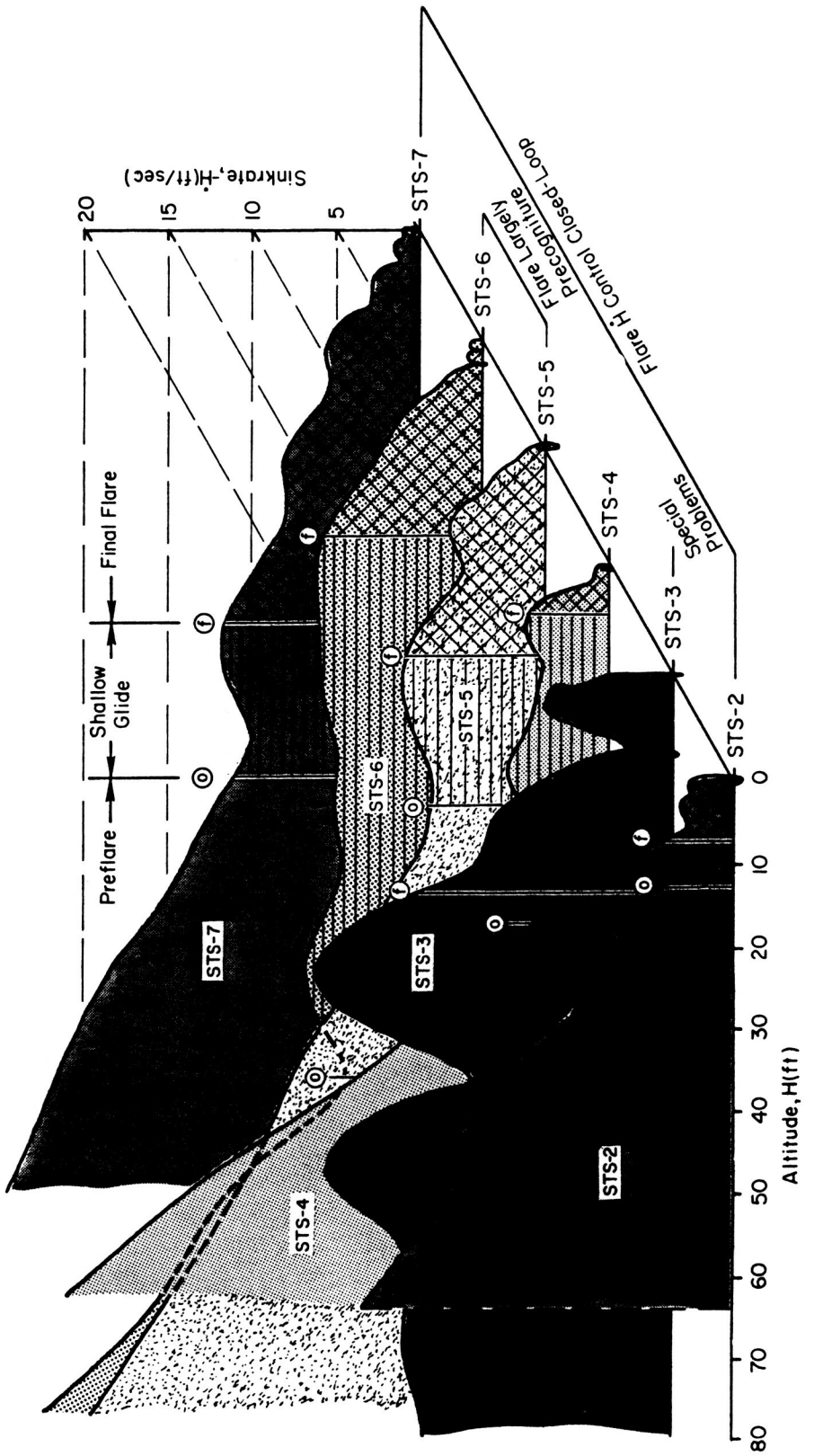

Figure 58. Composite of STS-2 Through -7 Approach and Landing Hodographs

rate of -10 ft/sec or less followed by a flare at close to the vehicle path response time constant. While there appears to be little difference in task accomplishment between these three hodographs, the time traces for the pilot's RHC inputs in Figs. 50, 52, and 54 indicate a definite decrease in activity, and therefore workload as the landing aids (ground and HUD) came into use. The STS-3 landing bears little resemblance to the others due to the late manual takeover and over-control problems. Again all of the above has obvious implications on pilot workload, landing performance, and possible safety for emergency landings at less well-equipped or more restricted landing sites.

b. Flare and Touchdown Performance Parameter Summary

While there is value in focusing on the details of the individual flights and seeking explanations of pilot activity on a flight-by-flight basis, such conclusions, strictly speaking, apply only to the individual flights and not to the characteristics of the vehicle in general. This motivates use of the quantitative model of Fig. 32 to draw conclusions which apply to the Orbiter and landing task as a whole from the ensemble of landings.

The model of Fig. 32 is about as simple as possible, and involves roughly a half dozen parameters that can be extracted from the time traces at the times identified as initiation of shallow glide ⓘ and final flare ⓕ in the hodographs. The parameters thus extracted are summarized in Table 6 and Figs. 59 and 60.

Figure 59a compares the initial glide speeds for STS-2 through -7, and shows fairly high consistency -- particularly after STS-3. However, there is considerable variation in the initial glide altitude at the main gear (Fig. 59b) even if the anomalous STS-3 case is neglected.

Figure 59c shows the shallow glide slope variable. The shallow glide slope is difficult to extract precisely from the flight data; these values were obtained by averaging $\dot{H}/V$ over the shallow glide region. The values obtained are all less than the nominal 1.5 deg except for STS-3, and show a significant variation. However, after the

TABLE 6. SUMMARY OF GLIDE AND FLARE MODEL PARAMETERS EXTRACTED FROM SHUTTLE FLIGHT DATA

Mission #	V_o fps Cine	H_o ft Cine	γ_o deg Cine	$K_{\dot{V}}$ ft/sec^2 Cine	V_f fps Cine	H_f ft Cine	T_f sec Cine	X_g ft Cine	X_f ft Cine
STS-2	355.00	13.00	-0.82	6.78	342.00	7.50	2.00	451.00	1539.00
STS-3	470.00	111.00	-1.70	7.41	432.00	27.00	2.15	2100.00	1923.00
STS-4	440.00	43.70	-0.73	7.69	380.00	6.20	1.26	2985.00	1981.00
STS-5	443.00	43.00	-1.07	7.84	412.00	25.00	2.85	933.00	3318.00
STS-6	412.00	89.70	-1.46	8.00	360.00	23.20	2.42	2593.00	2468.00
STS-7	451.00	66.50	-1.42	7.84	439.00	47.50	4.60	775.00	4282.00
Mean	428.50	61.83	-1.20	7.59	394.17	22.73	2.55	1639.50	2585.17
Std Dev	37.07	32.99	0.35	0.41	36.17	13.80	1.04	965.28	942.33

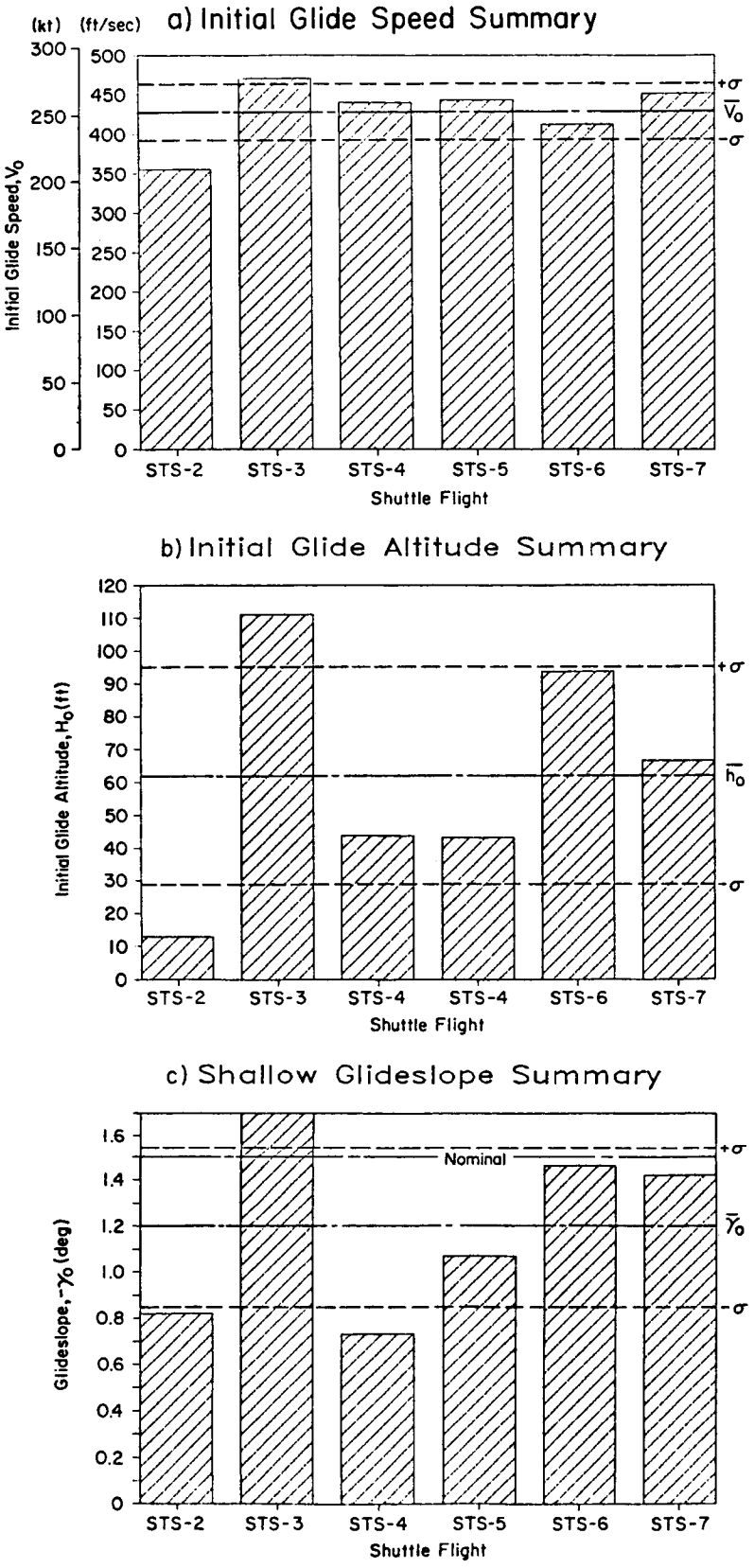

Figure 59. Summary of Shallow Glide Parameter Values

HUD became available on STS-6 and -7, the shallow glide is close to the nominal -1.5 deg.

The initial flare speed summary of Fig. 60a shows variation similar to that of the V_o summary in Fig. 59a. This is consistent with the constant deceleration model following the conclusion of preflare. Velocity at any point in the trajectory is thus a function of time, and touchdown time is controlled via sink rate.

The main gear flare height summary of Fig. 60b shows considerable variation over the six flights, and does not appear related to H_o. This is to be expected since not all flights exhibited shallow glide of significant duration.

The key control variable which the pilot selects in the hypothesized multi-stage landing strategy is the flare time constant T_f. The "available" range of T_f is a critical point for flying qualities of the Orbiter in landing. The vehicle can respond to flare law requirements as long as the flare time constant required is greater than the flare time constant available, i.e., the "path lag" T_{θ_2}. Thus, we expect to find flare time constants not less than T_{θ_2} which, for the shuttle landing, is about 2 sec. This reference "boundary" is indicated in the flare time constant summary of Fig. 60c, and reveals that the observed flare time constants are all near to T_{θ_2} except for the STS-4 and -7 landings. As noted in conjunction with Figs. 47b and 53, the flare time constant for STS-2 and -5 could be either 2 or 2.85 sec. Thus, both values are reflected here. In the STS-4 landing (Fig. 51), if the initiation of final flare (f) had been selected at 10 sec on the trace instead of 11 sec, T_f would be very close to 2 sec. Thus, the STS-4 T_f may well have been 2 sec since, as indicated earlier, identification of the point of flare initiation is based on an iteration between the various traces and there is acknowledged uncertainty in the points selected.

T_{θ_2} is not a "hard" limit since the pilot can attempt to flare faster than T_{θ_2}, as he may have in STS-4. It does represent a reference beyond which we may expect that the pilot will have increased difficulty

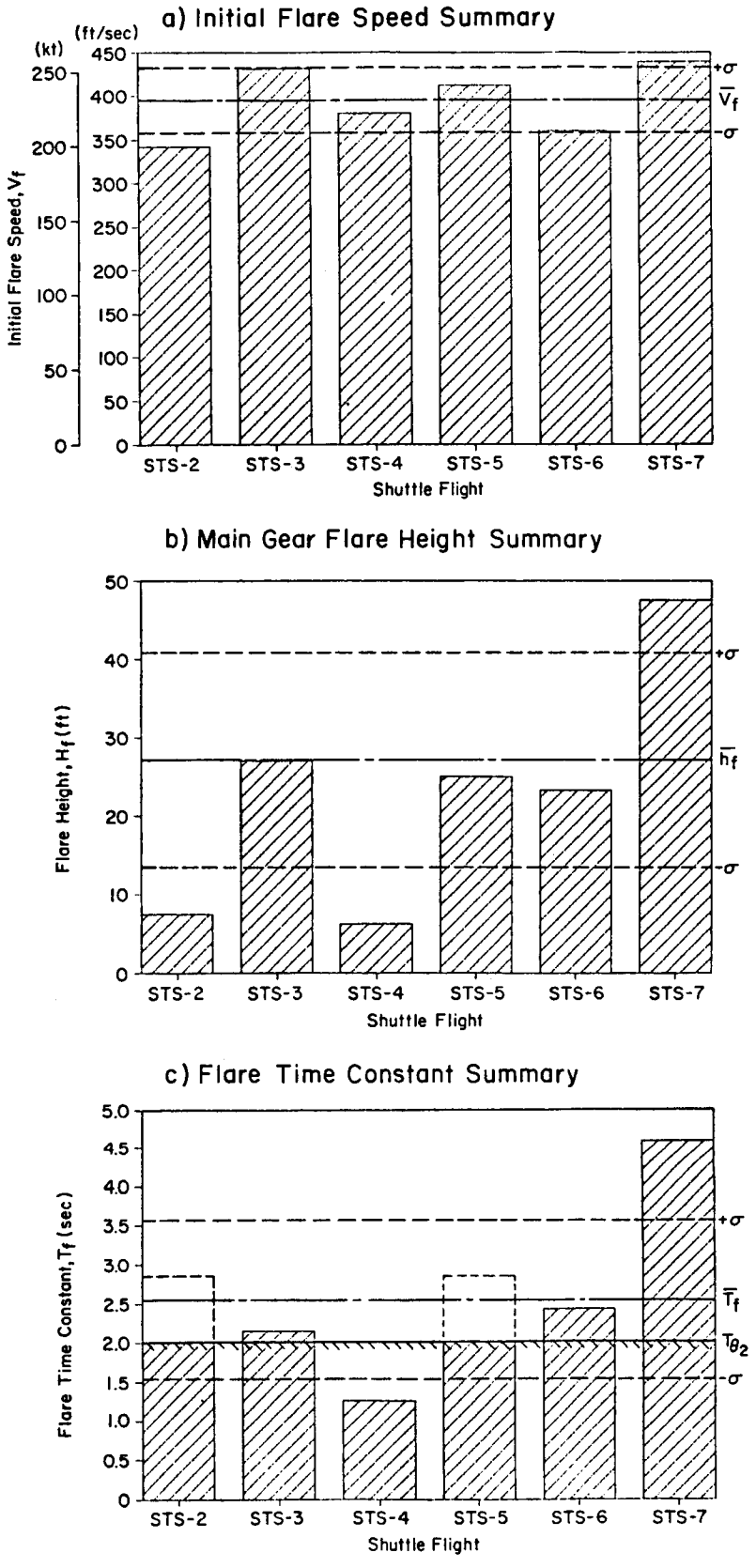

Figure 60. Summary of Final Flare Parameter Values

in achieving the desired flare performance, and consequently may be dissatisfied with the vehicle flying qualities in landing. The real interest here is to define the circumstances under which a pilot might be forced to "push the T_{θ_2} limit" to achieve a satisfactory landing.

The values of touchdown sink rate at the nose, $\dot{H}_{TD}$, speed, V_{TD}, and glide and flare distance, X_T, derived from the STS-2 through -7 cine-theodolite data are summarized in Table 7. The distance is measured from the assumed end of preflare as identified from the hodographs. In addition, touchdown sink rate at the nose was translated to the main gear based on vehicle geometry and pitch rate. Main gear sink rate, vehicle speed, and glide distance at touchdown are plotted in bar chart form in Fig. 61. Various constraints from Table 4 are also shown as boundaries in Fig. 61. These constraints are best estimates based on early autoland design information (Ref. 8), and do not necessarily reflect the latest shuttle mission policies. More importantly, they do not necessarily drive the pilots who have internal criteria we are trying to discover. However, they provide a consistent representative set for comparison.

TABLE 7. SUMMARY OF TOUCHDOWN SINK RATE AND SPEED

Mission	$\dot{H}_{TD}$ nose (fps) Cine	q_{TD} (deg/sec) MMLE	$\dot{H}_{TD}$ wheels (fps)	V_{TD} (fps) Cine	X_T (ft) Cine
STS-2	-0.70	0.10	-0.84	314.00	1990
STS-3	-2.50	0.40	-3.04	398.00	4023
STS-4	-0.40	0.40	-0.94	342.00	4966
STS-5	-0.20	0.05	-0.27	348.00	4251
STS-6	-0.50	0.00	-0.50	305.00	5061
STS-7	-1.40	0.00	-1.40	357.00	5057
Mean	-0.95	0.16	-1.17	344.00	4225
Std Dev	0.79	0.17	0.91	30.35	1078

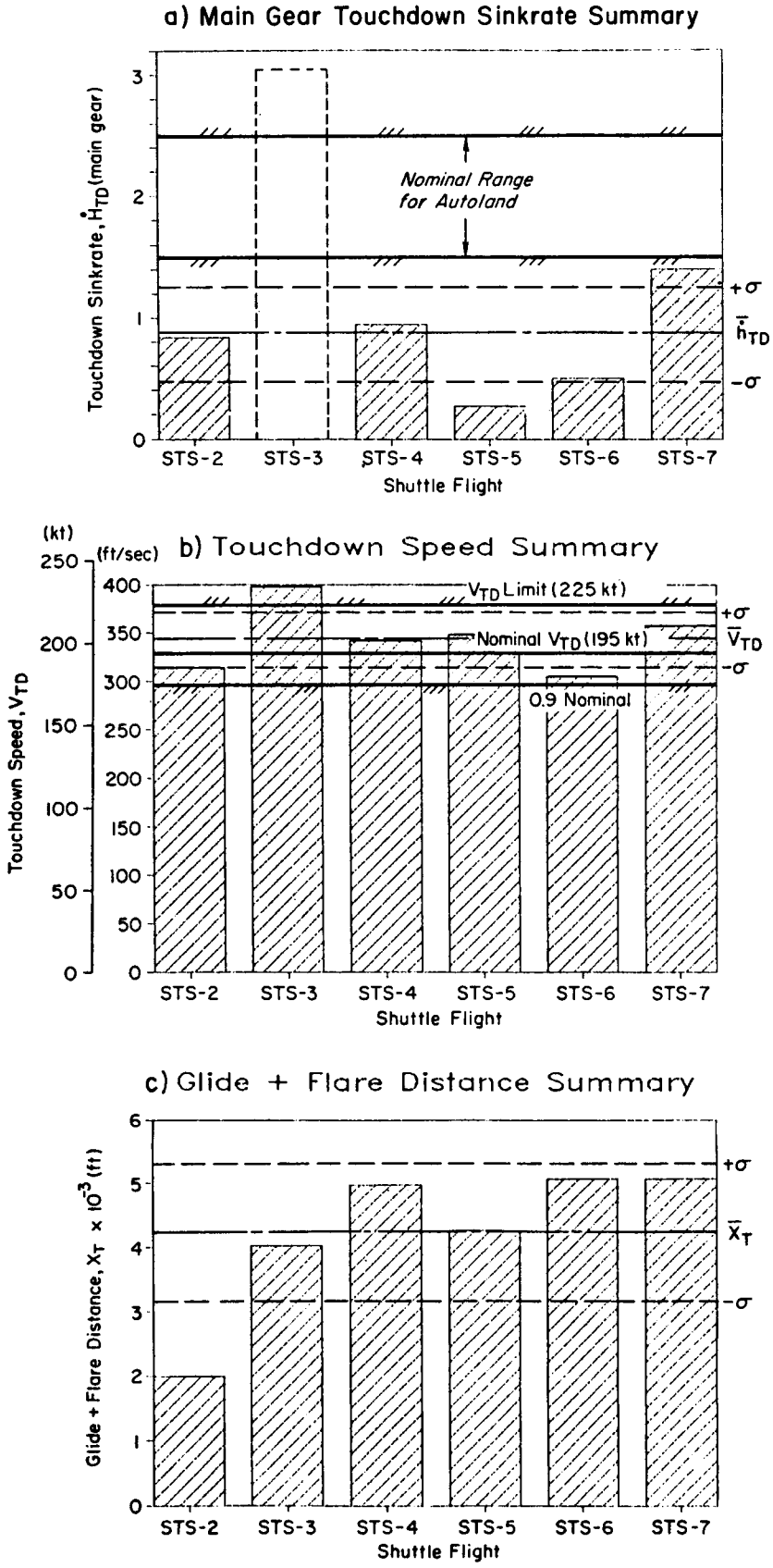

Figure 61. Touchdown Parameter Summary Chart

The touchdown sink rate summary in Fig. 61a indicates that all landings were well within the 6 fps (crosswind) sink rate limit, and only the STS-3 landing exceeded the assumed nominal region. However, that landing could have exceeded the 6 fps limit if the vehicle had touched down about 1 sec earlier. All of the other landings have sink rates below 1.5 fps, and tend to indicate a target value close to 1 fps. Indeed a major conclusion to be derived from these data is that the touchdown sink rate, when STS-3 is excluded, is remarkedly uniform for all flights -- mean $\dot{H}_{TD} \doteq 0.86$ ft/sec with a standard deviation of 0.38 ft/sec -- and differ markedly from the autoland based nominal.

The touchdown speed summary in Fig. 61b shows that the 225 kts touchdown speed limit was exceeded only in the STS-3 landing. Three flights were slightly higher and two slightly lower than the nominal 195 kts. One standard deviation in the achieved touchdown speed is less than the 30 kt difference between the upper limit and nominal V_{TD} values. If STS-3 is again excluded, the mean $V_{TD} \doteq 333$ ft/sec with a standard deviation of 22.5 ft/sec.

Figure 61c compares the total distance traveled from the end of the preflare pull-up (as identified in the hodographs) to touchdown. Establishing absolute constraints for distance is more difficult than for $\dot{H}_{TD}$ and V_{TD}, since reference must be made to the runway threshold. Further the effective distance constraints certainly vary more among the flights especially between lakebed and runway landings.

STS-2 was known to be low on energy and this is reflected in both V_{TD} and X_T. Despite this (and with the exception of STS-3) touchdown performance is quite consistent and adequate with respect to the Table 4 constraints. When it is recognized that this performance is attainable with both precognitive and tight closed-loop control of sink rate, this implies excellent and flexible performance for the pilot-vehicle system.

The data of Fig. 61 also tends to indicate that most importance is being attached to touchdown sink rate with touchdown velocity also being weighted heavily. The latter is consistent with Ref. 7 in which it was

stated that the difficulty of runway landings was reduced by setting V_{TD} criteria rather than X_{TD}.

c. Correlation with the Flare Strategy Models

It was noted in the previous discussions concerning the landing hodograph shapes and the flare time constants that two distinctly different flare techniques appear to emerge. The exponential flare is the only elementary strategy which produces a distinctly straight flare hodograph over a range of conditions with a flare time constant that can be other than T_{θ_2}. However, for sufficiently low altitude flares, open-loop "step θ" strategies will also approach straight line hodographs with an indicated flare time constant close to T_{θ_2} (Fig. 44). By considering the effective flare time constant in conjunction with the amount of RHC activity, it has been possible to separate landings which appear to be largely precognitive from those which are largely closed-loop. On this basis, the STS-5 and -6 landings appeared most strongly precognitive. They showed little RHC activity after flare initiation and flare time constants approaching $T_{\theta_2} \doteq 2$ sec. The four other landings showed more evidence of closed-loop control in flare. STS-7 in particular showed distinct characteristics of a closed-loop exponential flare ($\dot{H} \propto H$) with continuous RHC activity, and a flare time constant ($T_f = 4.6$ sec) much larger than T_{θ_2}.

Examination of pitch attitude time traces for these landings (Fig. 62) further reinforces these conclusions. The step attitude change to initiate both shallow glide and final flare is very apparent for STS-5 and -6 whereas a continuous, essentially exponential, change in pitch is seen in STS-7. The trace for STS-4 reflects almost a doublet attitude change to initiate shallow glide but this is then followed by a series of small step pitch changes. In all cases, however, the final pitch attitude "target" appears to be about 8 deg since this attitude is achieved some 3-4 sec prior to touchdown in almost all cases and then held constant until touchdown.

Since STS-4, -5, -6 landed on the runway while STS-7 landed on the lakebed (as did STS-2 and with a hodograph shape similar to STS-7) it

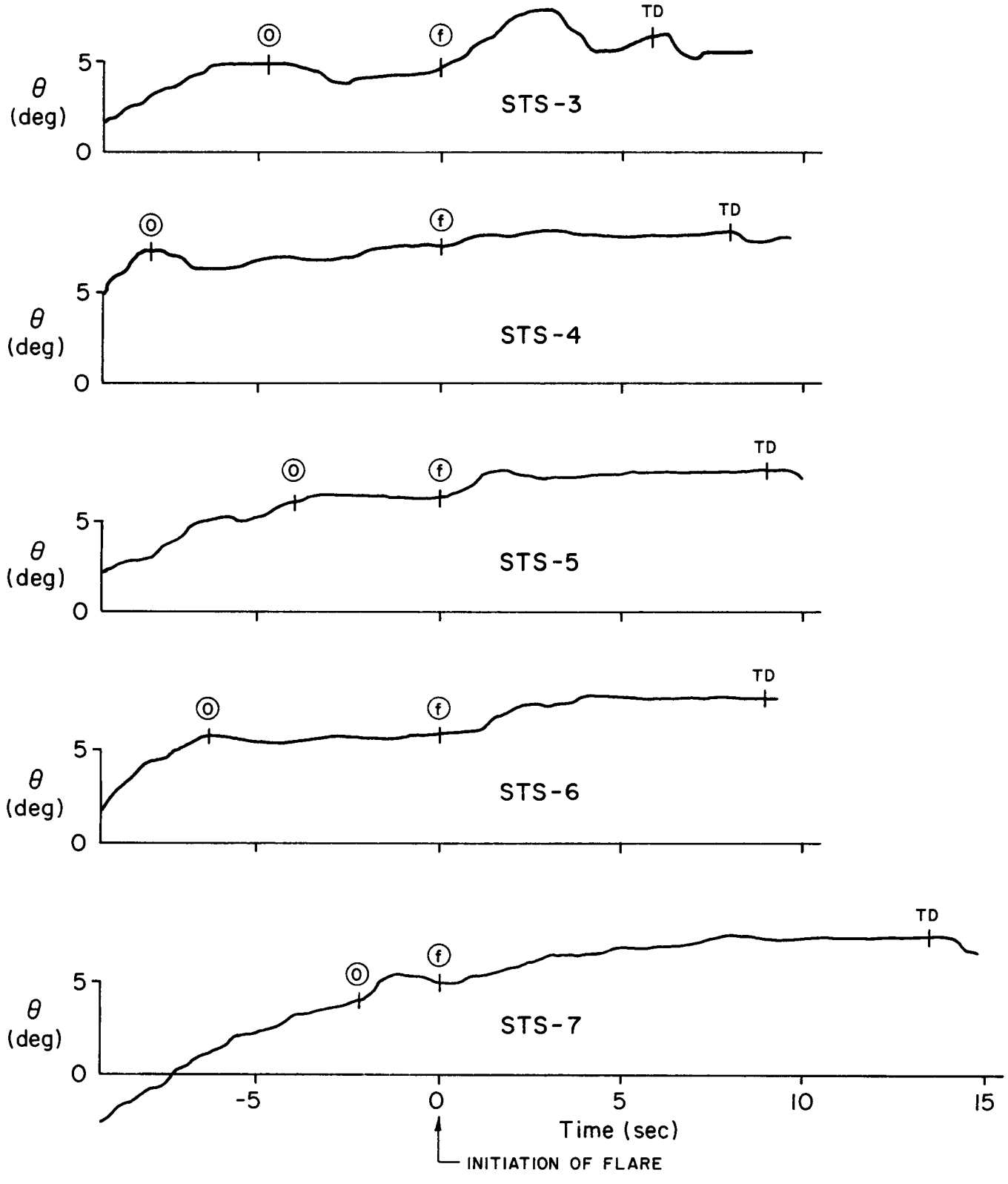

Figure 62. Comparison of Pitch Attitude Responses in the Shuttle Landing Flare

would appear that the landing surface (in particular runway length) and landing aids might be influencing the flare strategy. Unfortunately, the reason (or reasons) for this behavior is not so readily apparent. But it is of interest that the two lakebed landings show exponential flare characteristics which require a control law with sink rate decay proportional to altitude decay. Furthermore, STS-2 was landed with a minimum of landing aids while STS-7 enjoyed the full complement (Table 5).

The question that immediately comes to mind is "how did the pilot obtain sink rate information sufficiently accurate to perform the exponential flare?" It was noted in the discussion of the STS-4 landing that the "pilot" called out altitude and airspeed during the flare maneuver and the "commander" then estimated sink rate based upon the cadence of calls and adjusted pitch attitude accordingly. Assuming this is typical of all landings, this certainly provides reference information but is hardly sufficient to achieve direct outer loop path control with the precision reflected in Fig. 57. If, However, the commander has pitch attitude displayed in some manner (HUD, reference lines on windscreen, etc.) then he might extract perturbation sink rate information through the dynamic relationship of Eq. 42 which is shown in Bode asymptote form in Fig. 63.

When $T_f > T_{\theta_2}$ then the amplitude ratio between $\dot{h}$ and θ is constant and the phase lag decreases as T_f increases. Therefore, the change in sink rate is proportional to change in pitch attitude but with a small time lag. Once the commander has learned (through training) the relationship between pitch attitude and sink rate he can then employ a three parameter terminal control technique in which pitch attitude is increased proportional to altitude decay and timed such that pitch attitude reaches the 8 deg reference and velocity approaches 195 kt while the vehicle is still a few feet off the ground. The sink rate is thus reduced to approximately -1 ft/sec (per Fig. 61a) and the attitude is held constant until touchdown.

Now, upon reexamination of the hodographs (Figs. 51, 53, 55, and 57) and the pitch attitude traces of Fig. 62, it is apparent that the two

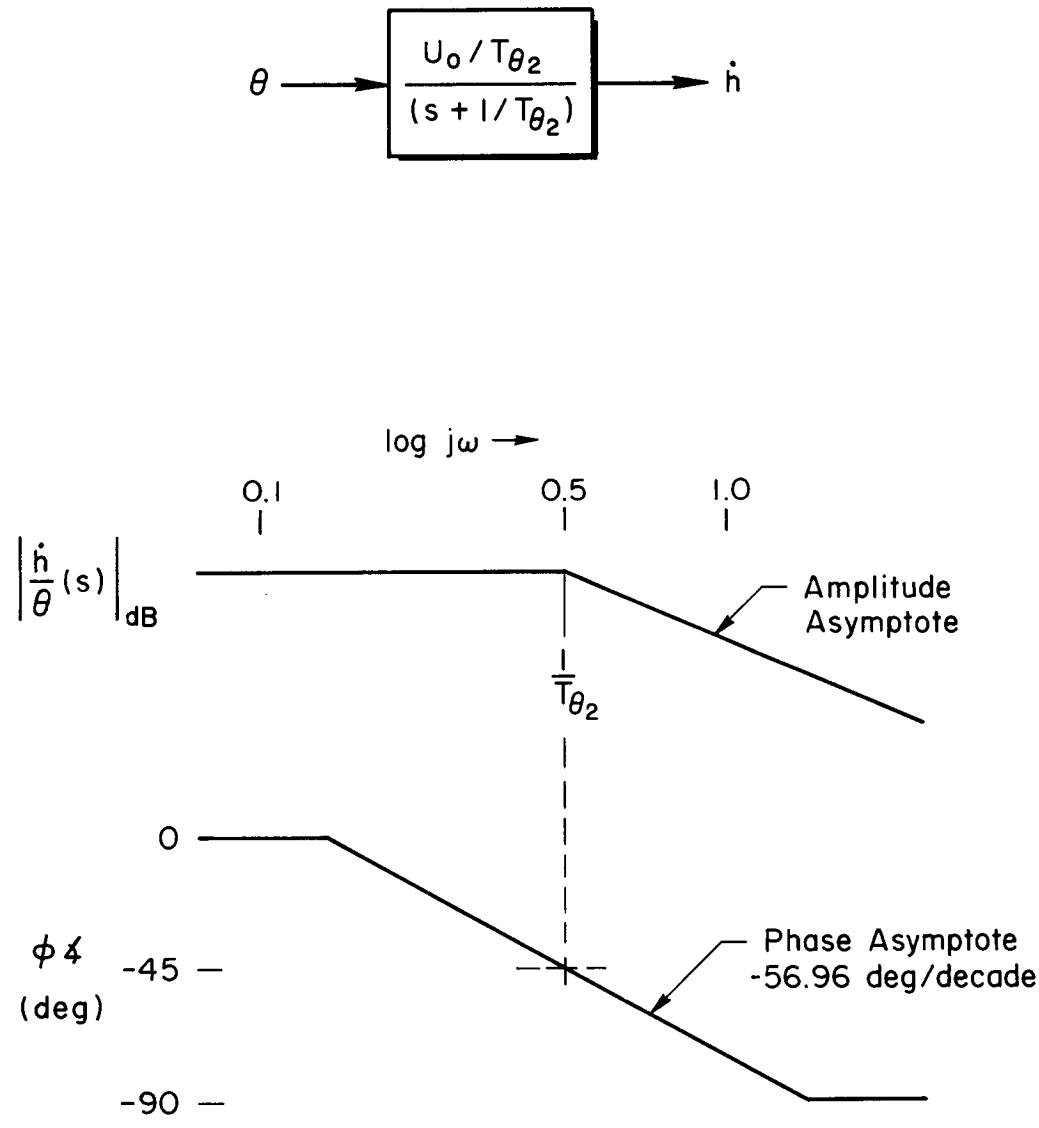

Figure 63. Bode Amplitude and Phase Asymptotes for First-Order Lag Approximation to $\dot{h}/\theta(s)$

flare strategies are really much the same. The difference between the "precognitive step θ" and the "exponential" flare is, in reality, merely a difference in the magnitude and number of steps employed. Or in other words, how tightly the attitude loop is closed. This in turn may be dictated by factors such as energy state relative to desired touchdown point, runway length constraints (runway vs. lakebed), etc.

It might be noted that this flare strategy will generally result in a flare time constant larger than T_{θ_2} since any attempt to maneuver at a response mode above $1/T_{\theta_2}$ will encounter an $\dot{h}/\theta$ amplitude ratio decrease, and a significant increase the time lag between θ and $\dot{h}$. This would drastically increase the pilots' workload.

3. Summary

One basic problem of the OFQ experiment has been to identify control strategies and loop structures employed by the different Shuttle crews in performing the critical task of final approach and flare. Due to operational constraints this has had to be accomplished in a non-intrusive, after-the-fact basis, without direct access to the flight crews.

Despite significant differences in landing conditions, aids available, and seemingly individualistic control strategies, it has been possible in the foregoing to reconstruct the landings to the point of identifying

- different segments of each approach and flare
- specific flight path parameters being controlled (strategy) in each segment
- loop structure employed (and hence vehicle dynamic ranges of special concern)
- "target" vehicle response and/or performance levels

This has been relatively straightforward for the steep glide through shallow glide segments for runway landings due, in part, to the various path aids available. However, the final flare segment has been more of

a challenge for all landings since at least two different control strategies appear to emerge. Both involve closure of pitch attitude as the inner loop and altitude as the outer loop in a four parameter (H, $\dot{H}$, θ, V) terminal control strategy. But at one extreme the maneuver consists of a precognitive step attitude change with the pulse input timed at an altitude and sink rate for which the basic vehicle path response will transition the vehicle from the shallow glide to a near nominal touchdown. This appears to be a relatively low gain closure of the inner loop since a pulse and wait type control activity is employed. At the other extreme, both loops appear tightly closed as the pilot performs an exponential flare in which pitch attitude (and hence sink rate) is adjusted proportional to altitude. The rapid stick pulsing is also indicative of lead generation in the presence of a K/s^2 controlled element. The choice between the two techniques may depend upon how soon (and well) the vehicle is stabilized on the proper shallow glide path.

The task remains to relate these findings to flying qualities requirements or criteria. This also is complicated by the fact that flight crews have not provided flying quality ratings, indications of workload, or any other commentary for the above task. For this we are forced to rely upon comparisons drawn from other information sources.

SECTION IV

DESIGN CRITERIA ISSUES FOR SHUTTLE CRAFT

In this section a review of flying quality criteria relevant to pitch attitude and flight path control is presented. It is shown that aircraft responses and criteria derived from conventional fighter aircraft are not generally applicable to large superaugmented aircraft such as the Shuttle. More appropriate pitch rate response and time delay criteria are suggested. Problems with pitch rate command/attitude hold (RCAH) control in the landing flare as opposed to attitude command/attitude hold (ACAH) are addressed, and the preference for the latter noted. Possible influence of the pilot's control manipulator configurations on the preference for ACAH over RCAH is also explored.

A. REVIEW OF FLYING QUALITY CRITERIA RELEVANT TO ADVANCED AIRCRAFT

1. Space Shuttle Longitudinal Flying Qualities Specification and Assessment

Because the Shuttle is always operated as a closed-loop system vehicle, the conventional MIL Spec open-loop aircraft format for flying qualities was considered to be inappropriate when the Shuttle specifications were being formulated. Instead Shuttle pitch axis flying qualities were specified (Ref. 30) in the time domain by an indicial response criterion with different normalized pitch rate boundaries for subsonic, supersonic, and hypersonic flight regimes. Since there is a dearth of comparative flying quality data for other than the subsonic conditions, only this regime will be considered herein. The initial circa 1973, subsonic response boundaries (Ref. 30) are shown by the dashed lines in Fig. 64. The solid boundaries of Fig. 64 reflect a later flight control system specification (Ref. 31) against which performance was verified (Ref. 32) prior to first flight.

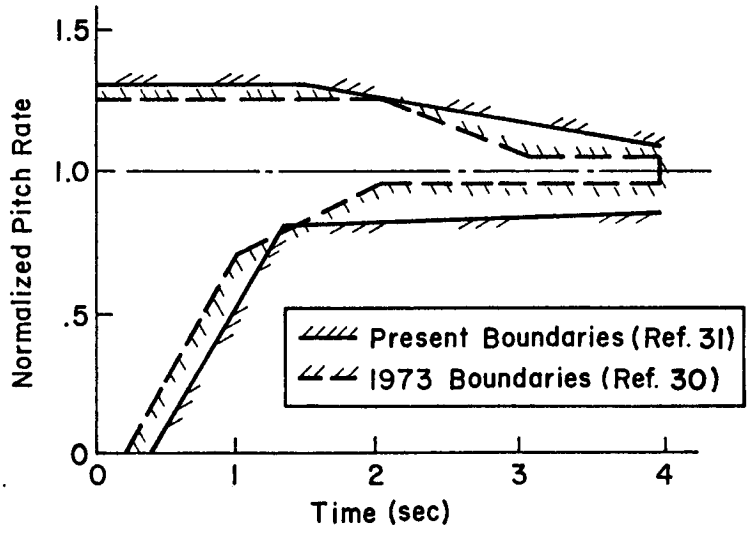

Figure 64. Specified Shuttle Pitch Rate Response Boundaries

The origins of and rationale behind the various boundaries are not well documented. The circa 1973 boundaries were presumably drawn primarily on the basis of simulation experience. The current (circa 1977) expanded boundaries also reflect piloted simulation of the Shuttle itself, and the allowable response excursions under conditions of various flight control component tolerance build-ups, off-nominal trajectory conditions, etc. It should be noted that the Shuttle boundary specification recognizes but one "level" of flying qualities because the fly-by-wire flight control system is quad-redundant, and theoretically there should be no change in flying qualities even in the presence of multiple dissimilar control system failures.

The simple time response boundary specification represents a significant departure from the specification concepts employed by the military (Ref. 33). Therefore a direct comparison of the Fig. 64 boundaries and time responses of other highly augmented aircraft configurations, plus a comparison of Shuttle response parameters with other existing or proposed flying qualities criteria, follows.

a. Evaluation Against NT-33 Flight Experience

Two flight experiments provide relevant dynamic response and accompanying flying quality rating data. These are the Landing and Approach Higher Order System (LAHOS) Study (Ref. 34) and the "Neal-Smith experiment" (Ref. 35). Both of these experiments were performed using the Calspan variable stability NT-33 aircraft, and both were designed to examine the effect of higher order control system elements which produce unconventional response modes. The basic approach to evaluation is to apply the Shuttle pitch rate specification to these data to see if it will discriminate between good and bad flying qualities. There is a conceptual problem with this approach, however. Although the NT-33 uses pitch feedbacks to augment the short-period, the attitude numerator zero remains conventional $(1/T_{\theta_2})$ since the airframe has significant static margin, and there is no forward loop integrator (hence, no $1/T_q$) equivalent to that in the Shuttle. Thus, the differences noted in the discussion concerning Fig. 20 must be kept in mind when comparing these data to the Shuttle specifications.

The LAHOS study was built around an approach and landing (Category C) task in which the evaluation flights were made through touchdown. A large number of configurations were evaluated, usually by two pilots with repeat evaluations being made randomly for many of the configurations. From these, six configurations have been selected as particularly relevant to assessment of the Shuttle pitch rate response criterion. These are divided into two groups. The first group shown in Fig. 65 consists of three configurations which exceed both the Refs. 30 and 31 Shuttle boundaries. These are characterized by rapid rise time and significant overshoot, and have overall pilot ratings equal to or better than 3-1/2, i.e., MIL Spec Level 1 flying qualities. In the LAHOS experiment, pilots gave a Cooper-Harper pilot rating for the overall task of approach and landing through touchdown. The ratings shown are two-pilot averages except for 3-c.

Figure 66 shows the three LAHOS configurations in the second group, i.e., those that do meet both sets of Shuttle response criteria. All

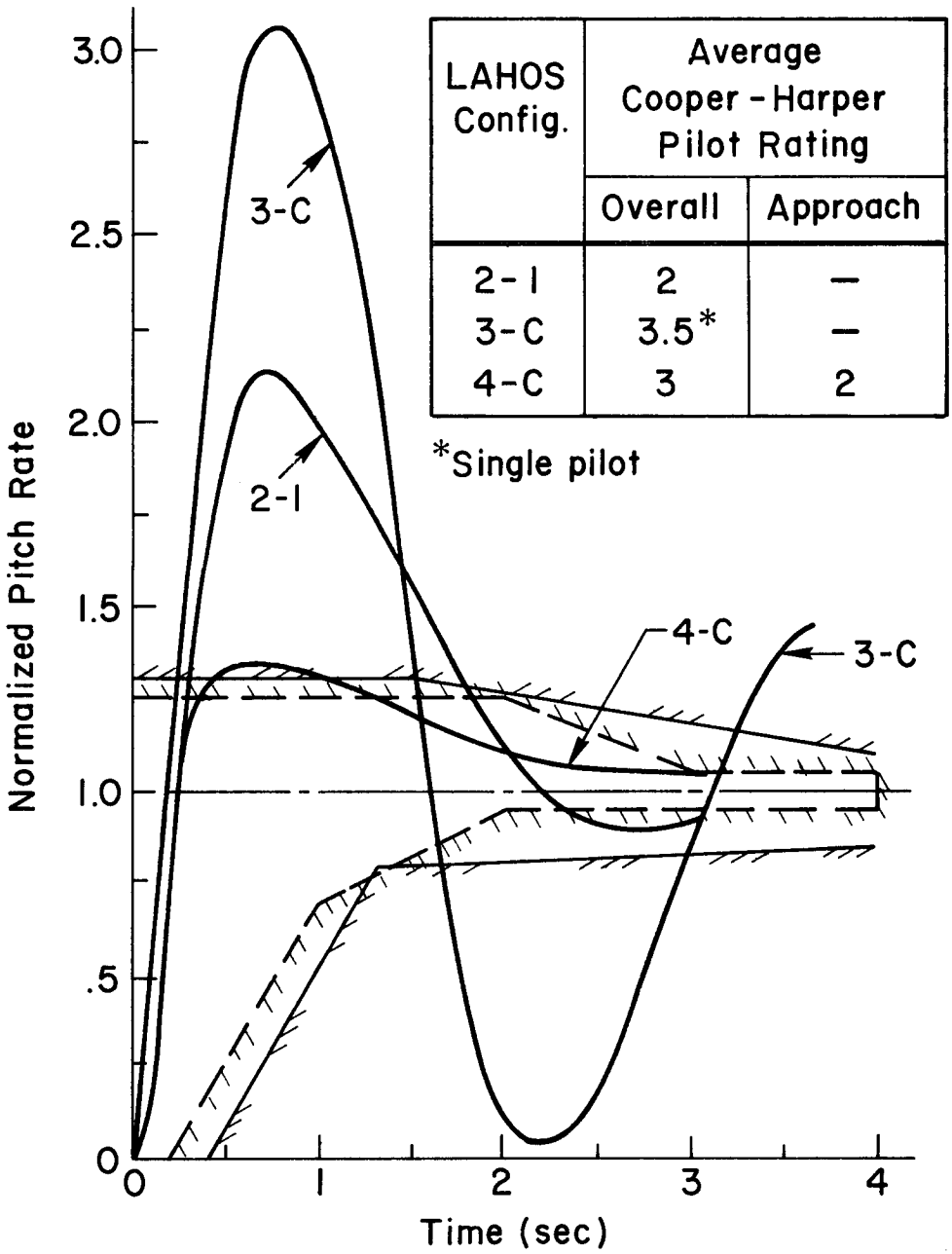

Figure 65. LAHOS Configurations Which Do Not Meet the Shuttle Pitch Rate Requirement

LAHOS Config.	Average Cooper-Harper Pilot Rating	
	Overall	Approach
4-0	6*	—
4-3	6.5	3.5
4-4	6.5	4.

*Single pilot

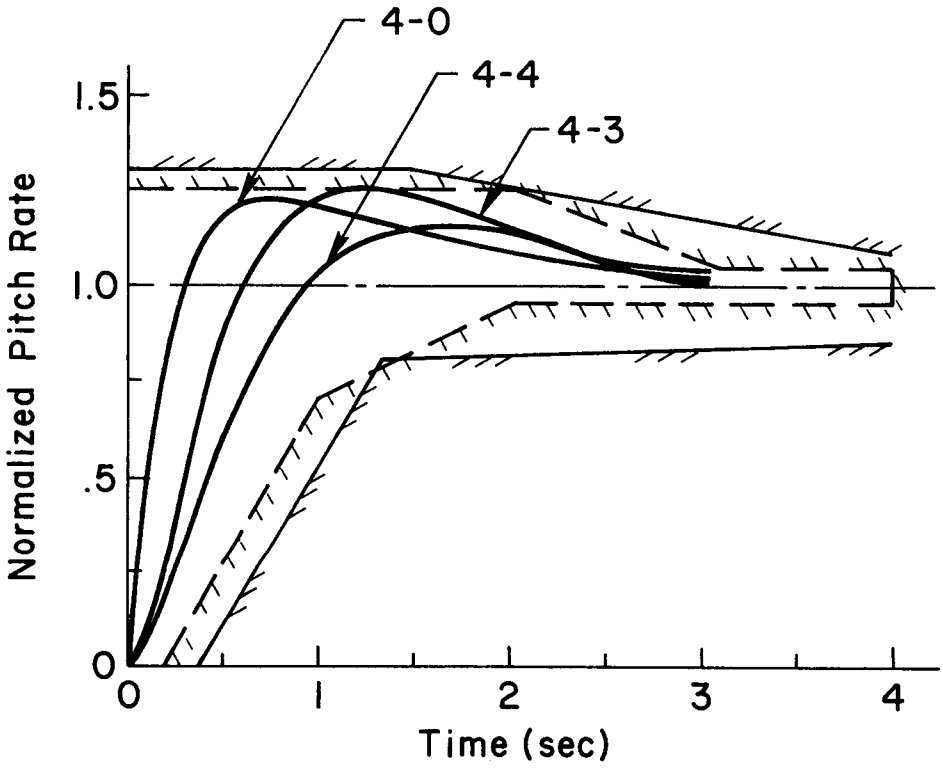

Figure 66. LAHOS Configurations Satisfying the Shuttle Pitch Rate Requirement

have overall pilot ratings between 6 and 7, i.e., flying qualities between MIL Spec Level 2 and Level 3. It should be noted that Configuration 4-0, which is the most rapidly responding of the three was rated by only one pilot; and thus, the rating cannot be considered as reliable as those for the other two configurations. These configurations, when compared to the previous group, are characterized by less overshoot, longer rise time, and greater effective time delay.

Thus in summary, the LAHOS data indicates that for six configurations relevant to the Shuttle, three configurations which did not meet the Shuttle response criteria had good (Level 1) flying qualities, and three which did meet the criteria had poor (Levels 2 to 3) flying qualities.

The Neal-Smith study was performed before LAHOS, and was similar in concept. However, the flight scenario was Category B (up-and-away flight), and the task was rather general with the pilots instructed to "rapidly acquire and track distant air and ground targets." It is felt that this task is analogous to the Shuttle tasks in the initial part of Terminal Area Energy Management (TAEM). Eighteen Neal-Smith configurations are compared to the Shuttle pitch rate response boundaries in Ref. 1, and give very similar results to the LAHOS results, i.e., configurations with good flying qualities ratings generally exceeded the Shuttle pitch rate boundaries; and conversely, those configurations with poor ratings generally met the criteria. However, to repeat, the LAHOS and Neal-Smith data obtained in a statically stable aircraft having a conventional $(1/T_{\theta_2})$ pitch numerator and no forward loop integration, may not be relevant to the larger Shuttle with its unconventional relationship between altitude and path dynamics.

b. Evaluation Against High Performance Aircraft

To provide further assessment of the Shuttle pitch rate response boundaries, the responses of four high performance aircraft in approach flight conditions were compared to the boundaries in Ref. 1. The four are the YF-12, the YF-17, and two fly-by-wire aircraft referred to as

"A" and "B." One of the latter incorporates forward loop integration during the approach and landing phase of flight.

Figure 67 shows the responses of two aircraft considered to have good landing flying qualities, the YF-12 and YF-17, compared to the Shuttle boundaries. It may be seen that the YF-17 response (which was obtained from an in-flight simulation of the YF-17 modified flight control system in the LAHOS program) exceeds the upper boundaries of both Refs. 30 and 31. However, these two configurations may be categorized as having both fairly rapid rise and settling times and very little initial delay.

Figure 68 shows the comparison for early versions of the two fighter aircraft, both of which were reported to have flying qualities problems in landing. These aircraft also overshoot the upper boundary, but have larger effective time delays, slower rise times, and much longer settling times than the YF-12 and YF-17 shown in the previous figure. For both modern fighters, the source of the delay is primarily high order lags within the control system including, in one, a significant computational delay in the digital flight control system. The characteristics for both aircraft have since been modified by reducing the delays and other FCS changes.

c. Assessment of the Shuttle Against Its Own Specification

Figure 69 shows a comparison of the Shuttle with its pitch rate boundaries. The response is the linearized models of Fig. 26 derived from the STS-4 flight data. It shows the Shuttle meets the criterion as presently defined. Compared to the YF-12 and YF-17 (Fig. 67), the Shuttle exhibits greater effective time delay, rise time, and settling time, and has considerably less overshoot. Compared to Modern Fighters A and B (Fig. 68), the most significant differences are the lower overshoot and longer rise time of the Shuttle. Extensive verification simulations with detailed models conducted by Shuttle contractors (Ref. 32) also have shown that the Shuttle generally satisfies the present criteria even for many off-nominal flight conditions. Figure 69 also includes

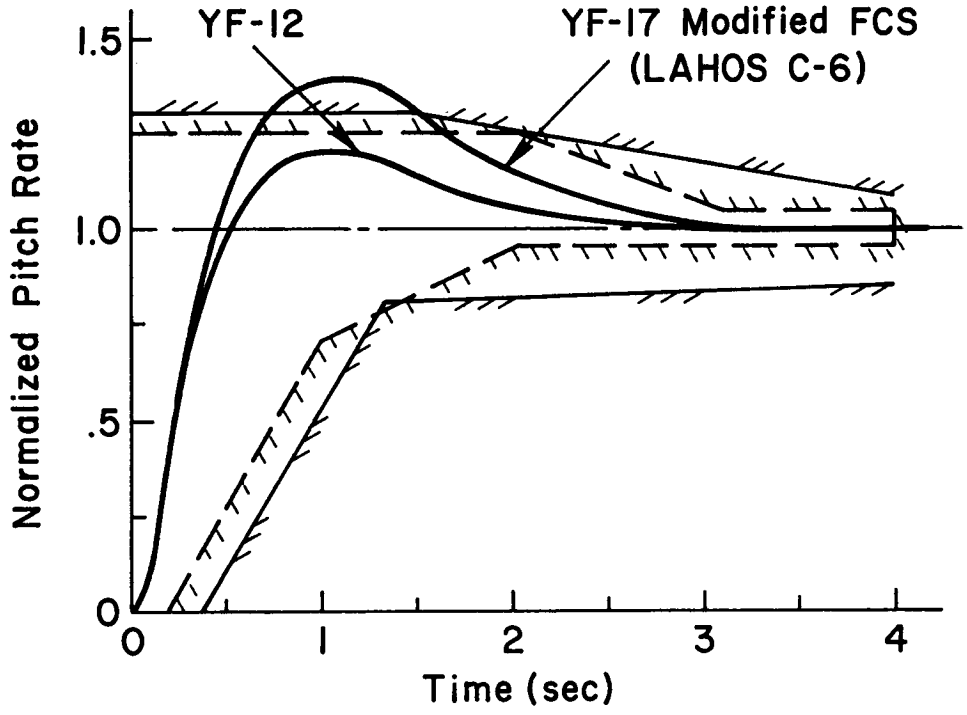

Figure 67. Comparison of the YF-12 and YF-17 Pitch Rate Responses to the Shuttle Requirements

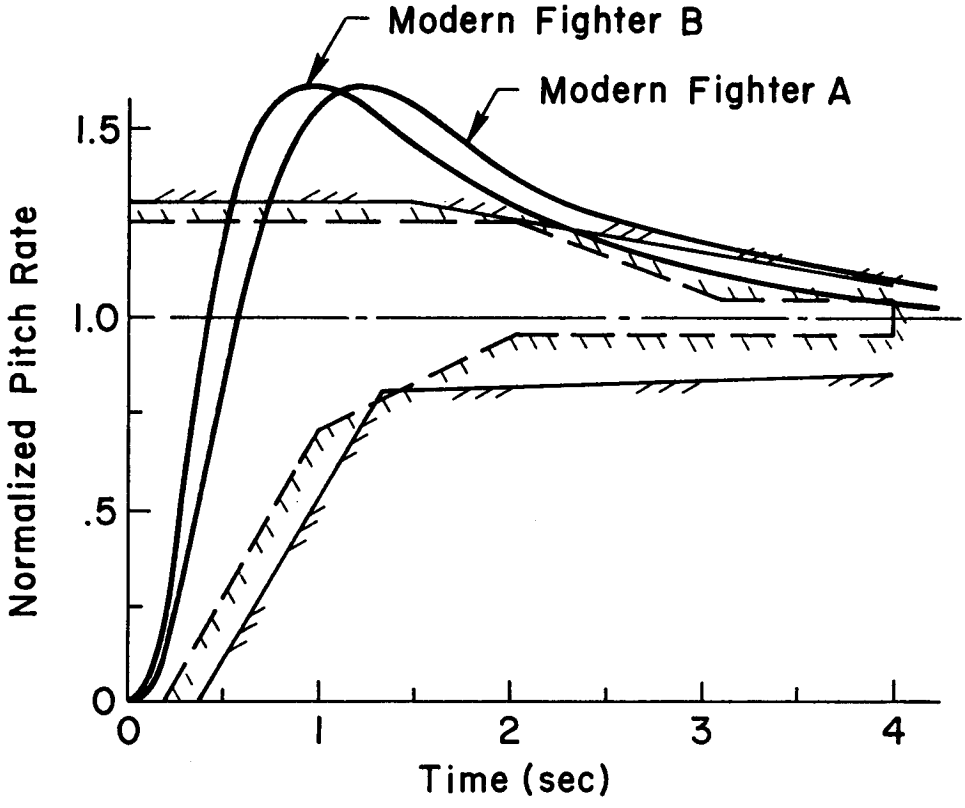

Figure 68. Comparison of the Fighter A and B Pitch Rate Responses to the Shuttle Requirements

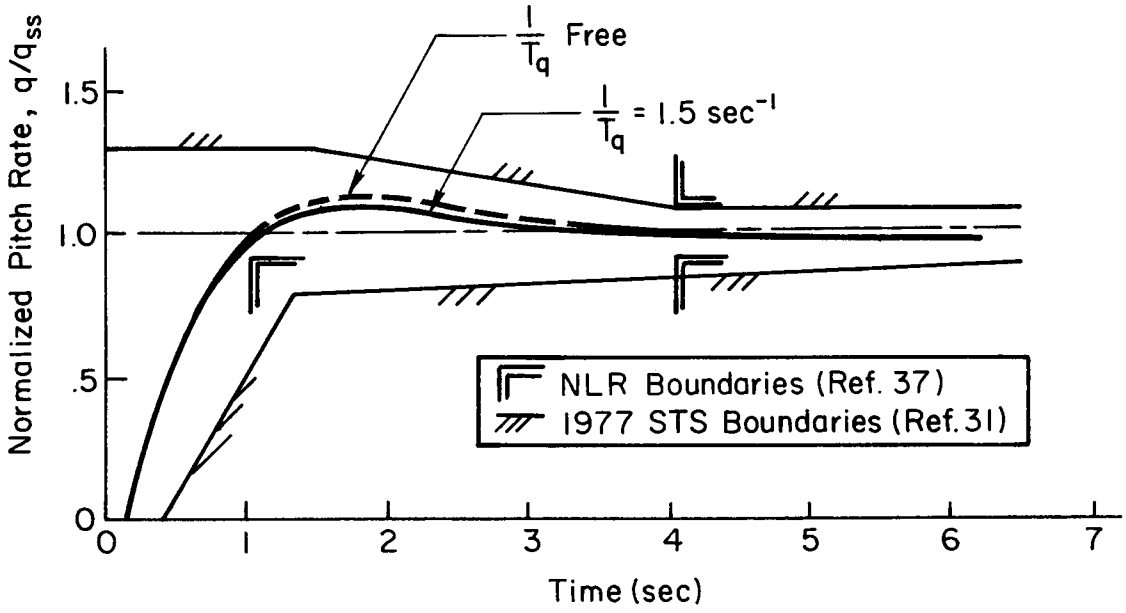

Figure 69. Comparison of Flight-Derived STS-4 Effective q/δ_{RHC} with $1/T_q$ Fixed and Free to the Shuttle Pitch Rate Response Specification

time response boundaries derived from the experiments of Refs. 36 and 37 discussed next, and show the Shuttle also meets these boundaries.

d. Assessment Against Class II and III Relaxed Static Stability Aircraft Simulation

Two recent simulation studies provide the best available data relevant to the flying qualities of "superaugmented" relaxed static stability aircraft. The program discussed in Refs. 36 and 37 involved simulation of a relaxed static stability (RSS) version of the Fokker F-28 medium transport on the NLR ground simulator and on the Calspan TIFS aircraft. A rate command/attitude hold FCS was employed, which was somewhat different in concept from the Shuttle system, however, some of the configurations are of interest.

A second TIFS simulation of interest is the Calspan "million pound airplane" study of Refs. 38 and 39, which was in part devoted to study of Shuttle related issues. Three "airframes" were simulated -- "long aft tail," "short aft tail," and "canard" -- which essentially differed

only in Z_{δ_e}, and therefore in instantaneous center of rotation location for elevator inputs. Other variables in the experiment were the two FCS designs (one of which was identical to the Shuttle concept), effective time delays, and pilot location.

1. NLR Experiments. The NLR experiment, Refs. 36 and 37, employed an FCS (shown conceptually in Fig. 70) somewhat more general than the Shuttle system. In particular, the feedback time constant, T_q, and the feedforward time constant, τ_m, were varied independently. The configurations of interest here are the four in the "F" series (see Fig. 71) in which $1/T_{q_1} = K_\theta/K_q$ was fixed at 1.40 sec^{-1} while $1/\tau_m$ was varied between 0.186 sec^{-1} and 0.870 sec^{-1}. The resulting pitch rate response to command transfer functions are tabulated in Table 8 in the form

$$\frac{q}{q_c}(s) = \frac{K(1/T_{\theta_1})(1/T_{\theta_2})(1/\tau_m)}{(1/T'_{sp_2})(1/T'_{sp_1})[\zeta', \omega'_n]} \tag{43}$$

This represents a "superaugmented" configuration to the extent that

$$\frac{1}{T'_{sp_2}} \doteq \frac{1}{T_{\theta_1}} = 0.0835 \text{ sec}^{-1}$$

$$\frac{1}{T'_{sp_1}} \doteq \frac{1}{T_{\theta_2}} = 0.715 \text{ sec}^{-1}$$

and thus

$$\frac{q}{q_c}(s) \doteq \frac{K(1/\tau_m)}{[\zeta', \omega'_n]}$$

The effective attitude zero is thus $(1/\tau_m)$. Unfortunately, only one value of $1/\tau_m$ is slightly greater than $1/T_{\theta_2}$, and thus these configurations do not provide data specifically relevant to the Shuttle path/attitude issue (i.e., the $1/T_q \gg 1/T_{\theta_2}$ situation). However, some tentative conclusions may be reached. In particular, the normalized time

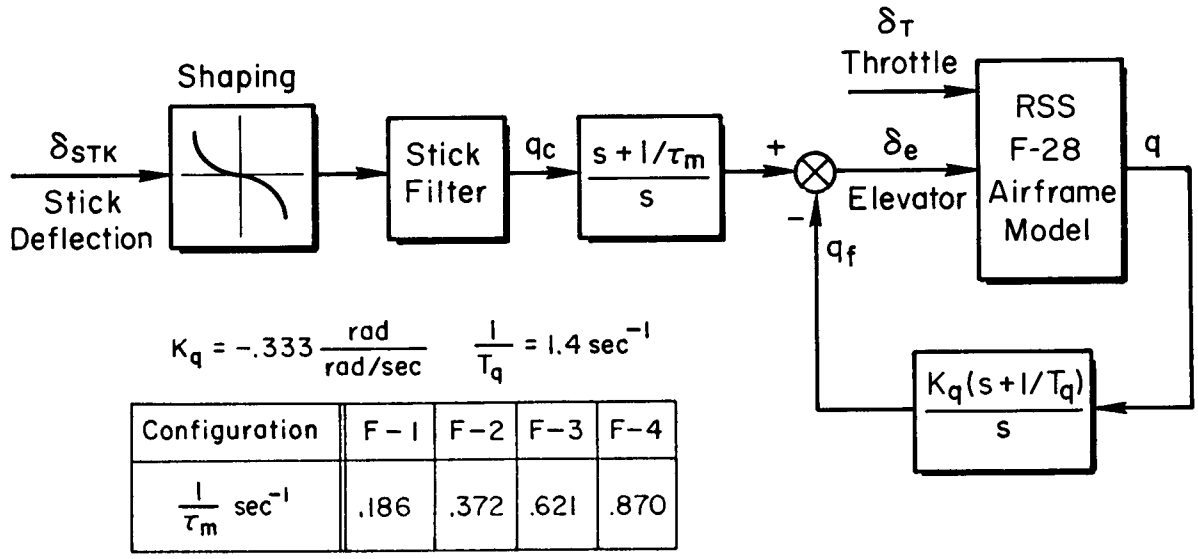

Configuration	F-1	F-2	F-3	F-4
$\frac{1}{\tau_m}$ sec^{-1}	.186	.372	.621	.870

Figure 70. Basic Structure of the FCS Used in the Ref. 37 Study

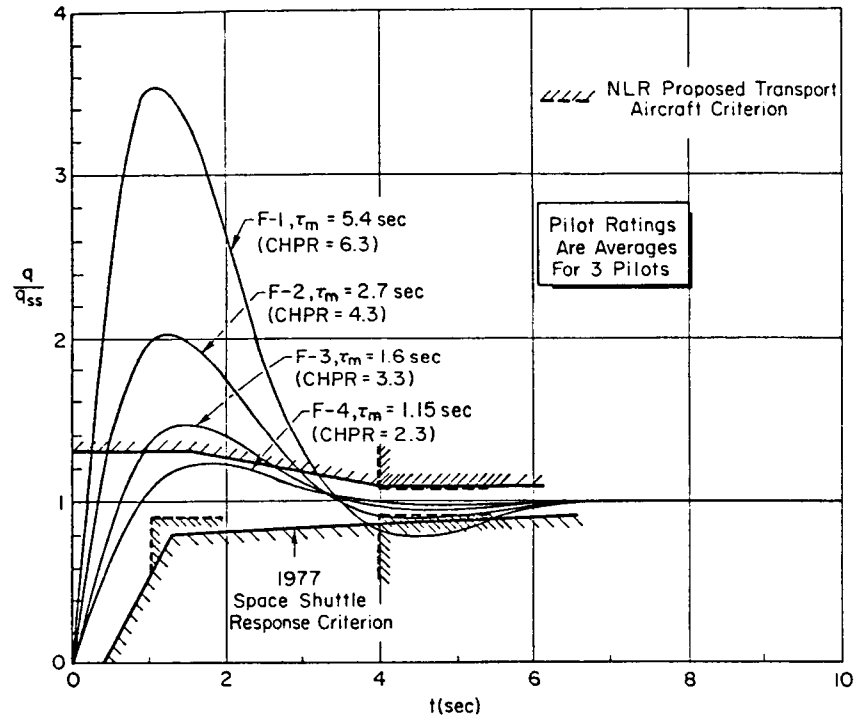

Figure 71. Normalized Indicial Pitch Rate Response of Ref. 37 "F" Configurations Compared to Exemplary Criteria (T_{θ_2} = 1.4 sec)

TABLE 8. $\frac{q}{q_c}(s)$ TRANSFER FUNCTIONS, F CONFIGURATIONS OF REFERENCE 37

CONF.	$\frac{q}{q_c}(s)$, $\lfloor\frac{\text{rad/s}}{\text{rad/s}}\rfloor$
F-1	$\frac{90.4(0.0835)(0.715)(0.186)}{\Delta'}$
F-2	$\frac{45.0(0.0835)(0.715)(0.372)}{\Delta'}$
F-3	$\frac{27.0(0.0835)(0.715)(0.621)}{\Delta'}$
F-4	$\frac{19.3(0.0835)(0.715)(0.868)}{\Delta'}$

$\Delta' = (0.0780)(0.857)(10.)[0.703, 1.194]$

responses to step commands, Fig. 71, show that increasing the frequency of the effective attitude zero (at least to $1/\tau_m \doteq 1/T_{\theta_2}$) improves flying qualities. It also shows that this variation increases rise time while decreasing overshoot. The Fig. 71 trend when compared to the LAHOS data correlation in Figs. 65 and 66, strengthens the argument that "superaugmented" aircraft have "unconventional" flying qualities. As an aside, it should be noted that the F-4 configuration is essentially a conventional aircraft in that the effective attitude lead is close to $1/T_{\theta_2}$. It is also of interest to note that the best-rated (Level 1) F-4 configuration (though not technically Shuttle-like as noted) satisfies the present Shuttle pitch rate specification.

Time domain pitch response criteria for transport aircraft, similar in concept to the Shuttle criterion, were proposed in the NLR study. They consist of rise time and settling time boundaries as shown in Fig. 71. The settling time requirement is only slightly "tighter" than the Shuttle spec, but the rise time requirement is notably more stringent. Interestingly, there is no NLR requirement proposed for overshoot.

2. TIFS Million Pound Airplane. The "million pound airplane" study (Refs. 38 and 39) provides an interesting comparison between what are perhaps the two fundamental approaches to augmentation of RSS aircraft, the Shuttle-type q, $\int q \rightarrow \delta_e$ system and the "M_α augmentor," a pure gain $\alpha \rightarrow \delta_e$ system. Either system will provide a stable vehicle, but with different side effects -- e.g., sensitivity to turbulence for the α system and neutral speed stability for the q system. On the basis of gross comparison between the two, the (higher gain) q systems were rated better by the evaluation pilots.

For the Shuttle-like pitch rate systems, several gain levels and two T_q values were used to vary the augmented aircraft response. Of these, only one configuration was (technically) similar to the Shuttle (i.e., $1/T_q > 1/T_{sp_1} > 1/T_{\theta_2}$). This was a short aft tail, extra high K_q configuration with $1/T_q = 2.0$ sec^{-1}. The effective augmented vehicle model is

$$\frac{q'}{q_c} = \frac{2.29(2.0)e^{-0.11s}}{[0.54,\ 2.14]} \tag{44}$$

which is quite close to the Shuttle OFT model (Eq. 8c). A step response for this dynamic model is shown in Fig. 72 to meet the Shuttle specification. Unfortunately, only a single pilot rating is available for this configuration (CHPR = 4). Pilot comments do not indicate a specific problem.

Three Ref. 38 "high K_q" pitch rate system configurations differ technically from the effective Shuttle dynamics in that $1/T_{sp_1} > 1/T_q > 1/T_{\theta_2}$. However, these configurations are superaugmented in the sense that the effective dynamics are dominated by the FCS parameters. Figure 73 shows the step response for one case, a short aft tail, high K_q configuration with T_q = 1 sec. The overshoot, while less than the maximum in the present Shuttle boundary, is extended somewhat further, and the rise time is also fairly large. Nonetheless, this pitch rate response is not too far removed from the exemplary boundaries. This configuration was evaluated by both pilots in the study, and received generally good ratings. In its second evaluation by one pilot, it was given a Cooper-Harper rating of 1, which is extremely unusual (the same pilot initially evaluated it as 4). The pilot commentary indicates initial problems in trim basically in attempting to "Keep the airspeed and attitude organized." After familiarization, however, the same pilot noted that "Airspeed control is excellent. Once I get it trimmed up, it virtually holds the airspeed, holds attitude, and stays trimmed in turns." The other pilot indicated that "airspeed control was good, predictable." His summary comment was "No major problems; an excellent airplane." From these comments it would appear that in precision path control, a superaugmented configuration may indeed exhibit good flying qualities. There does appear to be a potential familiarization problem, although this is rapidly overcome. This one flight data point goes a long way toward justifying a position that heavily augmented RSS aircraft, especially as they approach the superaugmented condition, cannot satisfactorily be judged by criteria or compared with data from conventional aircraft.

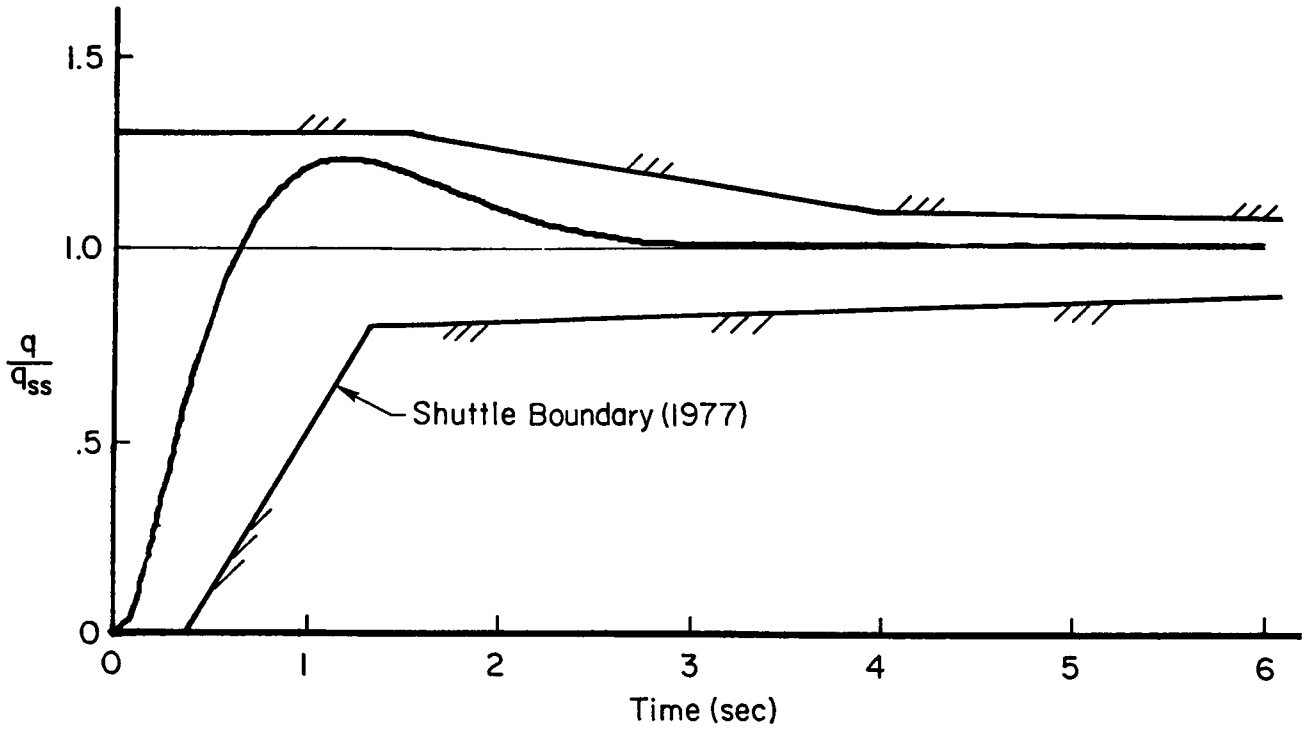

Figure 72. Normalized Indicial Pitch Rate Response to Stick Force, Ref. 38 Short Aft Tail, Extra High K_q, T_q = 0.5 Configuration

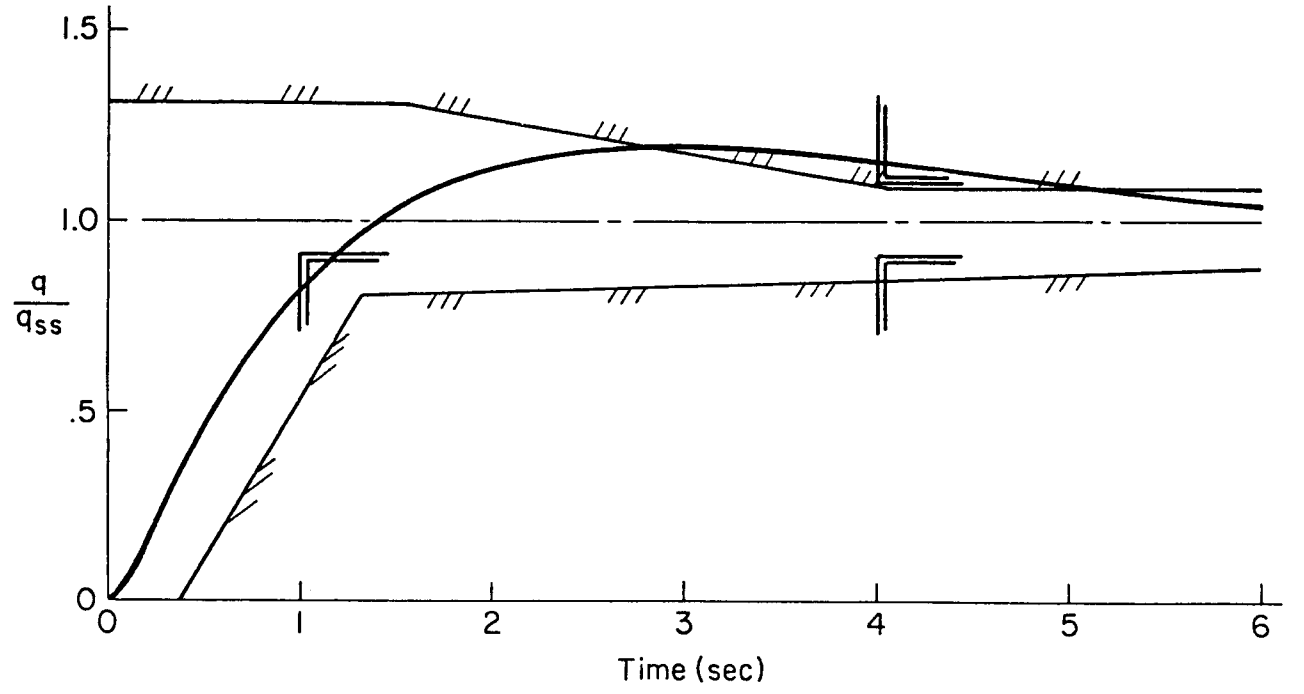

Figure 73. Normalized Indicial Pitch Rate Response to Stick Force, Ref. 38 Short Aft Tail, High K_q, T_q = 1 sec Configuration

e. Summary

The preceding has indicated that flying qualities assessments obtained with conventional (statically stable) highly augmented vehicles may not be applicable to Shuttle-like superaugmented vehicles. It has also shown that the Shuttle time domain pitch rate boundary compares favorably with the pitch rate response characteristics of RSS highly augmented vehicles rated Level 1. However, the Shuttle boundary may unduly restrict overshoot but not sufficiently restrict effective time delay and response rise time. It would appear that the NLR boundaries might be more appropriate for response rise time and settling time, and that new requirements might be needed to restrict effective time delay. One definite criticism can be made of the Shuttle specification; it considers pitch attitude control only without explicit regard for flight path control.

2. Assessment of the Shuttle Against MIL-F-8785C and Other Proposed Criteria

The Shuttle OFT, the Shuttle Approach and Landing Test (ALT) vehicle, the four aircraft of the preceding Section 1, and some additional "reference" aircraft were compared in Ref. 1 to the present U.S. Military flying qualities specification, MIL-F-8785C (Ref. 33). The MIL Spec was considered not as a superior approach, but rather because it is probably the most widely used and well established flying qualities specification. It therefore codifies much of the specification data and lore of flying qualities research and concepts.

MIL-F-8785C contains three requirements which are potentially relevant to Shuttle pitch control: "Short-period frequency and acceleration sensitivity" (Section 3.2.2.1.1); "Short-period damping" (Section 3.2.2.1.2); and "Dynamic characteristics" (Section 3.5.3, Table XIV). No problems are indicated with respect to short-period damping for any of the aircraft considered here, and this requirement will not be discussed further. However, application of short-period frequency requirements to the Shuttle presents some important conceptual problems that require some background discussion.

a. Consideration in LOES Modeling

It is widely recognized that application of the frequency domain specifications of the MIL Spec to highly augmented aircraft requires some form of "lower order equivalent system" (LOES) model. LOES models are generally formulated by numerically fitting a low order form to a high order system (HOS) transfer function numerically via a digital computer program. This form is specified a-priori with variable parameters to be adjusted to a best fit of the HOS. The LOES form is generally taken as that for a classical unaugmented airframe with the idea that at least some of the flying qualities data accumulated over the years for conventional aircraft could thereby be extended to highly augmented aircraft. By extension of this reasoning, the flying qualities specification formats developed for conventional aircraft could also be used for some highly augmented aircraft.

For longitudinal pitch attitude control, the LOES model is usually based on the short-period approximation, Eq. 23. This led to a controversy over whether $1/T_{\theta_2}$ should be allowed to vary in the numerical fitting process (the "galloping L_α" issue) or be fixed at the classical value of $1/T_{\theta_2} \doteq -Z_w$. The more or less generally accepted present view seems to be noted in Ref. 40 -- namely that the pitch attitude and path angle (or reasonable surrogates thereof), HOS transfer functions should be fitted simultaneously. For fairly conventional aircraft this produces a $1/T_{\theta_2}$ near the classical airframe value, and thus a generally acceptable alternative procedure is to fix $1/T_{\theta_2}$ at the airframe value during the fitting process. When this is done for the Shuttle OFT, the result is (Ref. 2)

$$\frac{q}{q_c}(s) = \frac{2.26(0.54)e^{-0.213s}}{[0.728,\ 1.104]} \tag{45}$$

This conventional LOES modeling concept is fundamentally different from the analytical LOES approach used to derive the literal approximation to q/q_c given in Eq. 8c. In particular, the significant difference

between $1/T_q \doteq \omega_e = 1.5\ \text{sec}^{-1}$ in Eq. 8c, and the considerably lower $1/T_{\theta_2} = 0.54\ \text{sec}^{-1}$, and $\omega = 1.104$ found in Eq. 45 should be noted. Also the effective time delay is larger in Eq. 45 than in Eq. 8c.

b. MIL Spec Short-Period Requirements

The short-period frequency and acceleration sensitivity requirement relates pitch attitude and path (normal acceleration) response through the Control Anticipation Parameter (CAP) defined in the time domain by Bihrle (Ref. 41) as

$$\text{CAP} \equiv \frac{\ddot{\theta}(0)}{n_{ss}} \tag{46}$$

which under the short-period approximation is

$$\text{CAP} = \frac{\ddot{\theta}(0)}{(U_o/g)\dot{\theta}_{ss}} \tag{47}$$

CAP is generally computed from an approximation (in frequency domain parameters) based on conventional (short period) airframe dynamics, i.e.,

$$\text{CAP} \doteq \frac{\omega_{sp}^2}{(U_o/g)(1/T_{\theta_2})} = \frac{\omega_{sp}^2}{n/\alpha} \tag{48}$$

For the Shuttle OFT, this gives CAP = $0.246\ \text{sec}^{-2}$ at $n/\alpha = 5.6$ g/rad. On this basis the Shuttle OFT (and ALT) would be Level 1 on the MIL Spec Category C short-period frequency requirements, Fig. 74, and would compare favorably to other large conventional aircraft.

However, this conclusion must also be qualified in light of the Shuttle's unconventional pitch attitude dynamics. Even if the concept

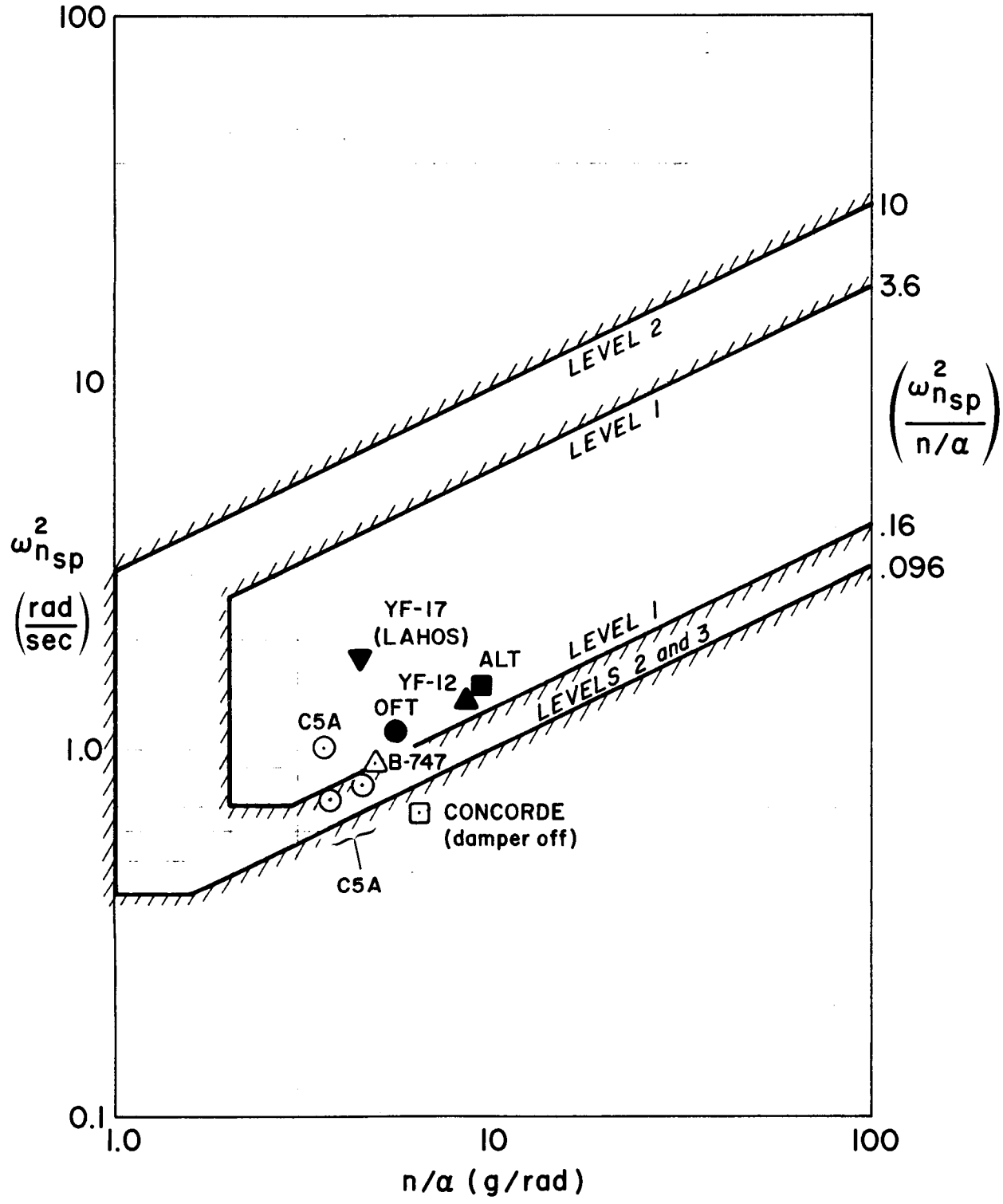

Figure 74. Comparison of Aircraft to MIL-F-8785C Short-Period Frequency Requirements - Category C, Class III, Based on Conventional LOES Model (from Reference 2)

of CAP is valid for the Shuttle, calculating it by Eq. 48 is not. Instead using the analytic LOES model Eq. 8c with Eq. 47;

$$CAP \doteq \frac{\omega_n^2}{(U_o/g)(1/T_q)} = 0.143 \text{ sec}^{-2} \qquad (49)$$

Since n/α is independent of pitch attitude dynamics, the 3 parameters of the MIL Spec short-period frequency requirements are for the OFT

$$\omega_n = 1.40 \text{ sec}^{-1},$$

$$CAP = 0.14 \text{ sec}^{-2},$$

$$n/\alpha = 5.6 \text{ g/rad}$$

This set of characteristics cannot be accommodated by Fig. 74, which implies the MIL Spec requirement is inappropriate for Shuttle-like superaugmented aircraft.

c. Effective Time Delay

The military flying quality (Ref. 33) specification defines effective time delay in terms of $\dot{\theta}/F_S$ or n_z/F_S, where τ_e is taken as the greater value of the two. Thus, τ_e is the effective time delay between pilot force at the manipulator and vehicle $\dot{\theta}$ or n_z response. By constrast, most of the available data concerning τ_e reflects measurements between manipulator displacement and vehicle response. Therefore, the feel system dynamics lag (delay increment) between force application and manipulator deflection is included in the Ref. 33 criterion; whereas it must be added to most other data in order to make a direct comparison. Typically, this feel system effective time delay contribution can be expected to be about 0.05 sec.

Figure 75 shows the effective time delay (τ) based on the conventional LOES for the Shuttle ALT and OFT (Ref. 2), and the four aircraft

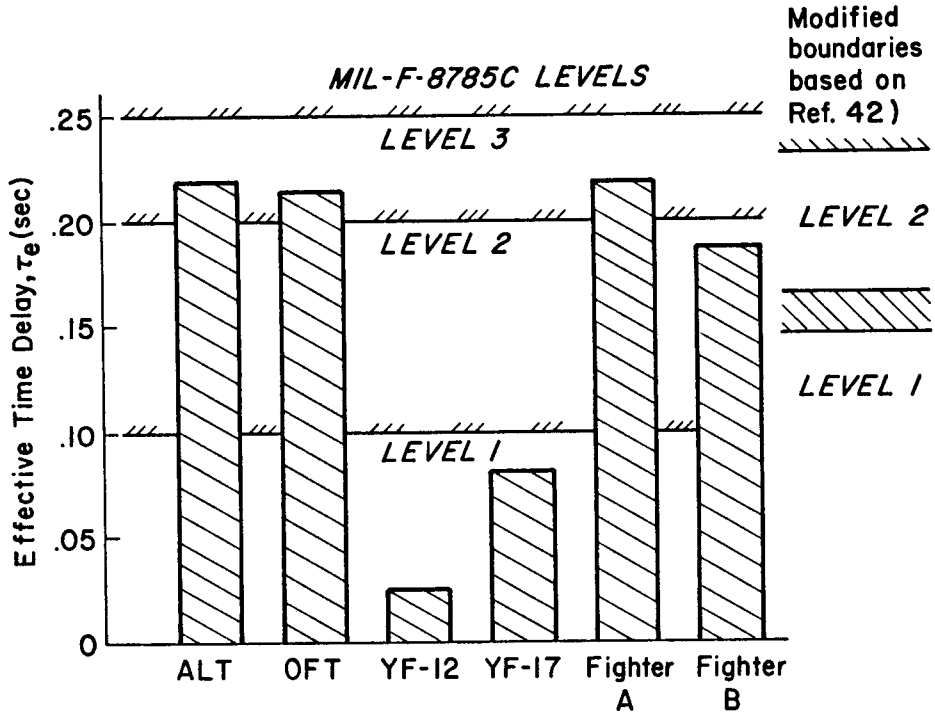

Figure 75. Comparison of Six Aircraft with MIL-F-8785C Time Delay Requirement (Based on the Conventional LOES)

examined previously compared to the time delay requirements of MIL-F-8785C. It may readily be seen that the two aircraft earlier identified as having good flying qualities, the YF-12 and YF-17, have the lowest effective time delay, and both are well within the Level 1 requirements of 8785C although the YF-17 would probably be Level 2 if the feel system contribution is to be added. The Shuttle configurations both have much larger time delays, which fall into the Level 3 region, and are comparable to Modern Fighters A and B noted earlier as having precision approach and landing problems. And to be further noted, the Fighter A τ_e is based on stick force input while Fighter B may be based on stick position input.

However, a comparison in Fig. 75 of flying quality level boundaries from MIL-F-8785C and from an experiment on the NASA-Dryden F-8 aircraft (Ref. 42) indicates the MIL Spec requirements (which are not well documented) may be overly restrictive. The Ref. 42 data based upon stick

position input indicates the Shuttle and both Fighters A and B to be Level 2, and the YF-12 and YF-17 to definitely be Level 1.

These difficulties with the present MIL Spec led to the following comparison of the Shuttle and the other reference aircraft to several new concepts for flying qualities criteria.

d. The CAP' Specification

As noted recently by Bischoff (Ref. 43), the control anticipation parameter must be redefined for aircraft with effective time delay since $\ddot{\theta}(0) = 0$ in this case. Bischoff defines on the basis of a unit step stick force input, a more general control anticipation parameter, CAP', as

$$CAP' \equiv \frac{\ddot{\theta}_{max_{HOS}}}{n_{ss}} \tag{50}$$

where the maximum pitch acceleration, $\ddot{\theta}_{max_{HOS}}$, will occur sometime after the input. CAP' is further extended to the conventional short-period LOES model giving an approximate form denoted CAP'_e.

Reference 43 does not address the question of the validity of extending CAP to systems with significant effective time delay, but does propose a specification by defining flying qualities levels in the $CAP'_e - \tau_e$ plane (see Fig. 76). The CAP'_e (vertical) boundaries shown for each flying quality level were defined by correlations of data from DiFranco (Ref. 44), Neal and Smith (Ref. 35), and the LAHOS study (Ref. 34), and thus are not transformations of the MIL Spec CAP boundaries. It should be noted that while the definition of the levels vary with flight category in the MIL Spec, they are apparently the same for all categories in Ref. 43. The time delay boundaries are the same as MIL-F-8785C, and are independent of CAP.

Figure 76 indicates the Shuttle OFT and ALT are Level 3 primarily upon MIL Spec LOES τ_e values, and would be Level 2 based upon the NASA Dryden τ_e boundaries (Fig. 75). Second, the Shuttle is in the Level 2

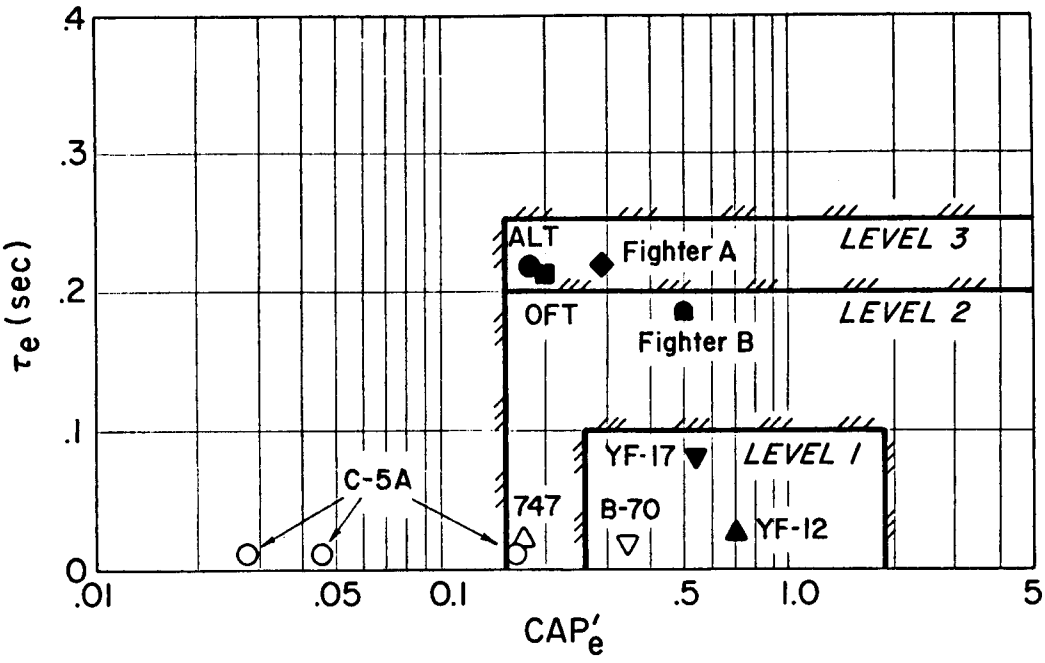

Figure 76. Comparison of Eight Aircraft with the Reference 43 CAP'_e Criterion

CAP'_e region not directly due to the use of CAP'_e (in place of CAP), but rather due to the redefinition of the lower boundary in Ref. 43 (i.e., Level 2 is $0.15 \leq CAP'_e \leq 0.25$; whereas in Fig. 74, Level 2 is $0.096 \leq CAP \leq 0.16$). Third, the Ref. 43 CAP'_e developments are based on the conventional LOES model, and must be qualified for the Shuttle as noted previously. However, the need to consider effective time delay in the use of CAP seems clear.

e. The Bandwidth/Time Delay Criterion

A new criterion for highly augmented aircraft (Ref. 45) has been developed for possible use in the new Military Standard planned to replace MIL-F-8785C. This criterion is based on direct use of the HOS $\theta/\dot{\theta}_c$ frequency response (Bode plot), and thus avoids the previously discussed problems related to LOES modeling and CAP. The criterion shown in Fig. 77 defines flying qualities levels in the pitch attitude bandwidth -- τ_p plane. "Bandwidth" as used here is defined as the highest frequency with at least a 6 dB gain margin, and at least a 45 deg phase

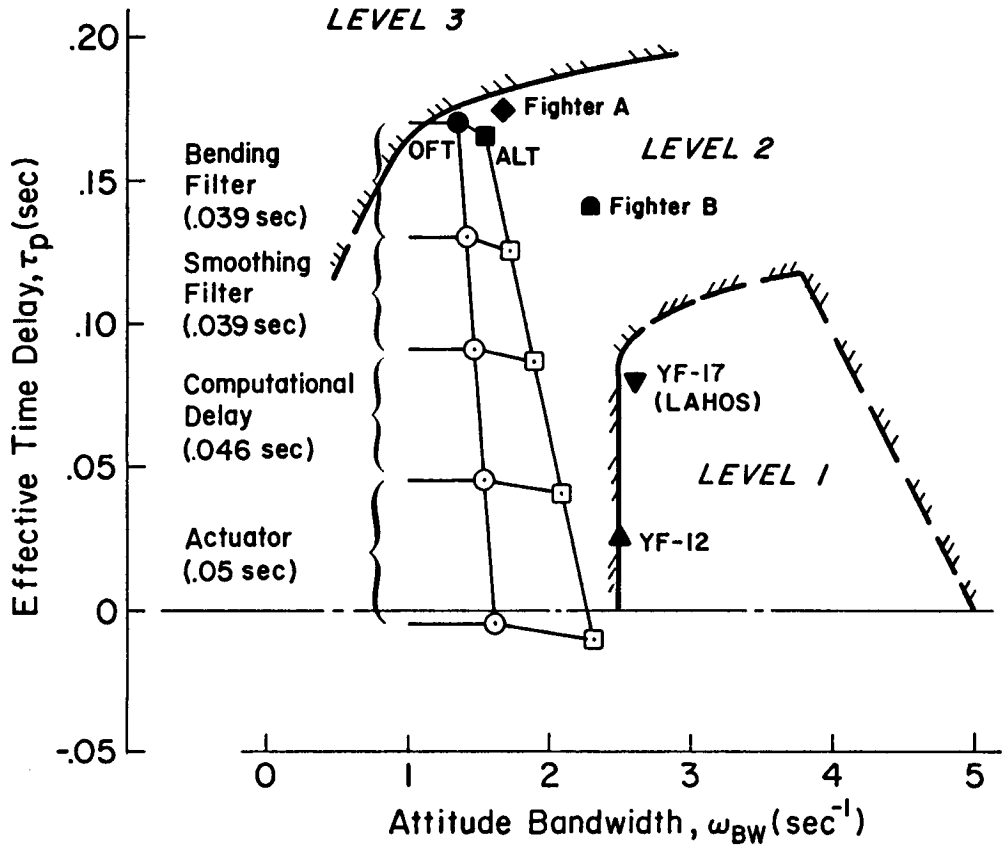

Figure 77. Comparison of the Shuttle ALT and OFT with Four Augmented Aircraft in the Bandwidth/Time Delay Plane

margin. The time delay parameter, τ_p, is defined on the HOS phase plot as

$$\tau_p = (\phi_{2\omega_{180}} + 180 \text{ deg})/(57.3 \times 2\omega_{180}) \quad (51)$$

which approximates $d\phi/d\omega$ near phase crossover (ω_{180}), and correlates well with the τ_e from analytic LOES modeling.

Figure 77 compares the ALT, OFT, and four other aircraft to the criterion. The Shuttle and Fighters A and B are Level 2. The YF-17 and YF-12 are borderline Levels 1 and 2; however, these latter points must

be considered approximate since their time delays are based on conventional LOES fits due to difficulty in applying Eq. 51 to aircraft with little time delay.

A "build-up" of the OFT and ALT time delay contributions by component is also shown in Fig. 77 based on the Eq. 7 approximation (which gives a τ slightly different than τ_p from Eq. 51). Reduction of the time delay increases bandwidth (by increasing phase margin); however, as shown in Fig. 77, the effect for the Shuttle is small and it appears that the Shuttle would not be Level 1 even with zero effective time delay. This somewhat surprising result occurs because the phase angle decrease due to time delay is small near the relatively low Shuttle bandwidth frequency. This situation may be examined for the OFT using the analytic LOES model, Eq. 8c, with zero time delay. Since $\omega_n \doteq 1.5\ \text{sec}^{-1}$, the bandwidth of

$$\frac{\theta}{\dot{\theta}_c} = \frac{1}{s}\frac{\dot{\theta}}{\dot{\theta}_c} \doteq \frac{\omega_n^2 T_q (1/T_q)}{s[\zeta,\ \omega_n]} \tag{52}$$

is $\omega_{BW} \doteq 1.5\ \text{sec}^{-1}$ (because $\phi_M \doteq 45$ deg there) which consistent with Fig. 77, is well below the Level 1 minimum ω_{BW} of $2.5\ \text{sec}^{-1}$.

f. Time Delay Criterion for Class II and III Aircraft

Large aircraft manufacturers have expressed dissatisfaction with the Ref. 33 time delay criterion because it has evolved solely from flight experimentation in the NT-33, and has not reflected large transport or bomber aircraft. At the opposite extreme based solely on C-5 ground based simulation, it is suggested in Ref. 46 that the LOES boundaries should be

$\tau_e < 0.4$	Level 1
$0.4 < \tau_e < 0.6$	Level 2
$\tau_e > 0.6$	Level 3

However, this is derived from an aircraft having a conventional mechanical control system with significant cable stretch, vehicle flexure, etc.

In the previously cited Ref. 38 very large aircraft in-flight simulation it was suggested that the amount of time delay that can be tolerated in the command path is inversely related to the dynamic bandwidth required to perform the task. For the very large aircraft investigated, the closed-loop attitude bandwidth was about 1.5 rad/sec (which is comparable to the Shuttle OFT in Fig. 77), and the associated time delay boundaries suggested were

$$PR = 3.5;\ \tau_e = \frac{0.3}{\omega_{BW}} = \frac{0.3}{1.5} = 0.2 \text{ sec}$$

$$PR = 6.5;\ \tau_e = \frac{0.4}{\omega_{BW}} = 0.27 \text{ sec}$$

$$PR = 10\ ;\ \tau_e = \frac{0.65}{\omega_{BW}} = 0.43 \text{ sec}$$

A Level 1 boundary of about this magnitude would be supported by Ref. 47, in which the LOES time delay for the B-1 in landing is given as τ_e = 0.158 sec, and the approach and landing handling is rated Level 1. Additional support can be obtained from the Ref. 48 conventional LOES fits to the F-3 and F-4 configurations of Table 8, which result in τ_e's of 0.141 and 0.145 sec, respectively, but have Level 1 handling quality ratings (see Fig. 71).

The idea of having allowable time delay inversely proportional to task bandwidth is inherently appealing for a wide range of vehicles. A plot of the Ref. 38 suggested boundaries of τ_e vs. ω_{BW} is presented in Fig. 78. It is immediately obvious that this criterion would allow much less time delay for a fighter tracking task at, say, 5 rad/sec than for a 1.5 to 2 rad/sec inner attitude loop closure in a transport aircraft landing task.

If one associates low closed-loop bandwidth requirements with "unstressed" tasks and vice-versa, then the trends of Fig. 78 are consistent with the flight results of Ref. 49 obtained in a fighter aircraft. The trends of Fig. 78 are also consistent with laboratory

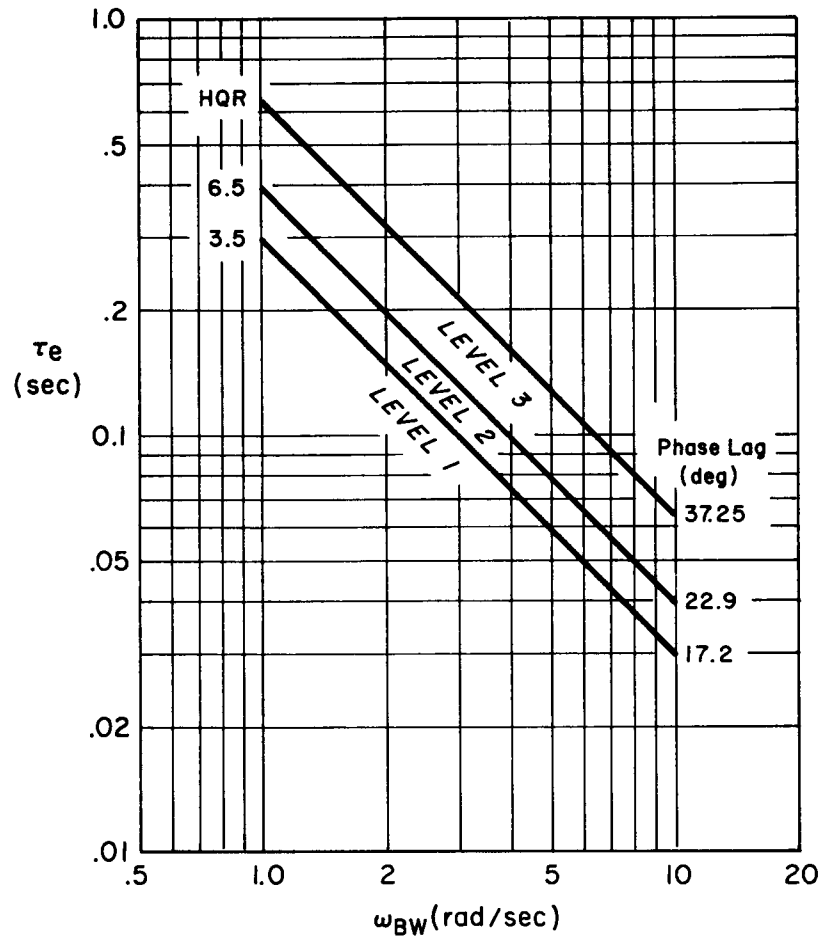

Figure 78. τ_e Inversely Proportional to ω_{BW}

experiment results reported in Ref. 11 where, for a desired tracking task closed-loop frequency, increasing τ_e required increased lead generation on the part of the pilot (with attendant degradation in HQR) or resulted in ω_c (with even stronger degradation in HQR).

Based upon the boundaries of Fig. 78, a time delay of $\tau = 0.156$ sec for the Shuttle (Fig. 26), and the dominant closed-loop frequency of 2-2.5 rad/sec exhibited in the time traces of Figs. 50, 52, and 54, one would anticipate a Level 2 flying quality rating for the landings of STS-4, -5, and -6. The 4-4.2 rad/sec PIO exhibited in Fig. 56 would forecast a near 10 rating for STS-7. Although HQR ratings are not

available from these flights, such ratings would appear overly pessimistic. Thus, additional research may be needed to properly place the boundaries.

g. Supersonic Cruise Research Vehicle Criterion

As a final comparison, Fig. 79 shows the terminal phase (landing) pitch attitude response criterion developed for the Supersonic Cruise Research Vehicle in Ref. 50. This criterion again involves the three parameters: effective time delay, effective rise time, and response overshoot/damping. Fixed boundaries were suggested for time delay and overshoot, e.g.,

LEVEL	t_1(sec)	$\Delta q_2/\Delta q_1$
1	0.12	0.30
2	0.17	0.60
3	0.21	0.85

Note that for a given overshoot (Δq_1), increasing Δq_2 leads to degraded flying quality rating, and hence provides a minimum damping ratio limit. For a given Δq_2, increasing Δq_1 leads to improved rating, and thus favors larger initial overshoot. Based on the Shuttle STS-4 time response of Fig. 26, the Shuttle would rate Level 1 on $\Delta q_2/\Delta q_1$, but Level 2 on t_1.

The rise time boundaries of Ref. 50 were established as inversely proportional to terminal speed so as to provide an upper and lower limit on rise time, Δt. Based on the nominal landing speed of 195 kt for the Shuttle, the effective rise time boundaries would be

$$0.026 < \text{Level 1} < 0.608 \text{ sec}$$

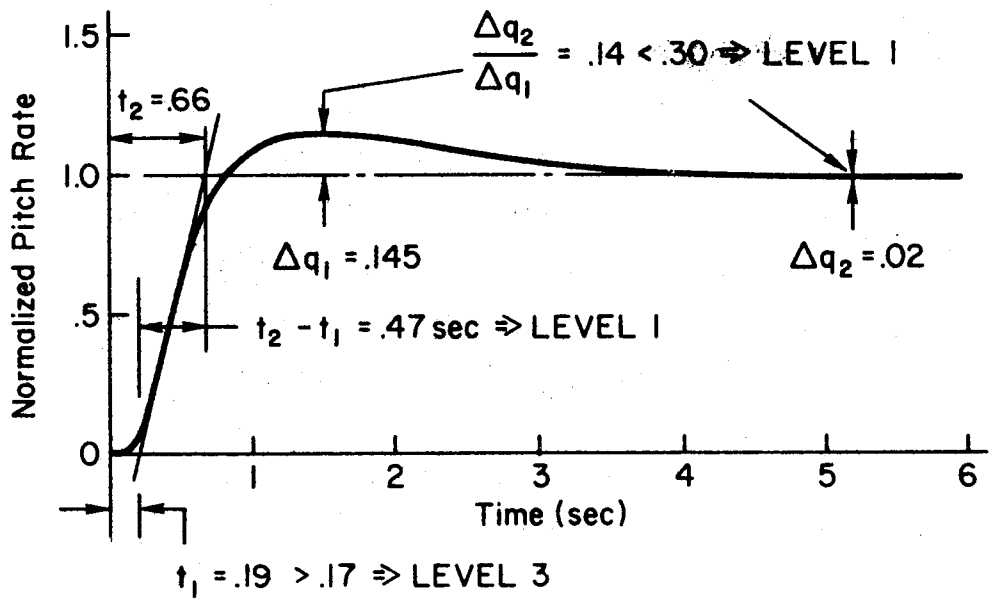

Figure 79. Application of the Supersonic Cruise Research Vehicle Specification to the Shuttle ALT

Again from Fig. 26, the effective rise time is determined to be 0.544 sec, and thus borderline Level 1.

The Ref. 50 criterion was applied in the Ref. 51 simulation investigation of very large aircraft flying qualities. Results indicated the criterion may be overly restrictive for aircraft with rate command/attitude hold augmentation. Figure 80 is a cross plot of the Ref. 50 time delay, t_1, and rise time, Δt, boundaries based on the Ref. 51 landing speeds. Parameter values for the four vehicle configurations are identified by the various symbols. Open symbols reflect unaugmented vehicle responses, and solid symbols reflect RCAH augmented vehicles. Averaged flying quality ratings given to each configuration are next to each symbol. Note that rise time boundaries appear overly restrictive for both the unaugmented and augmented vehicles, and the time delay boundaries appear inappropriate for the RCAH augmented vehicle. Time delay boundaries suggested by Ref. 38 as previously noted would seem much more appropriate.

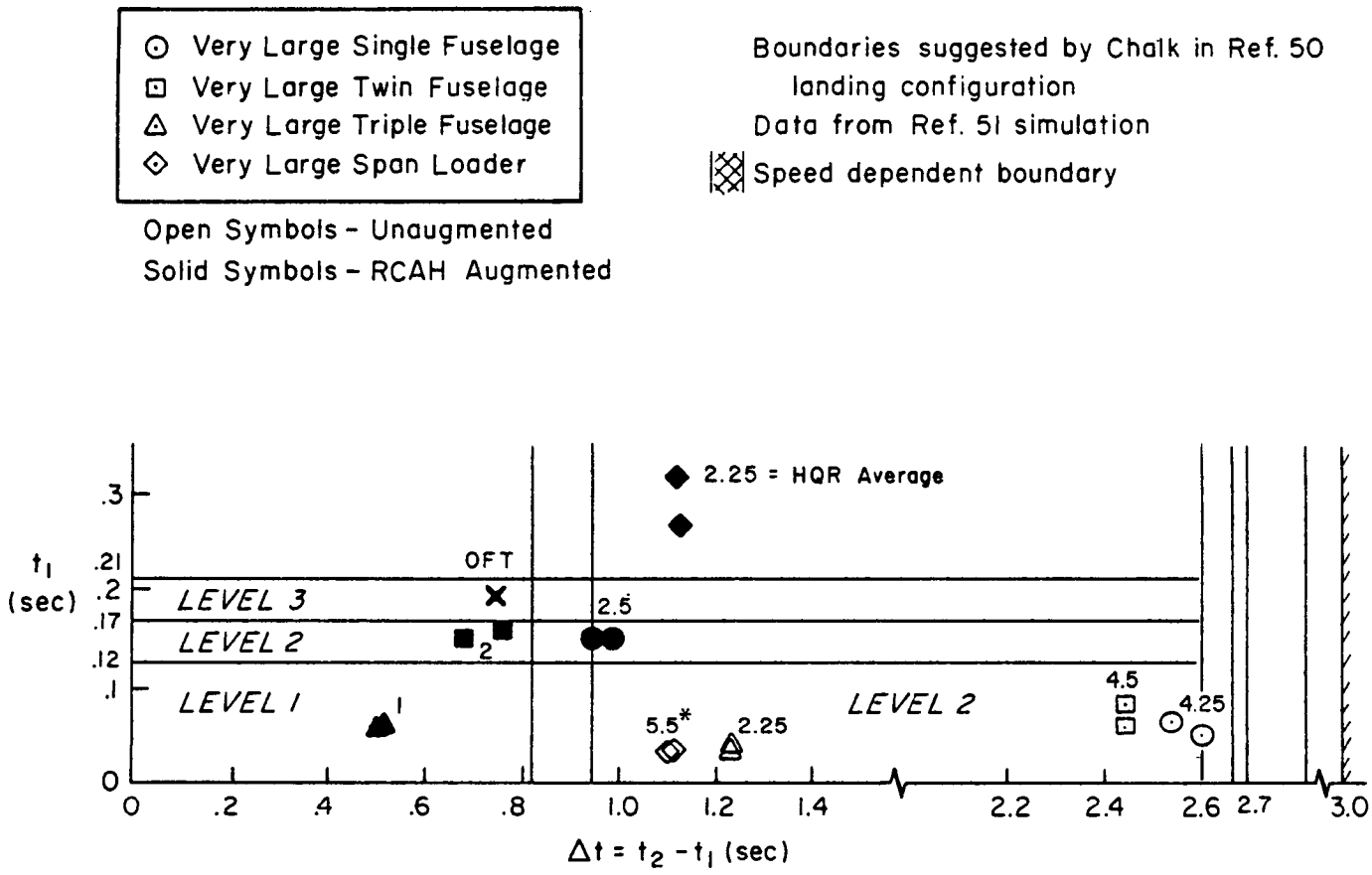

Figure 80. Suggested Delay Time vs. Rise Time Boundaries for Very Large Aircraft (from Ref. 50)

Time delay and rise time values for the Shuttle OFT STS-4 models are also identified in Fig. 80. Based on the Ref. 51 configuration ratings, Level 1 handling for the Shuttle would appear to be forecast.

h. Summary

The preceding has shown that Shuttle-like superaugmented vehicles do not fit in well with criteria from the Ref. 33 military flying quality specification. The concept of lower order equivalent system (LOES) modeling based on conventional aircraft dynamics as set forth in that spec, is inappropriate for RCAH superaugmented vehicles. The same is true for the various criteria (CAP, CAP', etc.) which relate to conventional aerodynamics dominated dynamic response modes.

Of the various effective time delay criteria reviewed, the one that appears the most promising for future Shuttle craft is the task bandwidth oriented τ_e criterion of Ref. 38. A modified version would appear to be a good companion to the NLR or basic Shuttle time response boundaries discussed in the previous subsection.

B. FLYING QUALITIES CONSIDERATIONS RELATED TO RESPONSE TO THE PILOT'S CONTROLLER

The previous review of flying quality specifications and criteria has been oriented toward one particular type of augmented vehicle configuration: the rate command/attitude hold (RCAH) system with a command prefilter G_i = constant. This has been necessary because the Shuttle employs such a configuration. There appears to be little argument that this type of control produces good flying qualities for up-and-away mission phases involving gross maneuvers, large attitude changes (as from hypersonic entry to subsequent deceleration to subsonic flight), etc. However, there is considerable controversy, and rightly so, as to whether other forms of augmentation or command filtering might be more appropriate for the terminal glide and landing flare.

In this subsection we will address other forms of command prefiltering which alter the effective vehicle low and mid-frequency responses. We will also briefly review how the control manipulator itself might influence pilot opinion and/or acceptance of different vehicle command response dynamics.

1. Command Filter (G_i)

a. Rate vs. Attitude Command -- Low Frequency

At this point we can address a current important issue in superaugmented FCS design, the low frequency θ/δ_p characteristics; specifically, the relative merits of rate command vs. attitude command mechanizations. A recent TIFS in-flight simulation study (Ref. 52) has focused renewed attention on this issue. In that study several basic pitch rate superaugmentation systems were simulated. The response to command was then

varied in the test matrix by modifying the command path filter G_i. It was found that significant improvements in pilot rating could be achieved by implementing a command path washout filter (Fig. 81), which created an attitude command characteristic. From this study and other experience, a widely held view has emerged that pitch rate command systems may be acceptable and even desirable in up-and-away flight, but attitude command systems may be preferable for the flared landing task.

To examine this issue, it is useful to compare an "up-and-away" task to the flared landing task as discussed above. In particular to compare "beam" tracking (e.g., the shuttle shallow glide ball-bar path aid) with the final flare. A generic pilot model adequate for glide slope tracking is shown in Fig. 82. (Strictly, the altitude quantity should be replaced by beam deviation; however, perturbation altitude and altitude rate are good approximations to beam deviation and rate). For beam tracking, the deviation rate and attitude perturbation commands are all constant in time and nominally zero, which presents the simplest possible command following task for the pilot. Furthermore, good displays of

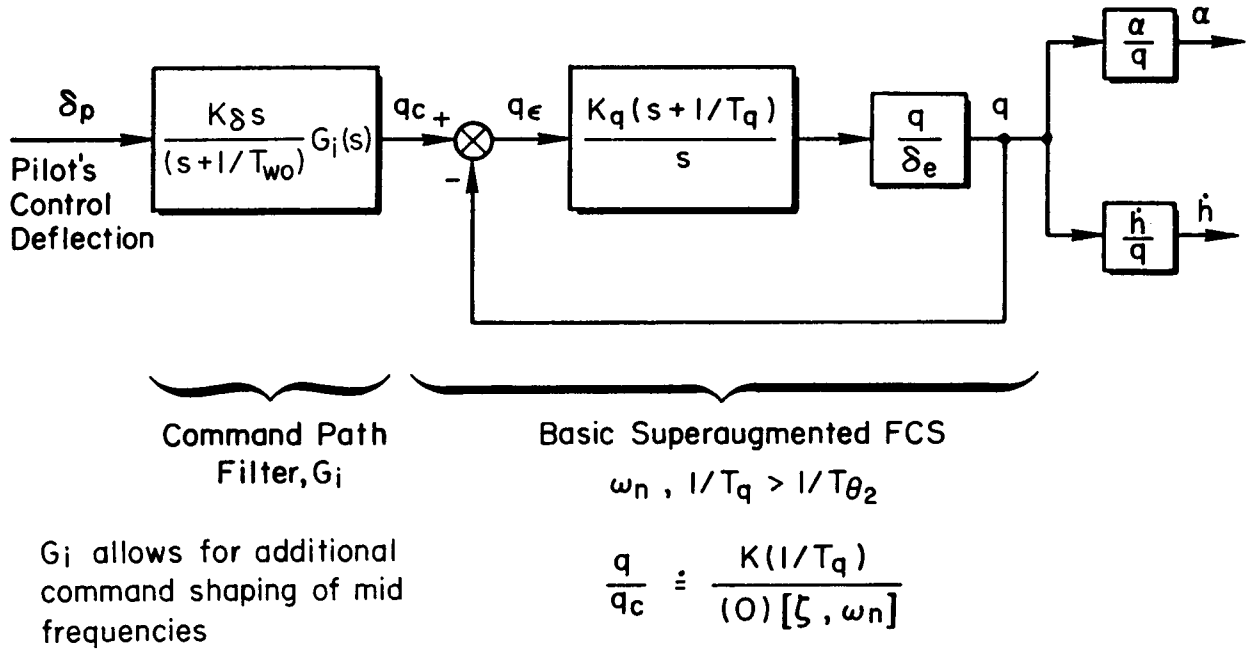

Figure 81. Superaugmented FCS with a Washout in the Command Path Filter

a) COMPLETE MODEL

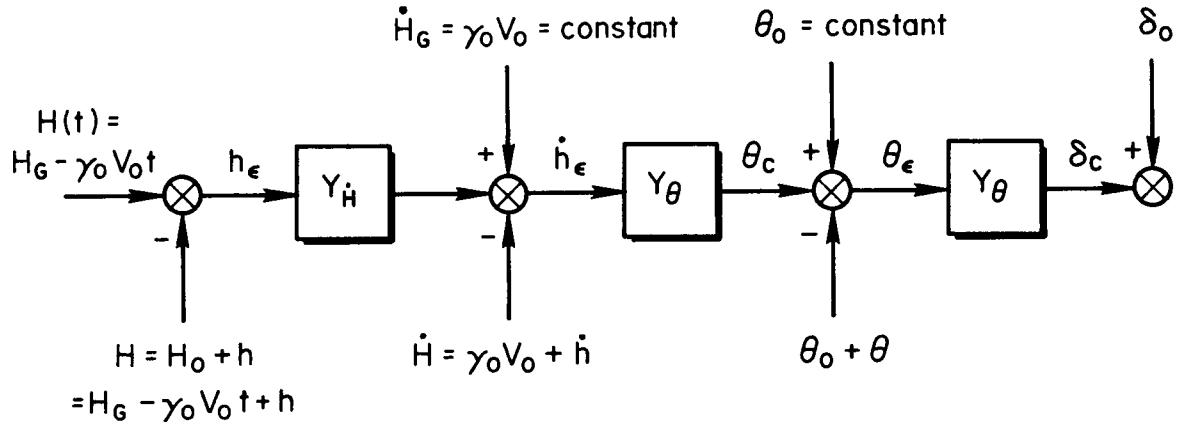

b) PERTURBATION MODEL

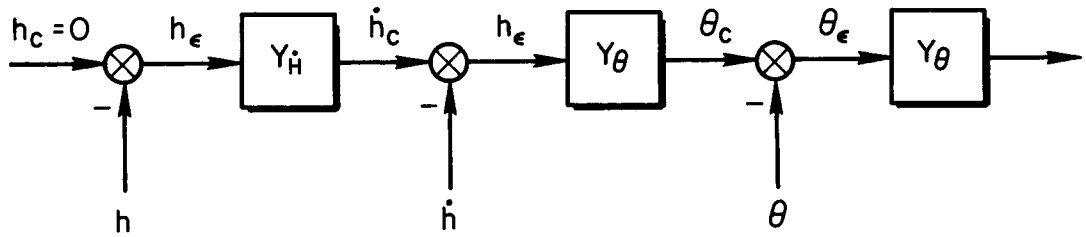

Figure 82. A Pilot Model for Glide Slope Beam Tracking

pitch attitude and/or beam deviation and rate are available from the HUD. Thus, manual closure of inner attitude or deviation rate loops to provide equalization for an outer beam deviation loop is quite feasible. For instance, if the character of the pitch attitude response to stick is a rate command system of fairly high bandwidth as shown in Fig. 83a, and the pilot has adequate cues for attitude, he can close an inner attitude loop of bandwidth, $\omega_{c\theta}$, to create an attitude command characteristic which provides proper equalization for the outer altitude loop closure. That is, the open-loop h/θ_c transfer function is "K/s-like" below $1/T_{\theta_2}$, and thus provides good gain and phase margin for closure of the outer loop. The only limitation on task performance is then $1/T_{\theta_2}$ (provided the aircraft attitude response has adequate bandwidth).

The situation is much more difficult for the flare maneuver. First, the reference values or commands for altitude, vertical speed, and pitch attitude nominally will <u>not</u> be zero or constant as in the beam tracking case, but instead may be complex time varying functions for altitude and possibly sink rate, and with pitch reference generated from the pilot's internal programs for flare as implied in Fig. 31. Further, since these references are programmed based on the pilot's perception of the vehicle responses developed in his training (which in shuttle operations is almost entirely in simulators), they may be somewhat inconsistent with each other for application to the actual aircraft. Finally and most importantly, the cues for altitude, sink rate, and pitch attitude will generally not be as good as in the beam tracking case since appropriate references will probably not be available. Specifically for the shuttle, neither the ball-bar or HUD provides flare references or guidance. Thus for flared landings in general, and for the shuttle landing in particular, closure of inner sink rate or attitude loops to provide equalization for the outer loop altitude closure will be more difficult than in beam tracking. However, the importance of the altitude loop in the flare is much greater than in the shallow glide, i.e., the consequence of a nonzero beam deviation at the end of the shallow glide slope is not as significant as an altitude error at touchdown.

a) INNER (ATTITUDE) LOOP CLOSURE

$$\frac{\theta}{\delta_p} = \frac{\omega_{c\theta}}{s} \left(\begin{matrix}\text{rate} \\ \text{command}\end{matrix}\right)$$

$$\frac{\theta'}{\theta_c} = \frac{\omega_{c\theta}}{(s + \omega_{c\theta})}$$

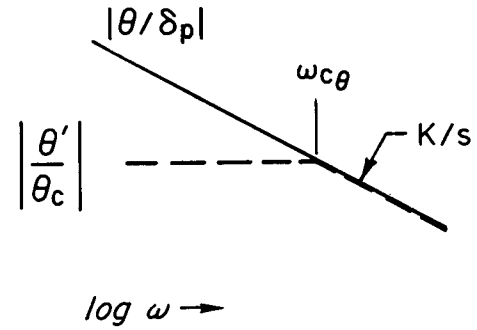

b) OUTER (PATH) LOOP CLOSURE

$$\frac{h'}{\theta_c} = \frac{V_o / T_{\theta_2}}{s(s + 1/T_{\theta_2})} \bullet \frac{\omega_{c\theta}}{(s + \omega_{c\theta})}$$

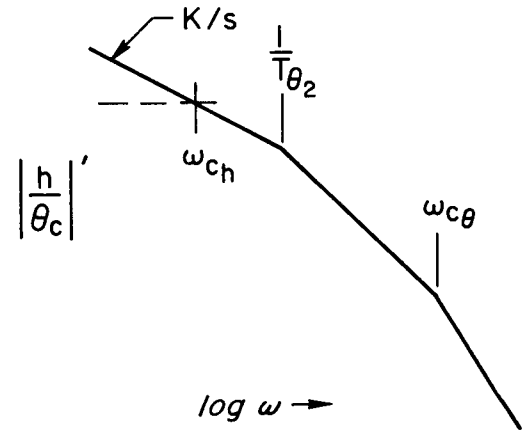

Figure 83. Closure of Inner and Outer Control Loops for Manual Beam Tracking with a Hierarchy of "K/s-like" Elements

The effect of pitch dynamics on closure of the altitude loop in flare without inner pitch loop closure is summarized in Fig. 84 for an ideal rate command system, and an ideal attitude command system. With a rate command system, the effective controlled element transfer function for the altitude closure is K/s^2 below $1/T_{\theta_2}$, and as noted previously, this elicits pulse type control of attitude. Generation of low frequency lead, i.e., below $1/T_{\theta_2}$, to improve the phase margin requires rapid control pulsing, and is associated with a very high workload task. Again a high value of $1/T_{\theta_2}$ would help somewhat. However, if the pitch response has an attitude command characteristic the situation, as shown in Fig. 84b, is much improved since the h/δ_p transfer function is K/s-like below $1/T_{\theta_2}$; yielding proportional control with phase margins approaching 90 deg. Thus, it appears that pilot's preference for attitude command characteristics over rate command characteristics in the flare, such as in the Ref. 52 study, can be explained in part by the advantage of attitude command for closed-loop altitude control without an inner pitch attitude loop closure.

b. Mid-Frequency Considerations

For superaugmented aircraft, unconventional characteristics at middle frequencies may have an important influence on path flying qualities. As noted in Section II, a basic superaugmented design (G_i = constant) like the shuttle will have a rate command ($\theta/\delta_p \doteq K/s$) characteristic out to essentially the dominant pitch mode frequency ω_n' and will have little pitch rate overshoot. There also will be an associated reduction in the α/δ_p and γ/δ_p bandwidths in the mid-frequency range (see Fig. 20). It should be noted that this effect will occur regardless of the low frequency ($\omega < 1/T_{\theta_2}$) command path filter characteristics.

The characteristics of the basic superaugmented attitude and path response to stick may be modified in the mid-frequency band by the use of a lead-lag command path filter (Fig. 85). The path-to-stick bandwidth may be increased by moving the $1/T^*_{\theta_2}$ breakpoint to lower frequencies, and if it is set to $1/T_{\theta_2} \doteq -Z_w$, the mid-frequency characteristics

a) RATE COMMAND

$$\frac{\theta}{\delta_p} = \frac{K_\theta}{s}$$

$$\frac{h}{\delta_p} = \frac{V_o / T_{\theta_2}}{s(s + 1/T_{\theta_2})} \quad \frac{K_\theta}{s}$$

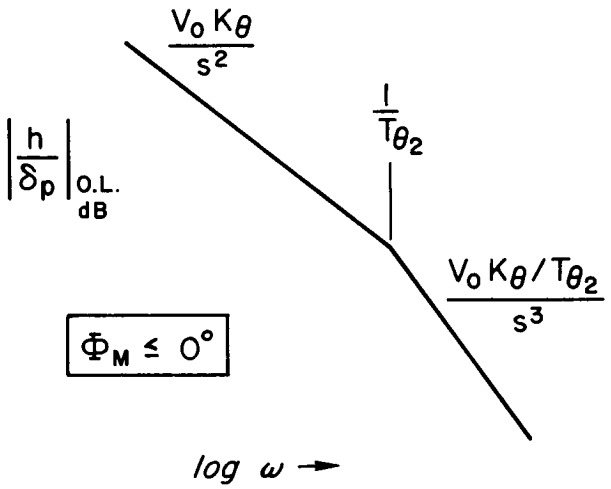

b) ATTITUDE COMMAND

$$\frac{\theta}{\delta_p} = K_\theta$$

$$\frac{h}{\delta_p} = \frac{K_\theta V_o / T_{\theta_2}}{s(s + 1/T_{\theta_2})}$$

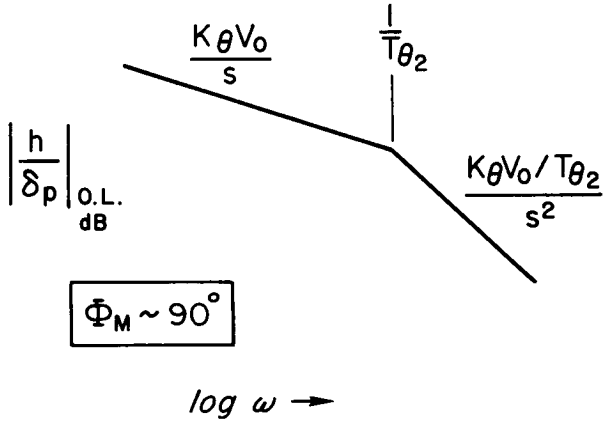

Figure 84. Pilot's Closure Problem for an Altitude Feedback Loop Without Inner Loop Equalization

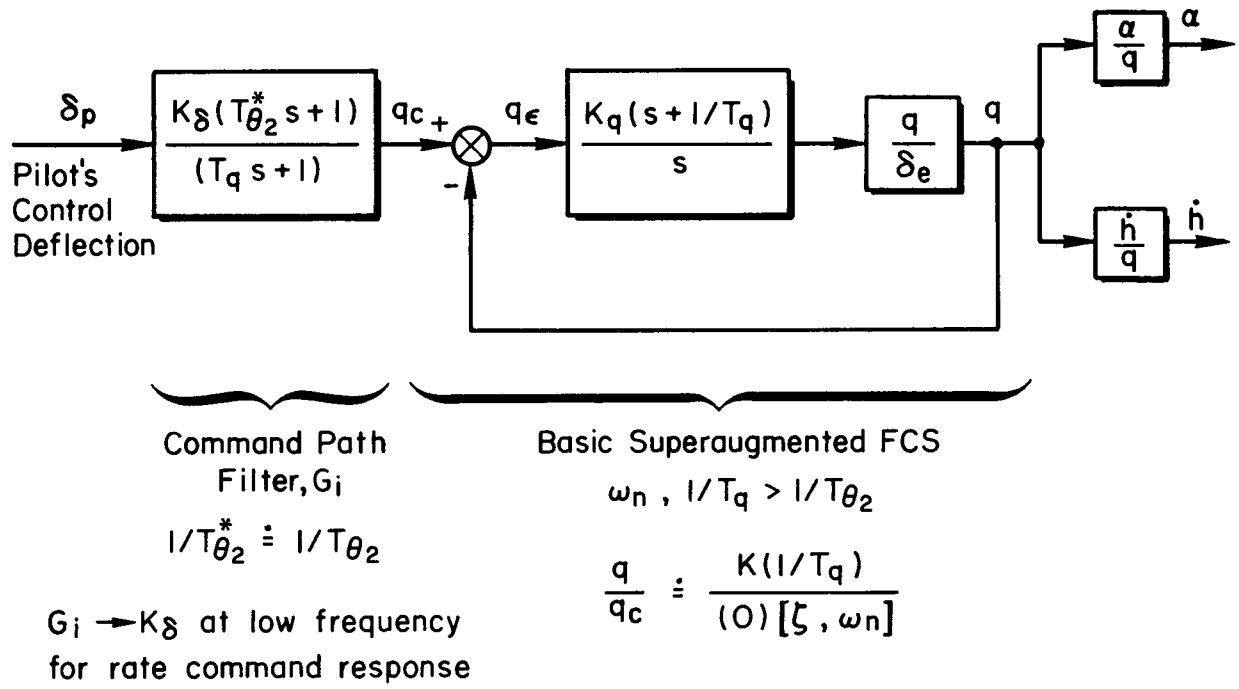

Figure 85. Superaugmented Design with a Lead-Lag Command Path Filter

of the γ/δ_p (or $\dot{h}/\delta_p$) response will be "pseudo"-conventional as in Fig. 86a. This reflects a potential increase in the γ/δ_p (or $\dot{h}/\delta_p$) bandwidth; however, the θ/δ_p response is also made more "conventional" by creating an "attitude command" response in the $1/T_{\theta_2} - \omega_n'$ shelf. This results in much more pitch overshoot in the initial response (Fig. 86b) to a pulse stick input, and therefore "quickens" the path response.

Such filters have been studied in two TIFS in-flight simulation programs, Refs. 37 and 52, with conflicting results. The Ref. 37 study indicated improved pilot ratings as $1/T^*_{\theta_2}$ was increased (more shuttle-like) while the Ref. 52 study indicated an opposite trend. There are several factors which may contribute to this conflict. First, if the pilot is attempting to accomplish an exponential flare (as observed in some of the shuttle landings) the large pitch overshoot and dropback response to pulse inputs could lead to oscillatory pitch attitude control. This could make the exponential flare much more difficult to perform. Recall that in the exponential flare, it was determined that the

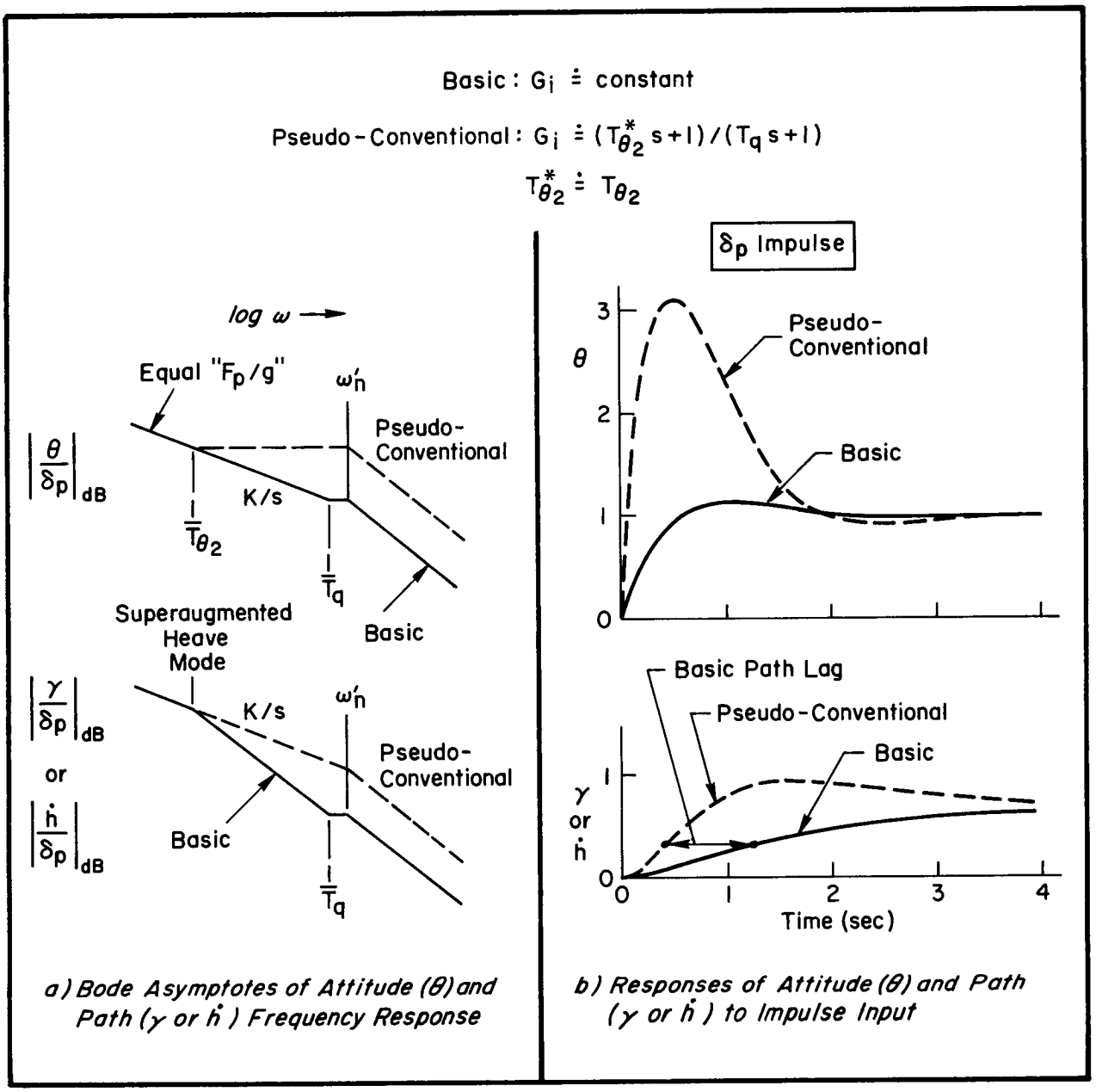

Figure 86. Comparison of Pitch Attitude and Flight Path Response to Command with Basic and Pseudo-Conventional Superaugmented FCS

pilot controlled attitude to asymptotically approach 8 deg as altitude asymptotically approached zero. A large θ overshoot response would also make control inputs more critical near touchdown due to the vehicle landing gear being far aft of the center of rotation.

On the other hand, the "psuedo-conventional" configuration may elicit smoother (less pulsive) pilot inputs and thus smoother attitude control. If the task involved control to the shallow glide, where γ or $\dot{H}$ errors are readily discernable, then the extended K/s region afforded by the "pseudo-conventional" also would be beneficial. Or if the landing flare were to be accomplished by a precognitive pulse input (again as observed in the Shuttle) the pseudo conventional configuration would result in a more rapid arrestment of sink rate.

Thus, arguments can be made for either command filter configuration. Unfortunately, for a single control point (e.g., elevator) aircraft the attitude and path responses cannot be changed independently and the designer is forced to make a tradeoff between pitch attitude and path response characteristics. However, for a two control point aircraft (i.e., an aircraft with a direct lift capability) independent feedbacks to the pitch control surface and the DLC surface could in theory be coordinated to effectively augment the superaugmented heave mode (i.e., augment Z_w) such that near ideal pitch and path characteristics could be achieved simultaneously.

There are considerable complications attendant to adding a second independent control surface (a "pop out" canard has been suggested for the Shuttle). Beyond the issues of weight, cost, and structure, there are flight control issues such as increased gust sensitivity if the heave mode frequency is raised. Thus, it is more than just an academic issue to know whether the attitude response or path bandwidth is the most important flying qualities issue in the mid-frequency range. These issues should be addressed in an appropriately designed simulation study.

2. Manipulator Considerations

In relating the Shuttle landing task and control response to results of other investigations, yet another aspect of the total system must be taken into account. This involves the manipulator (stick) input device contribution to the effective vehicle dynamics, and interaction with the human operator. For example, with an attitude command system, a flare strategy calling for a step attitude change requires a step manipulator displacement, and a ramp attitude change requires a proportional ramp manipulator displacement. With a rate command system, we have observed in the Shuttle flight traces that a ramp attitude change requires step manipulator input, and a step attitude change requires a manipulator pulse. Thus, manipulator activity is intimately tied to the augmentation configuration and vice versa. The interaction is further tied to the control task being performed, the control bandwidth and precision required, and human operator anthropometric and neuromuscular considerations.

For example, control over a rate command/attitude hold (RCAH) type system is most appropriate with a sidestick or similar wrist actuated manipulator. The smaller muscle systems involved in wrist movement are well suited to precise, rapid pulsive control. On the other hand, the wrist has quite limited fore and aft deflection freedom, and is not well suited to holding control displacement or force for extended time periods. A conventional center stick or control column is inappropriate for RCAH type systems because control inputs involve the larger muscle groups of the arm. These introduce larger neuromuscular latencies and are inappropriate for small precise pulsive activity. Also these manipulators generally entail high control system centering and breakout forces, which together with the arm limitations, further mitigate against small precise pulsive control.

For control over an attitude command/attitude hold (ACAH) system, a conventional centerstick or control column is most appropriate. Here the arm anthropometry is well suited to large displacements which might be involved with large attitude changes such as the Shuttle preflare

pullup and final flare, whereas the wrist joint might lock. Further, arm joint displacement and muscle tension receptors then provide valuable cues to the pilot concerning vehicle attitude, surface effectiveness, and/or energy conditions. While such cues would also be available from wrist action with a sidestick, limited wrist motion is just not compatible with maneuvering which requires large attitude changes.

In view of the above, it is important to note that the Refs. 52 and 53 TIFS in-flight simulation investigations of superaugmented vehicle dynamics (RCAH, ACAH, and "pseudo" conventional stick filter) in landing were accomplished with a conventional center control column configuration wherein the pilot controls pitch and roll with his left hand/arm, and throttle with his right hand/arm. Thus, this manipulator configuration may have biased the results to favoring the ACAH system. By contrast, the Ref. 37 investigation of similar dynamics configurations in the TIFS employed the NLR sidestick manipulator, and the RCAH system was found to be quite acceptable. Furthermore, the Shuttle manipulator was shown in Ref. 1 to have considerably lower breakout force and command gradient when compared to conventional aircraft sidesticks. The Shuttle manipulator also has the pitch pivot near the top of the hand palm whereas conventional sidesticks have the pivot below the hand. These differences would favor pulse type inputs and may contribute significantly to the acceptability of RCAH for the Shuttle. And finally, the manufacturers of the Airbus A-320 transport aircraft in citing their selection of a sidestick controller stated in Ref. 54: "Large movements of the control column are no longer needed when the aircraft is equipped with FBW controls. This is why we are looking into the possibility of using the sidestick, which is designed to interface with just the kind of flight control we plan to have in the A-320." The sidestick configuration has subsequently been selected for production.

3. Training Effects

Adverse pilot opinion of RCAH in landing has been noted for many years; however, a "training effect" has also often been observed in which pilot opinion may improve markedly with continued exposure to

RCAH, Ref. 55. Evidence of this training effect is implied in the recent comparison of the shuttle FCS to more "conventional" alternatives for landing on the Ames VMS simulator Ref. 7. The two groups of pilots who flew the various simulator configurations -- test pilots with primarily conventional aircraft experience vs. shuttle pilots -- had distinctly different preferences. The "conventional" test pilots generally preferred the more conventional alternatives while the shuttle pilots preferred the existing shuttle RCAH system with which they had extensive experience. Further circumstantial evidence of learning effects comes from the shuttle flight experience.

Accounting for such learning effects in an in-flight simulation study is difficult because of the limited exposures per test subject (a coordinated ground simulation effort might provide additional exposure at reasonable cost). Further the flying qualities rating procedures usually used have a "good/bad" dimension, but no distinct "conventional/unconventional" dimension; and thus may be "culturally biased" toward the aircraft characteristic the pilot is most familiar with. Indeed pilot commentary in Refs. 52 or 53 report indicates assessments might change if, "I could make four or five landings to get used to it."

C. PATH RESPONSE CRITERIA

The previous sections have focused primarily on pitch attitude response to controller inputs with vehicle c.g. path response related to attitude change by the time constant T_{θ_2}. Although pilot location is not normally considered to be a handling quality concern, the influence of pilot location on the effective altitude control high frequency zeros (which is of most interest for approach and landing) was noted in the pilot/vehicle analysis of Section II where, for the Shuttle configuration, a non-minimum phase zero results in an initial response reversal in which the pilot will go down before going up. This has been nicely demonstrated in the Ref. 38 "million pound airplane" in-flight simulation study which provides some of the best available data concerning

pilot/ICR location effects on the Shuttle. The configurations of interest are the three airframes (long aft tail, short aft tail, and canard) with the "high K_q" pitch rate system. These configurations all had essentially the same pitch attitude response. The primary difference was in the airframe Z_{δ_e} values and therefore in ICR location. The effective pilot location was then further varied with respect to the ICR for each airframe configuration.

Figure 87 shows represenative n_{z_p} and h_p time responses for the short aft tail configuration at those pilot locations. The $\Delta\ell_p$ = -10 ft approximates the Shuttle case, and demonstrates the response reversal due to the non-minimum phase zero. The figure also indicates the sensitivity of the response to moving the pilot forward (or the ICR aft).

Figure 88 shows Cooper-Harper pilot rating (CHPR) obtained in the Ref. 38 flight test plotted against the pilot location relative to the ICR. While there are some large rating variations for several of the configurations, there does seem to be a definite degradation of pilot rating for the two short aft tail configurations in which the pilot was less than 10 ft ahead of the ICR.

The fact that the short aft tail configuration with $\Delta\ell_p$ = 50 ft is consistent in CHPR ratings with the canard and long aft tail configurations indicates that it is pilot location with respect to the ICR rather than instantaneous center location per se that is relevant to path control problems.

The shuttle crews are keenly aware of the ICR, their location relative to it, and the time delay in seeing a path response change to their control inputs (Refs. 23 and 56). Control over the ICR location is best accomplished by providing a second control surface which can be operated independently or in conjunction with the pitch control surface. As the Ref. 38 investigation, this generally involves separate aft or canard surfaces.

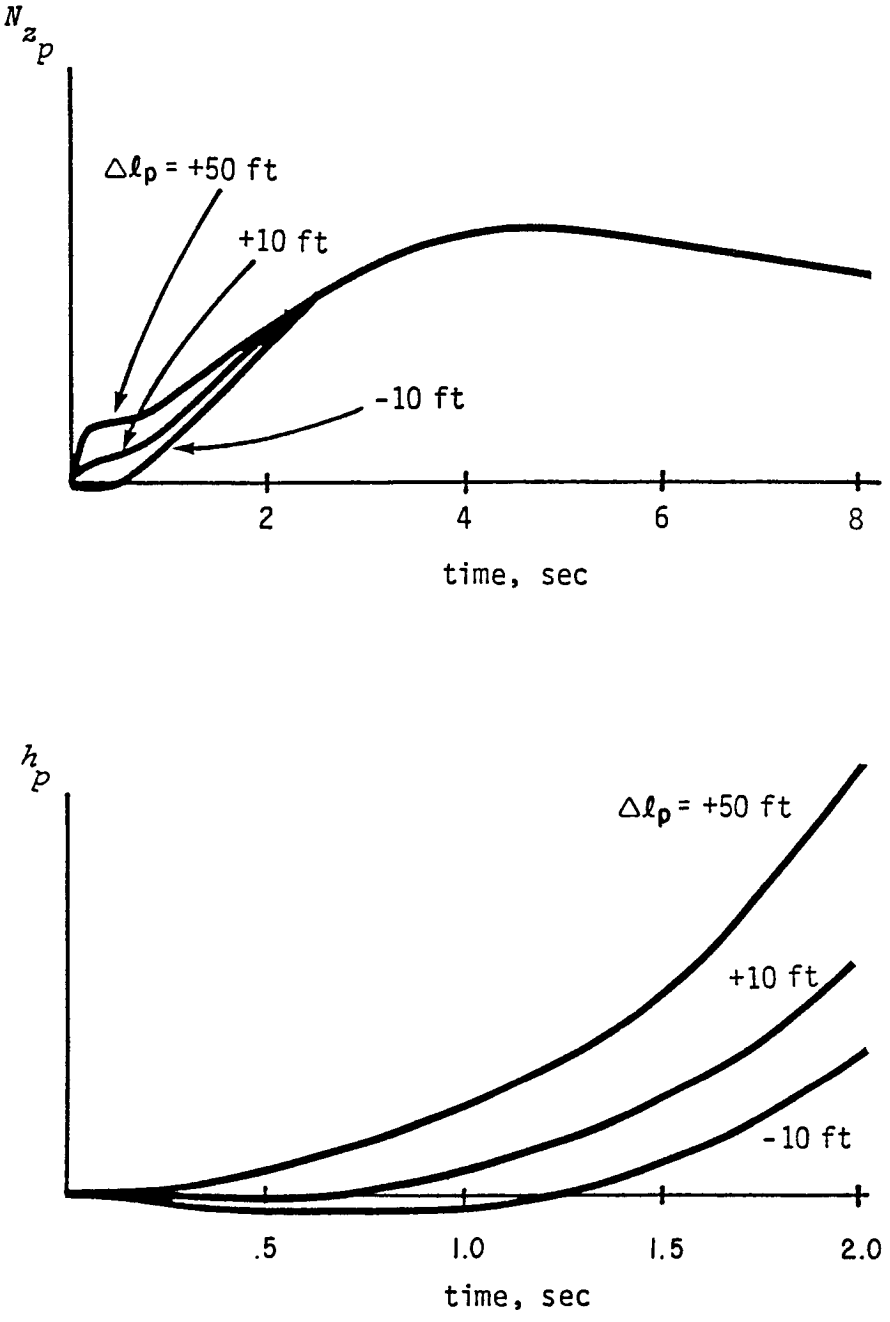

Figure 87. Normal Acceleration and Altitude at Various Pilot Stations in Short Aft Tail Configuration, High Augmentation, T_1 = A (from Reference 38)

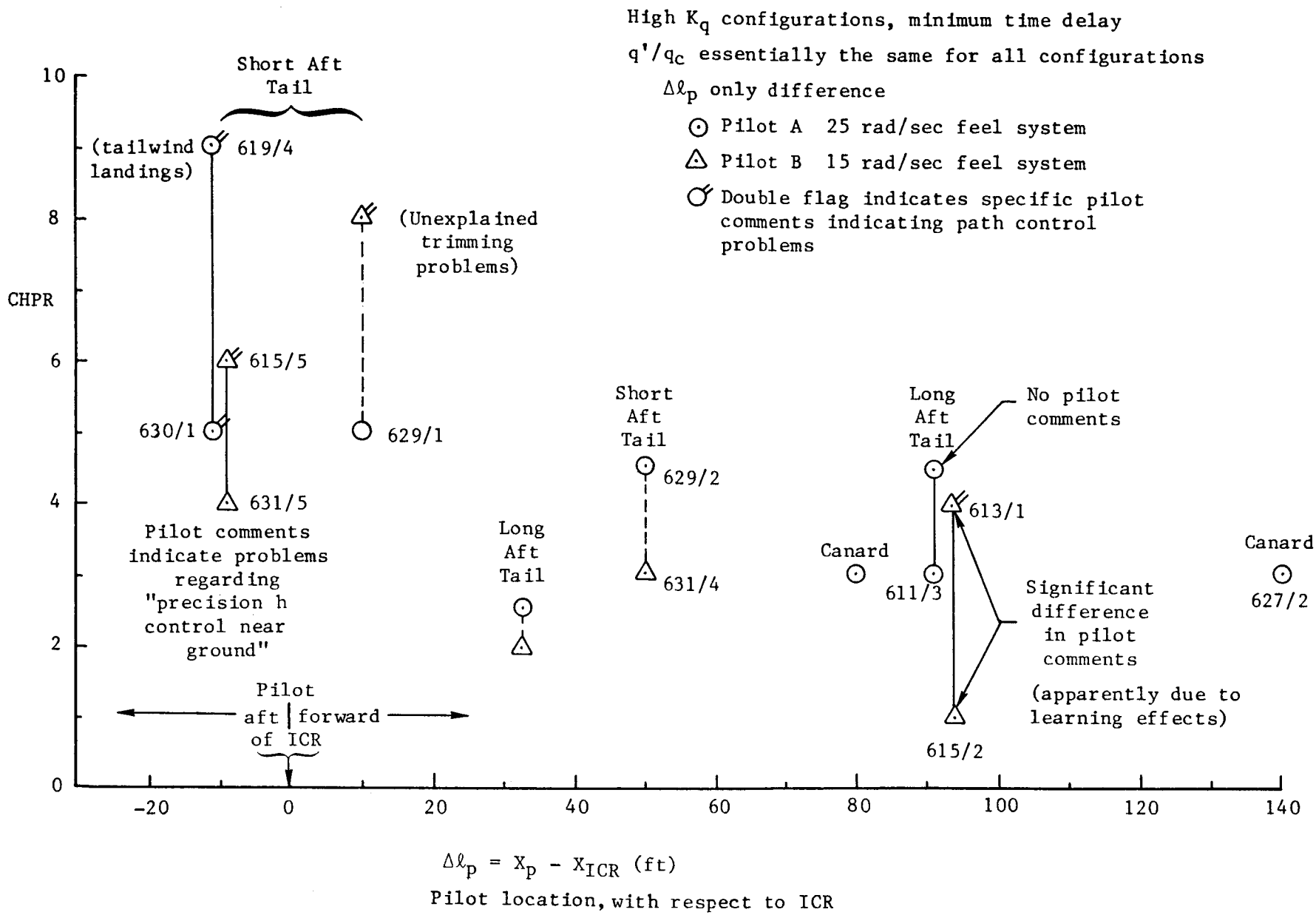

Figure 88. Variation of Pilot Rating with Relative Pilot/ICR Location, Reference 38 Data

SECTION V

SUMMARY, CONCLUSIONS, AND RECOMMENDATIONS

A. SUMMARY

The purpose of this program has been to assess the suitability of existing and proposed flying quality and flight control system criteria for application to the Space Shuttle, to help define optimum use of flight data in the development of flying quality criteria, and to assist the development of experiments for flying qualities and flight control systems design criteria for future shuttlecraft.

In summarizing the results of the four part study, this report started with the development of a simplified dynamic model of the Shuttle which shows its longitudinal characteristics to be significantly different from conventional aircraft -- the Shuttle is classified as a superaugmented aircraft. The Shuttle response dynamics are dominated by FCS centered parameters and with only two aerodynamic derivatives (M_{δ_e} and Z_w) having significant influence; all other aerodynamic coefficients and parameters being "swamped" by the closed-loop augmentation system.

In the simplified, superaugmented vehicle dynamic model, two closed-loop parameters are key to pitch response characteristics of concern, i.e., rise time, overshoot, and settling time. These two parameters are the numerator time constant, T_q (which arises from the proportional plus integral feedback of pitch rate), and the closed-loop bandwidth, ω_c. The latter is, in turn, a function of the loop gain $K_q M_{\delta_e}$. One additional parameter of importance is the effective time delay, τ, which results from computational throughput delays and the collective phase lag contribution of all filters, actuators, and dynamic modes at frequencies above ω_c.

Pitch frequency domain dynamic models extracted from flight data covering the approach and landing phase were then shown to closely match the theoretical model. This is taken as validation of both the simplified superaugmentation model approach and the non-intrusive fast Fourier

transform spectral analysis technique implemented in the (STI) FREDA program.

Attention was then turned to identification, again via non-intrusive methods, of the loop closure and control strategy employed by the STS crews in the preflare, shallow glide, and final flare segments of landing. The approach centered upon identification of path loci characteristics in the H, $\dot{H}$ phase plane from preflare through touchdown supported by time traces of pilot manipulator inputs and resulting vehicle perturbation responses.

Results indicate two basic flare strategies dominated the landings through STS-7: 1) a precognitive step θ, or 2) an exponential $h \sim \dot{h}$ or θ. For the Shuttle, both require precise control of the inner, θ loop to achieve the desired path control. There is some evidence (due to near PIO situations) that the pilots may be pushing the pitch response bandwidth limits.

Landing performance metrics show remarkably consistent touchdown values for sink rate, forward velocity, and distance from threshold. This despite widely varying conditions at the beginning of shallow glide and/or flare initiation. The one exception occurred when the pilot apparently had insufficient time to adapt to the vehicle dynamics and control task. The flight traces indicate adaption times of approximately 15-20 sec before settling into the control task. This adaption time should be recognized for any emergency takeover situations.

The shallow glide and touchdown performance tended to get more consistent as path visual aids (ground and HUD) provided more reference information. But, all landings met or exceeded desired touchdown performance criteria regardless of visual aids. Thus based upon task performance and a strict interpretation of the Cooper-Harper scale,* the overall vehicle flying qualities would appear to be no worse than a 4 (Level 2). Admittedly the pilots have all been exceptionally well

---

*4 = desired performance requiring moderate pilot compensation.
5 = adequate performance requiring considerable pilot compensation.

trained in the task. But again, in all cases examined here, this was the pilot's first landing in the real vehicle; all previous landings have been accomplished in simulators.

Comparison between key Shuttle longitudinal parameters and various existing or proposed flying quality criteria and design guides showed that most of these criteria developed on the basis of conventional fighter type aircraft are not appropriate for large superaugmented aircraft configurations. For superaugmented shuttlecraft, pitch response parameters and criteria investigated and proposed specifically for superaugmented-like Class II and III vehicles appear most applicable, i.e., NLR pitch rate response boundaries coupled with a task oriented effective time delay ($\tau_e \sim 1/\omega_c$). However, much remains to be resolved regarding path control of superaugmented vehicles. The biggest question revolves around the type of response desired for landing flare and how best to achieve it, i.e., RCAH vs. ACAH vs. separate path control. Based upon results reviewed in this study, dynamic analysis, etc., no specific conclusions can be reached except that more research is needed in which the <u>total</u> pilot/display/manipulator/effective vehicle/task interaction is considered. Prior experiments all seem to have overlooked or compromised one or more elements of this total system.

B. CONCLUSIONS

Specific lessons learned from the current Shuttle as design guides for future shuttlecraft flying qualities:

- Pitch rate response boundaries -- NLR boundaries most appropriate.
- Pitch rate bandwidth -- present 1.5 to 2 rad/sec is marginal at best and should be increased.
- Effective time delay -- present 0.15 sec is excessive and should be reduced compatible with pitch control task bandwidth.
- Path time constant -- present 2 sec is marginal at best and should be reduced.

- Effective vehicle dynamics in flare -- RCAH vs. ACAH still to be resolved.

- Manipulator -- design characteristics should be tailored to effective vehicle dynamics and control tasks (this undoubtedly will result in tradeoffs between orbital, entry, and landing control tasks).

- ICR location with respect to Pilot -- ICR should be located to minimize path mode apparent reversal or time lag response to flare commands.

C. RECOMMENDATIONS

- Current Shuttle dynamic response and flying quality parameter values collectively be considered minimum levels for future shuttlecraft.

- A series of carefully designed experiments be undertaken to identify and quantify interactive design guides and criteria between:

  -- manipulator design characteristics and effective vehicle dynamics configurations (including command filter)

  -- various methods of transitioning betwen RCAH and ACAH for final approach and flare.

  -- ACAH and RCAH with DLC in flare.

- Task hodograph and FREDA analysis techniques be applied in future simulations of Shuttle control tasks to verify and/or identify vehicle dynamic task characteristics and pilot strategy for comparison with actual vehicle and landing task.

REFERENCES

1. Myers, T. T., D. E. Johnston, and Duane McRuer, Space Shuttle Flying Qualities and Flight Control System Assessment Study, NASA CR-170391, Dec. 1981.

2. Myers, T. T., D. E. Johnston, and D. T. McRuer, Space Shuttle Flying Qualities and Flight Control System Assessment Study, Phase II, NASA CR-170406, Dec. 1983.

3. Myers, T. T., D. E. Johnston, and D. T. McRuer, Space Shuttle Flying Qualities Criteria Assessment, Phase III, NASA CR-170407, Feb. 1984.

4. Myers, T. T., D. E Johnston, and D. T. McRuer, Space Shuttle Flying Qualities Criteria Assessment Phase IV - Data Acquisition and Analysis, NASA CR-166618, May 1986.

5. Myers, T. T., R. J. DiMarco, R. E. Magdaleno, et al., Archive Data Base and Handling System for the Orbiter Flying Qualities Experiment Program, NASA CR-166622, Dec. 1986.

6. Arrington, J. P., and J. J. Jones (Compilers), "Shuttle Performance: Lessons Learned," NASA CP-2283, Part 1 and Part 2. Proceedings conference held at NASA Langley Research Center, Hampton, VA, 8-10 March 1983.

7. Powers, B. G., Active Control Technology Experience with the Space Shuttle in the Landing Regime, NASA TM 85910, AGARD FMP Symposium on Active Control Systems -- Review, Evaluation and Projections held in Toronto, Canada, 15-18 Oct. 1984.

8. Tsikalas, G. M., "Space Shuttle Autoland Design," AIAA Paper No. 82-1604-CP, presented at the AIAA Guidance and Control Conference, 9-11 Aug. 1982, San Diego, CA.

9. Brand, V. D., "Space Shuttle Development Update," Society of Experimental Test Pilots Report to the Aerospace Profession, 28th Symposium, ISSN 0742-3705, Sept. 1984, pp. 237-256.

10. Looney, B. J., "Post-DETAC HUD Monitor Description," Sperry Autoland Memo 57, Nov. 4, 1980.

11. Myers, T. T., D. T. McRuer, and D. E. Johnston, Flying Qualities and Control System Characteristics for Superaugmented Aircraft, NASA CR-170419, Dec. 1984.

12. Teper, G. L., R. J. DiMarco, and I. L. Ashkenas, Analyses of Shuttle Orbiter Approach and Landing Conditions, NASA CR-163108, July 1981.

13. McRuer, D. T., D. E. Johnston, and T. T. Myers, "A Perspective on Superaugmented Flight Control Advantages and Problems," presented at AGARD Flight Mechanics Panel Symposium on Active Control Systems-Review, Evaluation and Projections, AGARD CP-384, March 1985, pp. 3-1 thru 3-16.

14. Hoey, R. G., AFFTC Evaluation of the Space Shuttle Orbiter and Carrier Aircraft -- NASA Approach and Landing Test, AFFTC-TR-78-14, May 1978.

15. McRuer, D. T., I. L. Ashkenas, and D. Graham, Aircraft Dynamics and Automatic Control, Princeton University Press, Princeton, N.J., 1973.

16. Bendot, J. S., and A. G. Piersol, Engineering Applications of Correlation and Spectral Analysis, John Wiley & Sons, N. Y., 1980.

17. McRuer, D. T., and E. S. Krendel, Mathematical Models of Human Pilot Behavior, AGARDograph No. 188, Jan. 1974.

18. Covault, C., "Shuttle Crew Finds Performance Crisp," Aviation Week and Space Technology, Dec. 14, 1981.

19. Anon., "Flight Test Data Gained On Re-entry of Columbia," Aviation Week and Space Technology, Apr. 5, 1982.

20. Covault, C., "Third Shuttle Mission Being Assessed," Aviation Week and Space Technology, Apr. 26, 1982.

21. Covault, C., "Shuttle Re-entry Tests Vehicle Cross Range," Aviation Week and Space Technology, July 12, 1982.

22. Scott, W. B., "Shuttle Lands on Hard Surface Runway," Aviation Week and Space Technology, July 12, 1982.

23. Mattingly, Capt. T. K., and Col. H. W. Hartsfield, Jr., "Space Shuttle Progress Report," Society of Experimental Test Pilots Report to the Aerospace Profession, 26th Symposium, Sept. 1982, Vol. 16, No. 2, pp. 267-285.

24. Covault, C., "Liftoff Time Pivotal to Shuttle Events," Aviation Week and Space Technology, Nov. 1, 1982.

25. Anon., "Columbia Re-entry Tests Low-Mach Characteristics," Aviation Week and Space Technology, Nov. 22, 1982.

26. Covault, C., "Shuttle 6 Re-entry Aids Program," Aviation Week and Space Technology, Apr. 18, 1983.

27. Covault, C., "Shuttle Landing Shift Shows Flexibility," Aviation Week and Space Technology, July 4, 1983.

28. Brand, V., "Improving the Breed: Shuttle Development," Aerospace America, May 1985, pp. 78-80, 82.

29. Nagel, S. R., "Flying the Orbiter in the Approach/Landing Phase," Shuttle Performance: Lessons Learned, NASA CP-2283, Part II, 1983, pp. 1317-1329.

30. Klinar, W. J., D. W. Gilbert, C. T. Hackler, et al., Flying Qualities Requirements for the Orbiter Utilizing Closed-Loop, Fly-by-Wire Control of Vehicle Response Parameters, NASA MSC-07151, Rev. 1, 15 Dec. 1973.

31. Requirements/Definition Document, Flight Control, Part 1 Configuration, Performance and Functional Requirements, Rockwell International Report SD72-SH-0105, Vol. 1, Book 2, Part 1A, July 1977.

32. Ireland, R., and R. Woodle, Entry Primary Flight Control System Analytic Verification Test Report, Honeywell, Inc., STS 81-0119, Feb. 1981.

33. "Flying Qualities of Piloted Airplanes," MIL-F-8785C, Nov. 1980.

34. Smith, R. E., Effects of Control System Dynamics on Fighter Approach and Landing Longitudinal Flying Qualities (Vol. I), AFFDL-TR-78-122, March 1978.

35. Neal, P. T., and R. E. Smith, An In-Flight Investigation to Develop Control System Design Criteria for Fighter Airplanes, AFFDL-TR-70-74, Vol. II, Dec. 1970.

36. Mooij, H. A., W. P. de Boer, and M. F. C. van Gool, Determination of Low-Speed Longitudinal Maneuvering Criteria for Transport Aircraft with Advanced Flight Control Systems, National Aerospace Lab., NLR TR 79127 U, Dec. 1979.

37. Mooij, H. A., and M. F. C. Van Gool, "Handling Qualities of Transports with Advanced Flight Control Systems," AGARD CP-333, presented at AGARD Flight Control Panel Symposium on Criteria for Handling Qualities of Military Aircraft, Ft. Worth, TX, Apr. 1982.

38. Weingarten, N. C., and C. R. Chalk, In-Flight Investigation of Large Airplane Flying Qualities for Approach and Landing, AFWAL-TR-81-3118, Sept. 1981.

39. Weingarten, N. C. and C. R. Chalk, "In-Flight Investigation of Large Airplane Flying Qualities for Approach and Landing," AIAA Paper 82-1296, Aug. 1982.

40. Bischoff, D. E., "Longitudinal Equivalent Systems Analysis of Navy Tactical Aircraft," A Collection of Technical Papers; Proceedings of AIAA Atmospheric Flight Mechanics Conference, 8-10 Aug. 1977, Hollywood, FL, pp. 153-161.

41. Bihrle, W. Jr., A Handling Qualities Theory for Precise Flight Path Control, AFFDL-TR-65-198, June 1966.

42. Berry, D. T., B. G. Powers, K. J. Szalai, et al., "A Summary of an In-Flight Evaluation of Control System Pure Time Delays During Landing Using the F-8 DFWB Airplane," A Collection of Technical Papers; Proceedings of AIAA Atmospheric Flight Mechanics Conference, 11-13 Aug. 1980, Danvers, MA, pp. 561-571.

43. Bischoff, D. E., The Control Anticipation Parameter for Augmented Aircraft, NADC-81186-60, May 1981.

44. DiFranco, D. A., Flight Investigation of Longitudinal Short Period Frequency Requirements and PIO Tendencies, AFFDL-TR-66-163, June 1967.

45. Hoh, R. H., D. G. Mitchell, I. L. Ashkenas, et al., Proposed MIL Handbook -- Flying Qualities of Air Vehicles. Volume I: Proposed MIL Standard. Volume II: Proposed MIL Handbook, AFWAL-TR-82-3081, Nov. 1982.

46. Meyer, R. T., J. R. Knox, and S. A. Tingas, Suggested Revisions to MIL-F-8785C for Large (Class III) Aircraft, AFWAL-TR-83-3015, Feb. 1983.

47. Crother, C. A., and B. Gabelman, "Equivalent System Modeling of the Augmented B-1," Flying Qualities Design Criteria Proceedings of AFFDL Flying Qualities Symposium, AFWAL-TR-80-3067, WPAFB, OH, May 1980.

48. Mitchell, D. G., and R. H. Hoh, "Review of NLR Transport-Aircraft Longitudinal Study," Systems Technology, Inc., WP-1163-3, Aug. 1982.

49. Berry, D. T., "In-Flight Evaluation of Pure Time Delays in Pitch and Roll," Proceedings of AIAA Guidance, Navigation and Control Conference, AIAA Paper No. 85-1852, 19-21 Aug. 1985, Snowmass, CO, pp. 39-46.

50. Chalk, C. R., Recommendations for SCR Flying Qualities Design Criteria, NASA CR-159236, Apr. 1980.

51. Grantham, W. D., P. D. Smith, P. L. Deal, et al., Simulator Study of Flight Characteristics of Several Large, Dissimilar, Cargo Transport Airplanes During Approach and Landing, NASA TP-2357, Nov. 1984.

52. Berthe, C. J., C. R. Chalk, and S. Sarrafian, Pitch Rate Flight Control Systems in the Flared Landing Task and Design Criteria Development, NASA CR-172491, Oct. 1984.

53. Weingarten, N. C., and C. R. Chalk, In-Flight Investigation of Large Airplane Flying Qualities for Approach and Landing, AFWAL-TR-81-3118, Sept. 1981.

54. Aviation Week and Space Technology, 18 July 1983.

55. Stapleford, R. L., R. H. Klein, and R. H. Hoh, Handling Qualities Criteria for the Space Shuttle Orbiter During the Terminal Phase of Flight, NASA CR-2017, Apr. 1972.

56. Hartsfield, H. W., Jr., "Space Shuttle Orbital Flight Testing," The Society of Experimental Test Pilots, Twenty-Second Symposium Proceedings, 27-30 Sept. 1978, Vol. 14, No. 2, pp. 11-20.

1. Report No.	2. Government Accession No.	3. Recipient's Catalog No.
NASA CR-4049		

4. Title and Subtitle	5. Report Date
SPACE SHUTTLE FLYING QUALITIES AND CRITERIA ASSESSMENT	March 1987
	6. Performing Organization Code

7. Author(s)	8. Performing Organization Report No.
T.T. Myers, D.E. Johnston, and D.T. McRuer	H-1385
	10. Work Unit No. RTOP 506-48

9. Performing Organization Name and Address	11. Contract or Grant No.
Systems Technology, Inc. 13766 S. Hawthorne Blvd. Hawthorne, CA 90250	NAS2-11900
	13. Type of Report and Period Covered Contractor Report - Final
12. Sponsoring Agency Name and Address National Aeronautics and Space Administration Washington, DC 20546	14. Sponsoring Agency Code

15. Supplementary Notes

NASA Technical Monitor: Donald T. Berry, NASA Ames Reseach Center, Dryden Flight Research Facility, Edwards, California 93523-5000.

16. Abstract

This report is a summary of work accomplished under a series of study tasks for the Flying Qualities and Flight Control Systems Design Criteria Experiment (OFQ) of the Shuttle Orbiter Experiments Program (OEX). The tasks involved review of applicability of existing flying quality and flight control system specification and criteria for the Shuttle; identification of potentially crucial flying quality deficiencies; dynamic modeling of the Shuttle Orbiter pilot/vehicle system in the terminal flight phases; devising a nonintrusive experimental program for extraction and identification of vehicle dynamics, pilot control strategy, and approach and landing performance metrics; and preparation of an OEX approach to produce a data archive and optimize use of the data to develop flying qualities criteria for future space Shuttle craft in general.

This report concentrates on analytic modeling of the Orbiter unconventional closed-loop dynamics in landing, modeling pilot control strategies, verification of vehicle dynamics and pilot control strategy from flight data, review of various existent or proposed aircraft flying quality parameters and criteria in comparison with the unique dynamic characteristics and control aspects of the Shuttle in landing; and finally a summary of conclusions and recommendations for developing flying quality criteria and design guides for future Shuttle craft.

17. Key Words (Suggested by Author(s))	18. Distribution Statement
Flying qualities Manual flight control Manual landing control Space shuttle	Unclassified — Unlimited Subject category 08

19. Security Classif. (of this report)	20. Security Classif. (of this page)	21. No. of Pages	22. Price*
Unclassified	Unclassified	202	A10

For sale by the National Technical Information Service, Springfield, Virginia 22161.

☆ U. S. GOVERNMENT PRINTING OFFICE: 1987--726-123--45,003